

INVESTIGATING THE ROLE OF SUBCELLULAR
LOCALISATION OF AQUAPORIN 4 IN ASTROCYTES
AFTER TRAUMATIC SPINAL CORD INJURY

By ANDREA MELISSA HALSEY

A thesis submitted to the University of Birmingham for the degree of

DOCTOR OF PHILOSOPHY

Neuroscience and Ophthalmology

Institute of Inflammation and Ageing

College of Medical and Dental Sciences

University of Birmingham

UNIVERSITY OF
BIRMINGHAM

University of Birmingham Research Archive

e-theses repository

This unpublished thesis/dissertation is copyright of the author and/or third parties. The intellectual property rights of the author or third parties in respect of this work are as defined by The Copyright Designs and Patents Act 1988 or as modified by any successor legislation.

Any use made of information contained in this thesis/dissertation must be in accordance with that legislation and must be properly acknowledged. Further distribution or reproduction in any format is prohibited without the permission of the copyright holder.

Abstract

Traumatic spinal cord injury (SCI) is a debilitating condition that affects millions of people worldwide. Many people who receive a SCI suffer from paralysis and a reduced quality of life. Most of the complications of SCI occur secondary to the initial injury over a period of days to years. Currently, there are no pharmacological interventions to prevent secondary features of SCI, such as edema and scarring, meaning symptom management is the only available treatment option. The water channel protein aquaporin-4 (AQP4) is expressed in astrocytes and facilitates water flux across the blood-spinal-cord-barrier (BSCB). Previous work has demonstrated that AQP4 can be regulated by subcellular relocalization to the cell membrane, which alters its permeability, in a mechanism requiring calmodulin (CaM) and protein kinase A (PKA). AQP4 has been frequently associated with a number of secondary pathologies after SCI, including the formation of cytotoxic edema, and the migration of astrocytes preceding the formation of the glial scar border, both requiring a site-specific localization of AQP4. In this study, we aimed to investigate whether treatment with the inhibitors of subcellular AQP4 relocalization investigated *in vitro* could limit the formation of these secondary pathologies *in vivo*, using a rat dorsal column crush spinal cord injury model. This study illustrates that treatment with inhibitors of CaM, with the licenced drug trifluoperazine (TFP), or PKA, in a rat dorsal column crush SCI model, inhibited AQP4 localization to the blood-spinal-cord barrier, ablated SCI edema, lessened functional deficit, and reduced the size and density of the glial scar formed compared with untreated animals. In conclusion, this study demonstrates that targeting the mechanism of CaM/PKA-mediated cell-surface localization of AQP4 is a plausible approach for the treatment of traumatic SCI.

Acknowledgements

I would firstly like to thank Zubair Ahmed and Spinal Research UK for giving me the opportunity to do this PhD, and for providing me with invaluable training and networking.

A special thanks to Alex Conner and Roslyn Bill, for going above and beyond to provide me with encouragement, enthusiasm and a questionable sense of humour. “You’re welcome”. And to the other members of #TeamAQP: Phil Kitchen, Andrea Markou, Charlie Clarke-Bland, Mootaz Salman, Mohammed Abir-Awan, Zita Balklava, and Matt Conner, for always being so welcoming and helpful, and for providing many laughs!

Thank you to the Neuroscience and Ophthalmology group at UoB; a particular shout-out to Chloe Thomas, Gibran Butt, Sayed Rassul, Hannah Botfield, Lisa Hill, Callum Watson, and Maryam Esmaeili for teaching me so much and making the lab a happy place!

Finally, and most importantly, a sincere thank you to my family: Mum, Dad and Bennie for always being my biggest cheerleaders, Trina Reeves, Aaron Martin, Andrew Halsey, Nanna G and the Cornells for your love and support, and finally to my partner Oliver Cornell, for being the brightest light at the end of every dark tunnel throughout the last nine years, but the past three in particular!

Publications

- **Andrea M. Halsey**, Alex C. Conner., Roslyn M. Bill, Ann Logan. and Zubair Ahmed. (2018). Aquaporins and their regulation after spinal cord injury. (*Cells*). 7(10): 174.

- Philip Kitchen†, Mootaz M. Salman†, **Andrea M. Halsey†**, Charlotte Clarke-Bland, Justin A. MacDonald, Hiroaki Ishida, Hans J. Vogel, Sharif Almutiri, Ann Logan, Stefan Kreida, Tamim Al-Jubair, Julie Winkel Missel, Pontus Gourdon, Susanna Törnroth-Horsefield, Matthew T. Conner, Zubair Ahmed*, Alex C. Conner* and Roslyn M. Bill* (2020). Targeting aquaporin-4 subcellular localization to treat central nervous system edema. (*Cell*). 181(4): 784-799.e19. † **co-first authors**. doi.org/10.1016/j.cell.2020.03.037

Contents

Contents	v
List of figures	viii
List of tables	x
Abbreviations	xii
1 Introduction	2
1.1 Traumatic spinal cord injury (SCI)	2
1.1.1 Anatomy and physiology of the spinal cord	2
1.1.1.1 Spinal cord organization	2
1.1.1.2 Cell types and their functions in the uninjured spinal cord	5
1.1.2 Spinal cord injury overview	6
1.1.3 Pathophysiology of traumatic SCI	8
1.1.3.1 Primary injury	8
1.1.3.2 Secondary injury	9
1.1.3.3 Spinal cord edema	18
1.1.4 Animal models of traumatic SCI	20
1.1.4.1 Contusion models	21
1.1.4.2 Transection models	22
1.1.4.3 Compression/crush models	23
1.1.5 Current treatments for traumatic SCI	24
1.1.5.1 Rehabilitation	25
1.1.5.2 Pharmacological therapy	26
1.2 Aquaporins (AQPs) in the CNS	33
1.2.1 Human AQPs	33
1.2.2 Structure of mammalian AQPs	34
1.2.3 Localization and functions of human AQPs	36
1.2.4 AQPs in the brain and spinal cord	38
1.2.4.1 AQP1	39
1.2.4.2 AQP4	41
1.3 The role of AQP4 in SCI	46
1.3.1 Changes in AQP4 expression after SCI	46
1.3.2 Mechanisms of AQP4 involvement in SCI	47
1.3.2.1 Edema	47
1.3.2.2 Astrocyte reactivity, migration, and scarring	52
1.3.3 AQP4-mediated therapeutics for treating SCI	53
1.3.3.1 Reported inhibitors of AQP4	56
1.3.4 Targeting subcellular relocalization of AQP4 as a therapeutic intervention for SCI	59
1.4 Hypothesis and aims	61
2 Materials and Methods	64
2.1 In vivo	64
2.1.1 Animal surgery	64
2.1.1.1 Rat dorsal crush spinal cord injury model	64
2.1.2 Spinal cord DC crush injury treatment groups	65
2.1.3 Tissue preparation	66
2.1.3.1 Tissue for spinal cord water content	66
2.1.3.2 Histology	68
2.1.3.3 Spinal cord tissue homogenization and protein quantification	69
2.1.3.4 SDS-PAGE and Western blot	69
2.1.4 Histology and immunohistochemistry	70
2.1.4.1 Antibodies used for immunohistochemistry and Western blot	70
2.1.4.2 Fluorescence immunohistochemistry for spinal cord sections	71

2.1.5	Tissue microscopy	72
2.1.5.1	Confocal microscopy	72
2.1.5.2	Epifluorescent microscopy.....	72
2.1.6	Tissue image analysis.....	72
2.1.6.1	AQP4/GFAP colocalization.....	72
2.1.6.2	Relative membrane expression (RME).....	74
2.1.6.3	Relative perivascular AQP4.....	74
2.1.6.4	Total fluorescence (pixel intensity)	75
2.1.6.5	Protein area (albumin and macrophages)	76
2.1.6.6	Lesion and syrinx cavity measurement	77
2.1.6.7	Astrocytic scar density measurement.....	78
2.1.7	Western blotting	79
2.1.7.1	Polyacrylamide gel electrophoresis and western blot.....	79
2.2	In vitro experiments	80
2.2.1	Cell culture establishment/maintenance	80
2.2.1.1	Rat dorsal root ganglia neurons (DRGN)	80
2.2.1.2	Rat primary astrocytes.....	82
2.2.1.3	Human induced pluripotent stem cell (hiPSC)-derived astrocyte derivation.....	83
2.2.2	Immunocytochemistry	87
2.2.3	Primary rat astrocyte transfections.....	88
2.2.3.1	Polyethylenimine (PEI)	88
2.2.3.2	Lipofectamine	88
2.2.4	In vitro assays	89
2.2.4.1	DRG neurite outgrowth assay	89
2.2.4.2	Astrocyte scratch assay.....	90
2.2.4.3	Transwell migration assay	92
2.3	Statistics.....	95
3	Chapter 3.....	97
3.1	Rationale	97
3.2	Hypothesis and aims.....	99
3.3	Results.....	100
3.3.1	Comparing AQP4 membrane distribution across astrocyte cell bodies after traumatic spinal cord injury	100
3.3.1.1	Lesion site identification in spinal cord tissue.....	100
3.3.1.2	Determination of the localization of AQP4 in spinal cord astrocytes using confocal microscopy.....	101
3.3.1.3	Comparing AQP4 subcellular membrane distribution in astrocyte cell bodies	101
3.3.1.4	Treatment with TFP produces “punctate” AQP4 staining within astrocytes after DC SCI	105
3.3.2	Increased perivascular AQP4 was significantly reduced in vivo by treatment with calmodulin or PKA inhibitors	106
3.3.2.1	Increased AQP4 in astrocyte endfeet processes surrounding blood vessels after spinal cord injury at 3, but not 7 days after injury	106
3.3.2.2	Increased AQP4 fluorescence is specific to perivascular sites within the lesion epicentre	108
3.3.2.3	Treatment with calmodulin (CaM) inhibitors or protein kinase A (PKA) inhibitors prevents the increase in perivascular AQP4.....	110
3.3.3	Changes in total AQP4 protein.....	112
3.3.3.1	Western blot of AQP4 in spinal cord tissue after DC injury	112
3.3.3.2	Fluorescence intensity of AQP4 in spinal cord tissue after DC injury.....	113
3.3.3.3	Foxo3a nuclear localization after spinal cord injury is prevented by treatment with TFP or H-89	115
3.4	Discussion	117

3.4.1	Summary of results	117
3.4.2	Distribution of AQP4 in astrocytes in spinal cord tissue.....	117
3.4.3	AQP4 relocalization in vivo	118
3.4.3.1	AQP4 distribution across astrocyte cell bodies	118
3.4.3.2	AQP4 perivascular localization.....	120
3.4.4	Changes in AQP4 protein levels in spinal cord tissue.....	123
3.4.5	Conclusions.....	126
4	Chapter 4.....	129
4.1	Rationale	129
4.2	Aims and Hypothesis	132
4.3	Results.....	133
4.3.1	Spinal cord injury (SCI) edema	133
4.3.1.1	Inhibitors of PKA and CaM significantly reduce spinal cord water content following moderate severity traumatic spinal cord injury	134
4.3.1.2	Reduction in spinal cord water content by TFP is Calmodulin-specific	135
4.3.3	Post-traumatic cell-free cavity formation	141
4.3.4	Treatment with TFP significantly improved neuronal conductivity after spinal cord injury	143
4.3.5	Effect of PKA or CaM inhibition on neurite outgrowth	145
4.3.5.1	TFP inhibits neurite outgrowth at concentrations 10uM or above	145
4.3.5.2	TFP inhibition of neurite outgrowth is mediated through inhibition of Calmodulin	147
4.4	Discussion	152
4.4.1	The effect of inhibiting CaM or PKA on CNS edema	152
4.4.2	Neurite sparing and sprouting	156
4.4.3	Summary.....	160
5	Chapter 5.....	162
5.2	Aims and hypothesis	168
5.3	Results.....	169
5.3.1	Inhibition of CaM or PKA significantly decreased the overall size of the scar, as well as the GFAP immunoreactivity at the scar border	169
5.3.2	Investigating the effect of calmodulin or PKA inhibition on the rate of astrocyte migration in vitro. 173	
5.3.2.1	Scratch wound closure assay.....	173
5.3.2.2	Transwell migration assay	180
5.3.3	Investigating the effect of AQP4 membrane relocalization on astrocyte migration in vitro	183
5.3.3.1	Transfection of eGFP-AQP4 into primary rat astrocytes	184
5.3.3.2	Differentiation of astrocytes from induced pluripotent stem (iPS) cell lines with EGFP-AQP4 knock-in.....	186
5.4	Discussion	192
5.4.1	AQP4 and astrocyte migration	193
5.4.2	In vivo immunohistochemistry of the astrocytic scar.....	195
5.4.3	The “glial scar” debate	198
5.4.4	Summary.....	199
6	General discussion	202
6.2	Limitations of study	205
6.2.1	Investigating AQP4 subcellular distribution in spinal cord tissue	205
6.2.2	Measurement of spinal cord edema.....	207
6.2.3	SCI model	209
6.2.4	Route of administration of drugs	209
6.2.5	Timepoints of drug administration	210

6.3	Future work	211
6.3.1	TBI translation	211
6.3.2	Scarring	212
6.3.3	Alternative applications of AQP4 relocalization mechanism	213
6.3.3.1	AQP4 and the glymphatic system: roles in sleep and neurodegeneration	213
6.3.4	Glioblastoma multiforme (GBM)	217
6.4	Summary	218

List of figures

Figure 1-1 Schematic representations of human and rat spinal cord anatomy.	4
Figure 1-2 A schematic demonstrating the mechanistic progression and interdependency of SCI pathogenesis.	16
Figure 1-3. Schematic representations of the difference between cytotoxic and vasogenic edema.	20
Figure 1-4. The secondary, tertiary, and quaternary structures of aquaporin proteins.	35
Figure 1-5 A schematic demonstrating the tissue specific expression of the various AQP isoforms (1-10).	38
Figure 1-6 A schematic representing the anatomic and subcellular localization of AQP4 in the human brain and spinal cord.	45
Figure 1-7. The proposed relationship between AQP4 and cytotoxic and/or vasogenic edema following primary injury over time.	51
Figure 2-1 A diagrammatic representation of dorsal column crush SCI at spinal cord level T8.	66
Figure 2-2 A schematic demonstrating area of tissue dissected for water content measurement.	67
Figure 2-3 Diagrammatic representation of the plane of parasagittal sectioning.	68
Figure 2-4. Method of preparing images for colocalization analysis between red and green channels.	73
Figure 2-5 Representative images of rat spinal cord tissue immunostained for AQP4 (green) and RECA-1 (red), demonstrating the areas used to quantify perivascular and non-perivascular fluorescence (white lines).	75
Figure 2-6 Method of analysis for albumin area in immunolabeled spinal cord tissue.	77
Figure 2-7 A representative image of injured rat spinal cord tissue at 7 days post-injury demonstrating where the areas of uninjured tissue, lesioned tissue area and cell-free cavity were demarcated for analysis.	78
Figure 2-8 A representative image of injured rat spinal cord tissue at 7 days post-injury immunolabelled for GFAP (green), AQP4 (red), and DAPI (blue) to demarcate the astrocytic scar border.	79
Figure 2-9 A diagram illustrating the identification of DRG after removal of the vertebrae from the dorsal side of rat.	82
Figure 2-10 Phase contrast image demonstrating the visual difference between hiPSC colonies (arrow) and potentially differentiated hiPSCs (arrowheads).	85
Figure 2-11 Schematic of NPC monolayer culture protocol.	86
Figure 2-12 Methodology for selecting and measuring DRGs for neurite outgrowth assays.	89
Figure 2-13 A screenshot of the ImageJ window, demonstrating the area measured using the polygon tool to demarcate the scratch area of primary rat astrocytes.	92
Figure 2-14 A schematic detailing the methodology of quantifying relative number of migrated cells in transwell migration assays using calcein fluorescence.	94
Figure 3-1 Macrophage (CD68; green) immunohistochemistry in rat spinal cord, from either control, uninjured rats or those subject to dorsal column crush injury at 3 days post-injury.	100

Figure 3-2 Representative images of astrocytes in the uninjured rat spinal cord.	101
Figure 3-3 Mander's colocalization coefficients describing the abundance of green (AQP4) positive pixels colocalized with red (GFAP) positive pixels in astrocyte images autothresholded with Otsu's threshold clustering algorithm.....	103
Figure 3-4 Relative membrane expression quantification of confocal images of astrocytes.	104
Figure 3-5 Spinal cord tissue immunostained for AQP4 (green), GFAP (red) and DAPI (blue) at 3 dpi.	105
Figure 3-6 Confocal images of rat spinal cord tissue stained for RECA-1 (red) and AQP4 (green).	107
Figure 3-7 Confocal images of rat spinal cord tissue stained for blood vessels (RECA-1; red) and AQP4 (green).	109
Figure 3-8 Rat spinal cord tissue dissected from each treatment group labelled for AQP4 (green) and imaged at 10x magnification.	110
Figure 3-9 Confocal images of rat spinal cord tissue stained for blood RECA-1 (red) and AQP4 (green) and quantified for perivascular AQP4.	111
Figure 3-10 Western blot of tissue lysates obtain from rat spinal cords.....	112
Figure 3-11 Confocal images of rat spinal cord tissue immunostained for AQP4 (green). ...	114
Figure 3-12 Immunofluorescence micrographs of rat spinal cord tissue stained for Foxo3a (green) and DNA (DAPI, blue) 3 days after dorsal column (DC) crush.....	116
Figure 3-13 A schematic demonstrating the underlying mechanisms of Foxo3a-mediated changes in AQP4 transcriptional regulation.	125
Figure 4-1 Mean water content differences after spinal cord injury at 3 days post-injury in rat T8 dorsal column crush models.	133
Figure 4-2 Water content of the thoracic spinal cord 3, 7, and 28 days after dorsal column (DC) crush and treatment with CaM or PKA inhibitors (CaMi or PKAi).	135
Figure 4-3 Water content of the thoracic spinal cord 3 days after DC crush to investigate the mode of action of TFP.	137
Figure 4-4 Immunohistochemistry of extravasated albumin in spinal cord tissue 7 days post-injury.	139
Figure 4-5 Immunohistochemistry of extravasated albumin in spinal cord tissue 28 days post-injury.	140
Figure 4-6 Immunohistochemistry of GFAP (green) and DAPI (blue) in rat spinal cord demonstrating the occurrence of cell-free cavity formations within the fibrotic scar area at 7dpi.	142
Figure 4-7 Compound action potential (CAP) areas (mV x ms) recorded at spinal cord level C4/5 after stimulation at level L1/2.....	144
Figure 4-8 Representative images of DRGNs immunostained against β III-tubulin (green) and DAPI (blue) 72hrs after treatment with either 0 μ M, 1 μ M, 10 μ M, or 100 μ M TFP.....	146
Figure 4-9 Quantification of various parameters of neurite outgrowth in cultured dorsal root ganglia neurons treated with increasing doses of trifluoperazine (TFP).	147

Figure 4-10 Representative images of DRGNs immunostained against β III-tubulin (green) and DAPI (blue) 72hrs after treatment with either 10 μ M TFP, 8.66 μ M W-7, 1.3 μ M L-741,626 (D2Ri), 0.724 μ M terazosin (A1Ri), or no treatment (control).	150
Figure 4-11 Quantification of various parameters of neurite outgrowth in cultured dorsal root ganglia neurons treated with 10 μ M TFP, 8.66 μ M W-7, 1.3 μ M L-741,626 (D2Ri), 0.724 μ M terazosin (A1Ri), or no treatment (control).	151
Figure 4-12 Treatment with inhibitors of AQP4 expression and subcellular relocalization after cytotoxic edema in vivo improves sensory and locomotor functional recovery.	158
Figure 5-1 A schematic representing the distribution of cell types at various time periods after traumatic spinal cord injury.	165
Figure 5-2 A schematic demonstrating the mechanisms of astrocyte membrane expansion and stabilization for the purpose of migration.	167
Figure 5-3 Immunohistochemistry of GFAP (green), AQP4 (red) and DAPI (blue) in rat spinal cord to demonstrate the morphology of the astrocytic scar barrier containing the entire lesion wound cavity at 7dpi.	170
Figure 5-4 Immunohistochemistry of CD68 (green) and DAPI (blue) in rat spinal cord to demonstrate the extent of macrophage infiltration to the spinal cord lesion site at 7dpi.	172
Figure 5-5 Optimization of cell culture conditions for an <i>in vitro</i> scratch wound closure assay using primary rat astrocytes.	176
Figure 5-6 The effect of TFP or H-89 treatment on the rate of scratch wound closure in primary rat astrocytes.	178
Figure 5-7 Initial optimization of two methods for calculating transwell migration.	182
Figure 5-8 Percentage number of migrated cells 24hrs after plating, as determined using the Calcein fluorescence method.	183
Figure 5-9 Representative phase-contrast images of primary rat astrocytes transfected with 0.5 μ g eGFP-AQP4 cDNA using various concentrations of polyethylenimine (PEI).	185
Figure 5-10 Optimization of Lipofectamine-2000-mediated transfection of eGFP-AQP4 cDNA construct into primary rat astrocytes.	186
Figure 5-11 Characterization of hiPSC differentiation into hiNPCs.	188
Figure 5-12 Characterization of hiNPC differentiation into hiPSC-derived astrocytes.	190
Figure 5-13 hiPSC derived astrocytes imaged at 0, 4, and 8hrs post-scratch using a CellIQ automated live-cell imaging machine.	191
Figure 6-1 A schematic of the glymphatic system. CSF flows in paravascular spaces lined with astrocyte endfeet.	215

List of tables

Table 1-1 A summary of all clinical trials carried out in neuroprotective or neuroregenerative agents studied in the context of traumatic spinal cord injury..... 32

Table 2-1 Further information on antibodies used for immunohistochemistry, immunocytochemistry and Western blotting, including species, source, and dilution volumes..... 70

Abbreviations

AD	Alzheimer's Disease
AIS	ASIA impairment scale
ANOVA	Analysis of variance
AQP	Aquaporin
ASIA	American Spinal Injury Association
ATP	Adenosine Triphosphate
AZA	Acetazolamide
BBB	Blood-brain-barrier
BSA	Bovine serum albumin
BSCB	Blood-spinal cord-barrier
CaM	Calmodulin
CaMKII	Ca ²⁺ /Calmodulin-dependent protein kinase II
CAP	Compound action potential
CD68	Cluster of Differentiation 68 (Monocytes)
cDNA	Complementary DNA
CNS	Central Nervous System
CPE	Choroid Plexus Epithelium
CRISPR	Clustered regularly interspaced short palindromic repeats
CSF	Cerebrospinal fluid
CSPG	Chondroitin sulfate proteoglycan
CVR	Cell Volume Regulation
Cx43	Connexin-43
DAMPs	Damage-associated molecular pattern molecules
DAPI	4',6-diamidino-2-phenylindole
DC	Dorsal column
DMEM	Dulbecco's Modified Eagle Medium
DMSO	Dimethyl sulfoxide
dpi	Days post-injury
DRG	Dorsal root ganglia
DWI	Diffusion weighted imaging
ECM	Extracellular matrix

EDTA	Ethylenediaminetetraacetic acid
eGFP	Enhanced green fluorescent protein
FLAIR	Fluid-Attenuated Inversion Recovery
Foxo3a	Forkhead box O3
GBM	Glioblastoma multiforme
GFAP	Glial fibrillary acidic protein
GLT-1	Glutamate transporter 1
H-89	N-[2-(p-Bromocinnamylamino)ethyl]-5-isoquinolinesulfonamide dihydrochloride
hiPSC	Human induced pluripotent stem cell
HMGB1	High mobility group box protein 1
ICP	Intracranial pressure
IgG	Immunoglobulin G
IgY	Immunoglobulin Y
IH	Infinite horizon impactor
IL-1	Interleukin-1
IL-6	Interleukin-6
ISF	Interstitial fluid
KSPC	Keratin sulfate proteoglycan
MAPK	Mitogen-activated protein kinase
MCAO	Middle cerebral artery occlusion
MP	Methylprednisolone
MRI	Magnetic resonance imaging
MTT	3-(4,5-Dimethylthiazol-2-yl)-2,5-Diphenyltetrazolium Bromide
NASCIS	National Acute Spinal Cord Injury Studies
NBA	Neurobasal A
NF- κ B	Nuclear factor κ B
NKCC1	Sodium/potassium/chloride co-transporter 1
NMO	Neuromyelitis optica
NO	Nitric Oxide
NPC	Neural progenitor cell
OAP	Orthogonal arrays of particles

OPC	Oligodendrocyte progenitor cell
PBS	Phosphate buffered saline
PDL	Poly-D-Lysine
PDVF	Immobilon-P polyvinylidene fluoride
PEI	Polyethylenimine
PFA	Paraformaldehyde
PKA	Protein Kinase A
RME	Relative membrane expression
ROI	Region of interest
SC	Spinal cord
SCI	Spinal Cord Injury
TBI	Traumatic Brain Injury
TEA+	Tetraethylammonium
TFP	Trifluoperazine
TGF- β	Transforming growth factor beta
TGN-020	2-(nicotinamide)-1,3,4-thiadiazole
TID	trypsin inhibitor DNase
TM	Transmembrane
TNF- α	Tumour necrosis factor alpha
WHO	World Health Organization
WT	Wild-type

Chapter 1

Introduction

This chapter has been published in the literature review: Halsey, A. et al. (2018). "Aquaporins and their regulation after spinal cord injury". *Cells*. 7(10): 174.

1 Introduction

1.1 Traumatic spinal cord injury (SCI)

The central nervous system (CNS) is comprised of the brain and spinal cord. The spinal cord functions as an intermediate conduit between the brain and the periphery. The brain coordinates the more complex, higher-level functions, including processing the sensory information received from the spinal cord tracts, and coordinating the appropriate motor responses back to it. Injuries to the CNS, including traumatic brain injury (TBI), spinal cord injury (SCI), and stroke have a collective incidence of between 500 – 650 per 100,000 people worldwide (Feigin et al., 2019).

1.1.1 Anatomy and physiology of the spinal cord

1.1.1.1 *Spinal cord organization*

The spinal cord is the caudally extending part of the CNS, between the base of the brain stem and the lumbar region of the vertebral column. It protrudes through the foramen magnum of the skull into the first spinal column, and is surrounded by the three CNS membranes (from inner to outer); the pia, arachnoid, and dura mater, containing cerebrospinal fluid (CSF), and the vertebral column, which protects and supports the cord. The cord can be divided into four rudimentary segments (from rostral to caudal); cervical, thoracic, lumbar, and sacral. This can be further divided into segments, with number of each varying between rat and human; human cords contain eight cervical, twelve thoracic, five lumbar, five sacral, and one coccygeal (Figure 1-1Ai), whereas rat cords contain eight cervical, thirteen thoracic, six lumbar, and four sacral (Figure 1-1Bi) (Frostell et al., 2016). When viewed longitudinally, the spinal cord

is symmetrical along the medial sagittal plane, with both portions carrying identical but unilateral tracts. The core of the spinal cord in this plane is comprised of grey matter, which contains all of the spinal cord neuronal cell bodies and can be divided into the dorsal horn, intermediate grey, ventral horn and central gray matter (Figure 1-1Aii) (Mercadante and Tadi, 2020). Surrounding the grey matter is white matter, which contains myelinated and unmyelinated nerve fibres and can be divided into funiculi; dorsal, lateral, and ventral. The composition of white matter to grey matter differs at different points along the cord. Nerves protrude from the spinal cord and exit or enter between vertebrae at their respective levels through dorsal or ventral roots, which combine outside the vertebrae in spinal nerves, named after the spinal cord level from which they protrude (Watson and Kayalioglu, 2009). Spinal cord nerves are arranged into tracts, according to the type of information they carry, and whether or not they are ascending or descending the length of the spinal cord (Watson and Harrison, 2012; Liang et al., 2011). Ascending tracts (i.e those carrying sensory, somatosensory, and information from the periphery to the brain) are formed from neurons within the dorsal root ganglia, that protrude their axons through the dorsal root into their white matter tracts. They include the dorsal column-medial lemniscus, spinocerebellar, spinothalamic, and spino-olivary tracts. Descending tracts (i.e, those carrying motor information, including that of muscle tone, balance and posture, from the brain to the periphery) originate in various parts of the brain and hindbrain, and project down through the spinal cord, where they synapse with lower motor neurons that carry information out of the spinal cord to the periphery via the ventral root (Nógrádi and Vrbová, 2007). There are also a small number of intrinsic pathways that relay information between ascending and descending tracts, and regulate propriospinal

functionality (Flynn et al., 2011; Edgley, 2001). Functional outcomes following SCI therefore largely depends on the level at which the spinal cord is injured, as well as the neuronal tracts that are damaged.

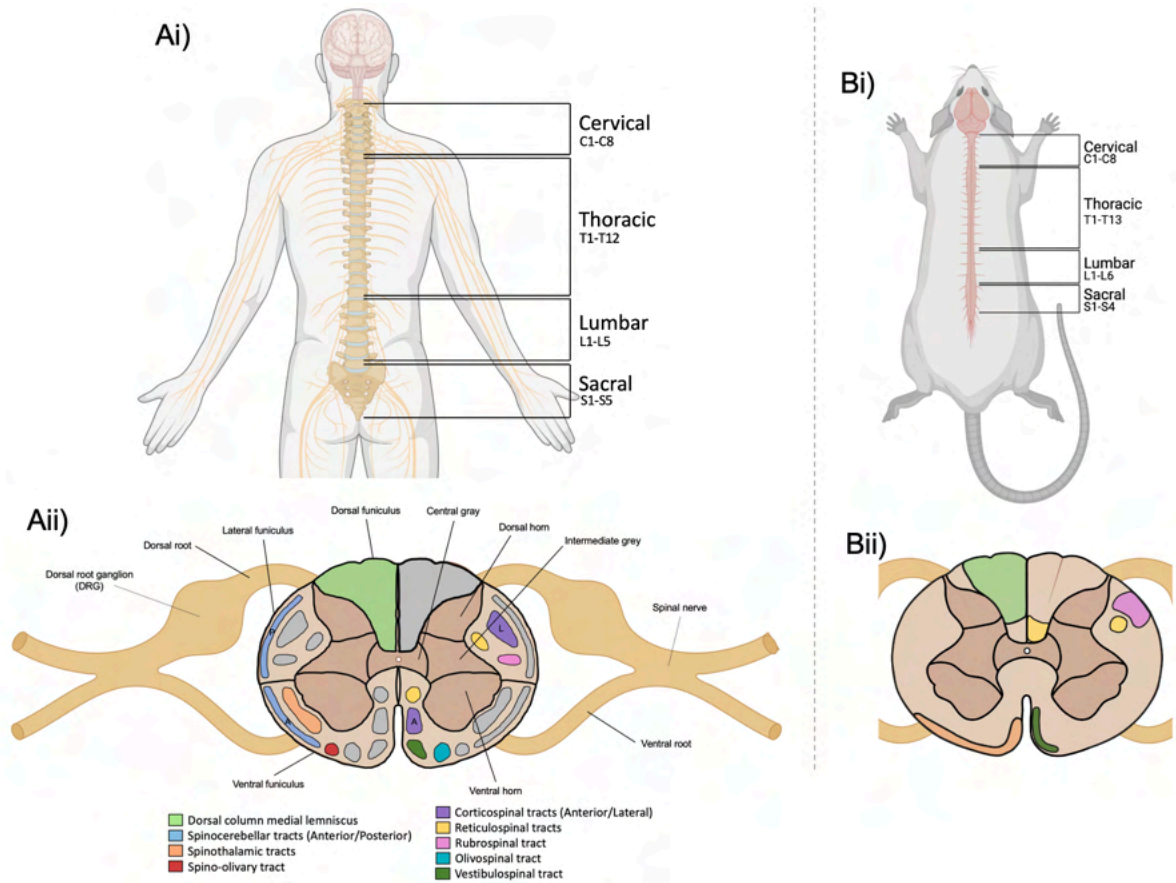


Figure 1-1 Schematic representations of human and rat spinal cord anatomy.

The longitudinal axis of both the human (Ai) and rat (Bi) the spinal cord is divided into 4 regions; cervical, thoracic, lumbar, and sacral, each with a defined number of spinal nerves protruding from between the numbered vertebrae, which differs between species. Aii) View of a cross-section of spinal cord within the lumbar region, as an example, labelled for the white and grey matter divisions, white matter tracts, and motor/sensory exit/entry points. The left half of the spinal cord contains coloured-in regions representing ascending tracts, whereas the left half

of the cord contains the coloured-in regions representing descending tracts. Bii) A representative view of a cross section of lumbar spinal cord in rat, highlighting the main location differences for some tracts compared to human. Made using biorender.com.

1.1.1.2 *Cell types and their functions in the uninjured spinal cord*

The spinal cord consists of a heterogeneous combination of cell types similar to those present in the brain, including neurons arranged into ascending and descending tracts and fibres, glia (e.g. astrocytes, oligodendrocytes, microglia, and ependymal cells), endothelial cells forming the spinal cord vasculature, and some endogenous progenitor cells (Nógrádi and Vrbová, 2007). Neurons are mostly of the sensory, motor, or interneuron subtype, which are arranged into distinct laminae depending on their neuronal characteristics and specificity (i.e. in terms of axonal size, receptor expression, degree of myelination). Glia are a collective of non-neuronal cells that do not generate electrical impulses, but have alternative functions, such as maintaining tissue homeostasis and modulating synaptic function. Oligodendrocytes are a type of cell from neural progenitor origin that produce myelin, a fatty substance that is used to ensheath and therefore insulate neuronal axons to increase the speed of electrical transmission (Nave and Werner, 2014). Microglia are resident immune cells, which under physiological conditions, known as a “resting” state, constantly monitor the biochemical environment through their extensive assortment of receptors, becoming “activated” upon signals related to stress, hypoxia, and inflammation (Raivich, 2005). Ependymal cells are cilia/microvilli-coated cells that line the central canal of the spinal cord, and function to produce and direct flow of cerebrospinal fluid (CSF).

1.1.1.2.1 *Astrocytes*

Astrocytes are known as the “star-shaped” cells of the CNS, owing to their extensive and highly complex array of processes that can extend to down to nanoscale thickness. Making up approximately 40-50% of all glia, they cover an extensive proportion of explicit territories, making close contacts via “endfeet” at the apex of their processes. These territories include neuronal synapses, blood vessels, and at the pial surface, where endfeet almost completely cover or surround the areas to ensure high levels of sensitivity. The functions of astrocytes at these locations is extensive, and can be summarized as homeostatic support on a cellular, molecular, and metabolic level (Verkhratsky and Nedergaard, 2018). They maintain the optimal metabolic environment through their ability to generate glycogen, providing additional energy for neurons when required, and modulate neurotransmission by removing and recycling released neurotransmitters, and releasing precursors for the generation of new neurotransmitter molecules (Hertz et al., 2007; Oliet et al., 2001). They are able to regulate appropriate neuronal plasticity, and promote synaptogenesis and/or neurogenesis where necessary (Schousboe et al., 2013). Astrocytes are also able to regulate the molecular environment of the CNS through their ability to transport ions and water into and out of the CNS via their close interactions with CNS vasculature (Simard and Nedergaard, 2004).

1.1.2 Spinal cord injury overview

The spinal cord coordinates the body’s sensation, movement and autonomic reflexes; elements that are vital for human functionality. As such, damage to the spinal cord can be profound on the wellbeing and quality of life for the individual. A SCI can be broadly

categorised into being of traumatic or non-traumatic origin; the former being the result of external physical insult (for example, a car accident), the latter being the result of a much more diverse range of internal insults (for example, a tumour) (Ahuja et al., 2017). Furthermore, traumatic injuries can be further broadly divided into “incomplete” and “complete” injuries. An incomplete injury describes direct damage to part of the cord, and results in “preservation of any sensory and/or motor function below the neurological level”. A complete injury describes direct damage to the entire cord, resulting in “an absence of sensory and motor function in the lowest sacral (S) segments (S4-S5)” (Kirshblum et al., 2011). Clinically, the “completeness” of an injury can be determined using the American Spinal Injury Association (ASIA) impairment scale (AIS). The incidence of SCI is not well defined, probably owing to the highly varied nature of the condition and the complications in its guaranteed diagnosis. A recent world-wide review suggests that the worldwide prevalence of SCI is now estimated around 27.04 million people (Feigin et al., 2019). According to the World Health Organization (WHO), patients suffering with SCI have a much higher incidence of depression compared to overall population estimates and are up to 5 times more likely to die prematurely (World Health Organization, 2013; Post and van Leeuwen, 2012). Furthermore, SCI has a significant economic impact both on the individual and society. Most recent estimates suggest that employment rates of SCI sufferers is only 37%, on top of the costs of personal care. (French et al., 2007; World Health Organization, 2013). A recent study estimated that in the UK alone, the yearly cost of treating SCI patients is about £1.43billion, which equates to roughly £1.12million per patient, with variability depending on the extent of injury as determined by the AIS impairment scale; paraplegic and tetraplegic patients costing about £1.41 and

£1.87million per year, respectively. Collectively, SCIs constitute massive economic and social problems, for both the patient and the health care systems involved in treating the injury. As such, research is absolutely vital for investigating how spinal cord injuries manifest in such a devastating way, and for creating interventions to minimize damage and subsequently the burdens to which SCIs cause.

1.1.3 Pathophysiology of traumatic SCI

SCI can be the result of external insult (traumatic SCI), or from a separate condition that physically impacts the spinal cord (non-traumatic). Following a traumatic SCI laceration, contusion, or compression (the primary injury), a series of molecular cascades are triggered that result in neuronal and glial cell death from inflammation and/or ischemia/hypoxia. These molecular changes then lead to architectural and functional changes (the secondary injury), including the formation of a glial scar and cavities, and neuronal cell loss. Although the focus of this review is on edema, in the context of SCI over time following primary injury, no particular pathological feature can be explained in isolation from the big picture, and as such the current knowledge of the pathogenesis as a whole shall be discussed:

1.1.3.1 *Primary injury*

The initial mechanical injury, be it a transectional laceration, distraction, contusion or compression, results in damage to the cell types present in the spinal cord; mostly neurons, astrocytes, myelinating oligodendrocytes, and the spinal cord vasculature. Damage to these cell types leads to a biochemical cascade that disrupts their functionality, including neuronal signalling, water transport, and blood-spinal cord

barrier integrity (Dumont et al., 2001). These events lead to further secondary cascades that cause sustained damaged and spinal cord dysfunction that can be reflected symptomatically, and the severity of the primary injury is often a strong prognostic index of the secondary mechanisms and functional outcome (Coleman and Geisler, 2004).

1.1.3.2 *Secondary injury*

Secondary injury can be broadly categorized chronologically into acute (0-48hrs), subacute (48hrs to 2 weeks), intermediate (2 weeks to 6 months), and chronic (6 months onward) phases from the onset of the primary injury. Each of these stages encompasses a multitude of pathophysiological mechanisms, each intrinsically overlapped in their relationship to one another, and each affecting the manifestation and magnitude of subsequent stages. Many agree that these mechanisms work in a cascade of cumulative or multiplicative effect, and therefore understanding these mechanisms in isolation and in relation to one another is vital for understanding the big picture and developing methods of dampening it. Each of the elements described can be visualized in the schematic depicted in

Figure 1-2.

Acute phase (<2 days): The initial primary injury leaves the spinal cord in a state of necrosis and apoptosis due to the initial neuronal damage, as well as the cessation to local blood supply, resulting in ischemia and hypoxia (Tator and Koyanagi, 1997). Furthermore, the damaged blood supply can result in haemorrhage, which alongside ischemia, is a major trigger for highly destructive inflammatory processes to start

through the release of pro-inflammatory cytokines and chemokines (e.g. IL-6 and TGF- β) (Logan et al., 1994). These signalling molecules result in the activation and infiltration of numerous innate and adaptive immune cells including neutrophils, macrophages and lymphocytes (Pineau and Lacroix, 2007; Fleming et al., 2008). This response is necessary to clear the post-apoptotic debris that may inhibit the survival or potentiate further apoptosis of other neurons (Neumann, H. et al. 2009). However, this mass immunogenic response can also cause damage to healthy tissue, including the endothelium of vessels, leading to further disruption of the BSCB. The destruction caused by activated immune cells then triggers several further intra- and extra-cellular signalling cascades, leading to localized cell death, swelling, and further damage from the cytokines and free radicals released. This inflammation may persist for weeks, or even months, after its onset (Fehlings and Nguyen, 2010). However, despite the damaging nature of the inflammation present, more recent studies suggest that the activity of the immune system at CNS injury site also contributes to building an environment aiding neuroprotection and/or pro-regeneration (Fleming et al., 2006). As such, the contribution of neuroinflammation to the pathogenesis of SCI remains complex and an area of interest in research.

As a result of the primary injury and molecular changes that occur within the acute phase, there is also frequently observed alterations to systemic functions. These are clinical manifestations that occur due to the damaged nerve supply to tissues, and can affect motor function, sensory stimulation, thermoregulation, respiration, gastrointestinal function, and autonomic function (termed neurogenic shock) (Krassioukov and Claydon, 2006; Laird et al., 2006; Ebert, 2012). Neurogenic shock is

generally defined as a combination of bradycardia and hypotension, but also involves the cessation of adequate vasomotor sympathetic control within tissues below the level of the SCI, resulting in mismatched muscle tone from parasympathetic activity (Cadotte and Fehlings, 2012). Frequently, patients will also experience spinal shock involving the loss of reflexes in regions caudal to the injury due to lack of innervation from the brain (Ko et al., 1999).

Subacute phase (2 days – 2 weeks): Naturally due to the excessive ischemia that occurs in the acute phase, as well as the release of intracellular substances due to mechanical damage, the tissue enters a stage of dysregulation in ionic homeostasis. Many of the damaged and surrounding neurons become excitotoxic as a result of excessive levels of sodium and calcium within neurons and glia due to high levels of glutamate and ATP in the extracellular environment (Shields et al., 2000; Weber, 2012). This probably occurs due to the breakdown of excitatory cell membranes or excess synaptic release from intracellular ion dysregulation (Guerriero et al., 2015). One of the major effects of this excess intracellular calcium is the activation of calpains, a cytotoxic and Ca^{2+} -dependent protease, which results in the degradation of many cellular proteins, including components of the cytoskeleton, neurotransmitter receptors, and mitochondrial ATP pumps (Pottorf et al., 2006; Xu et al., 2007). As such, further damage may then occur through mitochondrial dysfunction, cytoskeleton breakdown and further ionic dysregulation through loss of appropriate signalling responses. This destruction is further inflated by the activity of the CNS and extravasated peripheral immune systems (Anwar et al., 2016). These inflammatory cells cause further breakdown of cellular components, resulting in the production of

free radicals, which can cause oxidation of genetic material, lipids and other proteins vital for cellular function (Schwab et al., 2014). This process accentuates throughout the entire period of ischemia, which may persist way into chronic phases of SCI, depending on the nature and extent of the initial injury (Novy, 2006).

Intermediate phase (2 weeks to 6 months): Following the mechanistic and architectural changes resulting from the ischemic and inflammatory reactions of the earlier stages, several permanent changes have now occurred within the injury site and surroundings. The way that these changes manifest strongly determines the outcome of the SCI in the long-term. One of the first changes involves the demyelination of neurons within the white matter proximity of the lesion (Totoiu and Keirstead, 2005; Hassannejad et al., 2019). Neurons that were both directly affected or unaffected by the primary injury may become damaged or dead as a result of the damage to oligodendrocyte cell bodies near to the initial lesion that results in Wallerian degeneration of the myelin and death of oligodendrocytes (Guest et al., 2005; Abe et al., 1999). This loss of myelination affects the neural conductivity of surviving neurons and can cause them to retract (George and Griffin, 1994), and thus efficient remyelination is key to retaining neuronal functionality and promoting regeneration. However, similarly to neurons, oligodendrocytes exist in the adult spinal cord as post-mitotic cells, unable in themselves to compensate for the requirements of remyelination required. Remyelination of demyelinated neurons has been reported mostly between 2 and 12 months after the primary injury (Salgado-Ceballos, H. et al., 1998). This occurs mostly through the activation of a population of neural progenitor cells (NPCs) and oligodendrocyte progenitor cells (OPCs), which rapidly divide and alter in

morphology in response to injury (McTigue et al., 2001). However, it remains controversial as to whether the demyelination that occurs has any functional impact in the chronic stages of SCI and beyond (Lasiene et al., 2008), or indeed whether any regeneration that occurs has any functional benefit, as the myelin debris produced from the initial degeneration of myelin may be inhibitory for the formation of new oligodendrocytes and myelin (Kotter et al., 2006).

Another major formation is that of the “glial” scar, which develops at around 4 weeks following primary SCI in response to the onset of astrogliosis and increased inflammation in the lesion epicentre. The scar has two major compartments, which include different cell types and molecular environments. The fibrotic region contains many infiltrated fibroblasts, macrophages, and pericytes, which create a core for the scar, and secrete extracellular matrix proteins such as collagen, which can create an inhibitory environment for neuronal regeneration, as well as creating a physical barrier for growth (Anderson et al., 2014; Fehlings and Hawryluk, 2010). Surrounding the fibrotic region is the glial limiting membrane comprised of recently proliferated and migrated astrocytes, microglia, and NG2+ glia, where the fibroblast/extracellular matrix (ECM) core meets the glial scar, formed in a mesh-like arrangement of intertwined processes (Wanner et al., 2013). The different cell types present within the scar and during its formation each have different roles. In acute stages of scar formation, astrocytes proliferate, switch to a reactive phenotype, become hypertrophic and migratory, and reorganize their processes to the external border of the damaged tissue area to form the initial scar (Saadoun, 2005; Wanner et al., 2013; Sun and Jakobs, 2012). At later stages of scar formation, these reorganized astrocyte processes tightly

link, creating a glial limitans, which creates the barrier between lesion and non-lesion territory (Sofroniew, 2009; Khakh and Sofroniew, 2015). Resident NG2+ oligodendrocyte precursor cells increase in proliferation and differentiation following injury, and are thought to contribute to remyelination by differentiating into Schwann cells or by inducing oligodendrogenesis (Hesp et al., 2015). For many years it has been accepted that due to the physical barrier formed by the scar, that it results in the mechanical blockade of effective axon regrowth, and thus limits the ability for damaged nerves to regenerate in mammals (Windle, W.F. et al. 1952; Silver, J. and Miller, J.H. 2004). Indeed, non-mammalian SCI appears to result in little to no 'scar' formation, and concurrently there also appears to be a degree of neuronal regeneration, in which axons are able to regrow over a "glial bridge" formed of migrated astrocytes (Goldshmit et al., 2012). Furthermore, reactive astrocytes that aid the formation and eventually surround the scar have been demonstrated *in vitro* to express high levels of molecules that are inhibitory for axonal growth, such as chondroitin and keratin sulfate proteoglycans (CSPGs/KSPGs). Enzymatic degradation of such molecules appears to be a very promising therapeutic target, having demonstrated the appearance of a regenerative phenotype in injured SC axons and functional recovery after SCI in rodents (Bradbury and Carter, 2011; Bradbury et al., 2002; Suzuki et al., 2017; James et al., 2015). However, some evidence does also exist to suggest that the glial scar is a necessary structure to limit the overall damage area, and thus reduce the number of neurons damaged.

Chronic (6 months onward): Chronic manifestations of SCI are elements of the pathology that persist for long into the future, often for the remainder of the patient's

life. A major part of this involves the demyelination of neurons in regions surrounding the injury site; a process that begins approximately 2 days after the primary injury with swelling and toxicity in oligodendrocytes, and develops chronically into the loss of myelin ensheathing neuronal axons. This demyelination has been shown to still be occurring as late as 450 days post-injury in rats (Totoiu and Keirstead, 2005; Guest et al., 2005). Demyelination is a devastating occurrence in the spinal cord, as it exposes the axon and disrupts impulse conduction. Furthermore, demyelination can result in Wallerian degeneration of injured neurons and their degradation and clearance from the cord (Buss et al., 2004; Becerra et al., 1995).

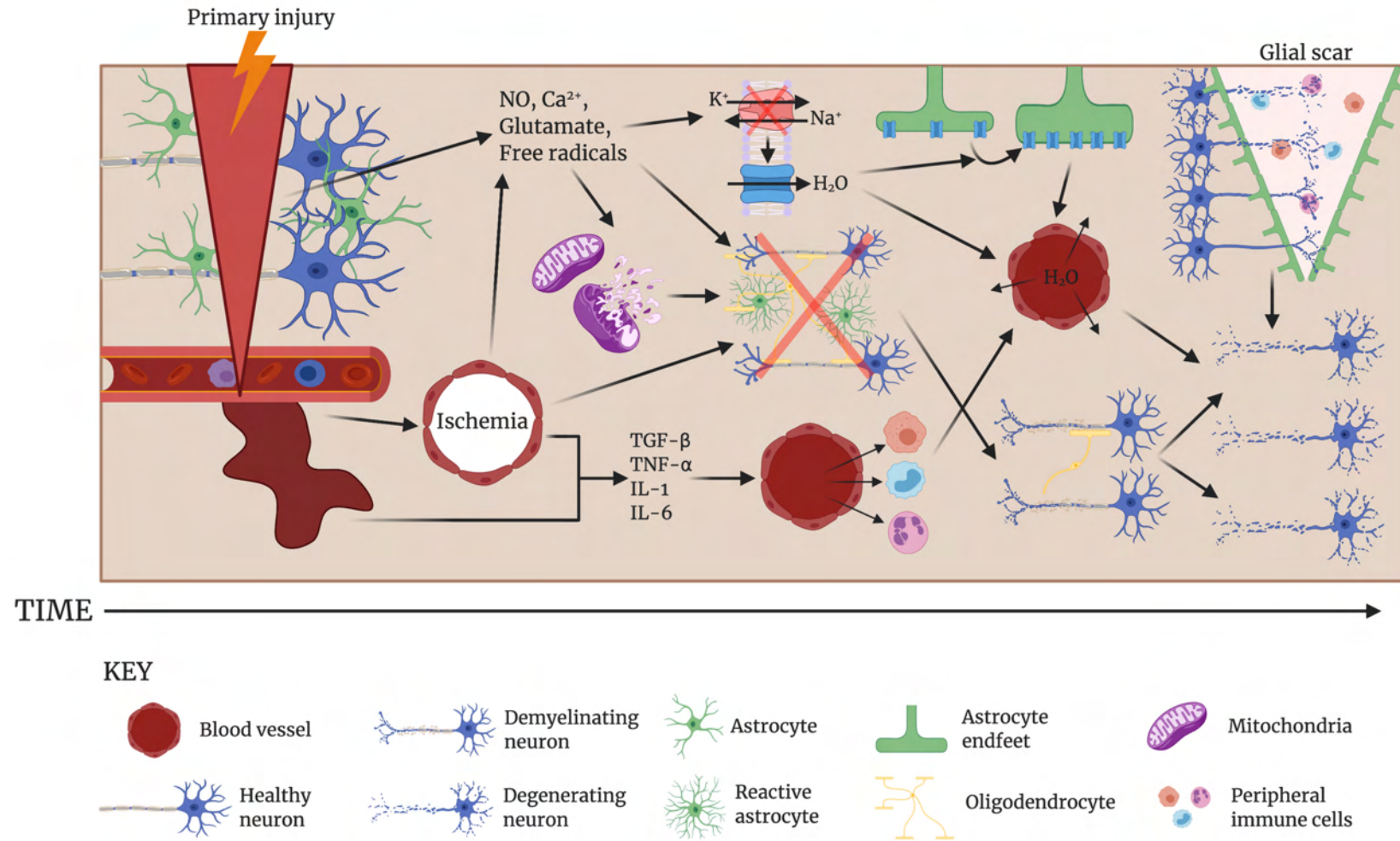


Figure 1-2 A schematic demonstrating the mechanistic progression and interdependency of SCI pathogenesis.

In the primary injury phase, the spinal cord becomes injured by a traumatic external insult, such as a laceration, distraction, contusion or compression. This primary injury results in mechanical damage to neurons, astrocytes, oligodendrocytes and blood vessels. From this primary damage, a series of secondary injury cascades occur that potentiate the primary injury. In the earlier stages, damaged blood vessels may haemorrhage, resulting in ischemia and release of inflammatory cytokines (e.g TGF- β , TNF- α , IL-1, and IL-6). These cytokines attract blood-borne inflammatory cells such as neutrophils, macrophages and leukocytes, which act to both clear up cellular debris, but also cause further damage to healthy cells by enhancing local inflammation, eventually leading to neuronal loss from inflammatory damage and through Wallerian degeneration through oligodendrocyte death and demyelination. Damaged neurons may secrete free radicals, nitric oxide (NO), glutamate, and Ca²⁺ which potentiate cellular damage by causing mitochondrial dysfunction leading to the loss of ATP, and by causing localized excitotoxicity. Collectively, these two events result in loss of Na⁺/K⁺-ATPase activity in astrocytes, which results in cytotoxic edema through increased water absorption through AQP4 in response to ionic dysregulation, eventually leading to vasogenic edema and spinal cord swelling and cavity formation, which obstructs and damages cells further.

1.1.3.3 *Spinal cord edema*

Edema of the spinal cord within the secondary pathogenesis of traumatic spinal cord injury is a clinically important feature that begins in the acute phase and persists through the sub-acute phase. It involves the accumulation of water within the parenchyma proximal to the primary injury (Leypold et al., 2008). Edema formation can be demonstrated in animal models of SCI within minutes from the epicentre of the primary injury and develops outward into a larger fluid-filled cavity within 48 hours and may persist for up to 14 days post-injury (Tator and Fehlings, 1991; Goodman et al., 1976b; Noble and Wrathall, 1989). Whilst the exact molecular mechanisms facilitating edema formation aren't clear, it's thought to occur due to both the swelling of neurons and astrocyte end feet (cytotoxic edema) and the disruption and leakage of the BSCB (vasogenic edema) (Figure 1-3). Cytotoxic edema is more prominent in astrocytes than in neurons owing to their sensitivity to K^+ levels for clearance (Song and Gunnarson, 2012). It is considered to happen as a response to a combination of local inflammatory mediators, ATP deprivation, and the local release of arachidonic acid produced via membrane lipid metabolism (Faden et al., 1987; Liu and Xu, 2012). Collectively, these factors influence dysfunction of ATP-dependent $Na^+ K^+$ -ATPase pumps, which drives excess Na^+ down its electrochemical gradient causing ionic imbalance (Kimelberg, 2004; Faden et al., 1987). To counter this, an excess of Cl^- ions is then driven into the cell to electrically neutralize it, which is followed by the influx of water into astrocyte endfeet, resulting in cell swelling (Rungta et al., 2015). Cytotoxic edema creates a premorbid driving force leading to ionic edema; a process whereby highly concentrated extracellular ions (e.g Na^+) are altered in their normal concentration gradients, which secondarily affects the driving force for secondary molecules (e.g Cl^-). This

dysregulation then affects the transendothelial concentration of Na^+ , where the blood concentration of Na^+ is significantly higher than that of the parenchymal concentration, creating a new Na^+ gradient, and leading to water flux into the parenchyma across the intact BBB, which is the first stage of CNS tissue swelling (Lo et al., 1987). The osmotic relationship across the blood-CNS barrier now creates a gradient, whereby water flux favouring the parenchyma occurs, and the capillaries (and potentially larger vessels) become less tightly restricted, aiding the formation of permeability pores, which results in vasogenic edema. Vasogenic edema describes the disruption of BSCB integrity, where molecules that are normally highly restricted in their passage across this barrier, can pass more freely, such as water, glucose, and some plasma proteins. Collectively, cytotoxic and vasogenic edema are both critical and associated processes. Even though cytotoxic edema itself may not necessarily produce mechanical or pressure-induced impact to the spinal cord, it may intensify the premorbid state of the tissue and the formation of vasogenic edema which ultimately leads to tissue swelling, raised intrathecal pressure, and obstruction (Kwon et al., 2009; Leonard et al., 2015; Leonard and Vink, 2015).

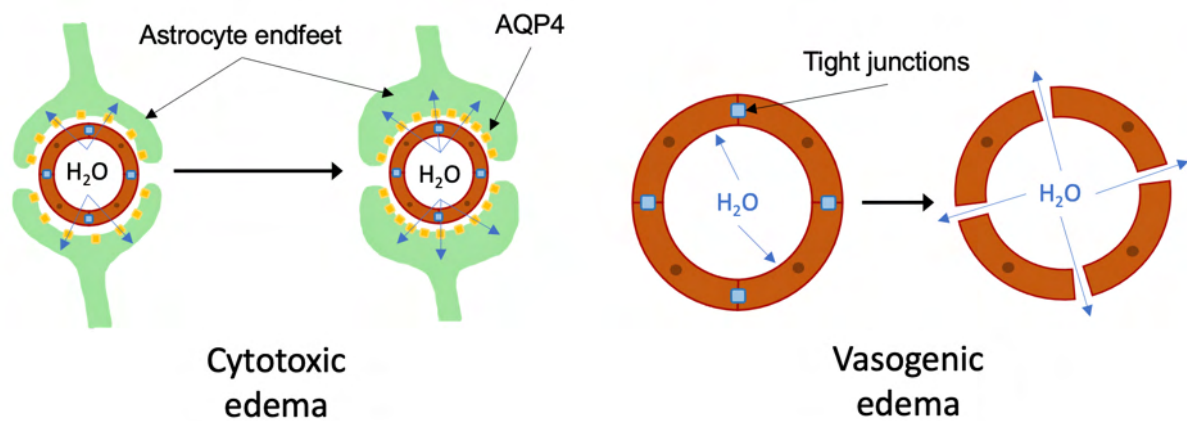


Figure 1-3. Schematic representations of the difference between cytototoxic and vasogenic edema.

Cytotoxic edema (left) involves the increased uptake of water and consequential swelling of cells, particularly astrocytes as depicted. Vasogenic edema (right) describes the increase in extracellular tissue water as a result of compromised integrity of the highly restricted blood-brain barrier at the level of the blood vessels.

1.1.4 Animal models of traumatic SCI

Animal models have proved invaluable in nearly all fields of medical research, and this is no exception with SCI. There are a number of advantages to generating good animals models over using simple clinical observation, including the ability to investigate histological features and changes in protein or gene expression. SCI models have allowed us to investigate many elements of the condition, from its pathophysiology to the efficacy and toxicology of potential therapeutics. One of the first models used to investigate SCI was reported in 1911 by Alfred Allen, in which dogs would undergo a laminectomy, followed by specified weight dropped onto the spinal cord inside a tube from a specified height, being recorded in impact as “gram-centimeters” (Allen, 1911). Since, more robust and quantitative methods of generating

animal SCI models have been developed, which more closely reflect those of various human SCIs. The species used in modelling depends on the type of model in question and the investigative intentions. These species range from rodents up to new world primates, each with their advantages and disadvantages, which will be briefly discussed. For models requiring genetic modifications, mice remain currently the most advantageous, as they can be genetically modified with much greater ease than any other rodent or higher mammal owing to the fact that mice were the first model used to develop embryonic stem cells (ES) that could be genetically modified *in vitro* (Evans and Kaufman, 1981), which didn't occur in rats until 2008 (Li et al., 2008). In fact, knockin/knockout transgenic rats were only first successfully developed within the last 10 years. Primates or other large animals most closely resemble human SCI, but are less frequently used owing to the expense and strong ethical regulations. Rats are the most commonly used species in modelling SCI, with 72.4% of all SCI studies using rats (Sharif-Alhoseini et al., 2017), as comparative studies have indicated similarities with human spinal cord injuries in terms of morphology and functional consequences, as well as the variety of different types of human SCI that can be closely replicated in rats (Metz et al., 2000; Rivlin and Tator, 1978; Guha et al., 1987a; Gruner, 1992).

There are a number of different types and subtypes of SCI that can be applied to animal models, each representing different primary or secondary variation in the condition. Below describes the three main categories of rodent SCI using in models; contusion, transection, or compression.

1.1.4.1 *Contusion models*

Contusion injuries represent 43.4% of all mechanical traumatic models utilized in the literature, according to the most recent data available (Sharif-Alhoseini et al., 2017). These models are an extension of the first recorded model of weight-drop, as previously described (Allen, 1911). Contusion SCI can be described as a transient, rapid injury to the spinal cord, and represents a vast majority of human SCIs that occur as a result of falls or motor accidents, resulting in very sudden impact to the spinal cord. Weight-drop was the first developed version of contusion injury, involving dropping a defined weight from a defined height on to the exposed spinal cord (Gruner, 1992). However, this model was then improved upon by such developments as the New York University (NYU)/Multicenter Animal Spinal Cord Injury Study (MASCIS) impactor, which records the parameters of velocity, height and time of the impact to monitor injury consistency. This was then improved upon further with the use of the infinite horizon (IH) impactor, which used controlled force instead of weight, with the motor rod connected to an external computer programmed to the desired velocity, depth, and dwell time. Interestingly, the representation of contusion model use across the literature still favours the older and less precise methods as being the most used; 37.5% of contusion injury studies have used the weight-drop model, 27.4% using the NYU/MASCIS impactor, and only 20.6% using the IH impactor (Sharif-Alhoseini et al., 2017). Whilst unsurprising given that the older models have been around for longer, it does open up the question as to whether a number of older studies using weight-drop might be better off repeated with a more controlled and replicable model.

1.1.4.2 *Transection models*

Transection models involve complete or partial severing of the spinal cord using a sharp object such as spring scissors or a scalpel (Lukovic et al., 2015; Arvanian et al., 2009). Partial severance can involve selective tracts or hemi-section depending on the functional requirements. Whilst being a fairly reproducible model, they do not represent most of the human SCI observed in clinic; as severance rarely occurs save for the occasional stab injury that impacts the spinal cord (Cheriyian et al., 2014). They are also not ideal models for studying molecular mechanisms of spinal cord injury. However, the model is very useful for examining regeneration, degeneration, and plasticity, and for generating and testing biomaterial scaffolds and/or neurotrophic factors intended to rebuild connections across the lesion area (Lavrov et al., 2006; Alilain et al., 2011; Edgerton et al., 2004; Lukovic et al., 2015). It has been an instrumental model in determining the efficacy of recently developed implantable neurotechnology to override lesion site damage and computationally bridge neural conductivity (Lavrov et al., 2006; Courtine et al., 2008; Wagner et al., 2018). It is also an interesting model for observing the effects of damage to specific spinal cord tracts on functionality, and to refine model development and functional testing (Barbeau et al., 1999; Heimbürger, 2005). It is possible that this model is the third most utilized in the literature not due to a large proportion of SCI researchers attempting to develop biomaterial scaffolds, but due to the ease and reproducibility of the model without the need for expensive equipment.

1.1.4.3 *Compression/crush models*

Compression models are similar to contusion models in that they occur as a result of a direct force to the exposed spinal cord. However in this instance, the force is

maintained for a defined period after initial impact, which more accurately represents the prolonged occlusion from displacement of the spinal column directly into the cord as a result of injury in humans. Compression SCI can be applied in a number of ways; the most popular method is to directly apply an aneurysm clip with calibrated force of compression directly to the exposed cord (Rivlin and Tator, 1978). This model allows for adjustment of force, size, and duration to alter the severity of the overall injury (Poon et al., 2007; Rong et al., 2018). Compression SCI can also be applied using calibrated forceps, where the distance and depth of the compression can be modified, but the compression impact itself comes from the hands of the experimenter (Blight, 1991). However, despite the potential for user variability, it has been demonstrated to exhibit graded severity and reproducibility of SCI (Plemel et al., 2008; McDonough et al., 2015). Balloon compression SCI represents 16.4% of all studies utilizing compression models. It involves the epidural or subdural insertion of a small catheter covered in a plastic sheet which when filled with air or saline through the catheter, inflates like a balloon next to the spinal cord (Vanický et al., 2001). Despite it being quite popular for use in rats, given that the size of the inserted 'balloon' can be modified, it is also a useful model in larger animals up to primates (Su et al., 2015; Fukuda et al., 2005; Nesathurai et al., 2006).

1.1.5 Current treatments for traumatic SCI

The approach to treating SCI is complex owing to the highly variable nature of the condition. Despite our increasing pathophysiological knowledge of SCI, including primary, secondary and tertiary damage mechanisms and consequences, current therapeutic approaches remain largely palliative. This includes pain relief, rehabilitating

symptomatic consequences such as muscle spasticity or bowel problems, and/or implementing methods of patient self-care for symptoms (Warms et al., 2002; Bracken, 2012). Whilst these are essential elements for rehabilitation, very little can be done in clinic to prevent the onset or minimize impact of secondary injury. Such therapeutics could minimise the need for existing palliative care, decrease the costs required to treat SCI patients, and could provide a higher quality of life for patients going forward.

1.1.5.1 *Rehabilitation*

Physical rehabilitation remains the only effective intervention offered to SCI patients. This aims to address and overcome the most common issues that patients will encounter after injury to minimise secondary complications (i.e loss of mobility, respiratory problems, bladder incontinence, sexual and reproductive health, and ulcer prevention), recover function, aid repair, and ultimately improve a patients quality of life and ability to live as independently as possible going forward. In the early stages of rehabilitation, the primary aims are to promote neurorecovery, intervene with any potential future complications, and maximise any lost function (Fawcett et al., 2007). Long-term aims, however, focus on elements of the injury that were unable to be minimized or addressed acutely, including functional compensation (i.e the use of assistive equipment) or physiotherapy. The specific recommendations for an individuals rehabilitation programme will be formed once the patient is medically stable. There are a number of variables that influence the clinical decision making, and ongoing literature reviews shape these recommendations based on recent evidence. For example, some of the recent recommendations from Fehlings et al., (2017) outline the most suitable type and timing of rehabilitation, including the use of functional

electrical therapy to improve hand and upper extremity function in patients with acute and subacute cervical spinal cord injury, and offering body weight support treadmill training where possible. Despite these exhaustive rehabilitation efforts, very little evidence exists that can demonstrate a direct improvement in patient outcome based on the type and timing of rehabilitation offered (Teeter et al., 2012; Whiteneck et al., 2012). Therefore, other interventions such as surgery and pharmacological treatment are also necessary for patient welfare and improvement following SCI.

1.1.5.2 *Pharmacological therapy*

There are a number of therapeutic strategies that have successfully made it into clinical trials for the treatment of SCI, which may be broadly categorized as neuroprotective and neuroregenerative. The former describes interventions targeting the pathophysiology of secondary features after injury, whereas the latter describes agents intended to enhance neurite sprouting or endogenous repair mechanisms in surviving neurons. A summary of neuroprotective or neuroregenerative drugs that have been or are currently being assessed in clinical trials are described in Table 1-1. However, to note, of all of the drugs and clinical trials listed in this table, only one has made it to clinic; methylprednisolone (MP), a corticosteroid found to aid preservation of the blood-spinal cord barrier and spinal cord blood flow by scavenging free radicals produced as a result of the primary injury. MP is thought to inhibit the inflammatory response that causes some of the secondary damage (Hall and Braughler, 1982; Braughler and Hall, 1982). MP demonstrated success in during the National Acute Spinal Cord Injury Studies (NASCIS) I, II & III demonstrating a significant improvement in neurological function up to 1-year when treated with a high dose (30mg/kg body weight +

5.4mg/kg/hr for 48 hours following) within 8 hours post-injury (Bracken et al., 1992, 1990a, 1997). However, the use of this drug, particularly for treatment of SCI, remains highly controversial, with many in the field being unconvinced of its effectiveness or benefit. Indeed, a recent meta-analysis of data from clinical trials and observational studies determined that MP treatment had no association with improvement to motor or sensory recovery, but was associated significantly with a number of dangerous side effects, including respiratory tract infection and gastrointestinal haemorrhage (Liu et al., 2019b). As such, MP is now not recommended for treatment in SCI patients, resulting in there being no recommended pharmacological agent currently in use to treat or prevent the myriad of secondary effects present after spinal cord injury. Many of the pharmacologic agents currently in clinical trials, as outlined in Table 1-1, target either the promotion of outgrowth of surviving neurons after SCI, reduction in further neuronal cell death, and limiting excitotoxicity or neuroinflammation. Only one of these drugs, Gacyclidine, has demonstrated any benefit in modifying the reactivity of astrocytes and the formation of the scar (Feldblum et al., 2000). None of the drugs currently in clinical trials for treatment of SCI have demonstrated any benefit for treating post-SCI edema, creating a significant and important niche for treatment of traumatic SCI that remains to be filled.

Category	Treatment	Pre-clinical effect	Complete clinical trial(s)	Outcomes of clinical trial(s)	Follow-up/ongoing	Sources
Neuro-protective	Methylprednisolone (MP)	Exacerbation of edema; anti-inflammatory effect; inhibits lipid peroxidation; attenuates demyelination.	NASCIS I - 1,000 mg IV bolus per day for 10 days NASCIS II - 30 mg/kg IV (<1hr) & infusion of 5.4 mg/kg/hr for 23hrs. Compared with Naloxone. NASCIS III - 30 mg/kg IV (<1hr) & infusion of 5.4 mg/kg/hr for 24 or 48hrs. Compared with tirilazad mesylate. All assessed using ASIA motor scoring	NASCIS I – No evidence of functional or neurological recovery. NASCIS II – Significant improvement up to 1yr post-injury if treated with IV bolus within 8hrs. NASCIS III – significant improvement seen up to 1yr post-injury if treated with IV bolus within 3hrs with 48hr regimen	No evidence of long-term benefit to patient recovery in clinic. Increases risk of side effects such as respiratory tract infection or gastrointestinal hemorrhage. Contraindicated for patients with diabetes or the elderly.	(Bracken et al., 1984; Green et al., 1980; Cabrera-Aldana et al., 2017a; Bracken et al., 1990b, 1992; Liu et al., 2019b; Bracken et al., 1997, 1990a; Anderson and Means, 1985; Barnes, 1998; Lee et al., 2008)
	Gacyclidine	Non-competitive NMDA receptor antagonist – limits apoptosis and inflammation, and minimizes glial scar formation by inhibiting astrocyte proliferation	Multicenter, randomized, placebo-controlled trial - 0.005 mg/kg, 0.01 mg/kg, and 0.02 mg/kg IV bolus <2hrs post-injury, and again at 4hrs post-injury	Multicenter, randomized, placebo-controlled trial – improved ASIA scores up to 1 month, but no improvement after 1 year, except in those with incomplete cervical injury treated with 0.02 mg/kg.	Not yet moved to clinic.	(Gaviria et al., 2000a, 2000b; Hirbec et al., 2001; Feldblum et al., 2000)
	Nimodipine	Calcium channel blocker – improves blood flow	Single-centre, Randomized, Placebo-Controlled Trial – Patients subject to decompression treated <8hrs post-injury with 1) Nimodipine - 0.015 mg/kg/h for 2 h followed by 0.03 mg/kg/h for 7 days; 2) Methylprednisolone - 30 mg/kg over 1 h, followed by 5.4 mg/kg/h for next 23 h; 3) Both drugs; 4) Placebo	Single-centre, Randomized, Placebo-Controlled Trial – no benefits observed after 1 year.	Not yet moved to clinic. Subsequent studies have demonstrated benefits in spasticity after experimental SCI in mice. Adjunct treatment with adrenaline improves SC blood flow and electrophysiology post-injury.	(Pointillart et al., 2000; Fehlings et al., 1989; Guha et al., 1987b; Marcantoni et al., 2020; Ross and Tator, 1991)
	GM-1 ganglioside	Induction of neurotrophin synthesis; modulation of neurotrophin signalling; activation of Trk receptors; promotion of neuronal cell survival; promotion of neurite outgrowth	Single-centre, Randomized, Placebo-Controlled Trial – 100 mg GM1 per day for up to 32 days, starting >72rs after injury. Multicenter, double-blind, randomized, placebo-controlled trial - patients with major SC, motor deficiency in one lower limb and ASIA score ≤15. All treated with 30 mg/kg IV MP followed by either A) initial IV bolus 600 mg followed by 200 mg/day or; B) initial 300 mg followed by 100 mg/day GM-1.	Single-centre, Randomized, Placebo-Controlled Trial – significant improvement in ASIA motor score and Frankel grades after 1 year. Multicenter, double-blind, randomized, placebo-controlled trial –Significant improvement in difference between ASIA and Benzel scores at 8- and 16-weeks, but no difference at 26 weeks after treatment onset.	Not yet moved to clinic	(Geisler et al., 1991; Skaper and Leon, 1992; Ferrari and Greene, 1996; Rabin et al., 2002; Geisler et al., 2001b, 2001a; Bose et al., 1986)
	Thyrotropin Releasing Hormone (TRH)	Tripeptide – anti-oxidation, membrane stabilization, enhanced blood flow,	Single-centre, Randomized, Double-Blind, Placebo-Controlled Trial – 0.2mg/kg IV bolus or placebo within 12hrs, followed by 0.2mg/kg/hr infusion	Single-centre, Randomized, Double-Blind, Placebo-Controlled Trial – Some benefit demonstrated at 4 months in both	Not yet moved to clinic	(Faden et al., 1984; Faden et al., 1989; Feuerstein et al., 1983;

		antagonization of excitotoxic agents	over 6hrs. Neurological scores measured using Sunnybrook scale and NASCIS motor and sensory scales.	scores for incomplete SCI patients, but not complete SCI patients. Small sample size resulted in non-definitive outcome.		Mcintosh et al., 1993; Pitts et al., 1995)
Fampridine	Rapidly inactivating, voltage-dependent, potassium channel blocker	Multi-centre, double-blind, randomized, placebo-controlled, phase II, parallel-group trial – patients with neurologic impairment secondary to SCI within 18 months of injury and 6 months of stable neurological status treated oral b.i.d in dose titration (0mg – 25mg) for 2 weeks, followed by 20 or 40 mg for 4 weeks, and then 2 weeks downward titration.	Multi-centre, double-blind, randomized, placebo-controlled, phase II, parallel-group trial – low dose treated groups displayed significant improvement in both spasticity and subject global impressions after 5-8 weeks.	Not yet moved to clinic. Significant side effects associated with high dose including hypertonia, generalized spasm, insomnia, dizziness, asthenia, pain, and constipation.		
Magnesium with Polyethylene Glycol (PEG)	NMDA antagonism – limits excitotoxicity and neuroinflammation, resulting in sparing of healthy tissue	Phase I/II, randomized, placebo-controlled trial – 30 minute intravenous infusion of AC105 or saline placebo at 6, 9, or 12 hours post-injury followed by 5 additional 30 minute infusions every 6 hours.	Trial discontinued due to low patient enrolment.	N/A		(Streijger et al., 2016; Wiseman et al., 2009; Kaptanoglu et al., 2003)
Minocycline	Reduced oligodendrocyte and neuron death	Single-centre, double-blind, randomized, placebo-controlled trial – treatment with 400 mg/day between 7hrs and 14 days post-injury. Assessed with ASIA motor scoring.	Single-centre, double-blind, randomized, placebo-controlled trial – improvement demonstrated for cervical, but not lumbar injury at 1year	Not yet moved to clinic. Phase III clinical trial still in enrolment.		(Casha et al., 2012; Stirling et al., 2004; Teng et al., 2004; Yune et al., 2007; Festoff et al., 2006; Lee et al., 2003)
Granulocyte macrophage colony-stimulating factor (GM-CSF)	A cytokine glycoprotein - Mobilization and migration of bone marrow cells to injury sites	<ol style="list-style-type: none"> Multicenter, open-label, prospective controlled trial - 10 µg/kg/day IV bolus of GM-CSF for 5 consecutive days. Assessed using Japanese Orthopaedic Association (JOA) score. Single-centre, non-randomized, comparative study – patients with chronic incomplete or complete SCI within 6 months of injury and 3 months of stabilization were treated subcutaneously with 5 µg/kg/day G-CSF for 7 consecutive days. Assessed with ASIA motor scoring. Multicenter Prospective Nonrandomized Controlled Trial - 10 µg/kg/day IV bolus of GM-CSF for 5 consecutive days in acute TSCI patients. Assessed with ASIA motor scoring. 	<ol style="list-style-type: none"> Multicenter, open-label, prospective controlled trial – one-month follow-up showed improved neurological function from treatment compared to control. Single-centre, non-randomized, comparative study – significant motor improvement in non-complete chronic SCI, but not complete. Multicenter Prospective Nonrandomized Controlled Trial – slight neurological recovery, but in a small number of treated patients. Multi-centre, double-blind parallel randomized, placebo-controlled trial – increased 	Not yet moved to clinic. A multicenter phase III randomized-control, double-blind, parallel group comparative study (IIA00217) due to finish April 2019 in acute, cervical, incomplete SCI patients treated with 5 days of IV G-CSF.		(Park et al., 2005; Yoon et al., 2007; Derakhshanrad et al., 2018; Sakuma et al., 2012b, 2012a; Inada et al., 2014; Saberi et al., 2014)

			<p>4. Multi-centre, double-blind parallel randomized, placebo-controlled trial – patients with incomplete upper motor neuron type injury received 300 mg/day of G-CSF for 7 days starting within 6 months of injury.</p> <p>5. Single-centre, phase I/II, non-randomized trial – 5 or 10 µg/kg/day IV bolus of GM-CSF for 5 consecutive days. Assessed using Japanese Orthopaedic Association (JOA) score.</p> <p>6. Single-centre, phase I/II, open-label and nonrandomized trial – bone marrow stem cells directly injected around lesion site within 14 days of injury, and then injected subcutaneously with GM-CSF for first 5 days for each subsequent month for up to 2 weeks (subacute), 8 weeks (acute) or >8 weeks (chronic) Assessed with ASIA motor scoring.</p>	<p>mean ASIA scores and functional improvement as measured by SCIM-III instrument.</p> <p>5. Single-centre, phase I/II, non-randomized trial – suppressed progression of myelopathy but highly variable between patients.</p> <p>6. Single-centre, phase I/II, open-label and nonrandomized study – subacute and acute treated patients demonstrated neurological benefit at around 10 months post-operation.</p>		
	Glyburide	Sulfonylurea receptor 1 (SUR1)-regulated, TRPM4-channel, calcium-activated nonspecific cation channel blocker	Multicentre open-label pilot study – patients with acute cervical traumatic SCI with ASIA grade A, B or C on admission treated with initial oral dose of 3.125mg within 8hrs followed by 0.625mg every 6hrs for 3 days.	No functional outcomes measured, but feasibility of 8hr oral treatment determined for Phase II trial.	Spinal Cord Injury Neuroprotection with Glyburide (SCING) phase I/II clinical trial still underway using ASIA scoring of treated patients recruited with grade A/B/C C2–8 injuries to observe adverse events.	(Minnema et al., 2019; Popovich et al., 2012; Simard et al., 2012)
	Recombinant human hepatocyte growth factor (KP-100IT)		A Phase I/II Double-Blind, Randomized Clinical Trial of Safety and Efficacy. Cohorts of patients with modified Frankel grade A/B1/B2 at 72 h after SCI. KP-100 was administered intrathecally. Subjects were followed up for 168 days using American Spinal Injury Association (ASIA) scores.	KP-100 contributed to motor improvement at Days 140 and 168, most significantly in patients with Frankel grade A. No harmful adverse affects observed during this period.	Non-randomized, multicenter, confirmatory study currently recruiting in patients who have suffered a cervical spinal cord injury within the past 78 hours whose AIS classification was A at 66 - 78 hours after injury (CT number: NCT04475224)	(Kitamura et al., 2011, 2007, 2015; Nagoshi et al., 2020)
	Imatinib	Tyrosine kinase inhibitor	N/A	N/A	A phase II, single center, open-label, non randomized clinical study to assess the uptake, safety and tolerability of	(Kjell et al., 2015; Liu et al., 2019a)

					Imatinib in acute Cervical Spinal Cord Injury patients when administered via a gastric feeding tube (NCT02363361). Not yet recruiting.	
Neuro-regenerative	Anti-Nogo Antibodies	Neutralization of neurite outgrowth inhibitory NOGO-A from oligodendrocytes and myelin.	Phase I, open-label, multicenter cohort study. Four cohorts received dose-escalating ATI355 5 to 30mg in 2.5 mL/day continuous intrathecal infusion over 24 hours to 28 days. A further 2 cohorts received a bolus regimen of 6 intrathecal injections containing either 22.5 or 45 mg in 3 mL over 4 weeks)	Well tolerated up to 1 year post-trial. No adverse effects related to ATI355. Follow-up serum levels demonstrated dose-dependency.	Two further trials currently ongoing: NISCI trial: a phase 2, placebo controlled, randomized, double blind, multicenter, multinational study. Testing 6 intrathecal bolus injections, each of 45mg in acute SCI patients (NCT03935321). RESET trial: Part 1; a phase-1 multicenter, open-label, single ascending dose study investigating safety efficacy and tolerability of AXER-204. Part 2; a multicenter, randomized, double-blind, placebo-controlled, repeat dose study (NCT03989440).	(Chen et al., 2000; GrandPré et al., 2002; Guo et al., 2012; Kucher et al., 2018)
	Acidic Fibroblast Growth Factor (aFGF)	A heparin-binding protein that enhances regeneration	1. Phase I, open-label, prospective, uncontrolled human clinical trial. aFGF with fibrin glue applied post-duraplasty via laminectomy, followed by adjuvant booster at 3 and 6 months via lumbar puncture. 2. ASCENT (Asubio Spinal Cord Early Neurorecovery Treatment), a phase 2, multicenter, randomized, double-blind, Placebo-controlled, parallel group study. An IV bolus of SUN13837 was administered within 12hrs of injury, with a further 7 to 28 total doses over 27/28 days, followed by 22 week follow-up.	1. Significantly improved ASIA motor scores and in pinprick or light touch sensory scores at 24 months post-op. No adverse effects observed. 2. ASIA motor scores, total SCIM III, combined SCIM III Self-Care and Mobility scores showed nonsignificant improvements. No adverse effects observed.	A Multicenter, Randomized, Double-blind, Placebo-controlled Phase 3 Study to Evaluate the Safety and Efficacy currently recruiting (CT number: NCT03229031).	(Wu et al., 2011, 2008; Levinson, 2018; Rabchevsky et al., 2000)
	Cethrin®	Rho Antagonist – prevents Rho-mediated neurite retraction and growth cone collapse, Decreased apoptosis.	Multicenter, Phase I/II, Double-Blind, Randomized, Placebo-Controlled Trial – treated extradurally with 0.3, 1, 3, 6, or 9mg Cethrin in thrombin and fibrin sealant solution within 7 days of	Multicenter, Phase I/II, Double-Blind, Randomized, Placebo-Controlled Trial – improved ASIA motor scores at 12 months in both cervical and thoracic SCI patients, but biggest improvement	Phase II/III clinical trials planned but no announcements for enrolment yet.	(Dergham et al., 2002; Dubreuil et al., 2003; Sung et al., 2003; Laufs et al., 2000;

			injury. Assessed with ASIA motor scoring.	in cervical SCI patients treated with 3mg Cethrin		Fehlings et al., 2011)
	AXER-204	A decoy/trap protein for the myelin-associated inhibitors of axonal growth known as Nogo-A, MAG, and OMgp	N/A	N/A	Currently recruiting for a two-part trial to assess the safety, tolerability, pharmacokinetics, and efficacy. Part 1 is a multicenter, open-label, single ascending dose study in participants with chronic cervical spinal cord injury. Part 2 is a multicenter, randomized, double-blind, placebo-controlled, repeat dose study (CT number: NCT03989440)	(Wang et al., 2014, 2020)

Table 1-1 A summary of all clinical trials carried out in neuroprotective or neuroregenerative agents studied in the context of traumatic spinal cord injury. Information included in this table was sourced from pubmed and clinicaltrials.gov by searching for drug clinical trials related to traumatic spinal cord injury. Up to date as of 06/05/2021.

1.2 Aquaporins (AQPs) in the CNS

1.2.1 Human AQPs

Water can move rapidly into and out of most cells of the human body. This passive, bidirectional transport of water may occur directly across biological membranes, however the phospholipid bilayer can restrict the rate of water flow, depending on the properties of the cell (Solenov, 2004). As such, the rate of water transport can be increased through co-transport with other solutes and/or ions, such as salt (Loo et al., 1996), or through water channel proteins. This type of transport is important for maintenance of physiological homeostasis. A majority of rapid water transport occurs through AQPs (Day et al., 2014). AQPs are a family of transmembrane (TM) transporter proteins that facilitate the transcellular flow of water through biological membranes in response to changes in osmotic and/or hydrostatic pressure (Verkman and Mitra, 2000; De Groot et al., 2009). 13 functional human AQP isoforms have been discovered to date, with ubiquitous, yet differential expression across tissues of the human body (Harries et al., 2004; Horsefield et al., 2008; Magni et al., 2006). The initial discovery that AQPs were functional water channels came from transiently transfecting AQP1 into *Xenopus* oocyte cells, exposed to distilled water. By comparison to the control, non-transfected oocytes, there was significant swelling in the transfected oocytes. This was the result of increased AQP1 present within the cell membrane, allowing an influx of water to occur when the extracellular solution was hypotonic to the intracellular (Agre et al., 1993; Preston et al., 1992). The discovery of AQPs and the development of such models has allowed us to further our understanding in how cells and tissues regulate water flow under physiological and pathological conditions.

1.2.2 Structure of mammalian AQPs

AQPs appear to exist functionally in a common homotetrameric structure (de Groot, 2001), with recent evidence suggesting that each of the monomers behave as a functional water transport unit (Horner, 2015) (Figure 1-4). Like most TM transporters, AQPs have evolved to become highly specific for their transport molecules. AQP monomer structures exist in an “hour-glass” 3D conformation, consisting of a hollow, but constricted “pore” formed of six transmembrane α -helices (Murata et al., 2000; Fu et al., 2000). The most constricted region of this pore is approximately 2.8Å in size, allowing the continuous passage of one water molecule at a time, known as single file permeation (Agre et al., 2002; Cui and Bastien, 2011). The electrostatic factors controlling single file permeation are conferred by the hydrophilic residues lining each pore. This includes a tightly constricted region containing an aromatic/arginine motif and two α -helices, which repel the passage of protons and defines specificity of water molecules, and two Asn-Pro-Ala (NPA) motifs within the highly conserved B and E loops that form hydrogen bonds with water molecules to facilitate transport into the intracellular compartment of the AQP (Figure 1-4a). (Preston et al., 1993; Eriksson et al., 2013; Beitz et al., 2006). These features are what allow AQP monomers to facilitate such effective capacity and selectivity for water transport, allowing up to 3×10^9 molecules of water per second across in some water-selective AQPs, e.g AQP1, 2, 4 and 5 (Zeidel et al., 1992; Verkman and Mitra, 2000). Additionally, some AQPs termed ‘aquaglyceroporins’, also have selectivity for small polar molecules such as glycerol and urea (Wang et al., 2005). These AQPs (AQP3, 7, 9 and 10) have an altered architecture and polarity within the constricted region that accommodate for transport of larger molecules (Savage et al., 2003; Wang et al., 2005). As such, the pore is

slightly larger at approximately 3.8\AA and is lined with more hydrophobic residues to accommodate for interactions with the multiple types of different but specific molecules (Thomas et al., 2002; Fu et al., 2000).

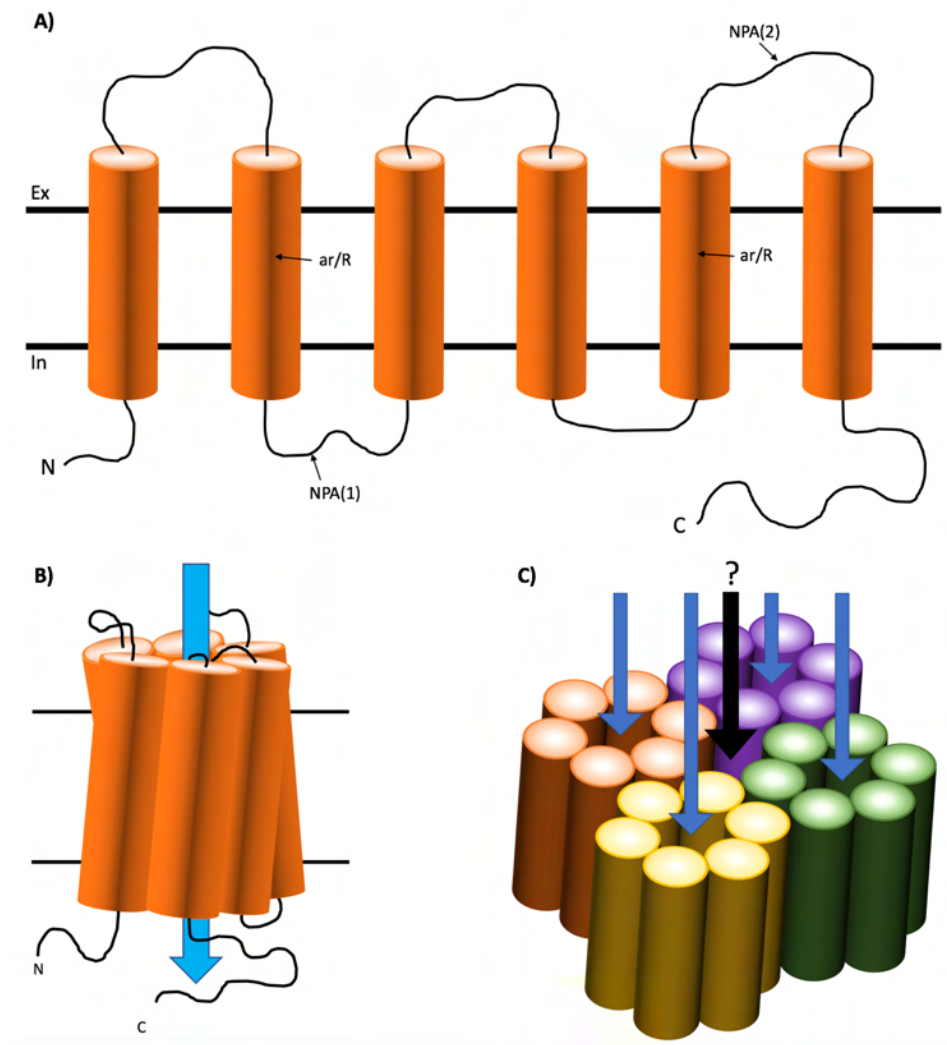


Figure 1-4. The secondary, tertiary, and quaternary structures of aquaporin proteins.

(A) The secondary structure of aquaporins contains six α -helices connected by three extracellular and two intracellular loops. Loops B and E contain NPA motifs and the fifth α -helices contain ar/R motifs, which is described in the text. (B) All six α -helices exist in a closely associated tertiary monomer structure with both ar/R motifs interacting at opposite sides of the pore and both NPA motifs interacting within the membrane. The route of water passage exists

in the transmembrane pore formed through the center of the three-dimensional barrel. (C) AQP monomers homotetramerize and create a five-pore quaternary structure. However, the function of the central pore, formed by the space between all four monomers, remains largely unknown. Published in Halsey et al., (2018).

1.2.3 Localization and functions of human AQPs

There are 13 functional isoforms of AQPs currently known within the human body, each with specific and localized expression patterns and functions. Different tissues in the body require transport of water as well as other substances such as glycerol, as described in section 1.2.2. The localization of the various isoforms of AQP reflects this, as demonstrated in Figure 1-5. For example, different cell types in the kidney collectively express nearly all known human AQPs (AQPs 1-4 and 6-11), whereas the spleen only appears to express AQP9 (Ishibashi et al., 1998). AQPs serve different physiological functions within the body, depending on their localization and isoform. Arguably the most important function of AQPs is to facilitate the maintenance of water homeostasis within tissues (Benfenati and Ferroni, 2010). This is achieved mostly through cell volume regulation (CVR) mechanisms, and ensures that the osmolarity within the cell is within a physiological range (Yeung et al., 2009; Mola et al., 2016). Other, more specific functions of aquaporins include, but are not limited to, water transport across kidney tubule epithelium through AQP2 (Deen et al., 1994), production of sweat and saliva through AQP5 (Nejsum et al., 2002), and blood-brain/blood-spinal cord water transport through AQPs 1 and 4 (Solenov, 2004; Oshio, 2004). Many of the physiological roles of AQPs have been determined using knockout models. AQP1 knockout mice display significant disturbance of function across many

tissue types, but most notably in their ability to concentrate urine in the kidney proximal tubule epithelium, but also in terms of cardiovascular homeostasis, peritoneal water flux, accumulation of excess amniotic fluid in pregnancy, angiogenesis, cell migration, lung physiology, epithelial fluid secretion, and gastrointestinal and hepatobiliary function (Hua et al., 2019; Saadoun et al., 2005; Luo et al., 2018; Ma et al., 1998; Bai et al., 1999; Wintmo et al., 2017). By contrast, AQP4 knockout models appear to exhibit very little deficit by way of urinary concentration (Ma et al., 1997). Instead, AQP4 knockout models appear to mostly cause disruption in the CNS by way of edema, astrocyte migration, and support of neural function, as will be discussed in section 1.3.2.

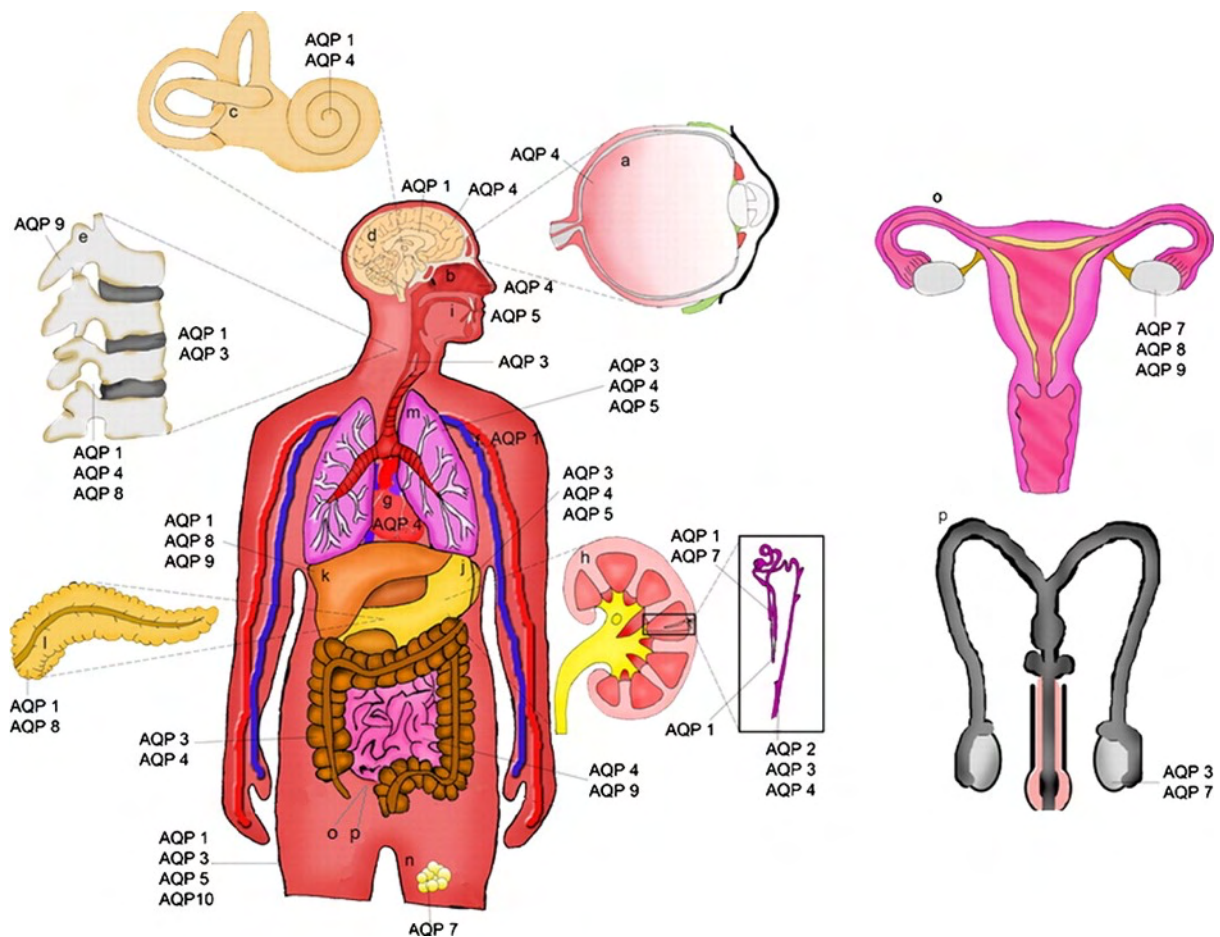


Figure 1-5 A schematic demonstrating the tissue specific expression of the various AQP isoforms (1-10).

AQP1 – inner ear, brain, spinal cord, liver, pancreas, skin, kidney, and some vasculature; AQP2 - kidney nephron; AQP3 - vertebrae, gastrointestinal tract, lungs, skin, and male reproductive organs; AQP4 – inner ear, retina, brain, spinal cord, olfactory epithelium, stomach, heart, lungs, gastrointestinal tract, and kidney; AQP5 – salivary glands, gastrointestinal tract, lungs, and skin; AQP7 – kidney, adipocytes, and male and female reproductive organs; AQP8 – liver, pancreas, and female reproductive organs; AQP9 – osteoclasts, gastrointestinal tract, liver, and female reproductive organs; AQP10 – skin. Adapted from (Day et al., 2014).

1.2.4 AQPs in the brain and spinal cord

The CNS is comprised of a vast number of highly specialised cells, which can be broadly categorised into neuronal cells and glial cells. These all work in tight coordination to ensure that its responsibilities are efficiently fulfilled (Morest and Silver, 2003; Wiedemann, 2010). The functionality of the CNS is very tightly coupled to the ionic and osmotic environments within and surrounding the tissues. The basic principles of neuronal conductivity rely on a balance of intra- and extra-cellular concentrations of Na⁺, K⁺, and Ca²⁺ ions, which affect intra- and extra-cellular osmolarity, and vice versa. Changes in osmolarity determines the flow of water into cells and extracellular space from the blood. Furthermore, the brain exists within a finite space, determined by the size of the skull; water content within the brain directly affects intracranial pressure, which is asserted on the tissue (Ropper, 2012). Water levels must be effectively regulated to ensure that the brain volume doesn't become too high, which results in increased intracranial pressure (ICP), and could lead to conditions

such as intracranial hypertension (IH) (Uldall et al., 2017). The fluid-tissue interfaces that exist in the CNS are extremely restricted, including for water molecules. As such, to maintain the optimal osmotic environments, the CNS must ensure that efficient homeostasis is regulated to maintain functionality, which it achieves through the presence of AQPs. A number of AQPs are expressed functionally in various tissues through the CNS, including AQP1, 4, and 9 (Praetorius and Nielsen, 2006; Oshio et al., 2004). The roles of these AQPs in the CNS are similar to their function in any other tissue; they regulate water transport between intracellular and extracellular compartments for the purposes of volume regulation, local environment maintenance. However, their expression levels and functions within different regions of the CNS vary, and as the blood-CNS barriers are so tightly restricted, AQPs remain the only source of mass water transport into and out of the CNS.

1.2.4.1 *AQP1*

AQP1 expression has been reported in locations throughout the entire CNS, in multiple cell types including ependymal cells, astrocytes, and to a lesser degree, vascular endothelial cells (Praetorius and Nielsen, 2006). The most abundant expression of AQP1 is at the apical membrane of choroid plexus epithelium (CPE) ependymal cells in the brain – the tissue residing in the lateral, third, and fourth brain ventricles, responsible for production of cerebrospinal fluid (CSF) (Nielsen et al., 1993; Bering, 1955). It is the role of AQP1 to facilitate rapid and regulated water transport between the CPE and the ventricles in order to produce CSF. CSF production through AQP1 is thought to be very important for maintaining physiological intracranial pressure (ICP), as AQP1 knockout mice exhibit 56% lower ICP than controls (Oshio, 2004). There is

an observed 80% reduction in the water permeability of the luminal CPE membrane, but only a 25% reduction in CSF production (Oshio, 2004). This suggests two things; firstly, despite the passive nature of AQPs, their expression levels should not be interpreted directly as a representation of absolute water flow. This is because AQP1 within the CPE, as with most AQPs, does not actively control water flow, as this remains under the control of the local osmotic pressures they're exposed to. Secondly, there may be other non-AQP1-dependent mechanisms facilitating CSF production in the CFE, potentially via paracellular transport or through other aquaporins, such as AQP4.

In addition to ependymal cells, AQP1 also appears to be lowly expressed within some neuronal and glial cells in the brain. Immunolocalization studies evaluating the expression changes of AQPs following CNS insult have revealed that even in sham controls, a small level of AQP1 expression may be observed within the rat parietal cortex (Fukuda, 2012). Whilst the physiological role of AQP1 in these neurons remains unknown, evidence suggests that their upregulation in TBI models is involved in pain processing (Fukuda, 2012). Furthermore, whilst AQP1 is not detected in astrocytes in the healthy brain, it appears to upregulate following a subarachnoid haemorrhage and within astrocytomas in humans (Badaut et al., 2003; Saadoun et al., 2002), and following brain stab injury in rats (Mccoy and Sontheimer, 2010), which mechanistically has been shown in cell culture to occur in response to hypertonicity via a hypertonicity-response element in the AQP1 gene (Misawa et al., 2008; Umenishi and Schrier, 2002).

1.2.4.2 AQP4

AQP4 is expressed in high levels across the brain, spinal cord and retina, as well as in some peripheral nervous tissue, with highest expression levels detected in the cerebellum and spinal cord grey matter (Oshio et al., 2004; Hubbard et al., 2015; Oklinski et al., 2014). Furthermore, its expression has been localized in multiple cell types, including astrocytes, endothelial cells and some smaller populations of neurons (Nielsen et al., 1997; Oshio et al., 2004). Broadly, the functions of AQP4 in the CNS include the aiding of astrocyte signalling, regulation of local ion homeostasis, maintaining the integrity of the blood-brain barrier (BBB), modulating neuroexcitation at neuronal synapses, and cell volume regulation (CVR) (Hoffmann et al., 2009; Thrane et al., 2011).

1.2.4.2.1 Astrocytes

The most prominent expression of AQP4 in the CNS is within the membranes of polarized astrocyte perivascular endfeet surrounding blood-CNS and CSF-CNS interfaces in the brain and spinal cord (Mathiisen et al., 2010; Nielsen et al., 1997). Accordingly, AQP4 expression strongly co-localized with glial markers such as glial glutamate transporter-1 (GLT-1) and glial fibrillary acidic protein (GFAP) (Vitellaro-Zuccarello et al., 2005). It remains unknown whether AQP4 is the key to the polarization of astrocyte end feet, as predicted by its localized function, or whether it becomes tied to these regions by the polarized expression of other proteins such as agrin and α -syntrophin (Noell et al., 2007; Neely et al., 2001; Wolburg et al., 2009). AQP4-expressing astrocyte endfeet can be found throughout many locations of the CNS, with highest abundance surrounding blood vessels within the superficial laminae

of grey matter in the spinal cord, and the pial surface membranes of the brain. Expression can also be found to a lesser degree in astrocyte end feet surrounding the glial-limiting membrane, myelinated neuronal fibres, and the central canal in the spinal cord (Oshio et al., 2004; Oklinski et al., 2014). The identification of AQP4 at these locations eluded to the protein identity of the crystal-like intramembranous 'assemblies' that were previously observed in the brain, and termed orthogonal arrays of particles (OAPs). AQP4 was subsequently confirmed as the OAP protein constituent owing to their disappearance in *Aqp4*^{-/-} knockout mice (Verbavatz et al., 1997). These AQP4 assemblies are built from M1 and M23 isoforms of the protein monomer, and the relative abundance of these isoforms directly affects the polarization of AQPs to endfeet (Smith et al., 2014). Higher M23:M1 ratios favour larger OAP formations, which increases the water permeability of the endfeet (Furman et al., 2003). Collectively, the tissue and subcellular localization of AQP4 in the CNS eludes to the primary functions of AQPs in the CNS. For example, the strong expression of AQP4 around brain and spinal cord astrocyte-fluid interfaces strongly suggests that AQP4 has an important role in regulating water flow into, and out of, the CNS. Many of the physiological functions of AQP4 have been revealed using genetically modified mice models exposed to varied pathological conditions. One of the earliest examples of this was in *Aqp4*^{-/-} mice models, which were demonstrated to exhibit vastly reduced levels of post-ischemic edema following an induced ischemic stroke (Manley et al., 2000). Furthermore, AQP4 deletion within glial cells in mice results in a decreased uptake of water into the brain by 31% following hypo-osmotic stress. However, the overall brain dry mass doesn't change, suggesting that the role of AQP4 at the blood-brain (and potentially blood-spinal cord) barriers exists pathophysiologically, mediating water

absorption in hypo-osmotic conditions (Haj-Yasein et al., 2011). More specifically, AQP4 has been demonstrated to regulate cell volume homeostasis, by maintaining extracellular solute clearance. Primary astrocytes demonstrate a response to hypo-osmotic stress by rapidly increasing cell volume, a response which was absent from identical astrocytes with AQP4 knocked down (*Aqp4^{-/-}*) (Benfenati et al., 2011). Additionally, AQP4 is also expressed at other astrocytic processes located perisynaptically, but to a significantly lower density (Nielsen et al., 1997). It's documented that high-frequency activation of excitatory synapses results in a reduction in the extracellular space surrounding the synapse (Dietzel et al., 1980), however in *AQP4^{-/-}* mice, this reduction in volume is increased (Haj-Yasein et al., 2012). Therefore, AQP4 is thought to regulate perisynaptic volume by increasing water efflux in response to hyperosmolarity resulting from high-frequency activity and the resulting water absorption through astrocytic $\text{Na}^+/\text{K}^+/\text{2Cl}^-$ cotransporter 1 (NKCC1) into astrocytes. Most of the studies investigating roles of AQPs tend to focus on either the brain or spinal cord. As such, at this stage the translation of physiological function isn't conclusive. However, owing to the highly similar cellular and sub-cellular distribution, it's expected that the same or similar functional mechanisms of AQP4 occur throughout the whole CNS.

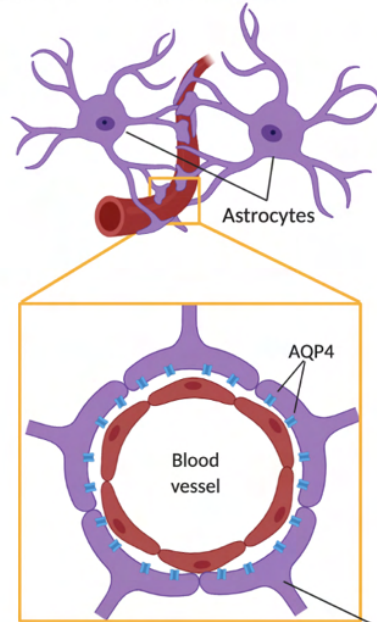
AQP4 expression also exists in a non-polarized distribution within fibrous astrocytes of the spinal cord white matter and optic nerve, and within Muller cells within the retina (Okłinski et al., 2014; Li et al., 2002). In the spinal cord, white matter astrocytes express AQP4 across the whole of the membrane, including along processes and at the cell body. These processes extend radially across the white matter regions – from borders

of grey matter to the outer glial limitans (Smith and Verkman, 2015). More specifically, these processes have been found to envelope myelinated neuronal fibres (Okłinski et al., 2014), however the physiological relevance of this expression remains unknown.

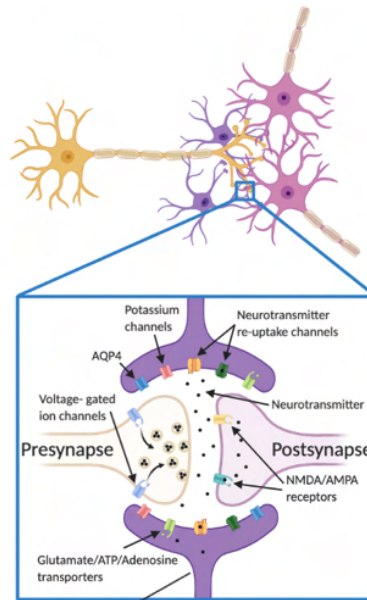
1.2.4.2.2 *Ependymal cells*

AQP4 expression can also be observed within the basolateral membrane of the ependymal cells surrounding brain-CSF barriers (Rash, 1998). This suggests that AQP4 has a physiological function in maintaining water transport between CSF and CNS parenchyma. Some studies suggest that ependymal AQP4 is involved in transependymal CSF flow and/or reabsorption, which when disrupted as in *aqp4*^{-/-} mice, results in sporadic hydrocephalus (Feng et al., 2009). However, more research is required to clarify the role. Ependymal AQP4 expression has been notably observed in the medial habenula of the brain, a region involved in many cognitive processes such as mood and anxiety regulation (Hubbard et al., 2015; McLaughlin et al., 2017).

A) Blood-brain barrier

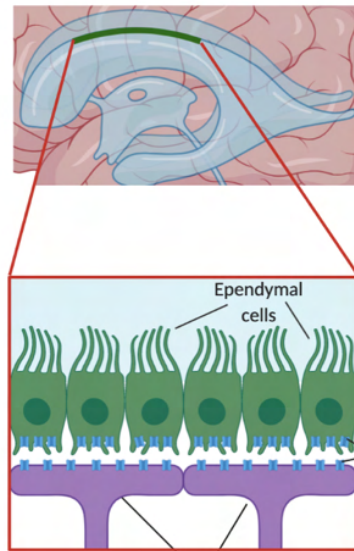


B) Tripartite synapse



Astrocyte endfoot

C) Ventricle lining



Astrocyte endfoot

D) Meninges

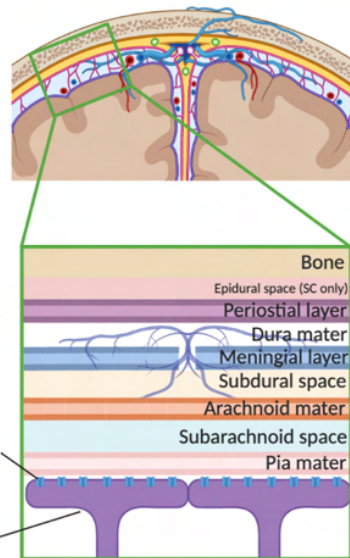


Figure 1-6 A schematic representing the anatomic and subcellular localization of AQP4 in the human brain and spinal cord.

Expression within astrocyte endfeet at the level of the pial surface and surrounding blood vessels is conserved between brain and spinal cord, however, expression in ependymal cells is only found within the brain within the choroid plexus.

1.3 The role of AQP4 in SCI

1.3.1 Changes in AQP4 expression after SCI

Following a traumatic spinal cord injury, AQP4 appears to increase in expression, on both a transcriptional and translational level. To date, only one study has attempted to investigate the changes in AQP4 expression after human traumatic SCI post-mortem. This study demonstrated increased amounts of AQP4 detected using immunohistochemistry within the white matter of chronically damaged cords (Nesic et al., 2010). Other studies in rodent models demonstrate that AQP4 protein levels are subject to change both on a cell-specific and tissue-wide scale, with the direction of expression change over time dependent on the type and severity of injury model used. One study shows that following contusion SCI, AQP4 appears to change in a bi-phasic manner, starting with an immediate decrease in protein expression between onset and 3 days post-injury, followed by a significant increase seen as much as 9 months post-injury (Nesic et al., 2006). The same group followed this study up by demonstrating that tissue analysed within the period of lower AQP4 expression exhibited distinct AQP4-negative and AQP4-positive astrocytes, and the regions of AQP4 positive staining were significantly higher than in control, uninjured tissue (Nesic et al., 2010). They also report that increased severity of injury and higher levels of functional impairment both produced longer periods of AQP4 downregulation. Other studies, however, report that the amount of AQP4 protein and mRNA increases as soon as 6 hrs post-injury, and can persist for as long as 168 days in rodents (Huang et al., 2019; Yan et al., 2018; Cabrera-Aldana et al., 2017a). The underlying causes of increased AQP4 expression are not yet well studied in the context of SCI, but given the extensive overlap in pathophysiology between SCI and TBI, particularly in the context of edema,

inferences can be made. Oxidative stress, which occurs within minutes after injury due to cessation of blood supply, results in the activation of many signalling pathways and transcription factors that increase the expression of AQP4. The p38/MAPK pathway appears to become activated in astrocytes following spinal cord injury, and increases in MAPK signalling in astrocyte cultures result in increased AQP4 mRNA production (Gao et al., 2009; Pan et al., 2010)

1.3.2 Mechanisms of AQP4 involvement in SCI

1.3.2.1 *Edema*

Edema is a clinically important feature in the progression of SCI, causing secondary damage through physical contortion and/or obstruction of surrounding nerve fibres and vasculature that were otherwise uninjured from the primary damage (Bozzo et al., 2011). Shortly following injury to the spinal cord, there is a significant increase in the amount of water accumulating in the parenchyma of the damaged region (Miyajima et al., 2007). Edema forms within the acute phase of secondary injury pathogenesis, and may persist for weeks. It is a vital element of SCI, as some studies report that the severity of the edema (generally the size and location of the swelling) is strongly correlated to the clinical outcome, particularly in terms of motor recovery (Flanders et al., 1999; Miyajima et al., 2007; Leonard et al., 2015). It's thought that edema causes exacerbation of the primary injury by raising intrathecal pressure within the spinal cord, causing further damage by reducing blood flow, leading to haemorrhage, BSCB disruption and subsequently further cell death (Leonard and Vink, 2015). However, as edema is often a quick-onset and long-lasting feature of SCI, it remains somewhat resistant to interventions, making it a great challenge to overcome or prevent. As such,

understanding the causes and molecular mechanisms involved in the formation or clearance of edema following SCI is important for developing ways of inhibiting it in order to improve or abolish the clinical outcomes resulting from secondary damage.

The mechanisms of edema formation in SCI are associated with dysregulation of water transport, leading to the swelling of astrocyte endfeet and the formation of fluid-filled cavities. This indicates that water homeostasis and the proteins involved in water transport may contribute to the resulting pathologies, and as such may offer themselves as therapeutic targets to prevent the secondary damage elicited from edema. The exact role of aquaporins in edema pathogenesis remains controversial owing to studies producing opposing results.

Some evidence indicates that AQPs are responsible for the formation of edema in the CNS following injury. Earlier support for this argument was found in ischemic stroke models resulting in cytotoxic edema, where swelling occurs within cells but spares the integrity of the BBB. *AQP4*^{-/-} mice exhibited 35% less cerebral edema compared to wild-type in stroke models, and significantly reduced astrocyte endfeet swelling (Manley et al., 2000). Further studies investigating SCI have also obtained similar conclusions, whereby inflammatory mediator IL-6 induces a High mobility group box protein 1 (HMGB1)-mediated signalling cascade resulting in the increased expression of AQP4 in astrocyte endfeet and subsequent increase in cytotoxic swelling (Sun et al., 2017). In *AQP4*^{-/-} mice, there is also reported functional and pathological improvement following contusion SCI where mice exhibited significantly higher motor scores and decreased edema than their WT counterparts up to 14 days post-injury

(Saadoun et al., 2008). AQP4 was also demonstrated to be a rate-limiting factor in the formation of CNS edema as in one study, glial cell-specific overexpression of AQP4 increased the rate of cytotoxic swelling and intracranial pressure (Yang et al., 2008a). More recently, a study showed that a novel compound, TGN-020, a suggested AQP4 inhibitor, may prevent the elevation of spinal cord water content and AQP4 expression cumulatively with the dose of the inhibitor after SCI (Yan et al., 2018). There is also evidence that myelotomy, which is a surgical procedure involving the removal of necrotic tissue after injury, prevents the formation of edema and concurrently prevents the increase in AQP4 expression after SCI (Hu et al., 2015). Collectively, studies focused on the roles of AQP4 in cytotoxic edema after acute injury suggest that AQP4 is a mediator in the formation of cytotoxic edema in the CNS.

Contrastingly, other studies focusing on vasogenic edema resulting from BBB/BSCB dysfunction demonstrate that AQP4 is crucial for facilitating the clearance of water. In *AQP4*^{-/-} mice, it was observed that vasogenic edema, as determined by water content, was significantly higher up to 28 days following compression SCI compared to control levels, which was not observed in the wild-type (WT). Furthermore, these *AQP4*^{-/-} mice also appear to have a poorer functional recovery following SCI than their WT counterparts (Kimura et al., 2010). Additionally, another study showed that when *AQP4*^{-/-} mice were subject to transectional SCI, the water content within the injured half of the spinal cord was significantly higher than the water content within the injured half of the spinal cord in *AQP4*^{+/+} mice 3 days post-injury (Wu et al., 2014b). This highlights the conflicting nature of AQP4 in traumatic CNS injury, and forces us to question the value of understanding the role of a given protein in the context of an

entire tissue from knockout studies. Indeed, many scientists are beginning to move away from transgenic knockouts as ways to study proteins in the context of injury or disease. This is particularly true in the context of physiologically relevant proteins, such as aquaporins, as the transgenic animals to survive must develop in a manner that overcomes their lack the missing water channel protein. In this light, another group looked at the role of AQP4 expression after injury by using siRNA to silence AQP4 expression post-injury, and found that 30% reduction in AQP4 decreased edema formation and improved neurological function acutely after injury (Fukuda et al., 2013).

It is important to resolve the differences observed between the roles of AQP4 in cytotoxic and vasogenic edema, as both of these elements have been demonstrated to occur following human traumatic SCI (Beggs and Waggner, 1975; Goodman et al., 1976a; Huang et al., 2019). Despite the fact that cytotoxic edema itself isn't thought to cause the significant tissue swelling that results in secondary injury, it is thought to be the ionic driving force that leads to vasogenic edema and the build-up of fluid-filled cavities that cause secondary damage (Faden et al., 1987; Liu and Xu, 2012; Kimelberg, 2004). As such, the traditional categorization of edema into "cytotoxic" and "vasogenic" is being increasingly considered as an oversimplification for two sides of a connected process. The conflicting evidence also suggests that in addition to the role of AQP4 in different types of edema, we must also consider the type of model used, as these studies appear to suggest that AQP4^{-/-} is beneficial following contusion SCI, but detrimental following compression SCI. Furthermore, there is a time element to be considered, as AQP4^{-/-} mice examined shortly after injury appear to have reduced edema and better behavioural functionality than those examined later. This suggests

that the role of AQP4 following SCI may be biphasic, having an edema-forming role immediately following injury, followed by resolution in later stages (Figure 1-7). Perhaps this biphasic phenomena of AQP4 is a result of it having two different functions; the pathological role of causing edema through encouraging cytotoxic and/or vasogenic edema, followed by the physiological role of maintaining ionic homeostasis by regulating water flow. There is a need for clarification on the role of AQP4 in different types/stages of edema formation and resolution, different models of SCI, severity of injury, and over a time course following injury, and an additional need to pay careful consideration to each of these elements when investigating or inhibiting the mechanisms underlying edema.

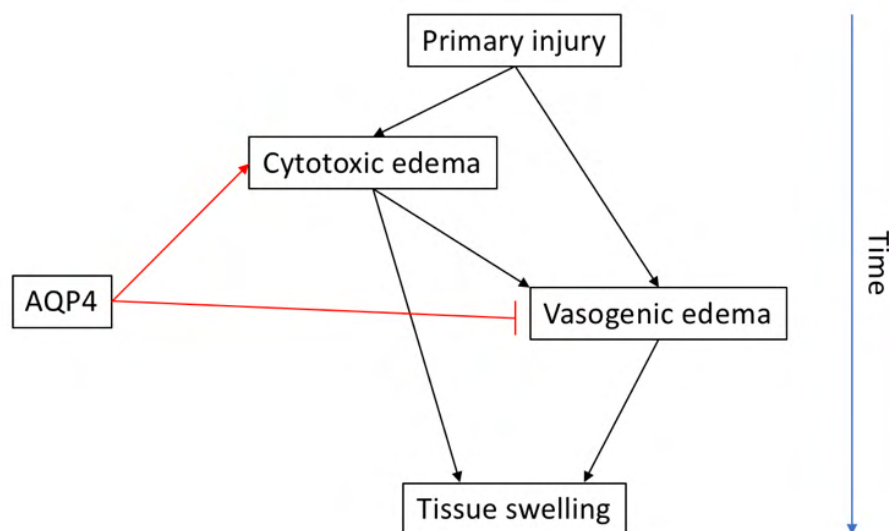


Figure 1-7. The proposed relationship between AQP4 and cytotoxic and/or vasogenic edema following primary injury over time.

AQP4 appears to facilitate cytotoxic edema, whilst aiding the clearance of vasogenic edema at later stages

1.3.2.2 *Astrocyte reactivity, migration, and scarring*

Reactive gliosis, as previously mentioned, is a state of response in astrocytes that coordinates the formation of scar tissue. Scarring, whilst important for the limitation of inflammation, and facilitation of tissue healing, is also highly inhibitory for axon regeneration, and therefore attempts at improving functionality after injury by promoting regeneration can be limited by the presence of a scar. Given the almost exclusive expression of AQP4 in astrocytes, it's unsurprising that it has been closely associated with astrocyte reactivity and the formation/stability of the astrocyte-limiting scar formed after traumatic injury (Sofroniew, 2009; Saadoun, 2005).

Most of the studies looking at the role of AQP4 in the context of astrogliosis and scar formation have used AQP4 knockouts to determine its role. AQP4 knockout mice have exhibited impaired formation of the scar in the contexts of SCI, TBI and MPTP-induced neurodegeneration (Lu et al., 2011; Saadoun, 2005; Fan et al., 2008). AQP4 knockout in astrocytes appears to slow the rate of migration in both transwell and scratch assay migration assays, with AQP4 appearing to be localised within the membrane at leading edge of the migrating astrocytes. Furthermore, AQP4 knockout minimizes the formation of morphological protrusions/processes that aid migration. AQP4 knockout also appeared to reduce the size of the scar present at 3 days after brain stab injury, which the authors attribute to the reduction in the migratory capacity of AQP4-null astrocytes (Saadoun, 2005). In another study, the migration of injected AQP4-knockout astrocytes site to the injury after brain stab injury appeared to be significantly slower than AQP4-expressing astrocytes (Auguste et al., 2007). The theory is, based on data

obtained in AQP1 studies, that AQPs at the leading edge of migrating cells facilitate increased local water influx, which expands the local membrane area to create protrusions wherein actin turnover can occur to form stable structures. As such, removing AQP4 prevents the ability of astrocytes to form these initial lamellipodia, disallowing them from moving through tighter spaces in the extracellular matrix to aid migration. The relationship between AQP4 membrane relocalization in astrocytes and actin remodelling has been demonstrated, however not in the context of directional migration. Instead, the authors report that in response to cAMP treatment, F-actin is required for the relocalization of AQP4, and demonstrate that AQP4 knockdown has no effect on the stellation of the astrocytes, but do not determine whether this affects their ability to migrate (Nicchia et al., 2008).

1.3.3 AQP4-mediated therapeutics for treating SCI

Despite the exhaustive list of therapeutic compounds that have been taken into clinical trials in the context of SCI treatment, there is no therapeutic strategy proven clinically effective for limiting or preventing edema after injury. The only methods used clinically to reduce the impact of edema after SCI are surgical decompression or osmotherapy. The latter is used to alter the systemic osmolarity with the aim of pulling water out of oedemous tissue. This is achieved by the intravenous administration of either saline solution or mannitol. It was first demonstrated in 1973 that mannitol administration significantly reduced edema after SCI in dogs (Parker et al., 1973). It was subsequently demonstrated to improve cerebral blood flow in the context of CNS vessel obstruction (Andrews et al., 1993), but was not brought into clinic in the UK. Subsequently, it was demonstrated that mannitol treatment significantly improves motor recovery,

decreases water content, and decreases BSCB breakdown in rat contusion SCI models. However, treatment with hypotonic saline solution appeared to be much more effective across each parameter (Zhang et al., 2019). Surgical decompression describes the removal of penetrating spinal fragments as a result of the injury or the vertebrae at the site of injury to create a space for the oedemous spinal cord to swell into, reducing the pressure (Fehlings et al., 2012). Early decompressive surgery has been determined as vital for any patient benefit; delay of more than 24 hours can prevent any significant improvement to neurological recovery (Furlan et al., 2011; Lee et al., 2018; Fehlings et al., 2012). However, in the UK, decompressive surgery rarely occurs before 72hrs post-injury, a timepoint by which tissue edema is well established, and therefore further tissue damage from raised intrathecal pressure has probably already occurred (Leonard et al., 2015). Therefore, although decompression is necessary, and shows significant benefit for recovery, it alone isn't sufficient for treating edema.

As previously discussed, altering the expression of AQP4 has been performed frequently in animal models, demonstrating benefits to edema and functionality following both direct genetic modifications or via compounds that affect expression downstream (Saadoun et al., 2008; Zeng et al., 2012; Kimura et al., 2010; Beitz et al., 2006; Fukuda et al., 2013, 2012). However, as a potential treatment route, altering protein expression might be problematic in the context of spinal cord edema as it appears the role of AQP4 in SCI pathogenesis is biphasic in its contribution to formation and resolution of edema. Hence, reducing expression of AQP4 may be beneficial for preventing formation of edema in the acute stages of SCI, but the AQP4

protein must then later continue be expressed to ensure its physiological functions are maintained, so finding a therapeutic agent that can affect AQP4 expression in the required timeframe remains a big challenge (Saadoun, 2005; Li and Verkman, 2001). The aforementioned drug methylprednisolone (MP), which is the only pharmacological agent used to treat acute SCI in clinic, has been demonstrated to increase the presence of edema, which the authors suggest is due to the prevention of AQP4 upregulation after SCI (Cabrera-Aldana et al., 2017a). However, 10 years prior to this, a clinical study had already demonstrated that MP administration at clinically recommended doses did not have a significant effect on the overall edema levels present after injury (Leypold et al., 2007). Some research of the compound curcumin, an acidic polyphenol material used in traditional Chinese medicine, reportedly inhibits the JAK/STAT pathway, and prevents upregulation of both GFAP and AQP4 by 3 days after contusion SCI, as well as promoting improved neurological function up to 2 weeks post-injury (Zu et al., 2014). There is still a big need for some form of early intervention to limit or prevent the onset of edema following SCI, which could ultimately prevent the necessity of such invasive measures as osmotherapy or surgery.

Some evidence does exist for the potential of short-term AQP4 knockdown in the form of siRNA treatment. This has been tested in rat pup traumatic brain injury (TBI) models; acute, transient reduction of AQP4 expression resulted in significantly reduced edema formation and BBB disruption (Fukuda et al., 2013). Furthermore, subsequent studies have also revealed that following TBI, AQP4 siRNA treatment reduced cytotoxic edema that appeared in the contralateral brain tissue of non-siRNA treated rats (Chen et al., 2016), suggesting siRNA treatment as a plausible strategy for inhibiting edema

following CNS injury. However, so far this has not been investigated in models of SCI, where effects on contralateral tissue isn't reflected. Furthermore, whilst the use of siRNA as therapeutic interventions is extremely promising on a molecular level, it remains limited in its clinical practicality due to a number of neurobiological hurdles in therapeutic administration. These include the restrictions imposed by blood-CNS barriers, stability of the siRNA as biological molecules, variation in genetics of individuals (Cho and Kim, 2016). There is also the added unknown of how quickly siRNA against AQP4 will take to have any observable effect in the desired tissue, how long the knockdown will persist, and whether this will have any impact on compensatory mechanisms (for example, upregulation of other AQP4 isoforms). Additionally, AQP4 knockout animals exhibit abnormal neuronal excitability, including prolonged seizures as a result of altered potassium currents (Binder et al., 2006; Amiry-Moghaddam et al., 2003), suggesting that special attention should be paid to the extent of knockdown achievable clinically.

1.3.3.1 *Reported inhibitors of AQP4*

Despite the aforementioned challenges faced in target specificity for AQP4 inhibitors, some proposed inhibitors have been investigated through computational and experimental screening. In the older literature, a number of anti-epileptic drugs, most notably the carbonic anhydrase inhibitor acetazolamide (AZA), demonstrated a reduction in edema after cerebral injury by non-specifically inhibiting AQP4 (Huber et al., 2009). However, as many predicted at the time due to a high rate of artefact in the oocyte swelling assays, these were all subsequently demonstrated not to have any influence on AQP4 inhibition (Yang et al., 2008b). However, astrocyte cell lines subject

to stretch-induced stress exhibited significantly less cell swelling and decreased AQP4 expression when treated with AZA compared to stretched, untreated cells, suggesting that AZA may still be a potential compound of interest for inhibiting edema, but not via AQP4 inhibition (Sturdivant et al., 2016). Other small-molecule inhibitors of AQP4 revealed at that time, such as the K⁺ channel blocker tetraethylammonium (TEA⁺) and bumetanide were also discredited as potential therapeutics for treatment of CNS edema due to their lack of specificity for AQP4 subtypes and lack of demonstrable evidence of reducing edema in vivo (Oliva et al., 2011; Detmers et al., 2006; Migliati et al., 2009). There have been more recent developments in the creating of more specific small-molecule inhibitors of AQP4. For example, 2-(nicotinamide)-1,3,4-thiadiazole (TGN-020), which has demonstrated benefit in reducing edema and overall brain volume increases after a number of ischemic brain conditions and spinal cord injury in rodent models, as well as reducing the size of the cavity formed within the scar (Igarashi et al., 2011; Pirici et al., 2018; Li et al., 2019). However, the precise mechanism by which TGN-020 produces this effect is questionable as there is no evidence to suggest that it is an AQP4-specific pore blocker. AER-270, a phenylbenzamide, is another small molecule proposed to be an AQP4 pore inhibitor, which has demonstrated a reduction in CNS edema (Farr et al., 2019). However, despite the molecule achieving a 70% maximal inhibition of rat AQP4, and only 20% maximal inhibition of mouse AQP4, the reduction in water content in both rat and mouse models is about proportionate, suggesting a mechanism not involving AQP4 inhibition. Given that AER-270 is also an inhibitor of NF-κB, which has also been shown to reduce edema after cerebral ischemia, this may be its mechanism of action (Li et al., 2016).

Attempts have also been made at inhibiting the functionality of AQP4 through the use of anti-AQP4 antibodies. Initially, this was investigated with the IgG anti-AQP4 autoantibody that exists in patients suffering with neuromyelitis optica (NMO). NMO is an autoimmune disease, whereby endogenous anti-AQP4 antibodies bind to extracellular epitopes of AQP4, resulting in complement-dependent cytotoxicity, inflammation and demyelination, which ultimately can lead to blindness and neurological deficit (Chang and Chang, 2020). However, subsequent studies determined that this AQP4-IgG had no effect on the permeability or membrane assembly of AQP4 in proteoliposomes (Rossi et al., 2012). This was probably due to the fact that the extracellular epitopes the antibodies bind to are within the large extracellular loop portions of the AQP4 protein, which are mostly situated quite far away from the pore, and therefore probably wouldn't affect the water permeability of AQP4 (Yu et al., 2011). Nevertheless, due to many NMO IgG binding studies using polyclonal serum, the specific epitope specificity for different autoantibodies is ambiguous. As such, AQP4 mutagenesis studies using multiple monoclonal recombinant anti-AQP4 antibodies to screen binding affinities reveal more dominant epitopes of binding in the extracellular domains, which is useful for narrowing down antibody specificity that may help develop new anti-AQP4 antibodies that can more effectively interfere with the pore region and therefore affect AQP4-mediated mechanisms (Owens et al., 2015). A new anti-AQP4 antibody therapeutic, 'aquaporumab' was generated which was an engineered version of the human monoclonal IgG that lacked the complement-dependent or antibody-dependent cytotoxic effector functions. This antibody showed promise in treating NMO patients by

blocking serum IgG binding to AQP4 with cytotoxic effects, but in the context of SCI and other AQP4-mediated pathologies, is still likely to be ineffective at inhibiting water movement across the pore (Duan et al., 2020).

1.3.4 Targeting subcellular relocation of AQP4 as a therapeutic intervention for SCI

Water transport is a dynamic and fluctuating process in most tissues in the human body, and therefore functional regulation of AQPs are critical to their activity. This is to ensure that water flow occurs at the appropriate cellular locations and permeabilities to which the cell or tissue requires. The most common and frequently observed method for regulating AQP activity is through 'gating'. This type of regulation was first reported in plant AQPs, such as spinach, where an intracellular loop physically barricades the pore following dephosphorylation at a local serine residue (Törnroth-Horsefield et al., 2006; Walz et al., 2009). Whilst this mechanism is used extensively in many biological membrane proteins, it is not thought to be involved in the regulation of AQP4.

The other rate-limiting factors regulating the water permeability of astrocytes through AQP4 include the rate of OAP aggregation at the cell surface, the rate of vesicle transport leading to AQP4 membrane delivery, and the relative amounts and/or density of AQP4 present. Turnover of the abundance of AQPs at the cell membrane via protein trafficking postulates that increased cellular water permeability may be the result of increased translocation of the AQP protein between the cell membrane and intracellular stores (short-term) and/or decrease in AQP endocytosis and recycling. Evidence for such a mechanism has been well demonstrated for AQP2 in kidney

endothelium (Noda and Sasaki, 2005). In this context, AQP2 is thought to be under the regulation of vasopressin; binding to its natural receptor, the vasopressin type 2 receptor (V_2), results in a G-coupled intracellular response leading to PKA activation, AQP2 phosphorylation, and its ability to translocate to the basolateral membrane (Fushimi et al., 1997; Katsura et al., 1997; Noda and Sasaki, 2005). In the context of AQP4, it was demonstrated that AQP4-mediated water permeability in transfected oocytes can be modulated via phosphorylation, and specifically that PKC-mediated phosphorylation results in decreased oocyte water permeability (Han et al., 1998). This phosphorylation-dependent increase in water permeability was found to also occur in response to vasopressin signalling, and involved the phosphorylation of Ser180 (Moeller et al., 2009).

Changes in water permeability were also detected in astrocyte cultures in response to glutamate signalling, involving the phosphorylation of Ser111 (Gunnarson et al., 2008). This suggests that astrocytes are able to turnover the amount and localization of AQP4 according to the circumstance and pathophysiological environment. Indeed, it was then determined that when astrocytes were cultured in either a hypotonic environment or treated with cAMP, AQP4 became significantly relocalized to the plasma membrane, and AQP4-containing vesicle turnover significantly slowed (Potokar et al., 2013). Subsequently, Kitchen, et al (2015) demonstrated that the increase in membrane abundance of AQP4 and cell swelling of astrocytes in response to hypotonicity is mediated through a Protein Kinase A (PKA)- and Calmodulin (CaM)-dependent mechanism, and that of the 5 PKA phosphorylation sites present, on Ser276 is necessary for the membrane relocalization response.

The subcellular distribution of AQP4 is also key for its functionality *in vivo*. Under physiological circumstances, AQP4 exists within the membrane of astrocytes, however this membranous distribution is extremely polarized to the endfeet membranes surrounding blood vessels and neuronal synapses, where AQP4 function is mostly required (Oklinski et al., 2014). The relative abundance of AQP4 at the perivascular endfeet has been demonstrated to increase as soon as 1hr after middle cerebral artery occlusion (MCAO) in the brain (De Castro Ribeiro et al., 2006), suggesting that the redistribution of AQP4 in response to various signals observed *in vitro* may also exist as a pathological response *in vivo*. One group previously demonstrated that the perivascular abundance of AQP4 increases at 3 days following closed cortical brain injury in mice models, and that the aforementioned drug AZA could inhibit this effect (Glober et al., 2019). However, no vascular marker was used to determine this localization, and no extra-lesional tissue was used as a negative control. Collectively, due to the previously demonstrated effects of AQP4 on edema formation and glial reactivity after such events as TBI or SCI, it is important to determine whether relocalization of AQP4 does occur *in vivo*, and what role this has in the secondary pathogenesis of such conditions. Furthermore, given that the molecular pathway that facilitates membrane redistribution of AQP4 has been discovered *in vitro*, it would be prudent to determine if treatment with these inhibitors has any beneficial effect on AQP4-mediated consequences of traumatic injury, such as edema and glial reactivity.

1.4 Hypothesis and aims

The hypothesis is that subcellular AQP4 relocalisation promotes SCI-induced edema, and treatment with inhibitors of AQP4 relocalization *in vitro* (PKA and CaM inhibitors) will be beneficial as acute treatments following spinal cord injury by a) preventing increased perivascular AQP4 relocalization, b) preventing onset of edema after SCI, and c) limiting the formation of the astrocytic scar by reducing astrocyte migration.

The aims of this project are to:

- 1) Determine whether there are any observable differences in the subcellular localization of AQP4 in a rat spinal cord injury model (chapter 3)
- 2) Investigate whether treatment with inhibitors of *in vitro* AQP4 relocalization prevent these observable differences (chapter 3)
- 3) To determine whether inhibitors of AQP4 relocalization affect overall edema in a rat spinal cord injury model (chapter 4)
- 4) Investigate whether inhibitors of AQP4 relocalization affect overall functionality of the spinal cord in a rat spinal cord injury model (chapter 4)
- 5) Investigate whether inhibitors of *in vitro* AQP4 relocalization affect the migration capacity of astrocyte *in vitro* and/or the astrocytic scar response *in vivo* in a rat spinal cord injury model (chapter 5).

Chapter 2

Materials and Methods

2 Materials and Methods

2.1 In vivo

2.1.1 Animal surgery

2.1.1.1 *Rat dorsal crush spinal cord injury model*

All animal surgeries were licensed by the UK Home Office and all experimental protocols were approved by the University of Birmingham's Animal Welfare and Ethical Review Board in strict accordance to the guidelines of the UK Animals Scientific Procedures Act, 1986 and the Revised European Directive 1010/63/EU and conformed to the guidelines and recommendation of the use of animals by the Federation of the European Laboratory Animal Science Associations. For each surgery, Female Sprague Dawley rats (Charles River, Margate, UK) weighing between 175-225g were used. Dorsal column (DC) crush at spinal cord level T8 was performed corresponding to previously published methods (Ahmed et al., 2010; Lagord et al., 2002). Prior to surgery, rats were first injected subcutaneously with 0.2ml of the analgesic Buprenorphine, and were then anaesthetised with 2.5-5% isoflurane and 2L/mg of oxygen. A partial laminectomy of the T8 vertebrae was first performed, followed by a bilateral DC crush of depth and width 1mm x 1mm in the spinal cord dorsal column at the T8 level using a calibrated watchmaker's forceps (Figure 2-1). Sterile black ink was coated on the tips of the forceps up to 1mm to ensure depth consistency, and also lesion site identification. Animals were allowed to recover, and were then killed by Schedule 1 methods (rising concentration of CO₂) for dissection of the spinal cord lesion site at specified times according to the research requirement (as described below).

2.1.2 Spinal cord DC crush injury treatment groups

All injured treatment groups in *in vivo* work involved an intraspinal injection of 2.5 μ L immediately following the dorsal column crush with forceps. Intralesional injections were performed using in-house pulled glass micropipettes (P1000 micropipette puller set to pull micropipettes with an internal tip diameter of 0.5 μ m; Sutter Instruments, Novato, CA, USA). The glass micropipettes were loaded with appropriate solutions, attached to the rubber tubing from butterfly needles and secured to a 5 ml syringe. Using a dissecting microscope, the tip of the micropipette was inserted into the lesion site, as determined by the presence of the ink from the crush, and solutions were pushed through, with air in the syringe, slowly over a 1 minute period, with a 20 s wait prior to withdrawal of the micropipette to alleviate backflow. (1) Uninjured controls, (2) DC injury (DC crush + intralesional injection of vehicle (PBS)); (3) DC injury + TFP (DC crush + intralesional injection of 4.9mM TFP); (4) DC injury + H-89 (DC crush + intralesional injection of 10 μ M H89); (5) DC injury + PKCi (DC crush + intralesional injection of 10 μ M Go 6983) (6) DC injury + W-7 (DC crush + intralesional injection of 164mM W-7); (7) DC injury + D2Ri (DC crush + intralesional injection of 6.6 mM L-741,626); (8) DC injury + A1Ri (DC crush + intralesional injection of 53mM terazosin). For all *in vivo* experiments, rats of each treatment group were randomized across mixed cages. The experimenter was blinded to the treatment groups prior to surgery by the anaesthetist who delivered and recorded the treatment for each rat. Groups were unanonymized during data analysis.

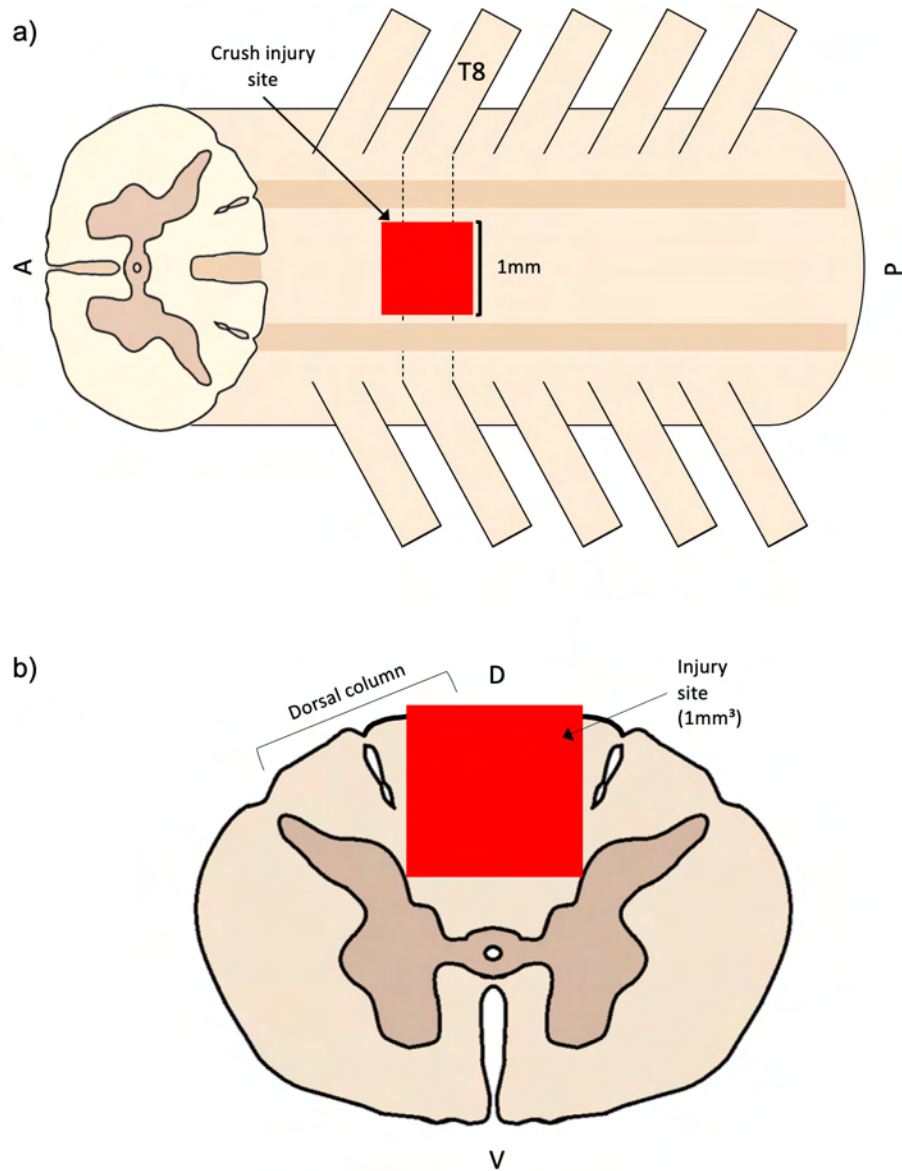


Figure 2-1 A diagrammatic representation of dorsal column crush SCI at spinal cord level T8. a) Dorsal view of spinal cord and b) cross sectional view of spinal cord, both demonstrating the primary lesion area crushed with forceps (red). Orientation: A – Anterior; P – Posterior; D – Dorsal; V – Ventral. Parts of this image have been modified from https://commons.wikimedia.org/wiki/File:Spinal_cord_-_Thoracic_cross_section.svg

2.1.3 Tissue preparation

2.1.3.1 Tissue for spinal cord water content

Water content was determined using a frequently utilized method of tissue dehydration (Li and Tator, 1999; Nestic et al., 2006). Immediately after sacrificing rats, spinal cord tissue was dissected 3 mm either side of the lesion site (Figure 2-2). Tissue was then weighed in Eppendorf tubes, dried at 95°C for 48 hours and reweighed. The percent water content was calculated as below:

$$\text{water content (\%)} = [(\text{wet weight} - \text{dry weight}) / \text{wet weight}] \times 100\%$$

48 hours was determined as the optimal timepoint for dehydration, after which no more loss in mass was observed. For all spinal cord water content experiments, “sham” groups did not receive any surgical or anaesthetic intervention, as this had been previously shown not to have any effect on the water content in the spinal cord (data not shown).

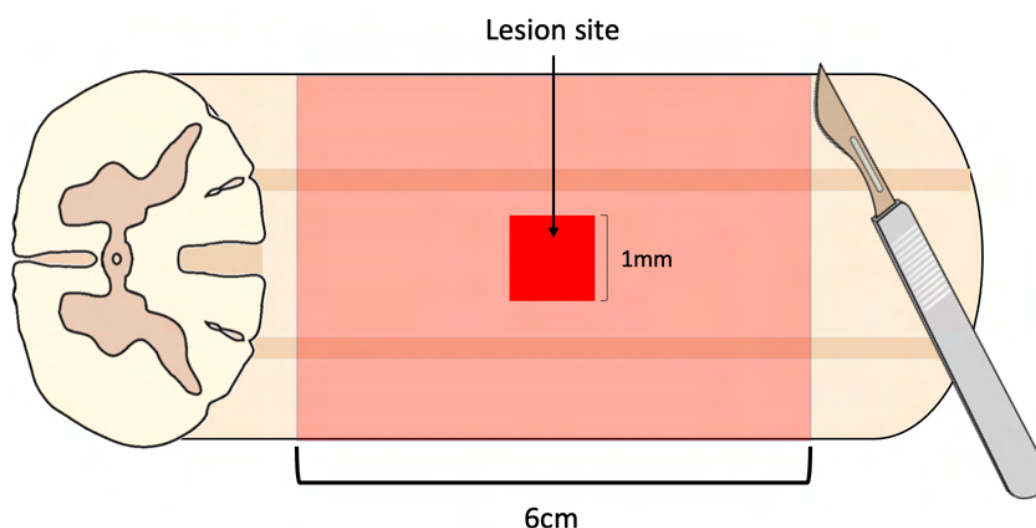


Figure 2-2 A schematic demonstrating area of tissue dissected for water content measurement.

Tissue was collected by dissecting the spinal cords at 3mm either side of the lesion epicentre to ensure edema was only measured within the injury area.

2.1.3.2 *Histology*

Rats were culled by rising concentrations of CO₂ in accordance with UK Home Office Animals (Scientific Procedures) Act 1986. Animals were then intracardially perfused with 4% paraformaldehyde in phosphate-buffered saline (PBS). Spinal cords were dissected ± 5 mm from the lesion site and cryo-protected in increasing sucrose concentrations in PBS, before being embedded in OCT Compound (ThermoFisher Scientific) and snap frozen on dry ice. Tissue was sectioned onto Superfrost Plus Slides (ThermoFisher Scientific, Loughborough, UK) at 15 μ m using a Bright cryostat (Bright Instrument, Cambridgeshire, UK) through the parasagittal plane of the cord (as demonstrated in Figure 2-3) and stored at -20°C until required.

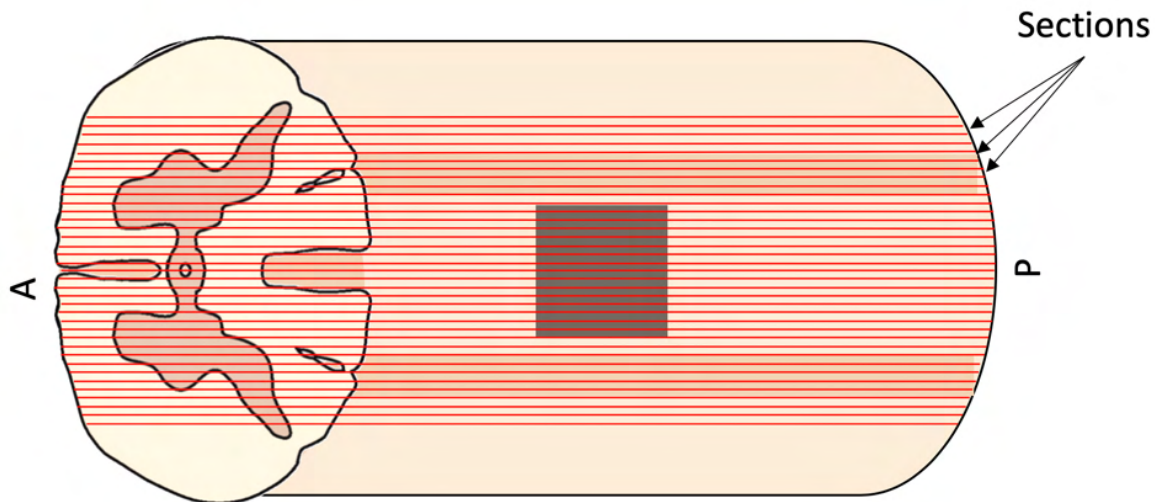


Figure 2-3 Diagrammatic representation of the plane of parasagittal sectioning.

1cm length of spinal cord tissue (± 5 cm from the crush site, or area matched control) was dissected, dehydrated using sucrose, and embedded in OCT. Sections were then sliced in the parasagittal plane of view.

2.1.3.3 *Spinal cord tissue homogenization and protein quantification*

Spinal cord tissue was dissected 3mm either side of the lesion site at level T8. This tissue was immediately snap-frozen on dry ice and stored at -80°C until processing. Total protein was extracted from each spinal cord tissue by homogenizing in 300µl of ice-cold lysis buffer (50mM Tris-HCL (pH 7.4), 300mM NaCl, 1% Triton X-100, 1X protease inhibitor cocktail (Sigma), 1X phosphatase inhibitor cocktail (Sigma)). Homogenates were incubated on ice for 30 mins to allow complete dissociation of proteins. Tissue lysates were clarified by centrifugation at 13,000 x g for 30 mins at 4°C to remove insoluble material. The supernatant was collected and stored at -80°C until required. Protein concentration in each lysate was assayed using a Bradford assay (Bradford MX, Expedeon). BSA protein standards were made up by diluting powdered BSA in the lysis buffer used to digest the tissue between 0 and 1000µg/mL. 1µL of each concentration BSA standard and tissue homogenate were added to 200µL Bradford reagent + 800µL dH₂O. They were incubated at RT for 5 minutes, and absorbance read at 595nm. The standard curve was plotted for the BSA standards, and the protein concentration of samples determined using the standard curve.

2.1.3.4 *SDS-PAGE and Western blot*

SDS-PAGE was performed using 1 mm thick 12% bis-tris acrylamide gels, which were handcast using BioRad handcasting equipment. Stacking gels were 4% acrylamide. 10 µg of protein from tissue lysates was loaded per well. Lysates were mixed with an equal volume of 2x Laemlli buffer (4% v/v β-mercaptoethanol, 4% w/v SDS, 20% v/v

glycerol, 0.02% w/v bromophenol blue, 120 mM tris, pH 6.8) and incubated for 10 mins at room temperature before loading. Electrophoresis was performed at 200V for 45 mins. Molecular weights were approximated using a commercial protein marker loaded into one well of each gel (New England Biolabs). After protein separation, gels were transferred to methanol-activated PVDF membranes using a wet electroblotting system (Bio-Rad). Electrophoresis was performed at 100 V for 1 h. Membranes were blocked using 10 mL 20% w/v powdered skimmed milk (BioRad) in 0.1% PBS-tween for 1 h on a roller in 50mL falcon tubes. After blocking, membranes were washed 3 times for 5 mins in 0.1% PBS-tween in upside-down micropipette tip boxes. Membranes were incubated in 5 mL of primary antibody diluted in 0.1% PBS-tween at the appropriate dilutions (see Table 2-1) overnight on a roller at 4°C.

2.1.4 Histology and immunohistochemistry

2.1.4.1 *Antibodies used for immunohistochemistry and Western blot*

Table 2-1 Further information on antibodies used for immunohistochemistry, immunocytochemistry and Western blotting, including species, source, and dilution volumes.

IHC = immunohistochemistry, ICC = immunocytochemistry, WB = Western blot

Primary antibodies				
Antibody	Detects	Host species	Dilution	Supplier (Cat. Number)
AQP4	Aquaporin-4 C-terminus	Rabbit	1:400 (IHC) 1:1000 (WB)	Abcam (ab128906)
CD31	Endothelial cell junction	Mouse	1:50 (IHC)	Abcam (ab119339)
RECA-1	Rat endothelial cells	Mouse	1:50 (IHC)	Abcam (ab9774)
GFAP	Glial fibrillary acidic protein	Mouse	1:200 (IHC/IF)	Sigma (G3893)
CD68 (ED1)	Macrophages	Rabbit	1:200 (IHC)	Abcam (ab213363)
β-III-tubulin	Neuronal microtubules	Mouse	1:400 (ICC)	Merck (T2200)

Foxo3a	Foxo3a transcription factor	Rabbit	1:200 (IHC)	Abcam (ab23683)
β -actin	Loading control	Mouse	1:10000 (WB)	Sigma (A2228)
Albumin	Serum albumin	Chicken	1:100 (IHC)	Abcam (ab106582)
Secondary antibodies				
Alexafluor-488	Mouse IgG	Donkey	1:400 (IHC/IF)	Invitrogen (A-21202)
Alexafluor-488	Rabbit IgG	Donkey	1:400 (IHC)	Invitrogen (A-21206)
Alexafluor-594	Mouse IgG	Donkey	1:400 (IHC)	Invitrogen (A-21203)
Alexafluor-594	Rabbit IgG	Donkey	1:400 (IHC/IF)	Invitrogen (A-21207)
Alexafluor-633	Mouse IgG	Goat	1:200 (IHC)	Invitrogen (A-21052)
Alexafluor-488	Chicken IgY	Goat	1:200 (IHC)	Abcam (ab150169)
HRP-linked	Rabbit IgG	Donkey	1:2500 (WB)	Santa Cruz (sc-2313)
HRP-linked	Mouse IgG	Goat	1:2500 (WB)	Santa Cruz (sc-sc-2005)

2.1.4.2 *Fluorescence immunohistochemistry for spinal cord sections*

Spinal cord tissue sections were removed from -20°C storage and thawed for 30 mins at room temperature, before being washed in PBS for 5 mins. Non-specific binding was blocked for 30 mins at RT using PBS containing 0.5% BSA (Sigma) and 3% normal goat serum in 0.5% Tween 20 (Sigma). Sections were incubated in primary antibody diluted in blocking solution (see sections on antibody dilutions) and incubated at 4°C in a humidified chamber overnight. Sections were washed three times in PBS and incubated in appropriate secondary antibodies (see sections on antibody dilutions) diluted in blocking solution for 1 hour at room temperature. Finally, sections were washed three times in PBS and mounted in Vectashield containing DAPI (Vector Labs). Sections were then viewed under an epifluorescent microscope (Zeiss).

2.1.5 Tissue microscopy

2.1.5.1 *Confocal microscopy*

Imaging was performed using an upright Leica Microsystems SP5 TCS II with multiphoton add-on and a 63x magnification apochromatically corrected (APO) oil lens. Laser properties were 488 Argon @ 20% (anti AQP4 – AlexaFluor 488; green); 594 HeNe laser at 29% (anti RECA1 – AlexaFluor 633; red of anti-GFAP – AlexaFluor-594; red); 800 nm multiphoton laser for DAPI (SpectraPhysics MaiTai; blue). X, Y resolution was 1,024x1,024 pixels for all images. Laser power, pixel size, scanning speed, smart gain and offset and beam splitting settings were kept constant for analysis of total AQP4 expression. To facilitate accurate acquisition and analysis to process expression of AQP4, smart gain and offset were adjusted using the quick LUT, glow over and under setting, to create a dynamic fluorescence range (0-255).

2.1.5.2 *Epifluorescent microscopy*

All tissue analysed for area of protein were imaged using an AxioPlan 2 epifluorescent microscope (Carl Zeiss, Germany) with a 10x or 20x dry aperture, and captured using an AxioCam HRc (Carl Zeiss). Images were taken sequentially across the spinal cord, ensuring that at least the entire lesion area was covered. Images were then stitched together using the Photoshop 2020 photomerge function.

2.1.6 Tissue image analysis

2.1.6.1 *AQP4/GFAP colocalization*

A number of methods for attempting to quantify the amount of AQP4 within the membrane/cytoplasm compartments of astrocytes of spinal cord tissue were attempted. Sections were taken across the lesion site within the dorsal column of rat spinal cord tissue. They were then co-immunostained for AQP4 (green), GFAP (red) and DAPI (blue) and imaged at 63X on a confocal microscope within the lesion site. At least 10 astrocytes were imaged per section, 3 sections per animal and a minimum of 3 animals per treatment group. The first method was to perform colocalization between AQP4 and GFAP. Each astrocyte identified (as determined by the limitations of GFAP immunofluorescence), was isolated to ensure background fluorescence from other cells or processes were not included. The channels were then split into green (AQP4) and red (GFAP) (Figure 2-4) and colocalization determined according to the Coloc 2 plugin on Fiji.

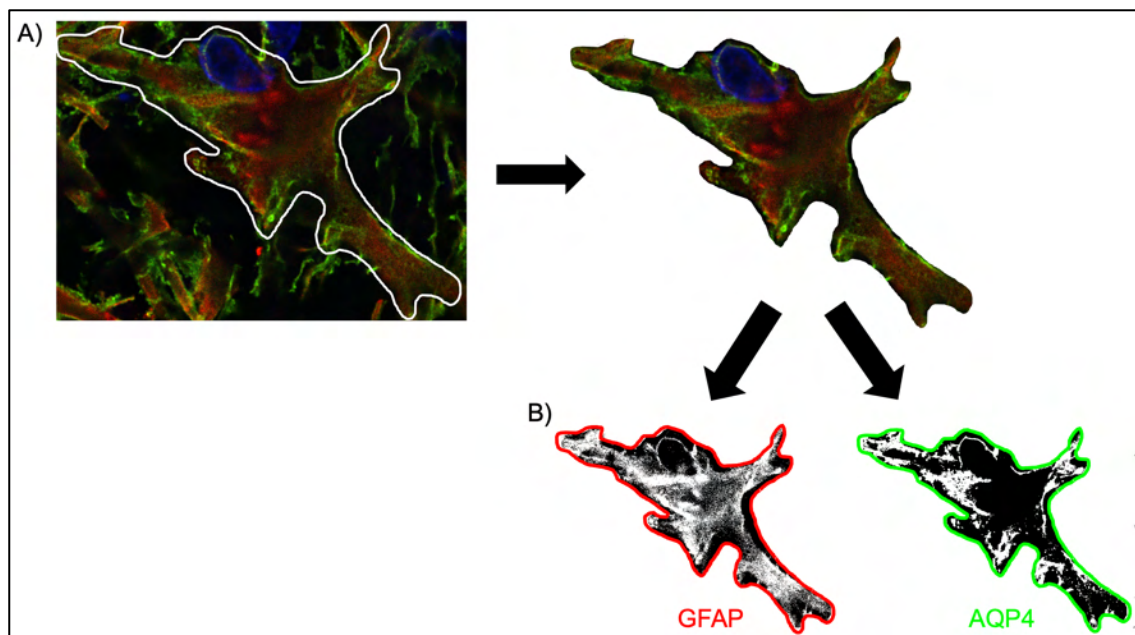


Figure 2-4. Method of preparing images for colocalization analysis between red and green channels.

The area containing the astrocyte cell body was isolated from “background” (A), and the channels were split into red and green (B).

2.1.6.2 *Relative membrane expression (RME)*

The second method used to quantify the amount of AQP4 at the membrane relative to intracellular utilized a method previously established by Kitchen et al., (2015) and Conner et al., (2010) in which fluorescence line profiles are extracted across a cell in ImageJ, and the fluorescence is then plotted over distance. Line locations were selected to avoid the nucleus and perinuclear region. The relative “membrane” and “non-membrane” regions were determined and the RME calculated using an in-house MATLAB code. A minimum of three line profiles distributed at regular intervals across the membrane and cytoplasm were measured for each cell. This method can be visualized in Figure 3-4.

2.1.6.3 *Relative perivascular AQP4*

Sections were taken across the lesion site within the dorsal column of rat spinal cord tissue at 3 and 7 days post-injury. Sections were co-immunostained for RECA-1 (red) and GFAP (green) and imaged at 40X on a confocal microscope within the lesion site. At least 10 regions of interest were imaged per section with an average of 5 blood vessels per ROI, with at least 3 sections imaged per animal and 6 animals per treatment group. Images were analysed using ImageJ. Regions of interest (ROIs) were outlined and mean value fluorescence was calculated (Figure 2-5). Relative expression values were calculated using ROIs along processes (non-perivascular) and around endothelial cells (perivascular), comparing the mean fluorescence values from each

group. For consistency, 10 values per group per image were collected wherever possible; images containing too few endothelial cells were discounted from the analysis.

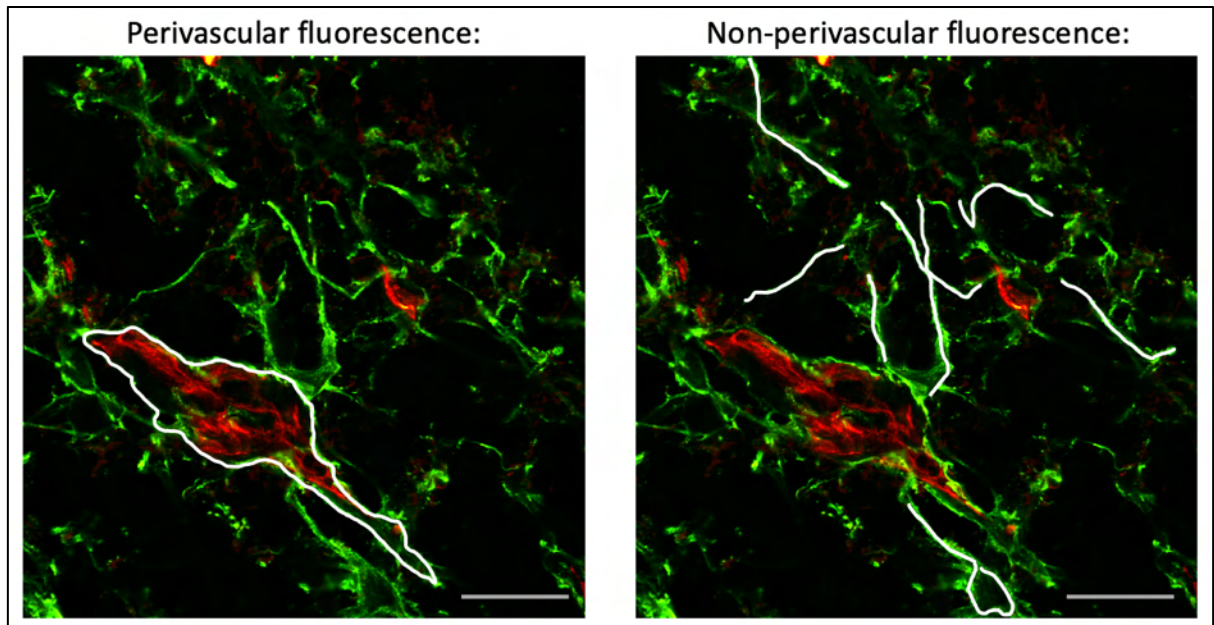


Figure 2-5 Representative images of rat spinal cord tissue immunostained for AQP4 (green) and RECA-1 (red), demonstrating the areas used to quantify perivascular and non-perivascular fluorescence (white lines).

Scale bar (grey) = 25 μ m.

2.1.6.4 Total fluorescence (pixel intensity)

To quantify total fluorescence, the entire original field of view was used (at X, Y resolution was 1,024x1,024 pixels for all images). In ImageJ, images were split into colour channels, and the green channel representing AQP4 fluorescence was converted to 8-bit, and quantified for mean gray value as a readout of signal intensity within the field of view. Data shown was all normalized to uninjured control.

2.1.6.5 Protein area (albumin and macrophages)

Using ImageJ, a region of interest (ROI) was selected as the middle 1.6mm of the cord section containing the lesion site, an area determined by examining all sections for the largest immunostained area. The colour channels were then split, and the threshold of relevant channels representing proteins of interest was adjusted to a level where no pixels were identified in a majority of the primary antibody-omitted samples to remove “background” (Figure 2-6).

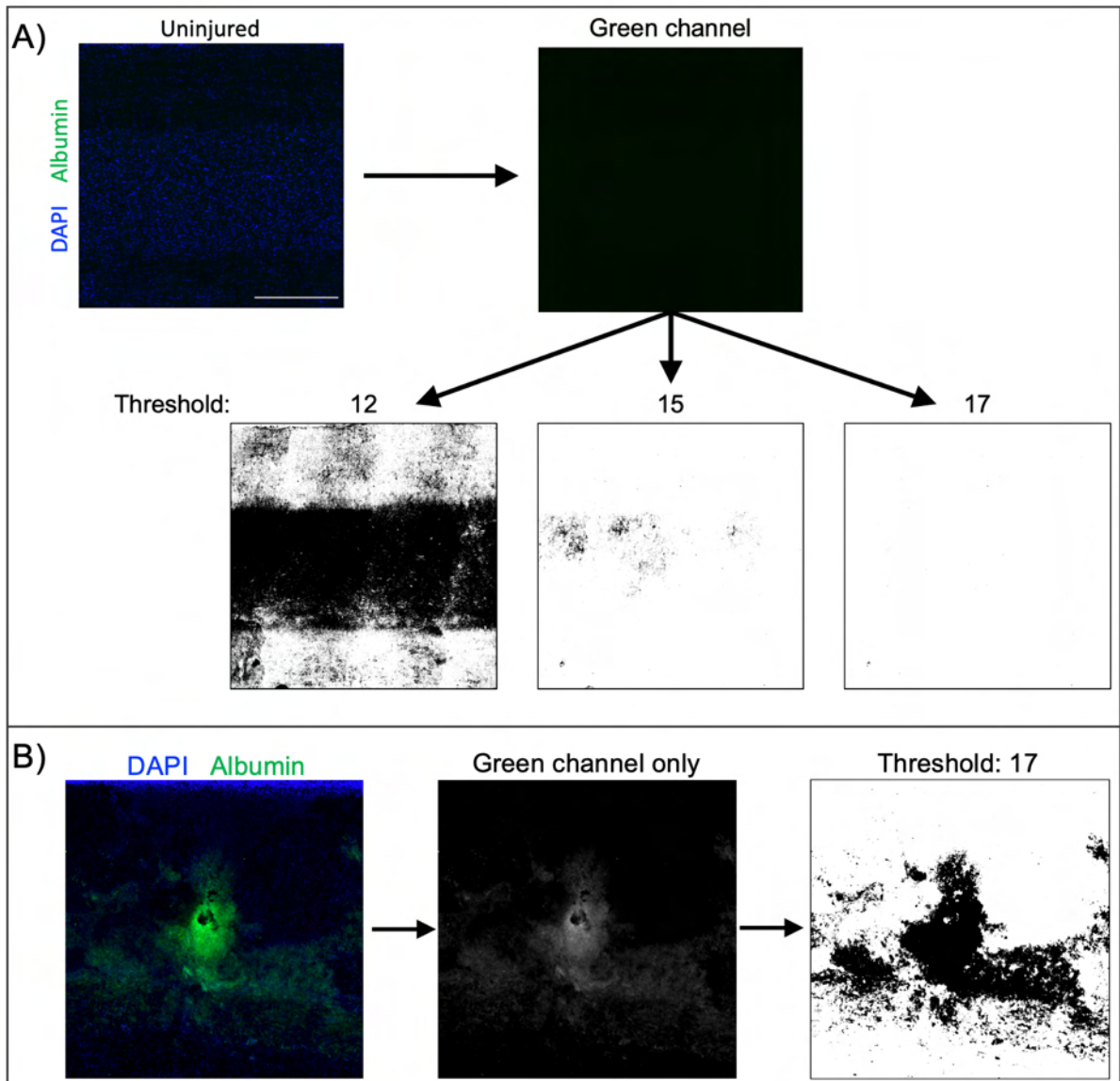


Figure 2-6 Method of analysis for albumin area in immunolabeled spinal cord tissue.

A) To determine the threshold level that removes background fluorescence, the green channel within negative control samples (uninjured tissue) was separated and the threshold increased until positive signal was below 1 for all negative control samples. B) The green channel for all other samples was then separated and thresholded to the level determined in (A).

2.1.6.6 *Lesion and syrinx cavity measurement*

Using the ImageJ freehand selections tool, the areas both within the boundary of the lesion scar border and the cell-free fluid-filled cavity area were demarcated and quantified. The scar border was determined as the limit of positive GFAP staining determined by the relevant cell morphology and positive immunostaining observed (Figure 2-7b). The cell-free fluid cavity area was determined as any area negative for both DAPI and background fluorescence (Figure 2-7c).

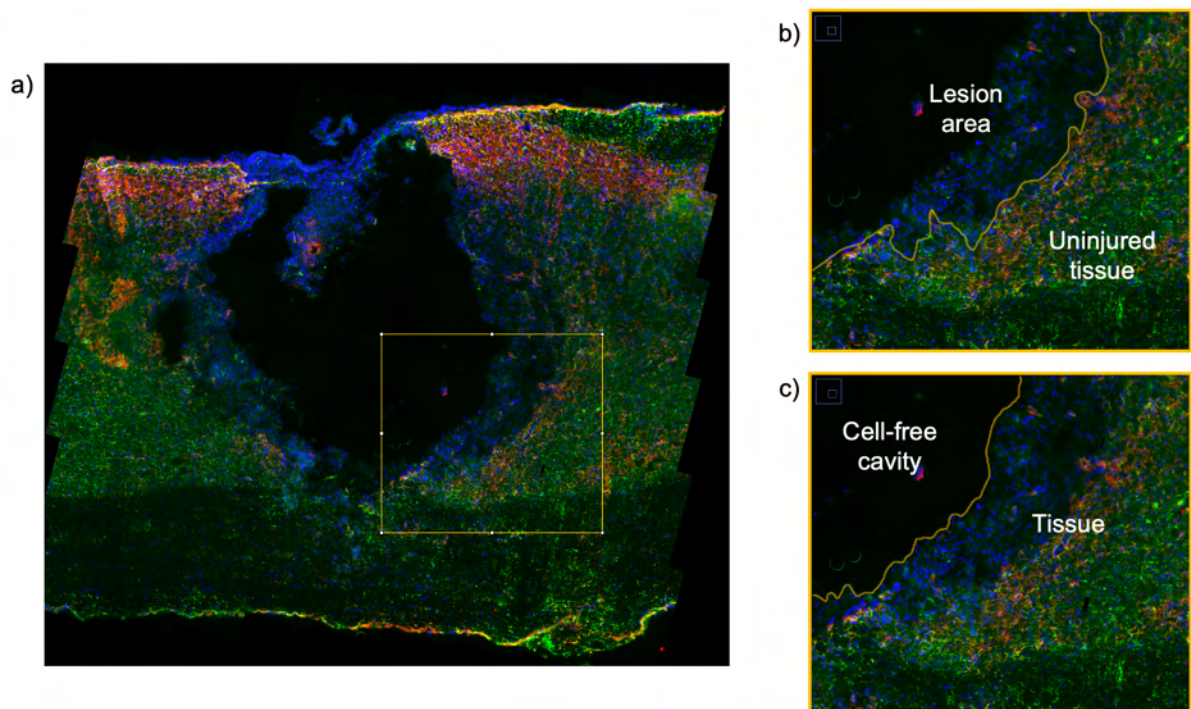


Figure 2-7 A representative image of injured rat spinal cord tissue at 7 days post-injury demonstrating where the areas of uninjured tissue, lesioned tissue area and cell-free cavity were demarcated for analysis.

2.1.6.7 *Astrocytic scar density measurement*

Using ImageJ, the y-axis coordinates at the top and bottom of the lesion area contained by the astrocyte scar border were measured. These were then entered into a random number generator to select 8 random numbers to 2 decimal places between the top and bottom coordinates. These numbers were then used to determine the y-axis coordinates that would be measured at the border of the lesion scar in areas of 75 μ m x 75 μ m (Figure 2-8, yellow boxes). Mean fluorescence within each of these areas was recorded and averaged. The background tissue fluorescence was also determined by measuring the mean fluorescence of tissue within the fibrotic scar, which is largely absent of astrocytes and therefore positive GFAP staining (Figure 2-8, blue freehand area).

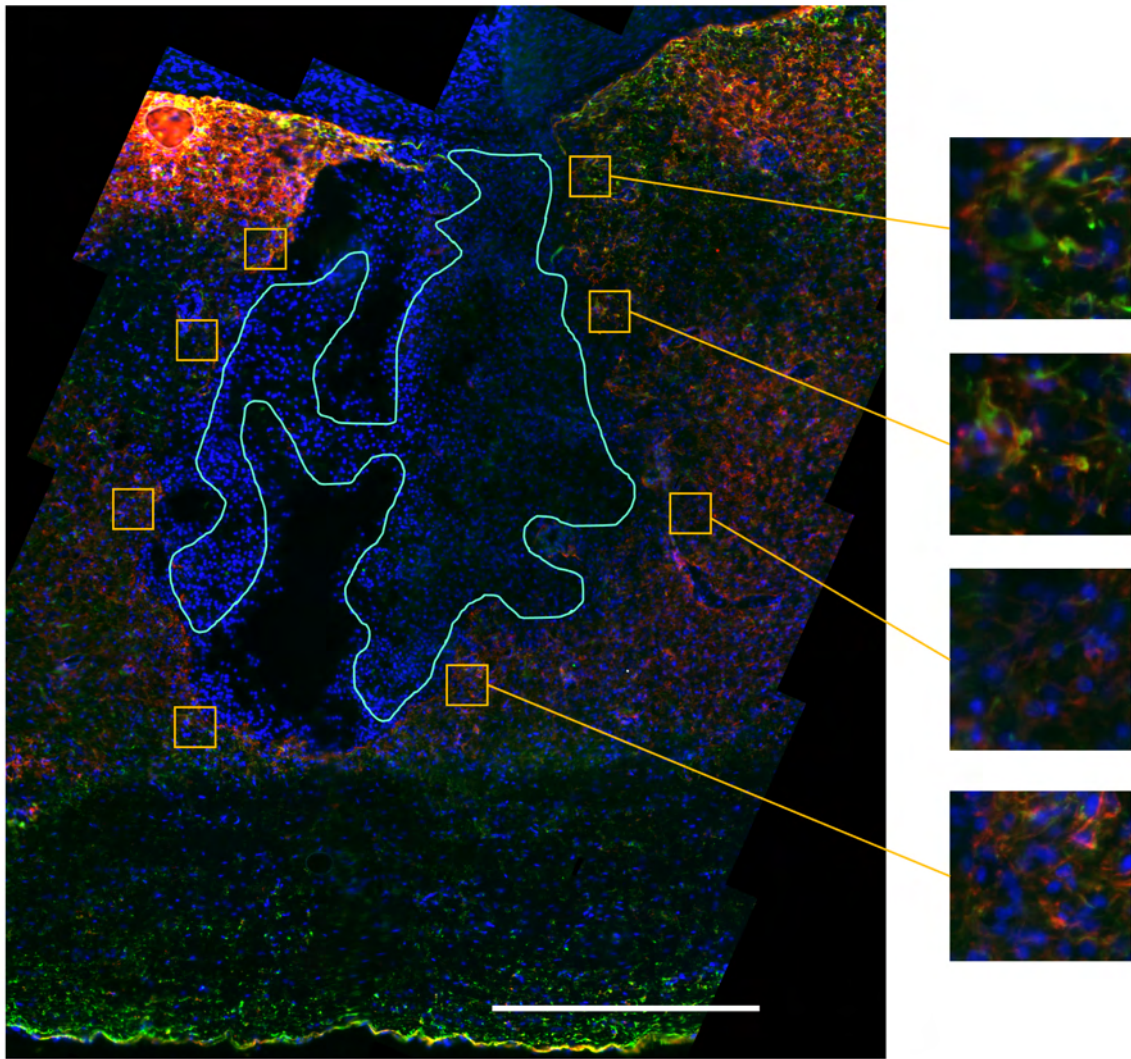


Figure 2-8 A representative image of injured rat spinal cord tissue at 7 days post-injury immunolabelled for GFAP (green), AQP4 (red), and DAPI (blue) to demarcate the astrocytic scar border.

Yellow boxes demonstrate the 8 hypothetical randomized 75µm x 75µm areas that were quantified for GFAP fluorescence. Area contained by light blue represents the hypothetical area quantified for background tissue staining within the green channel.

2.1.7 Western blotting

2.1.7.1 Polyacrylamide gel electrophoresis and western blot

Protein samples from each lysate were mixed with 2x Laemmli buffer (Sigma) at the appropriate concentrations determined from the DC assay. Lysates were then heated at 90°C for 4 mins, and loaded onto pre-prepared 12% Tris-glycine SDS-PAGE gels (Invitrogen, UK). Molecular weight standards (5µl of rainbow markers (Invitrogen)) were also loaded and proteins were electrophoretically separated for 1hr 50mins at 125V. Resolved proteins were transferred onto Immobilon-P polyvinylidene fluoride (PVDF) membranes (Millipore, MA, USA) for 2 hours at 25V. Membranes were washed in TBST (0.12% Tris-base, 0.88% NaCl, pH 7.4, 0.05% Tween20) for 5 mins and incubated in blocking buffer (5% dried skimmed milk (Marvel, Lincolnshire, UK) in TTBS) for 1 hour at RT. Membranes were then incubated with primary antibody (see antibody section) in TTBS, rolled in a 50mL falcon tube on a tilting platform overnight at 4°C, washed X3 in TBST before being incubated with appropriate HRP-labelled secondary antibodies (see antibody section) for 1 hour at RT. Membranes were washed x3 in TTBS. Protein bands were detected using an enhanced chemiluminescence (ECL) kit (GE Healthcare) according to the manufacturer's instructions. Membranes were stripped in a low pH stripping buffer (25mM glycine-HCl, pH 2, 1% SDS) and re-probed following the same protocol as above with primary anti-β-actin antibody (1/10,000).

2.2 In vitro experiments

2.2.1 Cell culture establishment/maintenance

2.2.1.1 *Rat dorsal root ganglia neurons (DRGN)*

Adult female Sprague Dawley rats weighing 170-220g (Charles River) were culled according to Schedule 1 methods of rising CO₂ concentrations inside a chamber. The whole spinal column was removed between the base of the skull and the hips, and kept on ice until dissection. The spinal cord was exposed by removing the vertebrae, and 4-6 pairs of lumbar DRGs (the largest DRGs that project through the dorsal column at T8) were dissected and washed in Neurobasal-A (NBA; Invitrogen, Paisley, UK) (Figure 2-9). DRGs were transferred to a petri dish containing 1.125% collagenase (Sigma, Poole, UK) in NBA, cut in half to allow penetration of the enzyme, and incubated at 37°C for 2 hrs. DRGs were diluted in NBA, dissociated via trituration, and clarified by centrifugation at 120xg for 10mins at RT. The supernatant was removed, 2ml of fresh NBA added, and the cell suspension was layered on a column of 1ml NBA and 1ml BSA (30%w/w) and centrifuged as before to separate cells by density gradient centrifugation. The supernatant and debris was removed, and 100µl trypsin inhibitor DNase solution (TID) (consisting of 20 ml CMF (10 ml HBSS 10X, 0.2 ml phenol red (0.5% in DRBS), 0.46 ml Sodium bicarbonate (7.5%), 60 mg BSA, 5 mg Soybean Trypsin Inhibitor, 0.2 ml Magnesium sulphate (3.8%)) was added to the cell suspension and triturated. Cells were counted, and cell suspension was diluted in supplemented NBA (2% B27 supplement, 0.25% L-Glutamine, and 0.5% gentimicin), and diluted to 3,000 cells/ml ready for plating in poly-D-lysine and laminin coated 8-well chamber slides (Fisher Scientific: 16260661).

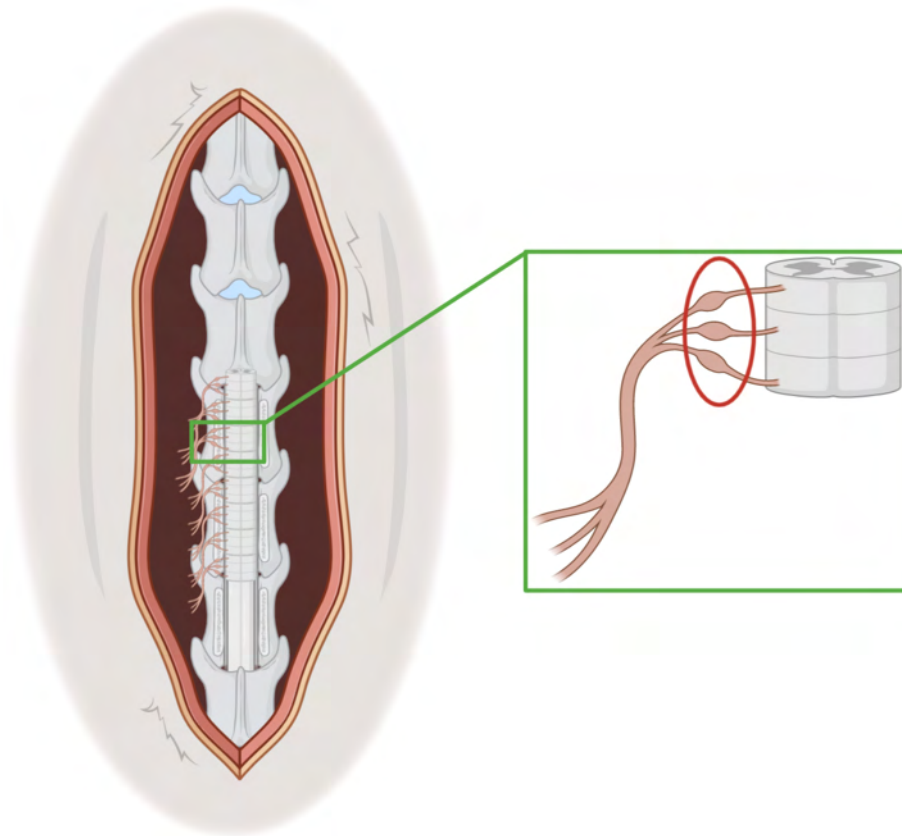


Figure 2-9 A diagram illustrating the identification of DRG after removal of the vertebrae from the dorsal side of rat.

DRG protrude from the spinal cord and are located nestled between vertebrae. The ganglia circled in red are dissected as close to the bulbs as possible. Made using biorender.com.

2.2.1.2 *Rat primary astrocytes*

Frozen rat primary astrocytes (N7745-100, Invitrogen) were thawed from frozen by swirling cryovial in a 37°C water bath, without submerging, and removed once the last bit of ice had melted. A 15ml centrifuge tube was then prewet with astrocyte media (Dulbecco's Modified Eagle Medium (DMEM) + 10% FBS + 1% N-2), and the media discarded. The cell suspension was added to the prewet centrifuge tube dropwise, followed by dropwise addition of 1mL warmed astrocyte media, and then 3mL astrocyte

media to make up 5mL of diluted cell solution. To remove the dimethyl sulfoxide (DMSO) from storage, the solution was centrifuged at 290 x g for 5 minutes, and the supernatant removed. Cells were resuspended in 2-3mL of warmed astrocyte media, counted, adjusted in volume for required cell density ($1 \times 10^4/\text{cm}^2$) and as appropriate (i.e in a T25 flask, 5ml containing 25×10^4 cells required). Cells were incubated in 36°C chamber (95% humidified, 5% CO₂). The media was changed 24 hours later when the cells had adhered, and then every other day.

2.2.1.3 *Human induced pluripotent stem cell (hiPSC)-derived astrocyte derivation*

2.2.1.3.1 *hiPSC establishment, culture, and colony formation*

HiPSCs were purchased from Applied StemCell, Inc. (Project C1815), which were genetically modified using CRISPR-Cas9 technology to introduce an iPS cell line with a eGFP reporter at the AQP4 locus. The following information was taken directly from the Applied StemCell Inc project final report. “ASE9209 cells were cultured and electroporated with gRNA C1815_AQP4_g1, Cas9, and C1815_AQP4_g1_donor. After stable puromycin selection for 10 days, a small portion of the cell culture, presumably with mixed population, was subjected to genotype analysis. Once the mixed culture showed eGFP insertion, it was subjected to single cell cloning process. In brief, the mixed culture was diluted to less than one cell/200µl culture media and dispersed into each well of a 96-well plate. The cells were allowed to grow for 4 to 6 weeks. Cells derived from such single cell cloning process were subjected to genotype analysis. PCR products were further purified and sequenced using Sanger to identify desired clones. Two heterozygous clones (14 and 23) were found to carry the desired

eGFP knock-in. Then the correct clones were subjected to expansion. After expansion, a portion of the cells were submitted to Sanger Sequencing to confirm their genotype. The cells were further cryopreserved in liquid nitrogen, ~ 1×10^6 cells per vial.”

Upon arrival, the hiPSCs were thawed, diluted dropwise into 9mL of pre-warmed StemFlex™ medium with swirling, and centrifuged for 5 min at 200g at 4°C. Media was aspirated, and the cell pellet was resuspended by gentle flicking in 3mL StemFlex™ medium + 10 µM Rock Inhibitor (Y-27632) and plated onto 3 wells of a 6-well plate pre-coated in Geltrex™. The media was changed within 16hrs of plating to StemFlex™ medium only, and then further changed daily until colonies begin to merge.

When colonies of hiPSCs started to merge, cells were incubated in 1 mL of 0.5 mM EDTA (in PBS) for 2-3 mins at 37°C. When cells at the edges of the colonies started to detach, EDTA solution was removed and replaced with 1mL StemFlex™ medium. Cells were then pipetted up and down gently 2-3 times to break into smaller clumps. Cells were then plated in a 1:6 dilution to fresh Geltrex™-coated wells of a 6-well plate.

2.2.1.3.2 *Neural progenitor cell (NPC) induction and maintenance*

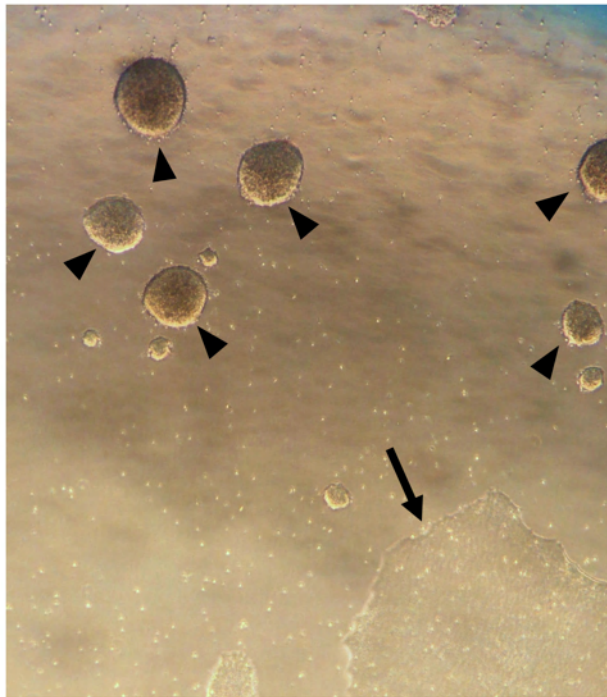


Figure 2-10 Phase contrast image demonstrating the visual difference between hiPSC colonies (arrow) and potentially differentiated hiPSCs (arrowheads).

Areas of potential iPSC differentiation were identified down the microscope as regions outside of colonies (arrowhead; Figure 2-10). These were demarcated using a felt pen, and were removed by scraping with a 200 μ L pipette tip. Undifferentiated colonies of hiPSCs (arrows; Figure 2-10) were then washed x1 with PBS, and incubated with StemPro® Accutase® (Gibco) at 37°C for 8-10 minutes. Cells were triturated with a 1000 μ L pipette tip 3-5 times to dissociate cells, transferred to a 15mL conical tube, topped up with 9mL DMEM/F-12 with 15 mM HEPES, and centrifuged at 300 x g for 5 minutes. Supernatant was aspirated and resuspended in 1mL STEMdiff™ Neural Induction Medium + SMADi + 10 μ M Y-27632 before being counted using Trypan Blue and a hemocytometer. Cell solution was made up to a concentration of 1 x 10⁶ cells/mL

and 2mL plated per wells of a 6-well plate pre-coated with Geltrex™. Media was changed daily to 2mL/well STEMdiff™ Neural Induction Medium + SMADi until ready to passage. After approximately 7 days, iPSC-NPCs were passaged 1:3 using the same method as above (yielding a cell solution with approximate concentration of 1×10^6 cells/mL) and plated on Geltrex™-coated wells of a 6-well plate. At passage 3, cells were plated in STEMdiff™ Neural Progenitor Medium at a density of about 1.25×10^5 cells/cm² on Geltrex™-coated wells of a 6-well plate, and the media changed daily. Full differentiation timeline can be observed in Figure 2-11.

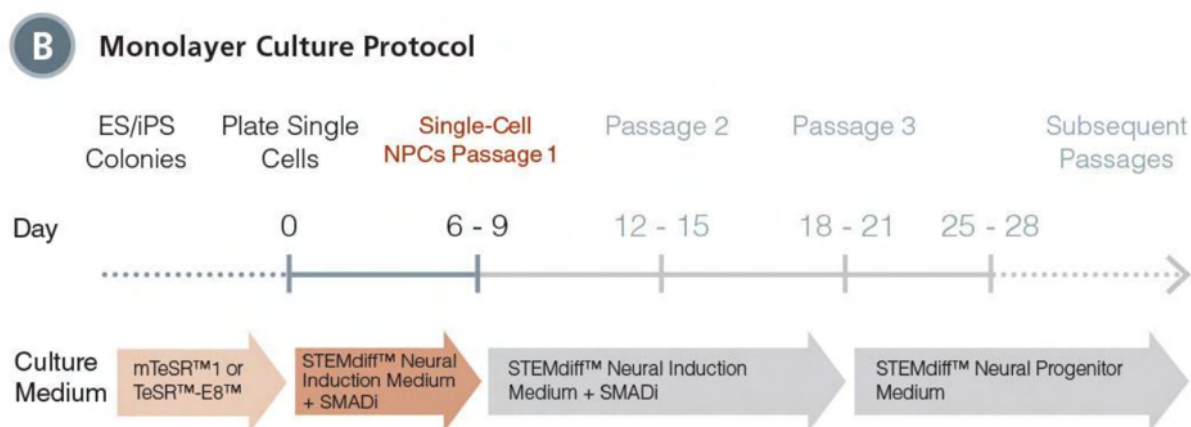


Figure 2-11 Schematic of NPC monolayer culture protocol.

Taken from the technical manual for “Generation and Culture of Neural Progenitor Cells using STEMdiff™ Neural System” associated with STEMdiff™ SMADi Neural Induction Kit (STEMCELL™ Technologies; catalog #08581).

2.2.1.3.3 hiPSC-derived NPCs to astrocyte differentiation

A population of replicative astrocytes were differentiation from the hiPSC-derived NPCs according to the protocol developed by TCW et al., (2017). hiPSC-derived NPCs

were detached using accutase, diluted to 10mL with DMEM (Gibco), centrifuged at 400 x g for 5min, and seeded as dissociated single cells after pipetting 3-5 times with a p1000 pipette at 15,000 cells/cm² on matrigel-coated plates in NPC maintenance medium. The following day, NPC maintenance medium was switched to fully supplemented astrocyte medium (ScienCell kit: 1801, astrocyte medium + 2% fetal bovine serum, astrocyte growth supplement and 10U/ml penicillin/streptomycin solution). From day 2, cells were fed every 48 hours for 20-30 days and split at 90-95% confluency (approximately every 6-7 days) to the initial seeding density (15,000 cells/cm²). At day 30, cells were split and seeded into either flasks for expansion, 6-well plates to lyse with RIPA buffer for Western blot, or into wells of 8-well chamber slides (Fisher Scientific: 16260661) for immunocytochemistry.

2.2.2 Immunocytochemistry

Cells plated into 8-well chamber slides were washed and fixed with either 4% paraformaldehyde, 4% formaldehyde, or 2% formaldehyde for 20 minutes at room temperature. Samples were then blocked with 3% BSA in 0.5% TritonX-100, and incubated overnight at 4°C in primary antibody solution (primary antibody diluted in 0.5% PBS-Tween20). The following day, cells were washed x3 with PBS and incubated for 2 hours at RT in the dark with secondary antibody solution. Cells were then washed again X3, the chambers removed, and a coverslip was mounted on top using VECTASHIELD® Antifade Mounting Medium with DAPI (Vector Laboratories: H-1200-10).

2.2.3 Primary rat astrocyte transfections

2.2.3.1 *Polyethylenimine (PEI)*

To transiently transfect primary rat astrocytes, eGFP-AQP4 cDNA (0.5µg per well of a 24-well plate) was added to serum-free media (30µl per well), followed by varying amounts of 1mg/mL PEI (0.5 to 3µL/well). The mixture was pulse vortexed for 10 seconds, incubated at room temperature for 10 mins. Solution was then added to 150µL/well media with serum. Cell culture medium was aspirated from cells and the transfection mix was gently added (180 µL/well). Cells were incubated at 37°C for 2 hours, and then topped up with 500µL/well full media. Cells were then placed into a Cell-IQ® automated cell culture and analysis machine at 37°C and 5% CO₂ to be imaged.

2.2.3.2 *Lipofectamine*

To transiently transfect primary rat astrocytes, 2.5µg eGFP-AQP4 cDNA was added to 250µL serum-free media. In separate eppendorfs, each containing 50µL serum-free media, different amounts of Lipofectamine-2000 reagent was added (2, 3, 4, 5µL/well). 50µL of the DNA solution was then added to each of the Lipofectamine solution (1:1 ratio) and incubated for 5 min at RT. 50µL was added to each well, and the media topped up with 450µL/well after 3-4 hours. At this time, were placed into a Cell-IQ® automated cell culture and analysis machine at 37°C and 5% CO₂ to be imaged ever 12 hours at x10 magnification using both phase-contrast and epifluorescent microscopy to detect the eGFP-AQP4 expressed.

2.2.4 In vitro assays

2.2.4.1 DRG neurite outgrowth assay

DRG cultures were allowed to settle and adhere to slides overnight, before being washed with PBS three times, and cultured for 3 days with relevant treatment medium. After 3 days, cells were washed x3 with PBS, and fixed at RT for 20 minutes with 4% PFA. Cells were washed and immunostained for β -III tubulin using the protocol detailed in section 2.2.2. Mounted cells were then imaged using an upright epifluorescent microscope (Zeiss) at 10x magnification. Each chamber well was divided into 9 squares, and the most central DRG neuronal body within the first field of view identified within each square was selected as the DRG imaged per square (Figure 2-12A). Images of complete DRGs and their processes were stitched together using Photoshop©. The length of each neurite of each DRG was measured using ImageJ (Figure 2-12B).

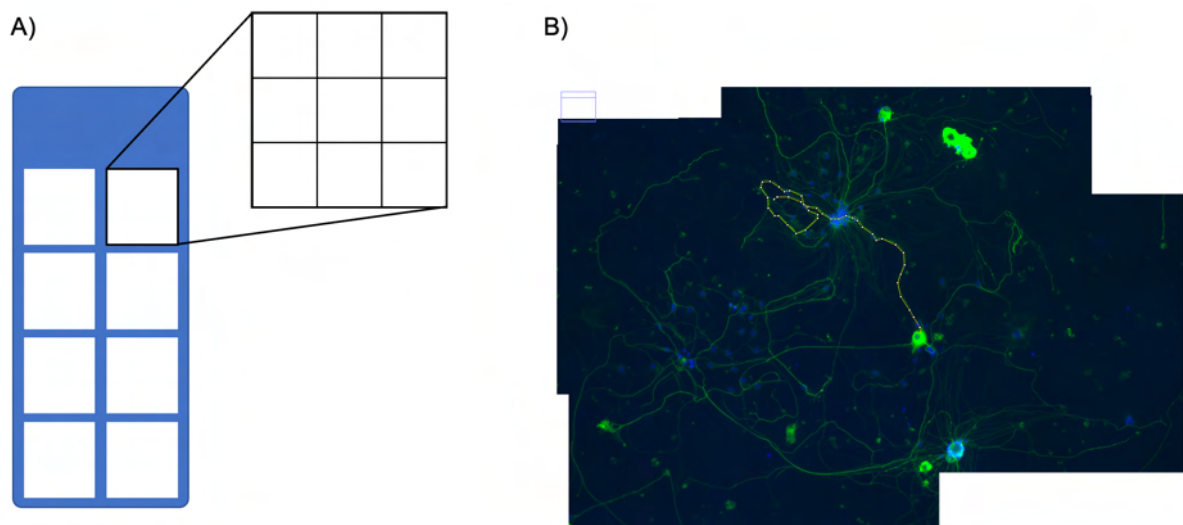


Figure 2-12 Methodology for selecting and measuring DRGs for neurite outgrowth assays.

(A) Each well of the 8-well chamber slides were divided into 9 sections. Within each of these sections, one DRG was selected to measure. (B) The neurites of each DRG were measured by drawing a segmented line along the neurite length, as determined by positive green fluorescence from anti- β -III tubulin immunostaining.

2.2.4.2 *Astrocyte scratch assay*

2.2.4.2.1 *Proliferation and viability determination*

To compare proliferation rates and cell viability across treatment groups, primary rat astrocytes plated in 24-well plates in standard rat astrocyte media (DMEM, 4.5g/L glucose, with L-glutamine and sodium pyruvate + 20% fetal bovine serum) until approximately 50-60% confluent. At t=0, the time of treatment, 3 wells were washed, detached using accutase, and the live/dead cells were respectively counted as baseline (100%) using a manual haemocytometer. The media on other wells was then changed to either standard rat astrocyte media with or without TFP/H-89 treatment, rat astrocyte media with only 1% serum, or AWESAM media (50% DMEM, 50% Neurobasal-A supplemented with B27, HB-EGF and Glutamax), as developed by Wolfes and Dean, (2018). After 96hrs, cells were washed with PBS, detached with accutase, and the live/dead cells were counted using a manual haemocytometer. From this, the proliferation rate was calculated as percentage increase in cell number counted at 96hrs across each treatment group relative to the baseline. Viability was counted as a percentage of cells counted that were alive.

2.2.4.2.2 *Cytotoxicity assay*

To measure any cytotoxicity of the inhibitors used, cells were cultured in 96-well plates until confluent. The media was then changed to various dilutions of each inhibitor in AWESAM media, and incubated at 37°C, 5% CO₂ for 96hrs. Each well was washed x3 with PBS, and the media replaced with 10µL 3-(4,5-dimethylthiazol-2-yl)-2,5-diphenyltetrazolium bromide (MTT) + 90µL AWESAM media and further incubated for 3 hrs. Each well was then washed with PBS, and 100µL of DMSO added to solubilize intracellular crystals formed. The plate was covered in tin foil and placed on a rocker for 20 minutes, and the absorbance read on a BMG Labtech LUMIstar Omega plate reader at 590nm.

2.2.4.2.3 *Scratch assay and quantification*

Primary rat astrocytes were plated in 24-well plates and cultured at 37°C and 5% CO₂ until 100% confluent. The confluent layer of cells was scratched evenly down the middle of the well using the tip of a 200µL pipette tip. A fresh pipette tip was used for each well to minimize deposition of lifted cells. Each well was then washed with PBS to remove any debris, and respective treatment added. Cells were then put into a Cell-IQ® automated cell culture and analysis machine (CM Technologies, Finland), and an area of 2,982 x 2,223µm covering the scratch area was programmed to be imaged every 6 hours over a 96 hour period. Images were then obtained and the area within the scratch at the start and end of the run were quantified to compare the area migrated across treatment groups. Area was quantified using the polygon section tool on ImageJ (Figure 2-13).

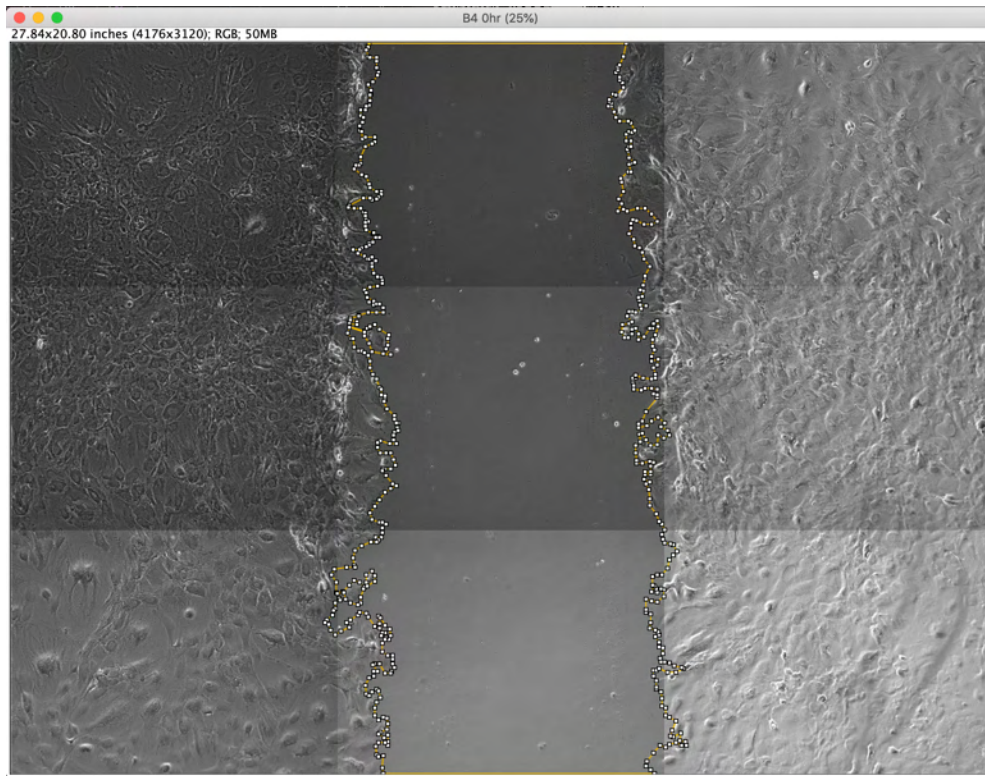


Figure 2-13 A screenshot of the ImageJ window, demonstrating the area measured using the polygon tool to demarcate the scratch area of primary rat astrocytes.

2.2.4.3 *Transwell migration assay*

2.2.4.3.1 *Migration assay*

Primary rat astrocytes were seeded into the upper chamber of a transwell insert within 24-well plates. The lower part of the chamber inside the well then contained astrocyte medium with either 1% or 20% serum (as in Figure 2-14a). 20% serum in the lower chamber would act as a chemoattractant for migration to the cells within the top compartment, whereas 1% serum in the lower chamber would not facilitate any chemoattraction (positive and negative controls, respectively). Plates were then cultured at 37°C and 5% CO₂ for 24 or 48hrs, after which the transwell inserts were

removed from the wells, and placed into fresh wells containing PBS. The media in the upper chamber was removed, and any remaining cells on the upper side of the transwell were removed by scraping with a cotton bud.

2.2.4.3.2 *Cell counting of transwell membrane*

After the cells in the upper level of the membrane (non-migrated cells) were removed, cells in the bottom chamber were washed once in PBS fixed by placing the membrane into a fresh well containing 4% PFA for 10 minutes at RT. The membrane was then washed again x3 with PBS, and the membranes removed using a scalpel. Membranes were then sandwiched between a glass slide and a coverslip using Vectashield mounting medium with DAPI to visualize the nuclei. Membranes were then imaged using an inverted epifluorescence microscope at 10x magnification, and 10 randomized fields of view were imaged across the membrane. The number of nuclei per field of view was then manually counted using ImageJ, and cell counts across the 10 fields of view per membrane were averaged.

2.2.4.3.3 *Calcein-AM fluorescence*

As depicted in Figure 2-14, after 24 hours of migration, transwells were moved into fresh wells containing 8 μ M calcein-AM in 1% serum media and incubated for 45 minutes to allow the cells on the bottom side of the membrane to take up the calcein-AM. The transwell was then washed x1 in PBS, and transferred into a fresh well containing accutase up to the volume just in contact with the lower side of the transwell membrane (approx. 300 μ L), and incubated for 10 mins to detach cells on the lower

half of the transwell membrane (migrated cells). Detached cells in accutase solution were then added to wells of black-walled 96-well plates in triplicate, and the calcein fluorescence was measured using a fluorimeter at ex/em 494/517nm, as a readout of the amount of cells in solution, and therefore the amount of migrated cells.

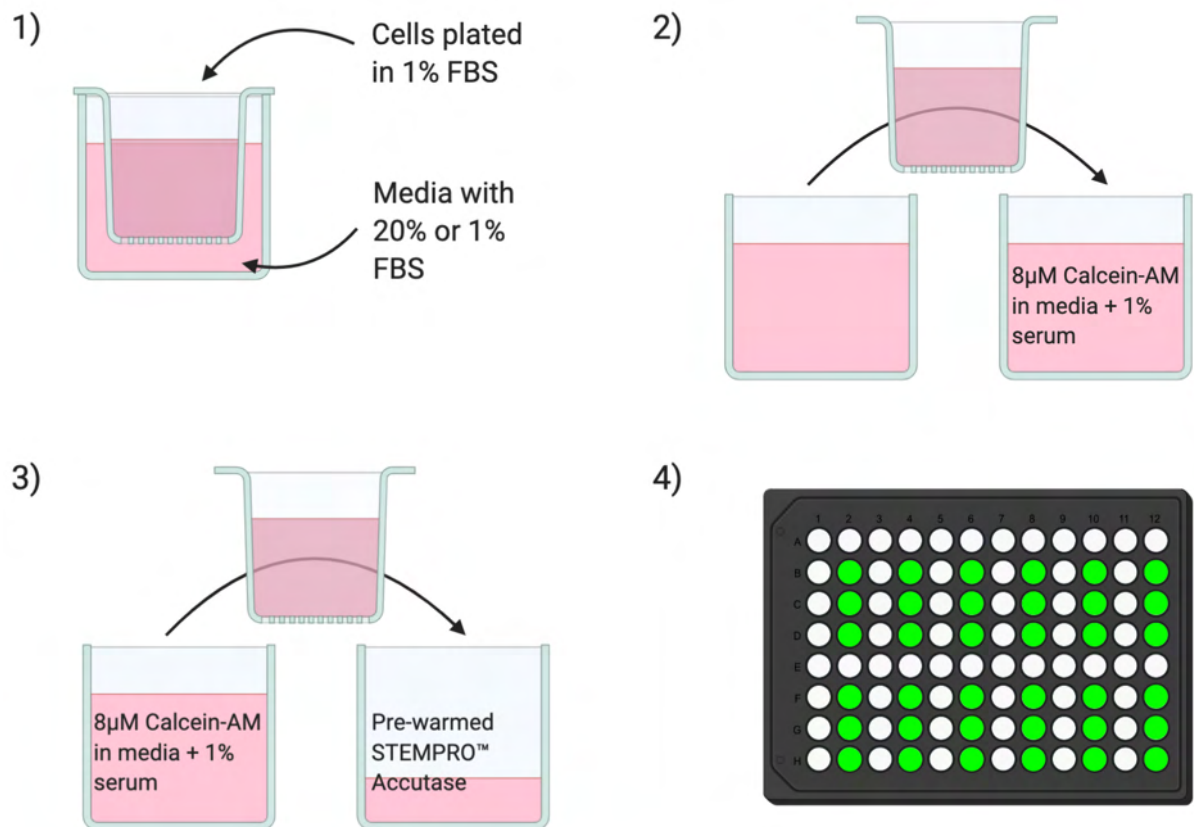


Figure 2-14 A schematic detailing the methodology of quantifying relative number of migrated cells in transwell migration assays using calcein fluorescence.

At the end of the transwell migration experiment, transwell inserts were moved from their culture condition (1) into fresh wells containing calcein-AM (2), incubated for 45 minutes, and placed into fresh wells containing PBS. Inserts were then transferred into fresh wells containing accutase solution (3) and incubated for 10 minutes to detach cells on the lower half of the transwell membrane. Detached cells in accutase solution were then transferred in triplicate to

black-walled 96-well plates for quantification of calcein to determine differences in number of cells in solution (4).

2.3 Statistics

Statistical analysis was performed in SPSS (IBM Corp., Armonk, NY, USA). The data were tested for normality using the Shapiro-Wilk test. For *in vitro* data that were normally distributed, ANOVA with a Bonferroni post hoc test was used to determine statistical differences between means. For *in vivo* data that was normally distributed, analysis of variance (ANOVA) with Tukey (immunohistochemistry) or Benjamini-Hochberg (water content experiments) post hoc tests were used.

Chapter 3

Investigating changes to AQP4 subcellular localization in an in vivo spinal cord injury model

Some of this Chapter is published: Kitchen P*, Salman M*, Halsey A*, Clarke-Band C., MacDonald J.A., Ishida H., Vogen H.J., Almutiri S., Logan A., Kreida A., Al-Jubair T., Missel J.W., Gourdon P., Tornroth-Horsefield S., Conner M.T., Ahmed Z., Conner A.C., Bill R.M. Targeting aquaporin-4 subcellular localisation to treat central nervous system edema. (2020). Cell 181: 1-16. ***Joint first authors.**

3 Chapter 3

3.1 Rationale

AQP4 is one of the major subtypes of AQPs expressed in the CNS (Halsey et al., 2018). In particular, it is highly expressed in astrocytes. AQP4 controls local CNS water homeostasis, both across the blood-brain barrier (BBB), and within the tissue parenchyma (Kimelberg, 2004). Water flow is important to maintain local ionic gradients, which are crucial for neuron conductivity and CNS function. Changes in local osmolarity occur due to release of locally absorbed solutes, such as glucose, or locally released metabolites and ions from neuronal conductivity. AQP4 allows astrocytes to rapidly respond and normalize the local osmolarity, a factor which will affect the ability of neurons to generate action potentials, and thus will affect the functionality of the local systems (Kimelberg, 2004, 2010). How astrocytes respond to these physiological events, and how much AQP4 contributes to local neuroprotection remains unknown. However, AQP4 appears to contribute both pathologically and physiologically in various CNS conditions. AQP4 expression appears to increase after spinal cord injury (SCI), and has been implicated in both the onset and clearance of spinal cord edema in conflicting studies. This has led to the belief that AQP4 is involved in the acute pathological facilitation of edema through cytotoxic swelling of astrocytes, but that its function is important for later clearance of excess water accumulation resulting from remaining compromised blood-spinal cord barrier (BSCB).

AQP4 facilitates water flow by osmosis. This means that water flow across astrocyte membranes depends on a combination of a) the relative osmolarities either side of the

cell membrane; b) the amount of AQP4 present at the membrane; and c) the localization of the AQP4 molecules across the complex morphology of the astrocyte. Whilst it's not possible to examine or interfere with the dynamic fluctuations in local osmolarity, it is possible to determine the molecular mechanisms that might result in changes to expressional regulation and subcellular distribution of AQP4. To this end, it was discovered that AQP4 membrane localization, and consequently astrocyte water permeability, can be regulated in astrocytes by a translocation mechanism of AQP4 between intracellular vesicular stores and the cell membrane (Kitchen et al., 2015; Conner et al., 2012; Salman et al., 2017). Primary astrocytes subject to hypotonicity or hypoxia will increase their surface localization of AQP4, and subsequently their water permeability. The underlying mechanism involves the activity of both calmodulin (CaM) and protein kinase A (PKA), as inhibition of both of these targets resulted in the prevention of AQP4 cell surface translocation (Kitchen et al., 2015).

3.2 Hypothesis and aims

Given that AQP4 facilitates the onset of spinal cord edema through astrocyte swelling, and that under traumatic stimuli, astrocytes increase the amount of membranous AQP4, it was hypothesized that after a SCI, the amount of cell surface AQP4 is increased, and that this can be prevented with treatment of CaM and PKA inhibitors.

The aims of the work presented in this chapter were:

- 1) To determine whether AQP4 is translocated to cell membrane of astrocytes after a traumatic injury *in vivo*, and to quantify this effect
- 2) To determine the anatomical sites of distinct AQP4 relocalization
- 3) To determine whether the proposed mechanism of AQP4 translocation is prevented *in vivo* after traumatic spinal cord injury by treatment with inhibitors of calmodulin or protein kinase A
- 4) To investigate whether inhibition of Calmodulin or PKA activity affects the expression of AQP4 after an *in vivo* spinal cord injury

3.3 Results

3.3.1 Comparing AQP4 membrane distribution across astrocyte cell bodies after traumatic spinal cord injury

To investigate changes in AQP4 localization in vivo, Sprague Dawley rats were subject to a dorsal column crush (DC) SCI, and spinal cords harvested, fixed and sectioned for immunostaining, as outlined in the methods (section 2.1.3.2).

3.3.1.1 *Lesion site identification in spinal cord tissue*

To confirm the success of the dorsal column (DC) crush injury, and to identify the limits of the tissue considered “injured tissue”. To achieve this, every 10 sequential sections obtained were stained for ED1 (CD68), a marker for macrophages which are normally excluded from the CNS, but extravasate into injured spinal cord tissue to contribute to clearance (Damoiseaux et al., 1994). This marker indicates that tissue has been injured, and indicates the limitations of “lesion site” tissue.

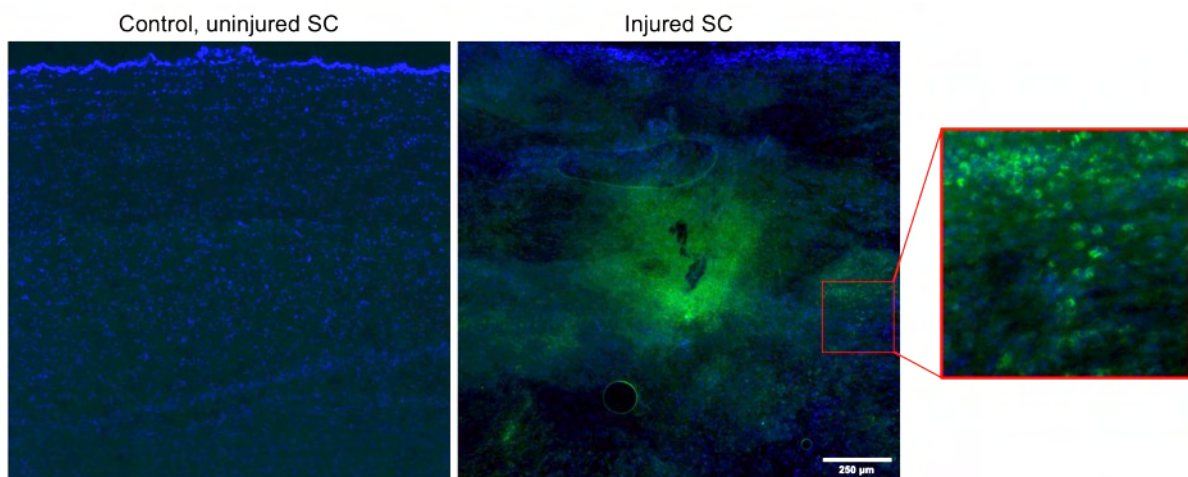


Figure 3-1 Macrophage (CD68; green) immunohistochemistry in rat spinal cord, from either control, uninjured rats or those subject to dorsal column crush injury at 3 days post-injury.

Insert represents higher magnification of boxed region demonstrating macrophage morphology. Blue staining corresponds to DAPI.

3.3.1.2 *Determination of the localization of AQP4 in spinal cord astrocytes using confocal microscopy*

AQP4 has been frequently reported to highly co-localize with GFAP in the spinal cord, however the sub-cellular distribution of AQP4 is mostly reported to exist at the endfeet of astrocytes, but not frequently reported within other areas of the cell membrane (Rash et al., 1998; Mathisen et al., 2010). High-magnification imaging of AQP4/GFAP co-stained spinal cord sections reveals that AQP4 can be found within, or proximal to the membrane of astrocytes at the cell body and in processes (Figure 3-2).

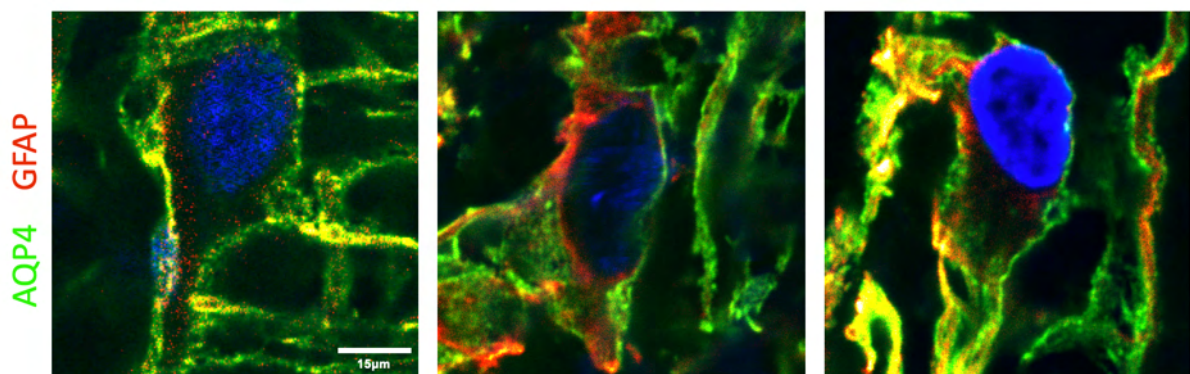


Figure 3-2 Representative images of astrocytes in the uninjured rat spinal cord.

Rat spinal cord tissue was stained for GFAP (red) and AQP4-4 (green) and imaged at 63x with a confocal microscope. Cell nuclei stained with DAPI (blue)

3.3.1.3 *Comparing AQP4 subcellular membrane distribution in astrocyte cell bodies*

Kitchen et al. (2015) demonstrated that when primary rat astrocytes were put under traumatic stress, for example hypotonicity, AQP4 relocalized to the cell membrane, resulting in cytotoxic swelling owing to the increase in water permeability of the cell. AQP4 subcellular distribution was compared between astrocytes imaged from tissue obtained from uninjured, control rats and those subject to a dorsal column crush injury. This was analysed using two independent different methods (see section 2.1.6.2).

Firstly, AQP4 localization was compared by isolating the cell bodies from astrocyte images and determining the co-localization between GFAP (an astrocyte-specific, cytosolic protein), and AQP4 (Figure 3-3). These values can be interpreted as “the amount of AQP4 signal within the GFAP labelled area”. Each of the images were auto-thresholded using Otsu's threshold clustering algorithm (Nobuyuki, 1979), which thresholds to “area of positive signal vs. area of no signal”, to ensure that co-localization was based on location rather than intensity of signal, owing to the fact that GFAP is a protein subject to variation in intensity under varying trauma conditions.

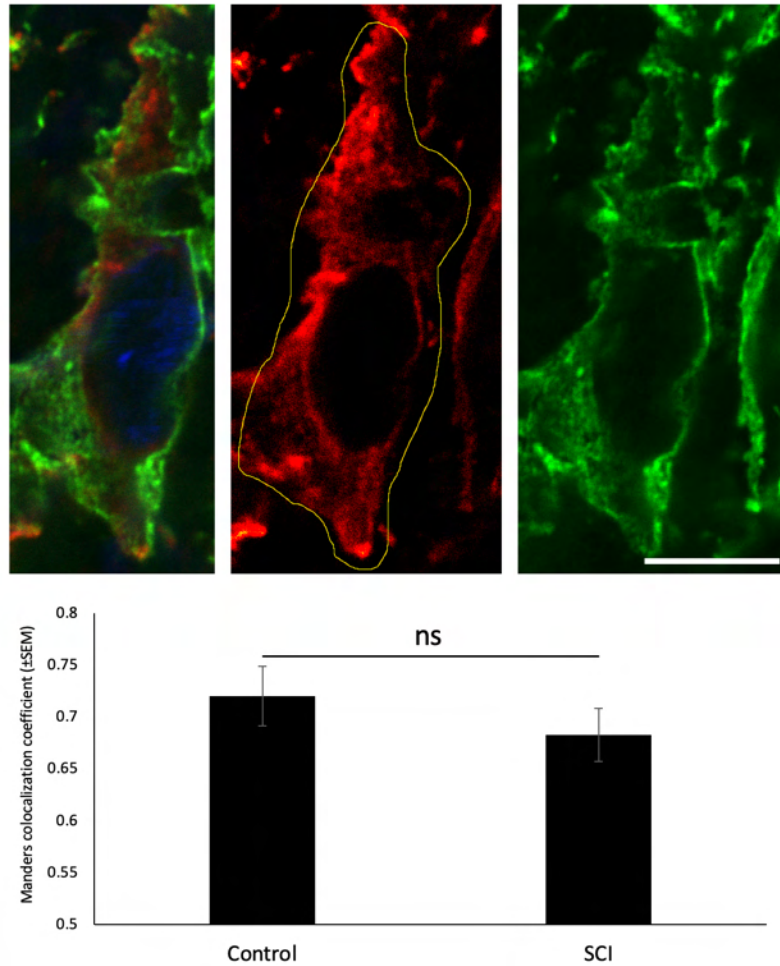


Figure 3-3 Mander's colocalization coefficients describing the abundance of green (AQP4) positive pixels colocalized with red (GFAP) positive pixels in astrocyte images autothresholded with Otsu's threshold clustering algorithm.

(* = $p < 0.05$. Yellow line indicates the area cropped to limit analysis to the astrocyte cell body. Scale bar = $25\mu\text{m}$. Analysed using one-way ANOVA followed by Bonferroni post-hoc test. $n = 3$, minimum of 10 astrocytes analysed per animal).

Secondly, the images were analysed using a method previously published (Kitchen et al., 2015), whereby the fluorescence intensity is recorded linearly across the cell soma (Figure 3-4a). The graph showing the fluorescence intensity readout of AQP4 over distance is shown in Figure 3-4b. The resulting coefficients describe the RME, and

corroborate that there are no significant changes in the amount of AQP4 present at the astrocyte cell membrane relative to amount present intracellularly (Figure 3-4c).

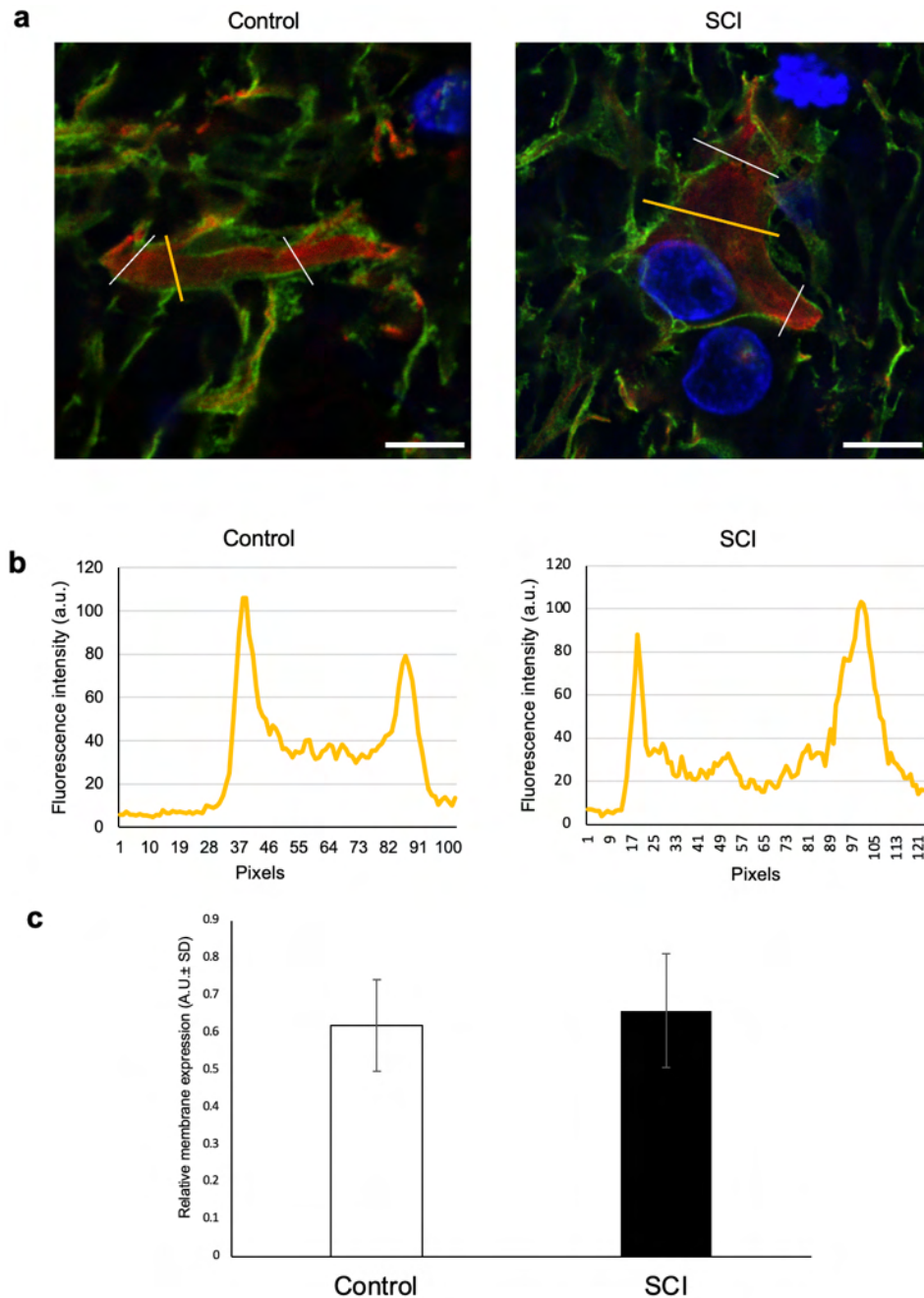


Figure 3-4 Relative membrane expression quantification of confocal images of astrocytes.

(a) Representative images of astrocytes stained for AQP4 (green) and GFAP (red) imaged by confocal microscopy, and examples of where linear readouts were plotted (white lines). (b)

Representative readouts of AQP4 fluorescence intensity across distance from the images in (a). (c) The relative membrane expression of AQP4 in astrocytes across each treatment group.

3.3.1.4 Treatment with TFP produces “punctate” AQP4 staining within astrocytes after DC SCI

Tissue from injured spinal cord treated with TFP at 3 days post-injury (dpi) appeared to exhibit a punctate AQP4 staining pattern within astrocytes, which is not as present within astrocytes imaged in tissue from uninjured or injured, untreated spinal cords. These puncta appear most predominantly within the narrower regions of astrocyte cell bodies where processes begin to form (Figure 3-5, arrows).

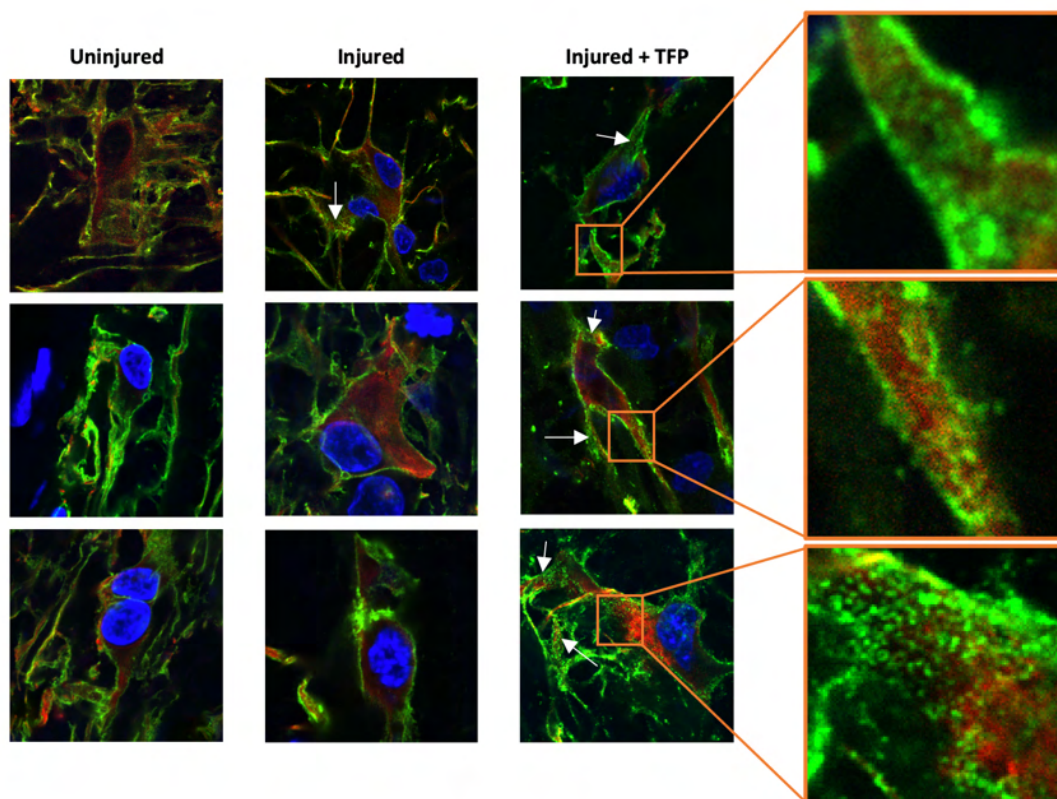


Figure 3-5 Spinal cord tissue immunostained for AQP4 (green), GFAP (red) and DAPI (blue) at 3 dpi.

Three representative images are shown per treatment group. Inserts for TFP-treated group magnify areas where punctate staining can be most identified.

3.3.2 Increased perivascular AQP4 was significantly reduced in vivo by treatment with calmodulin or PKA inhibitors

3.3.2.1 Increased AQP4 in astrocyte endfeet processes surrounding blood vessels after spinal cord injury at 3, but not 7 days after injury

At 3 dpi, there appeared to be an increased amount of AQP4 fluorescence surrounding many of the blood vessels in tissue obtained from injured rats compared to non-injured rats (Figure 3-6; white arrows identify astrocyte processes physically associated with endothelia, and were therefore assigned as astrocyte endfeet). This was quantified by measuring the fluorescence of AQP4 surrounding blood vessels, and normalizing to the fluorescence of AQP4 in non-vessel associated membrane (Figure 3-6; arrowheads). The amount of AQP4 surrounding blood vessels was significantly higher ($151.3 \% \pm 15.7\%$ of uninjured) in injured spinal cord tissue, suggesting that AQP4 relocalizes to astrocyte end-feet in response to injury. All sized blood vessels were included in the analysis. To note, the morphology of the AQP4-containing structures also appeared to change after injury in many of the images taken; at 3dpi, the AQP4-containing processes appeared to be much thicker and sparser. By 7dpi, AQP4 staining appeared to remain sparse, but the density of the processes appeared to be reduced (Figure 3-6).

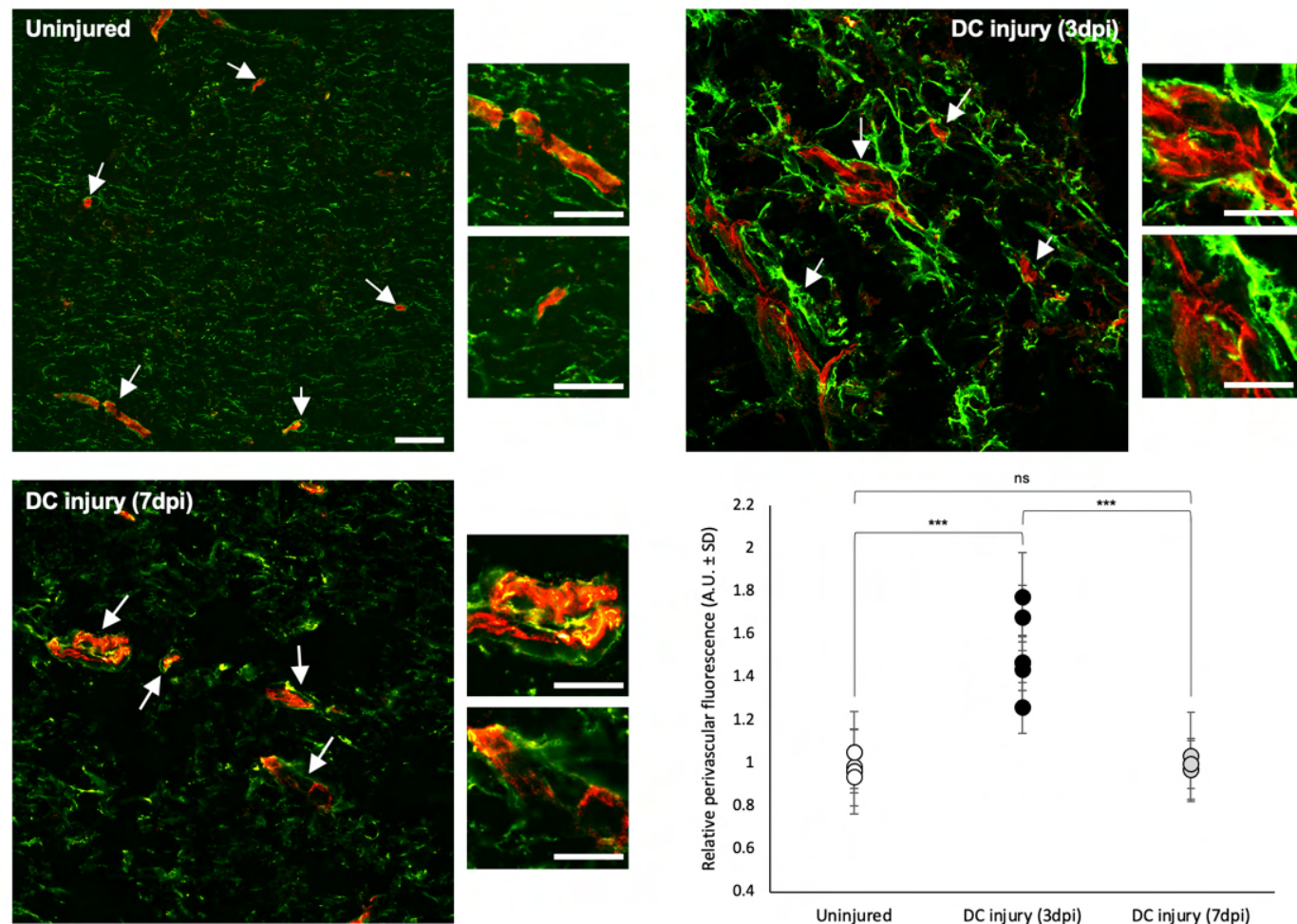


Figure 3-6 Confocal images of rat spinal cord tissue stained for RECA-1 (red) and AQP4 (green).

DC + Vehicle = dorsal crush + intraspinal injection of PBS (vehicle). Images shown are representative. Arrows indicate areas of sites used to quantify perivascular AQP4. Quantification of the relative fluorescence intensity of AQP4 (AQP4 intensity associated with RECA-1/AQP4 intensity not associated with RECA-1). Scale bars: 50µm, or 25µm for inserts. *** = $p < 0.001$.

3.3.2.2 *Increased AQP4 fluorescence is specific to perivascular sites within the lesion epicentre*

In addition to quantifying the perivascular fluorescence intensity of AQP4 within the lesion site, as in section 3.3.2.1, the perivascular fluorescence was also calculated in regions of injured tissue away from the lesion site for comparison. The distance selected was determined as that which was confidently outside the epicentre of the largest observed lesion area from all sections stained for CD68 (macrophages, as in section 3.3.1.1). The relative perivascular fluorescence of AQP4 surrounding blood vessels away from the lesion site was not significantly higher than in uninjured tissue (Figure 3-7; 0.945 ± 0.043 to 0.9909 ± 0.049), but was significantly less than the perivascular fluorescence observed within the lesion site (Figure 3-7; 0.945 ± 0.043 to 1.513 ± 0.184), suggesting that this effect is limited to the directly injured tissues at 3dpi.

In accordance with the literature (Okłinski et al., 2014), under physiological conditions, AQP4 localisation appears most significantly at the glial limitans (Uninjured, Figure 3-8), an area rich in AQP4-anchoring proteins such as laminin. Immunohistochemistry of spinal cord tissue from demonstrates that the strong glial limitans expression of AQP4 that exists in uninjured spinal cord (Figure 3-8; arrows) is actually diminished after injury, with AQP4 localization appearing more in the spinal cord parenchyma (Figure 3-8; DC injury group, arrowheads). This suggests that the relocalization directionality of AQP4 is a site-specific response towards the vasculature, and not simply determined by the presence of basement membrane proteins that are also present at the glial limitans.

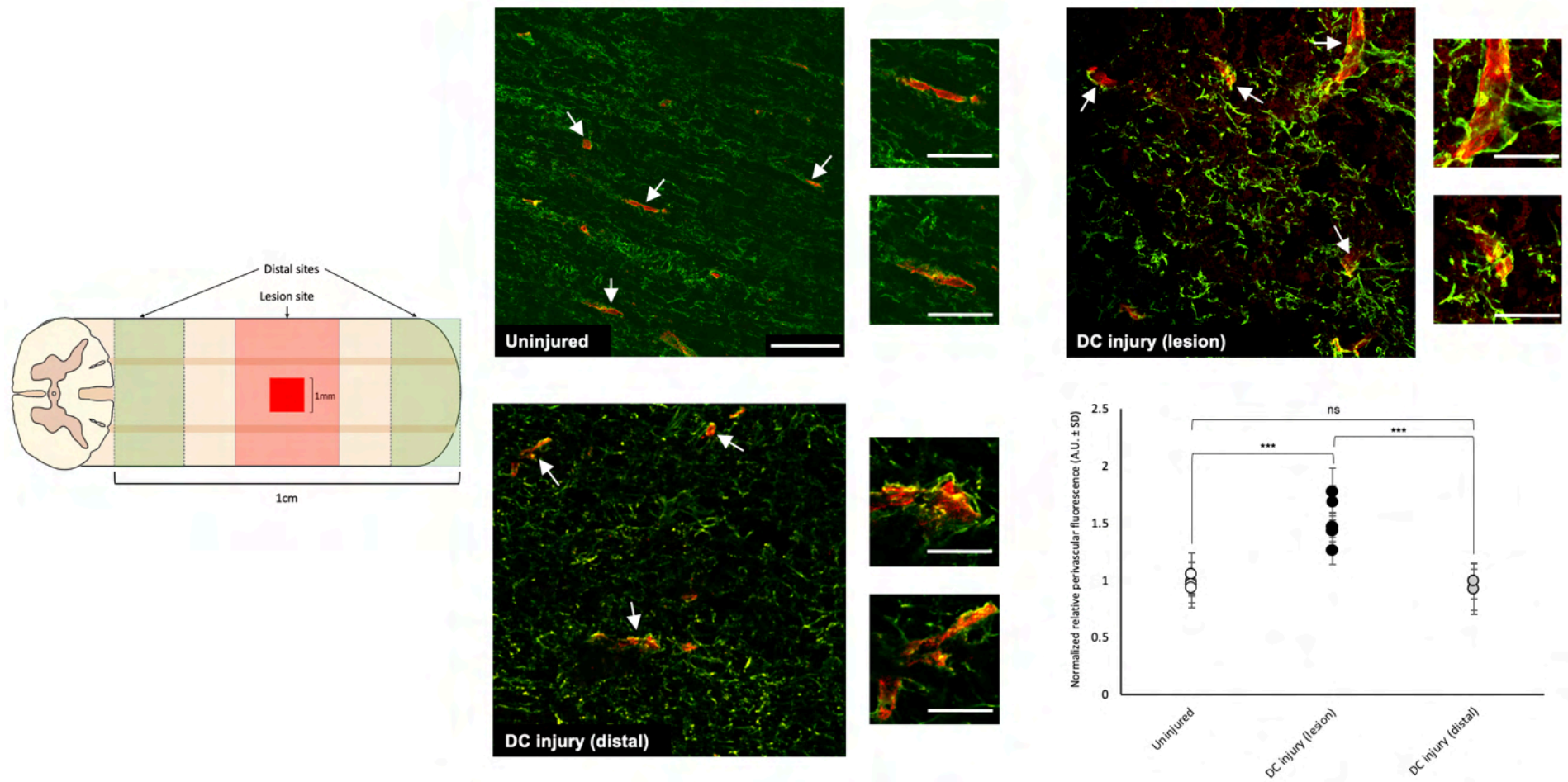


Figure 3-7 Confocal images of rat spinal cord tissue stained for blood vessels (RECA-1; red) and AQP4 (green).

DC + Vehicle = dorsal crush + intraspinal injection of PBS (drug vehicle). Images shown are representative. Arrows indicate areas of sites used to quantify perivascular AQP4. Quantification of the relative fluorescence intensity of AQP4 (AQP4 intensity associated with RECA-1/AQP4 intensity not associated with RECA-1). Scale bars: 50µm, or 25µm for inserts. *** = $p < 0.001$

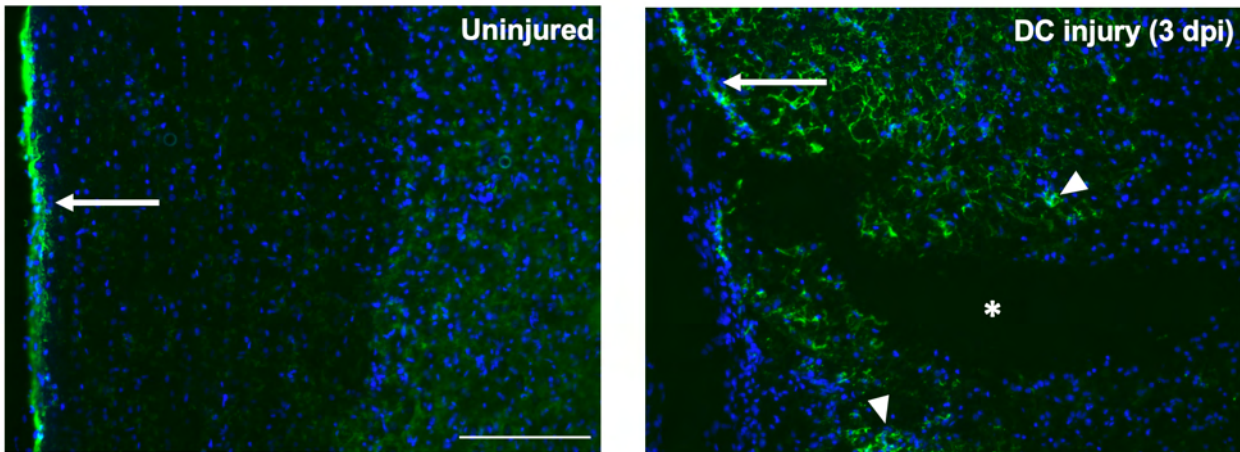


Figure 3-8 Rat spinal cord tissue dissected from each treatment group labelled for AQP4 (green) and imaged at 10x magnification.

Arrow indicates the localization of the glial limitans. Arrowheads indicate areas of increased tissue AQP4 fluorescence. Asterix indicates primary lesion site. Scale bar = 500 μ m.

3.3.2.3 *Treatment with calmodulin (CaM) inhibitors or protein kinase A (PKA) inhibitors prevents the increase in perivascular AQP4*

Previous data indicates that AQP4 subcellular relocation is regulated intracellularly through a mechanism dependent on both CaM and PKA (Kitchen et al., 2015). Quantification of perivascular AQP4 demonstrates that the significant increase observed in injured tissue (DC injury) compared to uninjured tissue at 3 dpi (Figure 3-9; 1.513 ± 0.184 to 0.9909 ± 0.049) was not observed in tissue from animals treated with either CaM inhibitor TFP (Figure 3-9; 1.035 ± 0.079) or PKA inhibitor H-89 (Figure 3-9; 1.025 ± 0.061). Data from either inhibitor treatment groups demonstrated no statistical difference from the uninjured group.

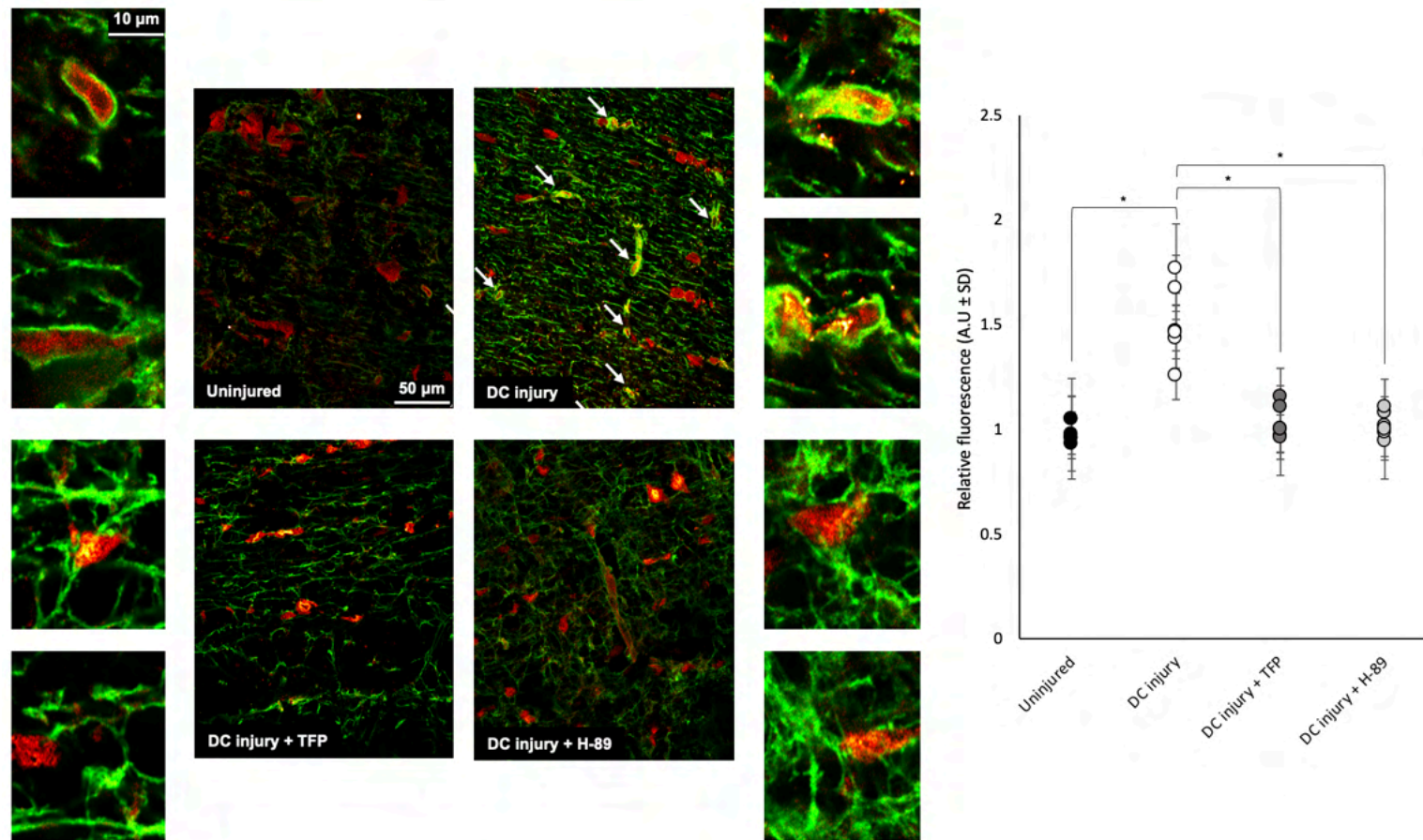


Figure 3-9 Confocal images of rat spinal cord tissue stained for blood RECA-1 (red) and AQP4 (green) and quantified for perivascular AQP4. DC + Vehicle = dorsal crush + intraspinal injection of PBS (drug vehicle); DC + CaMi = dorsal crush + intraspinal injection of CaMi trifluoperazine; DC + PKAi = dorsal crush + intraspinal injection of PKAi H-89. Images shown are representative. Arrows indicate regions of dense perivascular AQP4 localization. Quantification of the relative fluorescence intensity of AQP4 (AQP4 intensity associated with RECA-1/AQP4 intensity not associated with RECA-1).

3.3.3 Changes in total AQP4 protein

3.3.3.1 Western blot of AQP4 in spinal cord tissue after DC injury

Western blot revealed that the AQP4 protein band density from injured spinal cord tissue was significantly higher than from uninjured spinal cord tissue at 1dpi (Figure 3-10; 3.77 ± 0.72 to 1.00 ± 0.06). AQP4 band density was significantly lower in the TFP-treated group than in the vehicle-treated injury group (Figure 3-10; $1.15 \pm 3.77 \pm 0.72$), but not in the H-89-treated group (1.63 ± 0.62). The AQP4 band densities from tissue of either TFP or H-89 treated cord were significantly different to that of uninjured cords.

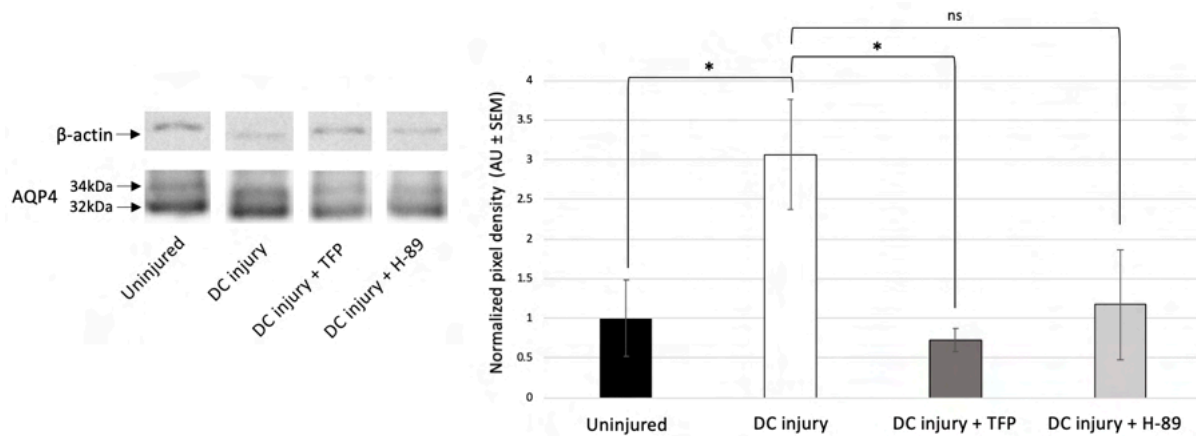


Figure 3-10 Western blot of tissue lysates obtain from rat spinal cords.

Treatment groups: DC + Vehicle = dorsal crush + intraspinal injection of PBS (drug vehicle); DC + CaMi = dorsal crush + intraspinal injection of CaMi trifluoperazine; DC + PKAi = dorsal crush + intraspinal injection of PKAi H-89. * = $P < 0.05$, $n = 3/\text{group}$. Quantification demonstrates densitometry of both 34kDa and 32kDa bands of AQP4 normalized to loading control (β -actin).

3.3.3.2 *Fluorescence intensity of AQP4 in spinal cord tissue after DC injury*

In support of the previous finding, images obtained from spinal cord tissue immunolabelled for AQP4 were quantified to determine differences in fluorescence intensity between treatment groups. Results indicated that the overall fluorescence of AQP4 is varied between each of the treatment groups, with images from the injured, untreated group being the most significantly fluorescent. Quantification of AQP4 fluorescence (fluorescence/area) confirmed that the overall fluorescence of AQP4 within the lesion site of injured, untreated tissue was significantly higher than in uninjured cord tissue (Figure 3-11; 2.08 ± 0.73 to 1.00 ± 0.26). Tissue from within the lesion site of both TFP- or H-89-treated animals exhibited significantly less AQP4 immunofluorescence compared that of injured, untreated tissue (Figure 3-11; 1.25 ± 0.28 , or 1.16 ± 0.29 , respectively), but not different to that of uninjured tissue.

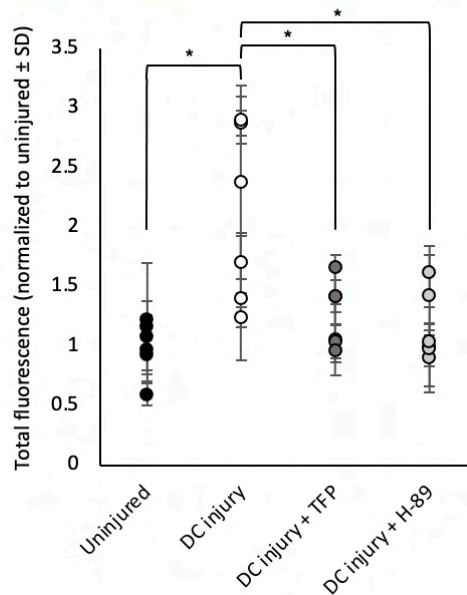
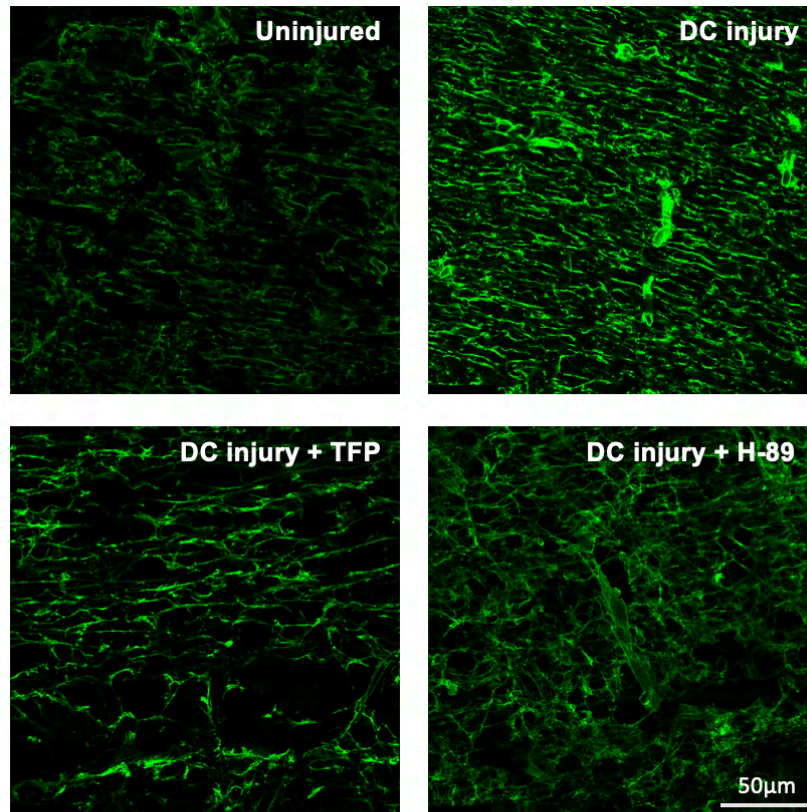


Figure 3-11 Confocal images of rat spinal cord tissue immunostained for AQP4 (green).

DC + Vehicle = dorsal crush + intraspinal injection of PBS (drug vehicle); DC + CaMi = dorsal crush + intraspinal injection of CaMi trifluoperazine; DC + PKAi = dorsal crush + intraspinal injection of PKAi H-89. Images shown are representative. Scale bar = 50µm. Quantification represents fluorescence intensity within the lesion site, or location matched area, across each of the treatment groups. * = P<0.05, n = 6/group.

3.3.3.3 *Foxo3a nuclear localization after spinal cord injury is prevented by treatment with TFP or H-89*

Forkhead box O3 (Foxo3a) is a nuclear transcription factor that regulates, among other things, the expression of AQP4, and has been shown to become localized to the nucleus of astrocytes in a TBI model that also demonstrates AQP4 upregulation and cerebral edema (Kapoor et al., 2013). In accordance with this evidence, Foxo3a appeared to become significantly localized to nuclei after spinal cord injury (Figure 3-12; DC injury). This effect is not observed in tissue obtained from uninjured animals, or animals subject to DC injury treated with inhibitors of CaM or PKA (Figure 3-12; Uninjured, DC injury + TFP, DC injury + H-89, respectively).

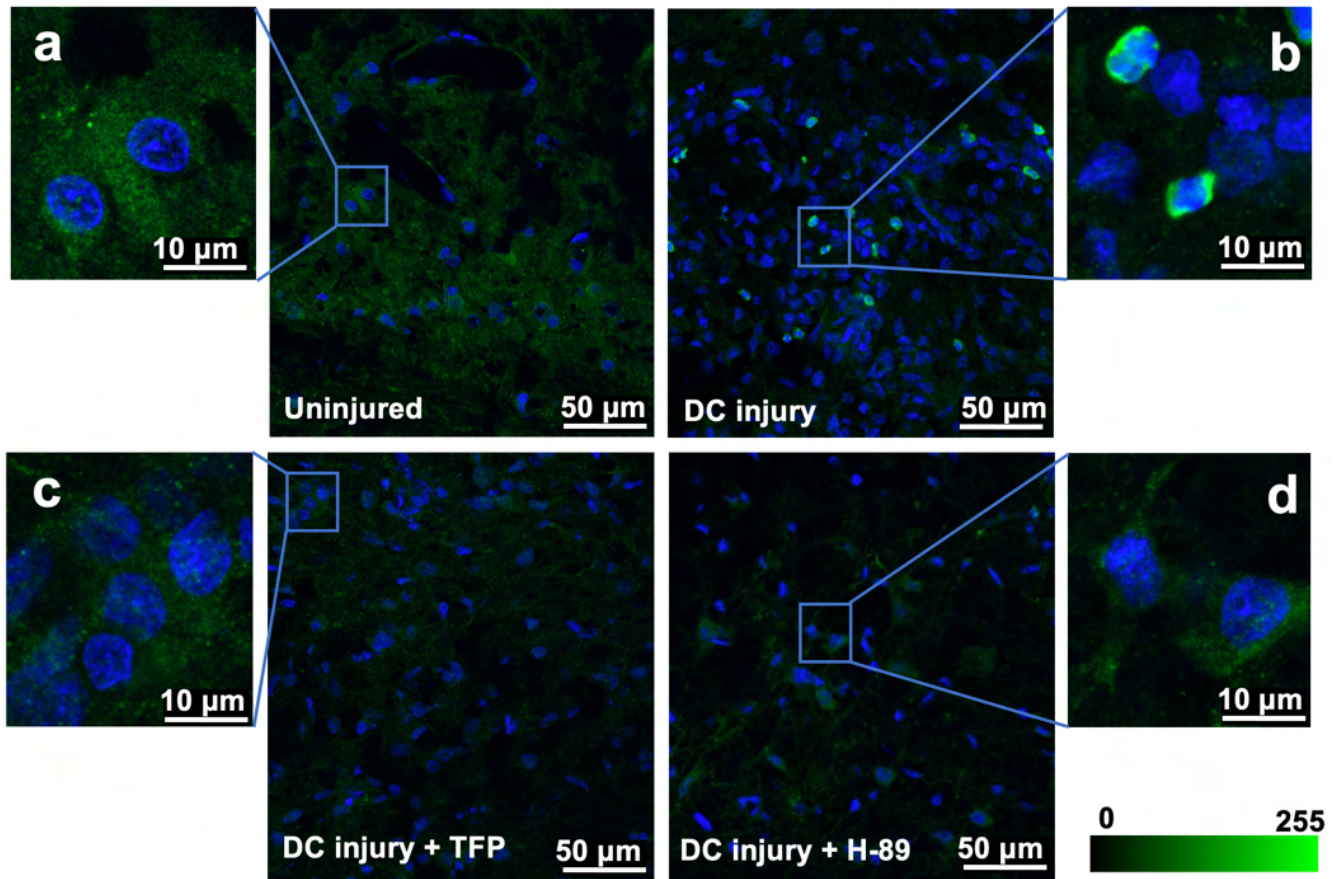


Figure 3-12 Immunofluorescence micrographs of rat spinal cord tissue stained for Foxo3a (green) and DNA (DAPI, blue) 3 days after dorsal column (DC) crush.

Treatment groups PBS (DC injury), TFP (DC injury + TFP) or H89 (DC injury + H-89) injected into the lesion site; zoomed-in images are shown for each panel . Insets show high power magnification of boxed regions. Scale bar = 50μm.

3.4 Discussion

3.4.1 Summary of results

The aims of this study were to determine the effects of DC injury on the subcellular localization of AQP4, and to determine whether treatment with inhibitors of AQP4 relocalization also had any effects *in vivo*. AQP4 appears to be localized across all astrocyte membranes in rat spinal cord tissue, and it not limited to the glial limitans, perivascular or perisynaptic sites. However, following spinal cord injury, the relative membrane expression of AQP4 at astrocyte cell bodies does not change, but the perivascular abundance of AQP4 appeared to increase significantly. When animals were treated immediately after injury with trifluoperazine (CaMi) or H-89 (PKAi), the increase in perivascular localization of AQP4 was not observed. Furthermore, after DC injury, there appeared to be an increase in the amount of AQP4, as well as increased nuclear localization of AQP4 transcription factor Foxo3a. Both of these effects were also inhibited when animals were treated immediately after injury with trifluoperazine (CaMi) or H-89 (PKAi). In summary, it appears that the subcellular localization and increase in expression of AQP4 after DC injury could be inhibited by treatment with inhibitors of CaM or PKA.

3.4.2 Distribution of AQP4 in astrocytes in spinal cord tissue

One interesting finding from this study was that AQP4 is expressed in most regions of astrocyte membranes. Most of the early literature characterized AQP4 as a protein expressed in astrocytes at their endfeet; surrounding blood vessels, neuronal synapses, and in contact with the glial limitans. Some studies even suggested that these were the exclusive sites of AQP4 localization (Rash et al., 1998). More recent

studies, including our present study, demonstrate that AQP4 can be found throughout the entire astrocyte cell membrane. High magnification confocal images of spinal cord tissue co-immunostained against AQP4 and GFAP (Figure 3-2) demonstrated that AQP4 can also be found in most astrocyte membrane domains, including the cell body and processes. Therefore, when considering features such as subcellular localization of AQP4, it is important to consider the entire cell, rather than simply sites of functional interest. Additionally, the images obtained in this study appeared to confirm that AQP4 is exclusively expressed in astrocytes, owing to the high abundance of co-staining with GFAP. However, whilst the images obtained support the exclusivity of AQP4 expression in astrocytes, in accordance with the literature, no data are shown to quantify this exclusivity, as the double AQP4:GFAP immunostain provided no positive or negative controls within the same sample to determine “total co-localization” or “no co-localization”.

3.4.3 AQP4 relocation in vivo

3.4.3.1 *AQP4 distribution across astrocyte cell bodies*

Perivascular AQP4 is important for maintaining BBB integrity, and for maintaining water influx and ionic homeostasis of CNS tissues. After spinal cord injury in mice, AQP4 appears to lose polarity from the BSCB, and instead take on a more even membranous distribution. However, no attempt at quantification was made (Wanner et al., 2013). In this study, we attempted to quantify the relative expression of AQP4 at different sites of the astrocyte in spinal cord tissue taken from rats with or without a spinal cord injury as a model of CNS trauma. No experimental methodology for this type of indirect semi-quantification of images obtained from neural tissue has been

published. To determine any differences in relative membrane expression of AQP4 in astrocyte cell bodies, AQP4 immunofluorescence was quantified in two ways; by comparing the co-localization of AQP4 and GFAP in isolated cell bodies of astrocytes, and by comparing line-profiles of AQP4 plotted across the cell bodies of astrocytes. The first method using co-localization essentially reveals “how much of the total AQP4 immunofluorescence exists within the GFAP stained region (i.e the intracellular compartment)”, as images were auto-thresholded prior to co-localization analysis using Otsu’s method (Nobuyuki, 1979). This creates two distinct populations of pixels; positive and negative. In this way, we remove the variability of signal strength on determining co-localization (i.e low signal intensity pixels from background staining are not considered). This is important given that the levels of GFAP (as a marker for astrocytes) significantly varies between uninjured and injured tissue, as GFAP increases in expression in activated astrocytes after SCI (Eng, 1985; Barrett et al., 1981). The data from our analysis suggested that there was no significant difference in the amount of AQP4 at the membrane relative to the intracellular domain. However, the limitations to this method may be the eradicating of signal intensity, we may be ignoring increased membrane or intracellular immunoreactivity. As such, a second method of determined relative membrane expression of AQP4 was used, adopting the same methodology used to investigate relative localization of AQP4 across astrocytes in vitro (Kitchen et al., 2015; Conner et al., 2010). This method considers the fluorescence intensity, rather than thresholded “area” of AQP4 and involves plotting line profiles of AQP4 immunofluorescence across the cell bodies of astrocytes, and calculating the relative “amount” (as determined by fluorescence intensity) in the assigned membranes compared to the intracellular compartments (see materials and methods for more information). The results of this analysis suggested that there was

no difference in the relative membrane expression of AQP4 between astrocytes imaged from uninjured and injured spinal cord tissue, in agreement with the co-localization analysis. However, this method too has limitations, in that the “membrane region” as determined by the algorithm is an estimation based on the two outer peaks of AQP4 fluorescence intensity. Ideally, a membrane specific marker would be incorporated into the immunohistochemistry to more definitively determine the membrane region, however triple staining immunohistochemistry (quadruple, if considering the inclusion of DAPI) is difficult to achieve, and no commercially available antibodies for membrane markers with compatible host species was found. Other astrocyte membrane markers, such as EAAT1 or EAAT2, could be co-immunostained with AQP4 to more specifically identify the membrane region, however both of these proteins also exist within intracellular stores, and trafficked to the membrane in activated astrocytes (Escartin et al., 2006; Holmseth et al., 2009; Underhill et al., 2015).

3.4.3.2 *AQP4 perivascular localization*

This study demonstrated that following DC injury, the amount of AQP4 surrounding blood vessels appears to increase relative to the amount of AQP4 at non-vascular sites, such as in processes and cell bodies. This is a particularly interesting result, as it suggests that previous evidence demonstrating the ability of AQP4 to translocate to the cell surface membrane in response to hypotonicity *in vitro* also appears to translate in response to tissue trauma *in vivo*. Furthermore, this event was only observed surrounding blood vessels within the lesion site (as determined by areas limited per cord by CD68 immunostaining), at 3 dpi, but not by 7 dpi. This suggests that the relocalization effect is an acute response of astrocytes to localized trauma, that can

be resolved as the secondary injury progresses. Most interestingly, the same CaM/PKA-dependent mechanism that regulates *in vitro* translocation of AQP4 also appears to have a role in regulating polarized translocation *in vivo*, as tissue analysed from rats treated post-injury with inhibitors of either CaM or PKA did not demonstrate any difference in perivascular fluorescence of AQP4 compared with tissue from uninjured rats. Instead, tissue imaged within the lesion site from either treated, injured groups appears to be very similar in perivascular AQP4 intensity than in uninjured tissue.

The site-specific perivascular relocalization of AQP4 is interesting from a mechanistic perspective, as *in vitro*, AQP4 relocalization has no polarity in response to hypotonicity or hypoxia, given that the entire cell is subject to the same conditions. It therefore poses the question; what is it about the perivascular microenvironment that causes specificity of AQP4 relocalization? It is possible that the supramolecular mixed-isoform composition of AQP4 clusters may contribute to this. It has been demonstrated that the M1- and M23- isoform relative composition and size of AQP4 clusters affect subcellular localization and function; it was concluded that perivascular AQP4 exists in larger OAP clusters than parenchymal AQP4, to which the M23 isoform is required (Smith and Verkman, 2015). This suggests that perhaps trafficking of AQP4 differs between isoforms, and that after SCI, increased amounts of the M23 isoform are translocated to the plasma membrane at the perivascular endfeet. However, there is no evidence to suggest that either isoform sit in any differing subcellular vesicular pools, or that either isoform is more susceptible to translocation. There is also another isoform of AQP4, AQP4e (also known as the Mz isoform), which also facilitates flow of water, and has been shown to increase in plasma membrane localization in

response to tonicity, which coincides with the decrease in AQP4-containing vesicle mobility (Potokar et al., 2013). However, no evidence exists to suggest that this isoform has any role in site-specific localization of AQP4 in vivo.

Another reason that perivascular relocalization of AQP4 may occur is due to the anchoring proteins that are present in the glial basal lamina, which exists underneath the astrocyte endfeet surrounding the blood vessels and in contact with the pial surface. It contains many proteins such as various laminins, collagens, heparansulfate proteoglycans, and fibronectin. It is well documented that AQP4 exists in the membrane in larger complexes called OAPs, which contain at least AQP4, but also other proteins, such as those previously listed. AQP4 co-localizes at the membrane with the dystrophin-dystroglycan (DDG) complex, and is required for the laminin-dependent membrane relocalization of the M23- isoform of AQP4 in cultured astrocytes. Furthermore, dynamin, a protein associated with the DDG, has been demonstrated to regulate the endocytosis of AQP4. Perhaps then, after a traumatic injury, there may be increased deposition or activity of the AQP4-anchoring complexes, such as the DDG, whilst other membrane domains within the brain parenchyma increase in their clearance or endocytosis of the protein (Tham et al., 2016). Agrin, a type of heparansulfate proteoglycan present at the glial basal lamina that binds to α -dystroglycan, is thought to confer polarity to astrocytes in terms of their recognition of endothelial sites. When added to astrocyte culture medium, agrin causes relocalization of AQP4 to the plasma membrane (Noell et al., 2007), in a similar manner to that observed by Kitchen, P et al. (2015) in response to hypotonicity. In agrin knockout mice however, AQP4 immunoreactivity surrounding blood vessels is not lost, but instead there appears a loss of OAPs, suggesting that its role is in the

clustering of AQP4 at the perivascular sites (Noell et al., 2009) that instead may infer stability.

It is well known that after a SCI, there is increased deposition of the extracellular matrix protein laminin throughout the damaged tissue parenchyma, and not strictly in the basal lamina domains (Soderblom et al., 2013; McKeon et al., 1991). Laminin deposition after contusion SCI has previously been evidenced across a time course, and demonstrates that at 1-3 days after injury, laminin deposition appears to increase in perivascular sites, but by 7 days after injury, laminin appears to exist in quite a dense network throughout the lesion site (Loy et al., 2002). Considering this evidence, it is conceivable that in early stages after traumatic injury where laminin deposition increases firstly at the perivascular basal lamina only, this may be what facilitates the polarized relocalization effect of AQP4 that is observed at 3 dpi. This may further explain why at 7 dpi, we do not observe increased perivascular AQP4, as more laminin deposition occurs within the tissue parenchyma, anchoring AQP4 to alternative sites. Additionally, comparing AQP4 immunostaining at the lesion site at a 10x magnification between injured and injured spinal cords, the distribution of AQP4 at 3dpi doesn't appear to increase significantly toward the glia limitans, and in fact appears to lose its polarity to this particular site. Collectively, our results suggests that the relocalization of AQP4 that we've observed in this study is not ubiquitous across the cell membrane of astrocytes, as it is in vitro, but is polarized to the perivascular endfeet sites due to the increase in anchoring proteins present at this site.

3.4.4 Changes in AQP4 protein levels in spinal cord tissue

In this study, an unexpected result was that the overall amount of AQP4 protein that increased after SCI was not observed when animals were treated with inhibitors of CaM or PKA. Given that we have observed relocalization of AQP4 at 3dpi in tissue from injured spinal cord tissue, but not in tissue from animals treated with CaM or PKA inhibitors, we hypothesized that this effect was unrelated to changes to AQP protein levels prior to this relocalization, and instead represented purely a difference in relocalization of existing protein. However, what we observed from tissue lysates obtained from the lesion sites of animals subjected to the same treatment groups was that preceding the timepoint of relocalization, at 1dpi, treatment with CaM or PKA inhibitors appeared to prevent the increase in AQP4 protein concentration (although this result was only significant between injured and injured + CaMi groups, which is probably due to the low n-number of samples used). We then decided to look back at the confocal images of AQP4 immunofluorescence within the lesion site of tissue obtained at 3dpi, and calculated the total fluorescence across multiple images taken within the lesion site, and it appeared to corroborate the same trend as demonstrated in the Western blot, that treatment with CaM or PKA inhibitors prevent the increase in AQP4 protein present after spinal cord injury. This led us to look into what mechanisms either of these proteins may affect AQP4 transcription. Foxo3a, a forkhead transcription factor that expressed ubiquitously in mammalian cells, has previously been demonstrated to modulated AQP4 expression in astrocytes (Kapoor et al., 2013). The transcriptional activity of Foxo3a is regulated by its localization; phosphorylation of Foxo3a by Akt inhibits its nuclear localization and retains it in the cytoplasm. Nuclear localization is achieved when Akt is inhibited, which retains Foxo3a in an unphosphorylated state, facilitating its entry into the nucleus. Akt activity is negatively regulated by PKA. As such, inhibition of PKA results in disinhibition of Akt,

phosphorylation of Foxo3a, and cytoplasmic retention, which prevents the increase in Foxo3a-mediated AQP4 upregulation (Figure 3-13).

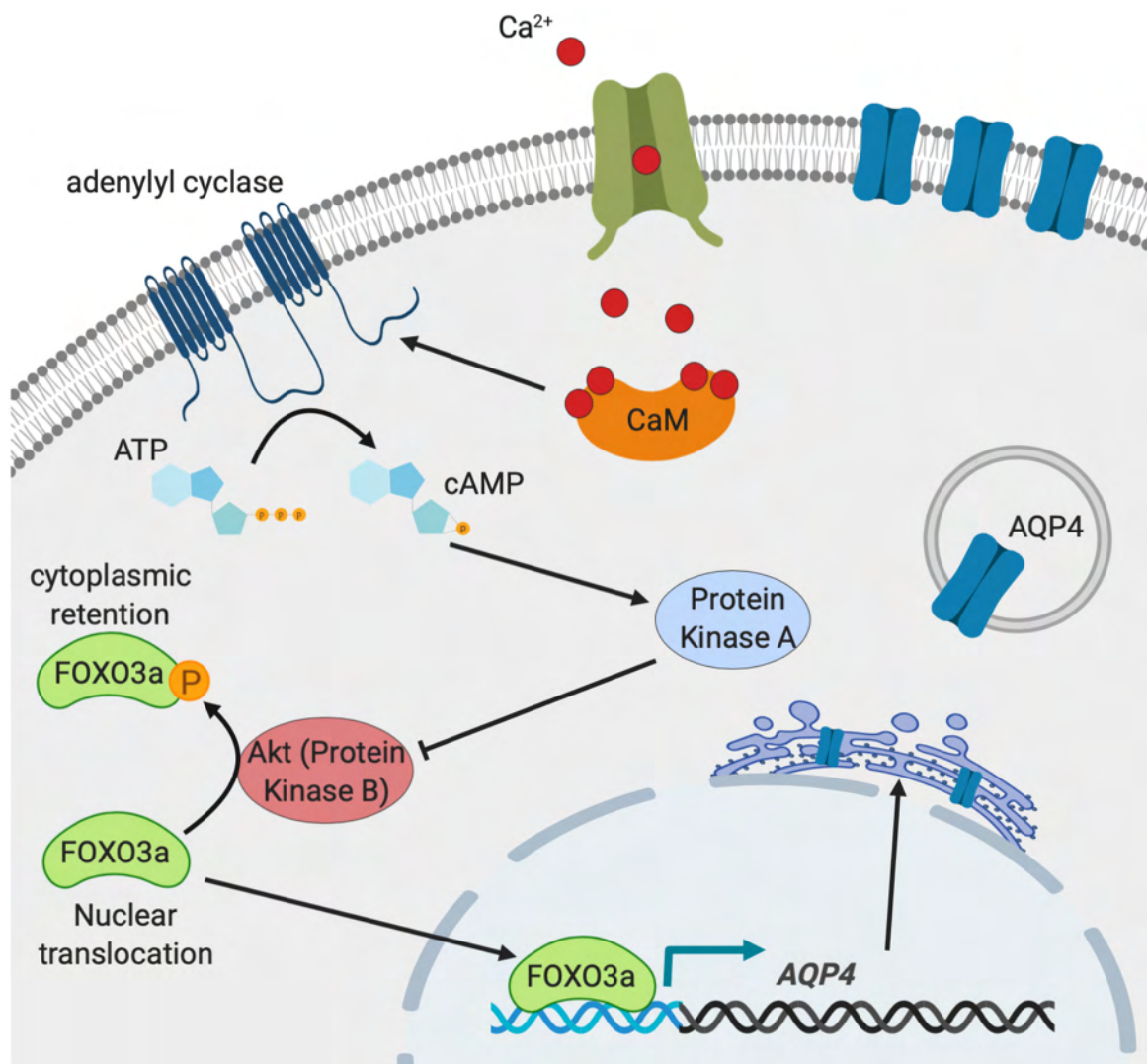


Figure 3-13 A schematic demonstrating the underlying mechanisms of Foxo3a-mediated changes in AQP4 transcriptional regulation.

Calmodulin (CaM) activation by calcium, and downstream Protein Kinase A activation by cyclic adenosine monophosphate (cAMP) inhibits Akt. Akt phosphorylates Foxo3a, which inhibits it from entering the nucleus. Once in the nucleus, Foxo3a can transcriptionally upregulate aquaporin-4 (AQP4).

Differences in nuclear localization of Foxo3a were investigated across all treatment groups. I observed significant nuclear localization of Foxo3a within the lesion site of spinal cord tissue from untreated injured animals, but not in tissue from uninjured animals, or injured animals treated with either PKA or CaM inhibitors (Figure 3-12). This suggests that the mechanism by which these inhibitors prevent the increase in AQP4 observed could be by preventing the increase in transcription. However, despite co-staining with GFAP, we can't determine whether the nuclear translocation is occurring within astrocytes, or other cell types, given that Foxo3a is ubiquitously expressed. Subsequent work by our group demonstrated that in primary rat astrocytes, Foxo3a undergoes nuclear translocation in response to hypotonicity, as well as an increase in PKA and Akt activity (Kitchen et al., 2020). Treatment with our CaMi, TFP, prevented this translocation and increase in PKA/Akt activity, suggesting that this relocalization observed in spinal cord tissue is likely to occur in astrocytes.

3.4.5 Conclusions

In summary, this study demonstrates that AQP4 subcellular translocation, as observed in response to hypotonicity and hypoxia in vitro, also occurs in vivo in response to traumatic injury in a rat DC injury model. This relocalization effect appears to be polarized toward the endfeet of astrocytes surrounding blood vessels acutely after injury. Treatment with inhibitors of PKA or CaM, which are necessary for in vitro translocation of AQP4, also appear to prevent translocation of AQP4 to perivascular endfeet in vitro. Furthermore, these inhibitors appear to limit the upregulation of AQP4 after a SCI by preventing the nuclear translocation of AQP4 transcription factor, Foxo3a. Astrocyte interfaces with blood vessels are vital for maintaining the integrity of the BBB. AQP4 appears to play an important role in the onset of edema after

traumatic CNS injury. AQP4 knockout appears to reduce the level of edema observed acutely after a traumatic CNS injury in mouse models, but worsens the long-term edema, suggesting a biphasic role of AQP4 to acutely regulate water flow into the CNS whilst a later phase where AQP4 is required to maintain water balance. As such, short term intervention of AQP4 dysfunction may be a promising target to reduce edema. Perhaps AQP4 dysfunction resulting in edema occurs as a result of the observed perivascular relocalization demonstrated in this study, and going forward, inhibition of PKA or CaM may confer benefit for prevention of CNS edema.

Chapter 4

Investigating the effects of inhibition of Calmodulin or Protein Kinase A on edema after traumatic CNS injury

Most of this chapter is published: Kitchen P*, Salman M*, Halsey A. M.*, Clarke-Bland C., MacDonald J.A., Ishida H., Vogen H.J., Almutiri S., Logan A., Kreida A., Al-Jubair T., Missel J.W., Gourdon P., Tornroth-Horsefield S., Conner M.T., Ahmed Z., Conner A.C., Bill R.M. Targeting aquaporin-4 subcellular localisation to treat central nervous system edema. (2020). *Cell* 181: 1-16. *Joint first authors

4 Chapter 4

4.1 Rationale

Edema is an important secondary pathology that occurs after SCI. It can exacerbate the primary injury by altering local osmotic and/or hydrostatic pressures and increasing intrathecal pressure. This disrupts local blood flow and causes ischemia, cell death and degeneration of axons (Kwon et al., 2009; Leonard et al., 2015; Leonard and Vink, 2015). Current therapeutic strategies to target post-traumatic spinal cord edema include 1) Osmotherapy, which involves the intravenous administration of osmotically active solutions, such as mannitol or hypertonic saline, to facilitate the movement of oedemous fluids from the intracellular and parenchymal spaces back into the blood. 2) Surgical decompression, involving removal of a section of bone from one vertebrae to allow the spinal cord space to swell into, in order to relieve the increase in pressure. Whilst both of these methods are still currently in clinical use as the best available options, their benefits remain questionable, most notably as neither of these treatment options offer a preventative measure for the edema, and instead only tackle the issue once it has already formed. Furthermore, the therapeutic window of effectiveness remains controversial, even in animal models of SCI (Fehlings and Perrin, 2006). There remains a niche for a treatment intervention that can prevent the onset of edema, rather than attempting to remove it at later stages. Edema begins to form within hours after the injury, and may persist for weeks to months after (Leypold et al., 2008; Miyanji et al., 2007). Therefore, developing and understanding of the cellular mechanisms responsible for the onset of edema will be crucial for developing any preventative measure.

The formation of post-traumatic spinal cord edema is generally considered to be biphasic in nature: acute ischemia as a result of SCI-induced ATP elevation and disruption in ion channel function causes cytotoxic edema, which involves the increased water uptake into cells, particularly in astrocytes (Rungta et al., 2015). The second stage involves breakdown of the normally highly restricted blood-spinal cord barrier (BSCB), which results in water influx into tissue, known as vasogenic edema (Sharma, 2005). The contribution of either of these towards the overall increase in edema remains unresolved; some studies suggest that cytotoxic edema alone can facilitate increased edema (Hudak et al., 2014), and some demonstrate that vasogenic edema is the only contributing type toward an increase in actual tissue swelling (Cabrera-Aldana et al., 2017b). However, cytotoxic edema is considered to be a cause of increased BSCB disruption, and worsens vasogenic edema by creating disruption to local ionic homeostasis in the perivascular regions (Kimelberg, 2004; Faden et al., 1987).

The role of AQP4 in edema is still unclear. It is thought that the rate-limiting factor mediating the onset of edema by facilitating cytotoxic edema is the abundance of AQP4 at the astrocyte endfeet interfaces with spinal cord vasculature, known as “perivascular endfeet” (Qiu et al., 2015; Zeynalov et al., 2008). However, perivascular AQP4 is also important for edema clearance and removal of water build up within tissue a result of vasogenic. AQP4 knockout mouse studies have demonstrated benefit for preventing edema and improving functionality in acute stages after injury (Manley et al., 2000; Saadoun et al., 2008), but worsening of edema and functionality at later stages (Kimura et al., 2010; Wu et al., 2014a). This suggests that by acutely preventing the pathological role of AQP4 in the onset of cytotoxic edema, we could

prevent edema without causing long-term detriment by temporarily removing the physiological AQP4 function. The data so far (see chapter 3) demonstrated that AQP4 appears to both upregulate and become significantly relocalized to perivascular sites after an SCI, and that treatment with CaM or PKA inhibitors prevents this effect at 3 days post-injury. These inhibitors also prevented membrane relocalization of AQP4 in cultured astrocytes in response to tonicity, as well as prevent astrocyte cell swelling (Kitchen et al., 2015). As such, it is hypothesized that CaM and PKA inhibitors may be beneficial for spinal cord edema by preventing excess water influx to astrocytes caused by the increased perivascular AQP4 observed acutely after injury, and that this prevention of edema will result in reduced functional deficit after SCI.

4.2 Aims and Hypothesis

Treatment with CaM or PKA inhibitors will prevent the onset of edema after SCI. To elucidate this, my aims are to:

- Determine the effect of CaM and PKA inhibition on spinal cord water content across time after moderate spinal cord injury
- To confirm that the mechanism by which TFP acts to improve edema after SCI is CaM-specific
- To determine the effects of acute treatment on later stage vasogenic edema
- To determine whether treatment with inhibitors of CaM or PKA are functionally beneficial, and whether this is as a consequence of reducing edema.

4.3 Results

4.3.1 Spinal cord injury (SCI) edema

The hypotheses outlined in section 4.2 will be addressed with the use of a rat dorsal column crush SCI model, (as described in section 2.1.1.1). Prior to the start of this project, Zubair Ahmed (Ph.D supervisor) determined that this model successfully produced edema, as measured by calculating % water content in the spinal cord after 3 days, in accordance with the literature (Yan et al., 2018; Wu et al., 2014a; Li et al., 2014). By comparison to normal, uninjured rat cords ($100\% \pm 1.61\%$ water content), injured spinal cords had a water content averaging at $108.50 \pm 1.62\%$, which was significantly higher (Figure 4-1, $p > 0.005$). As such, we suggest that the dorsal column crush model is suitable for investigating anti-edema drugs *in vivo* moving forward.

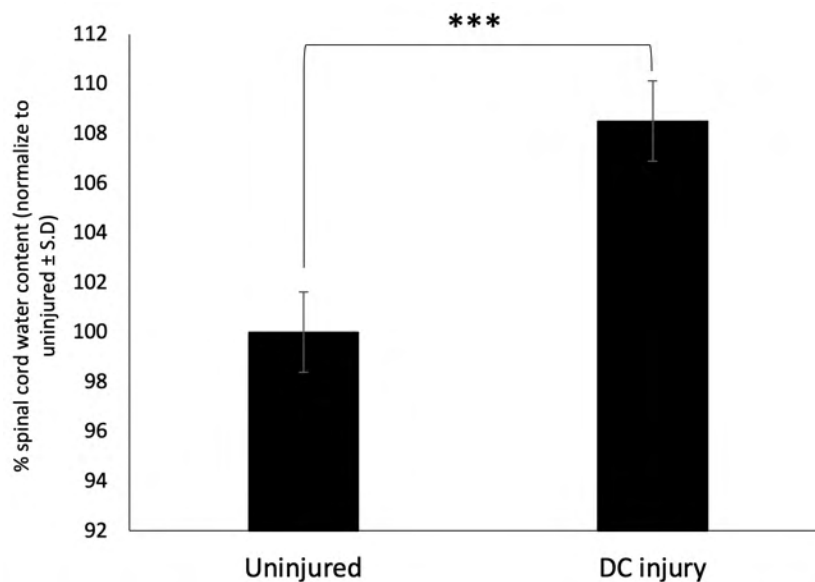


Figure 4-1 Mean water content differences after spinal cord injury at 3 days post-injury in rat T8 dorsal column crush models.

*** = $p < 0.001$ using independent t-test.

4.3.1.1 *Inhibitors of PKA and CaM significantly reduce spinal cord water content following moderate severity traumatic spinal cord injury*

In addition to the 3-day time point demonstrated in Figure 4-1, spinal cord water content was also measured at 7 and 28 days post-injury (dpi) in rats subject to DC crush injury. The water content of spinal cord lesion sites was significantly higher than in the spinal cords from uninjured control rats (normalized as 100%) at both 3dpi (Figure 4-2; $107.04 \pm 2.47\%$ to $100 \pm 1.61\%$) and 7dpi ($103.55 \pm 1.14\%$ to $100 \pm 1.61\%$). Spinal cord water content calculated from tissue obtained from rats who received a spinal cord injury followed by immediate intraspinal treatment with either calmodulin inhibitor TFP or PKA inhibitor H-89 (DC injury + TFP and DC injury + H-89, respectively), was significantly reduced compared to rats who received the injury and vehicle alone (DC injury) at both 3 (Figure 4-2; $102.34 \pm 1.38\%$ or $102.31 \pm 1.088\%$ to $107.04 \pm 2.47\%$) and 7 days post-injury (Figure 4-2; 99.79 ± 1.81 or 99.72 ± 0.87 to $103.55 \pm 1.14\%$).

At 28dpi, there was no significant difference between the DC injury group with either of the inhibitor groups, as the water content at this timepoint was already resolved to a level close to control (Figure 4-2; DC injury = $102.07 \pm 1.34\%$ to $100 \pm 1.61\%$), but demonstrates that these inhibitors do not appear to cause any increase in spinal cord water content at chronic stages.

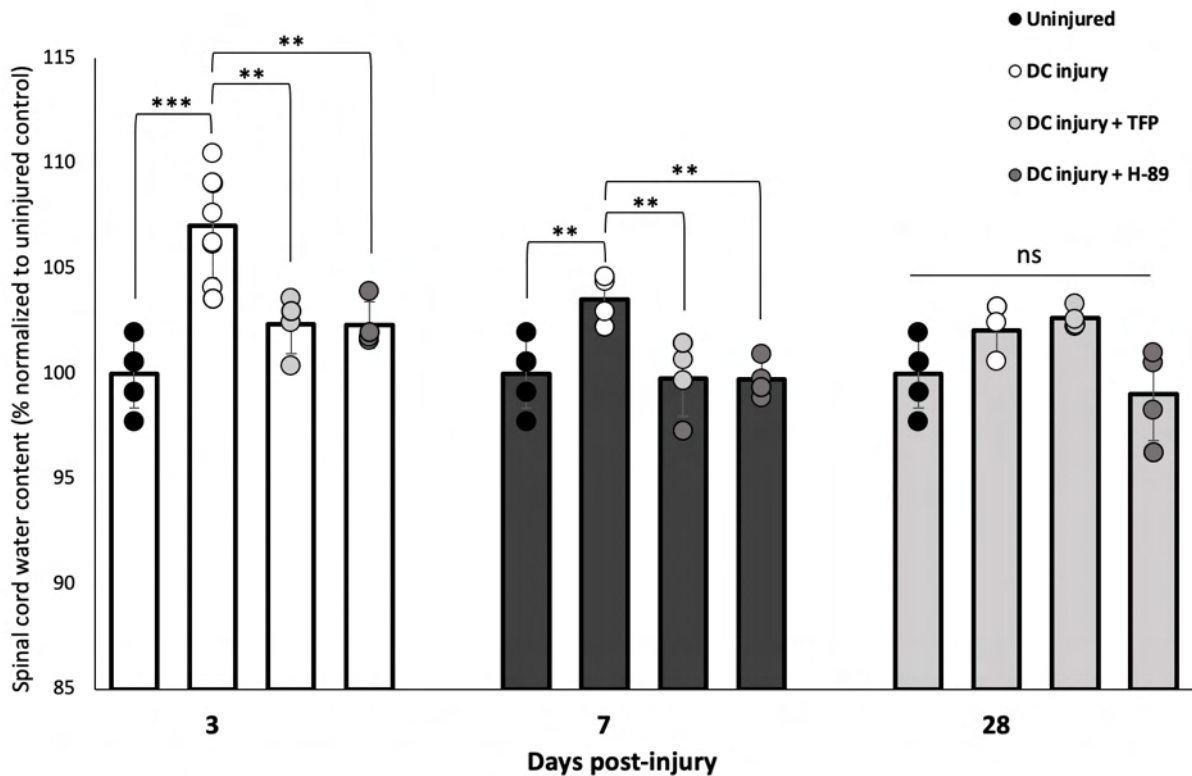


Figure 4-2 Water content of the thoracic spinal cord 3, 7, and 28 days after dorsal column (DC) crush and treatment with CaM or PKA inhibitors (CaMi or PKAi).

DC injury = T8 DC crush + PBS; DC injury + TFP = DC crush + intra-lesion injection of 50 µg trifluoperazine (TFP); DC injury + H-89 = DC crush + intra-lesion injection of 13 ng H89. All inhibitors were injected in a volume of 2.5 µl. Statistical significance was calculated by ANOVA followed by t-test with Benjamini-Hochberg correction * = $p < 0.05$, ** = $p < 0.005$, *** = $p < 0.001$.

4.3.1.2 *Reduction in spinal cord water content by TFP is Calmodulin-specific*

TFP is considered to have a broad polypharmacology, in that it is also an inhibitor of a number of other molecular targets including, most potently, dopamine D2 receptors and α_1 -adrenergic receptors (Seeman, 2002; Huerta Bahena et al., 1983). As such, we then repeated the water content study at 3dpi to determine the calmodulin

specificity of TFP treatment on preventing edema after a spinal cord dorsal column crush. To do this, we compared the spinal cord water content of injured, untreated animals (DC injury) with that of injured animals treated with D₂-receptor inhibitor L-741,626 (DC + D₂Ri), alpha₁-receptor inhibitor Terazosin (DC + A₁Ri) and an alternative calmodulin inhibitor W-7 (DC + W-7) in addition to TFP (DC + TFP) and H-89 (DC + H-89), as well as off-target inhibitor of PKC, Gö 6983. Data for all treatment groups is displayed in Figure 4-3. Treatment with the CaM inhibitor W-7, like TFP, produced a significant reduction in spinal cord water content at 3dpi (105.78 ± 3.05% to 98.58 ± 1.26%, p < 0.05). Treatment with the alpha₁-receptor inhibitor did not produce a significant difference in water content compared to injured, untreated cords (105.78 ± 3.05% to 105.15 ± 0.91%, p > 0.05). Treatment with both the dopamine D₂-receptor inhibitor and PKC inhibitor produced a significant increase in the percentage water content measured compared to injured, untreated cords (105.78 ± 3.05% to 107.96 ± 0.94%, p < 0.05 and 110.13 ± 2.42%, p < 0.05, respectively).

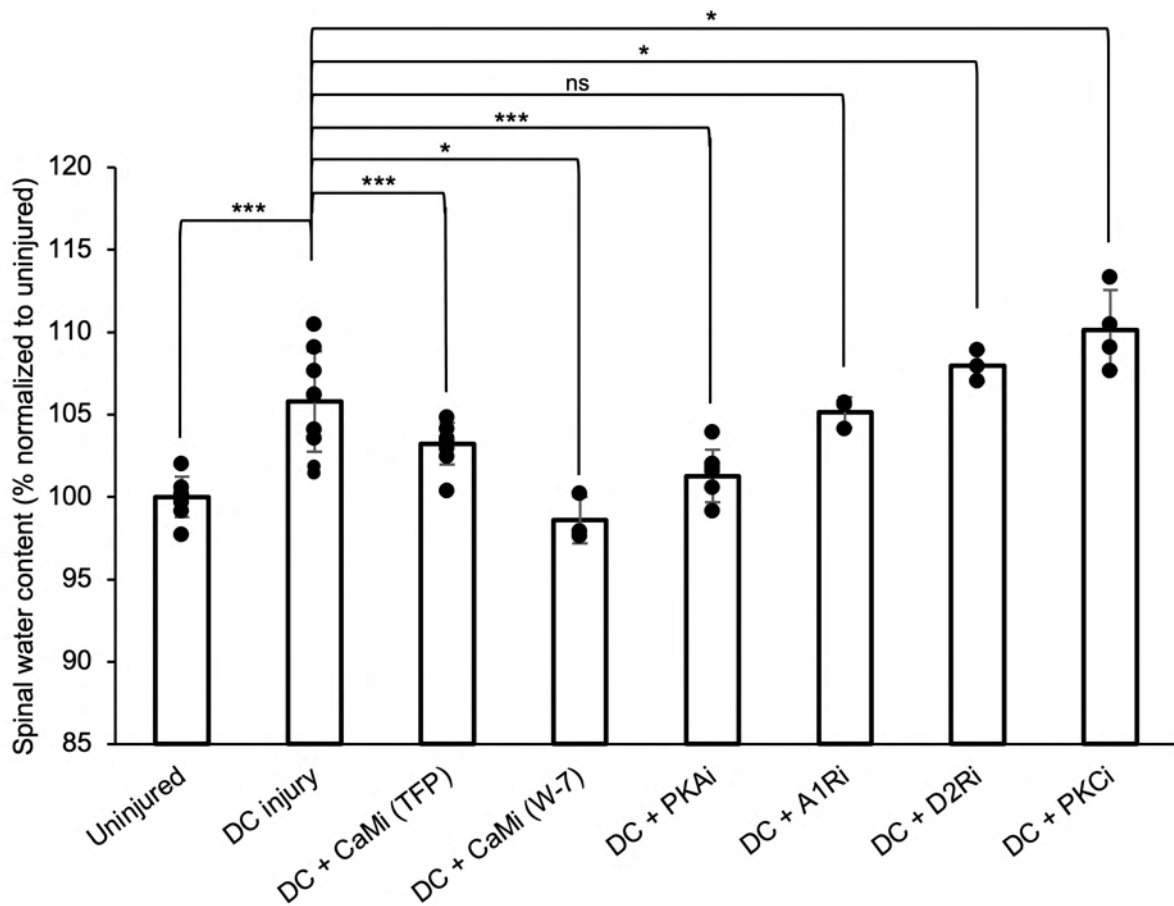


Figure 4-3 Water content of the thoracic spinal cord 3 days after DC crush to investigate the mode of action of TFP.

DC + CaMi = DC crush + intralesion injection of either 41 mM TFP or 164 mM W-7. DC + A1Rii = DC crush + intra-lesion injection of 53 mM adenosine A1 receptor antagonist (A1Ri), terazosin. DC + D2Ri = DC crush + intra-lesion injection of 6.6 mM dopamine D2 receptor antagonist (D2Ri), L-741,626. DC +PKCi = DC crush + intra-lesion injection of 9.94 μ M PKC inhibitor (PKCi), Gö 6983. All inhibitors were injected in a volume of 2.5 μ l; n= 3-12 rats per treatment group, normalized to uninjured controls across multiple experiments. Statistical significance was calculated by ANOVA followed by t-test with Benjamini-Hochberg

correction * = $p < 0.05$, ** = $p < 0.005$, *** = $p < 0.001$.

4.3.2 Vasogenic edema

Vasogenic edema is a secondary consequence of SCI, which can be propagated by the onset of cytotoxic edema (Michinaga and Koyama, 2015). Data in section 4.3.1.1 indicates that an increase in total water content within the spinal cord was prevented after crush injury by acute treatment with CaM or PKA inhibitors. As such, fixed, sectioned spinal cord tissue was stained for albumin, a mostly blood-borne protein, to determine the amount of penetration it has into the spinal cord parenchyma as a measure of BSCB breakdown, and by extension, the level of vasogenic edema that occurs within the tissue. Quantification of spinal cord sections stained by immunohistochemistry at 7 and 28 days post-injury demonstrate that in injured, untreated conditions, there is a significantly higher proportion of detected extravasated albumin compared to uninjured controls at both 7 days post-injury (Figure 4-4a-b,e; 21.30 ± 5.01 to 1.00 ± 0.62), and 28 days post-injury (Figure 4-5a-b,e; 24.65 ± 7.58 to 1.00 ± 0.51). Furthermore, in tissue obtained from injured animals treated with CaMi or PKAi, there was significantly lower amounts of albumin detected in the tissue at 7dpi compared to injured, untreated controls (Figure 4-4c-e; 5.37 ± 1.62 or 4.68 ± 1.47 , respectively). However, at 28dpi, only treatment with PKAi, but not TFP, significantly reduced the amount of albumin detected (Figure 4-5e; 2.76 ± 1.28 or 8.33 ± 3.26 , respectively).

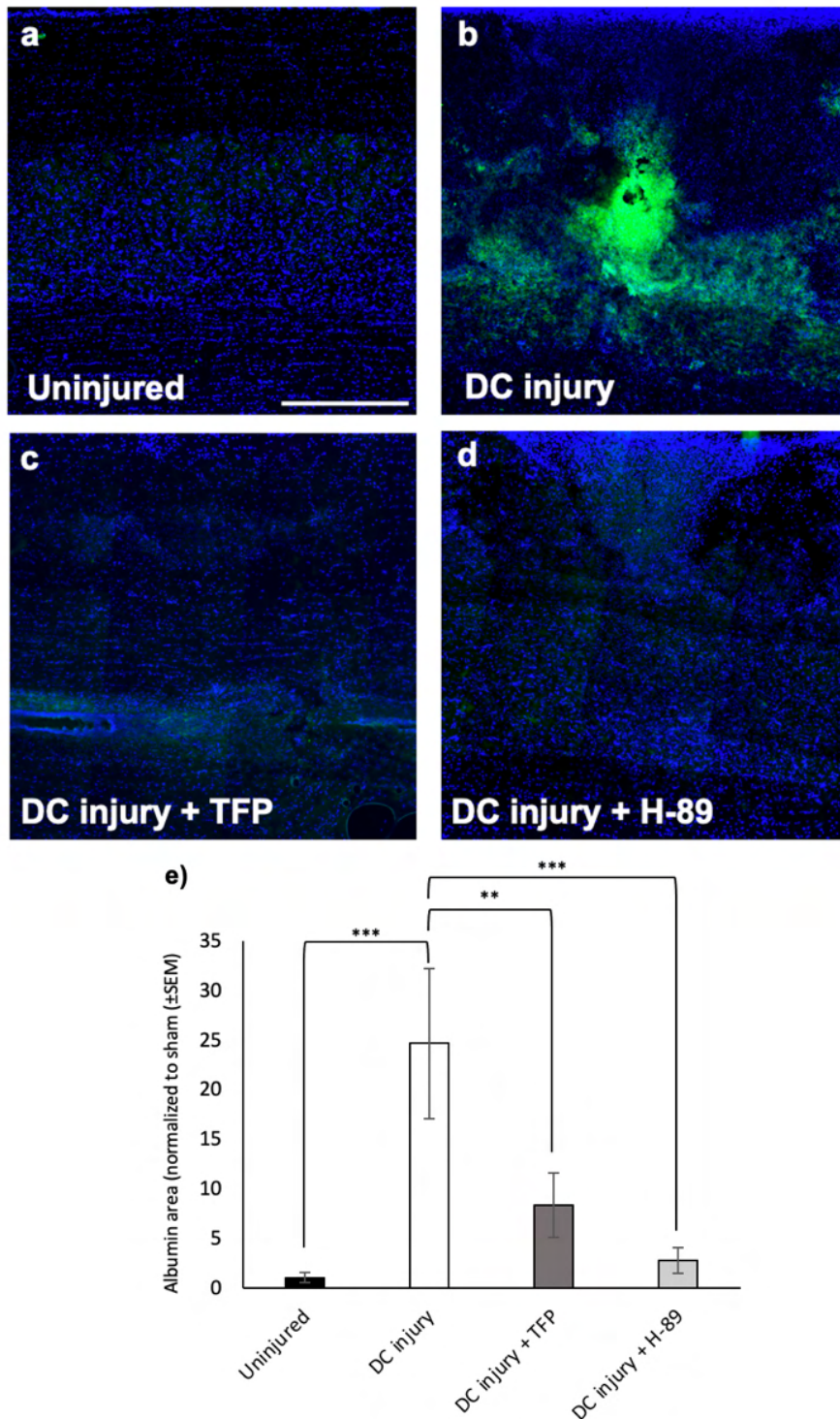


Figure 4-4 Immunohistochemistry of extravasated albumin in spinal cord tissue 7 days post-injury.

(a-d) representative images of spinal cords immunostained for albumin (green) and DAPI (blue) across each treatment group. (e) quantification of the area of albumin extravasation normalized to uninjured controls (n=3). * indicates $p < 0.05$, ** indicates $p < 0.01$, and *** indicates $p < 0.001$ by ANOVA followed by t-test with Bonferroni correction.

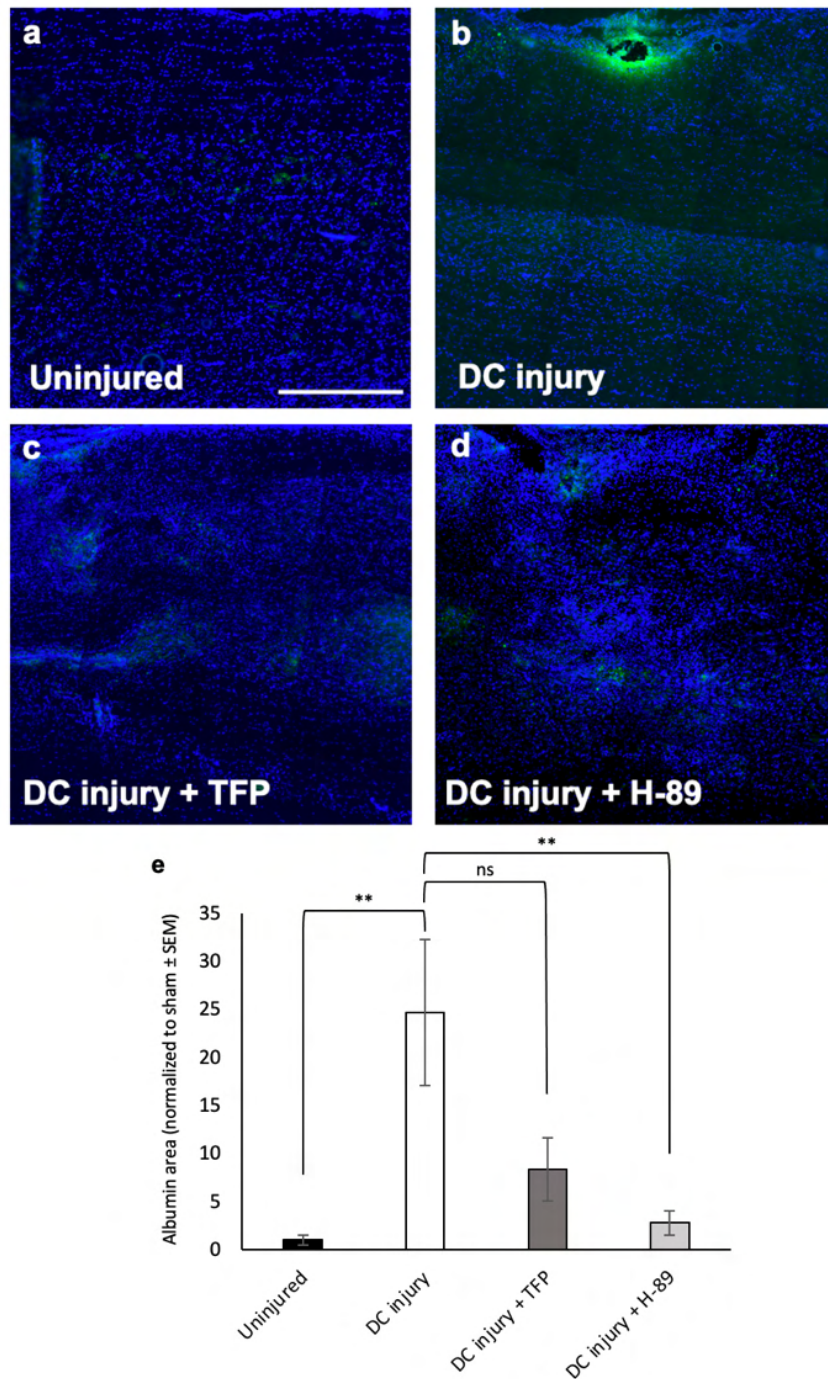


Figure 4-5 Immunohistochemistry of extravasated albumin in spinal cord tissue 28 days post-injury.

(a-d) representative images of spinal cords immunostained for albumin (green) and DAPI (blue) across each treatment group. (e) quantification of the area of albumin extravasation normalized to uninjured controls (n=3). Statistical significance was calculated by ANOVA followed by t-test with Bonferroni correction, * indicates $p < 0.05$, ** indicates $p < 0.01$, and *** indicates $p < 0.001$.

4.3.3 Post-traumatic cell-free cavity formation

Data from previous section demonstrated that treatment of injured rats with either TFP or H-89 reduces CNS edema, including via BSCB breakdown, which facilitates the flow of water into tissue parenchyma. The formation of fluid-filled cavities syrinx's may occur in both humans and adult rats after traumatic spinal cord (Surey et al., 2014). Byrnes et al., 2010 previously demonstrated that immunohistochemistry to demarcate the area of cavitation significantly correlated with the extent of lesion size determined by T2-weighted MRI imaging, which in turn also significantly correlated with functional outcome. As such, the effect of treatment with TFP or H-89 on lesion cavity size was measured in spinal cords sections. Sections were immunolabelled for GFAP (green) and cell nuclei (DAPI; blue), and the size of the fluid-filled cavity, as determined by the absence of cellular material (Figure 4-6). No measurable cavitation was seen or in uninjured controls. The volume of the spinal cord cavity measured was significantly reduced in cords obtained from animals treated with either TFP or H-89 ($0.212 \pm 0.115\text{mm}^2$ and $0.257 \pm 0.157\text{mm}^2$, respectively) compared to that from injured, untreated animals ($0.835 \pm 0.596\text{mm}^2$; Figure 4-6; $p < 0.05$).

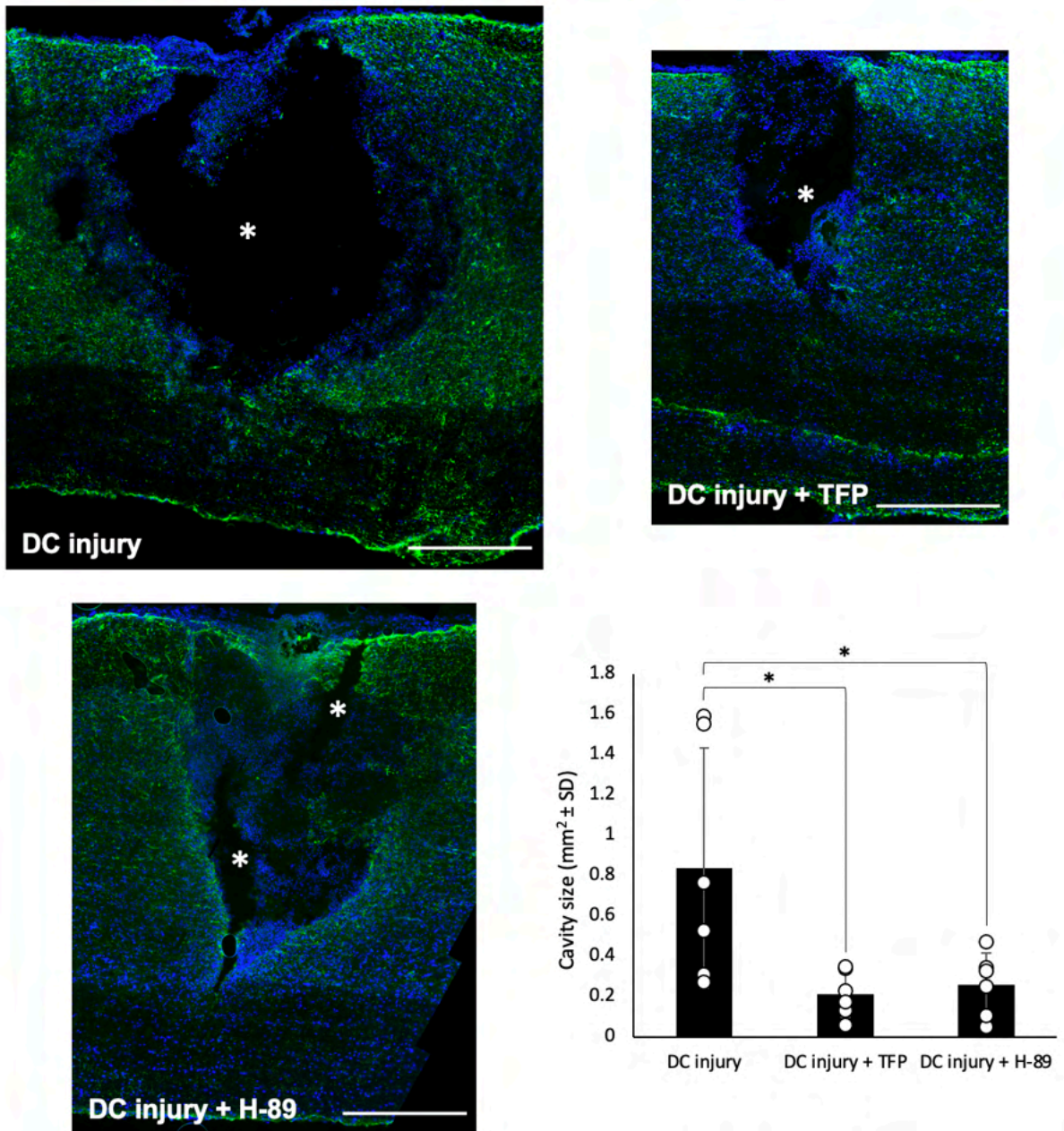


Figure 4-6 Immunohistochemistry of GFAP (green) and DAPI (blue) in rat spinal cord demonstrating the occurrence of cell-free cavity formations within the fibrotic scar area at 7dpi. Scale bar = 500 μ m. Total area of cell-free cavities was measured using ImageJ and statistical significance determined using a one-way ANOVA followed by Bonferroni post-hoc test. * = $p < 0.05$ ($n = 6$ /group).

4.3.4 Treatment with TFP significantly improved neuronal conductivity after spinal cord injury

To assess the neuronal functionality of the DC tracts, electrical conductivity was assessed as compound action potentials (CAPs) recorded across the lesion site at 6 weeks after DC crush spinal cord injury, in accordance with previously published methods (Lo et al., 2003; Hains et al., 2004). Data demonstrates negative (or repolarization) CAP traces across the DC lesion site (at spinal cord level T8), caused by stimulating at level L1/L2 and recording at level C4/C5 (refer to figure [insert once merged to direct to spinal cord level figure in introduction] for level orientation). The negative CAP traces in control (Sham), injured and untreated (DC+Vehicle) or injured and treated (DC+CaMi or DC+PKAi) animals were combined and analysed. The ablated negative CAP trace observed after injury only (DC + vehicle) was significantly restored following treatment with either CaMi TFP or PKAi H89 (Figure 4-7a). The CAP areas (Figure 4-7a) 6 weeks after injury in DC+CaMi and DC+PKAi-treated rats were significantly higher ($45.5 \pm 0.2\%$ and $52.5 \pm 0.7\%$, respectively) of that observed for control animals (Sham). Furthermore, the mean CAP amplitudes (Figure 4-7) were also significantly improved following treatment with TFP or H89 at stimulus intensities 0.4mA and above. These results demonstrate that treating CNS edema with either TFP or H89 reduces injury-induced deficit in cross-lesional neuronal conductivity.

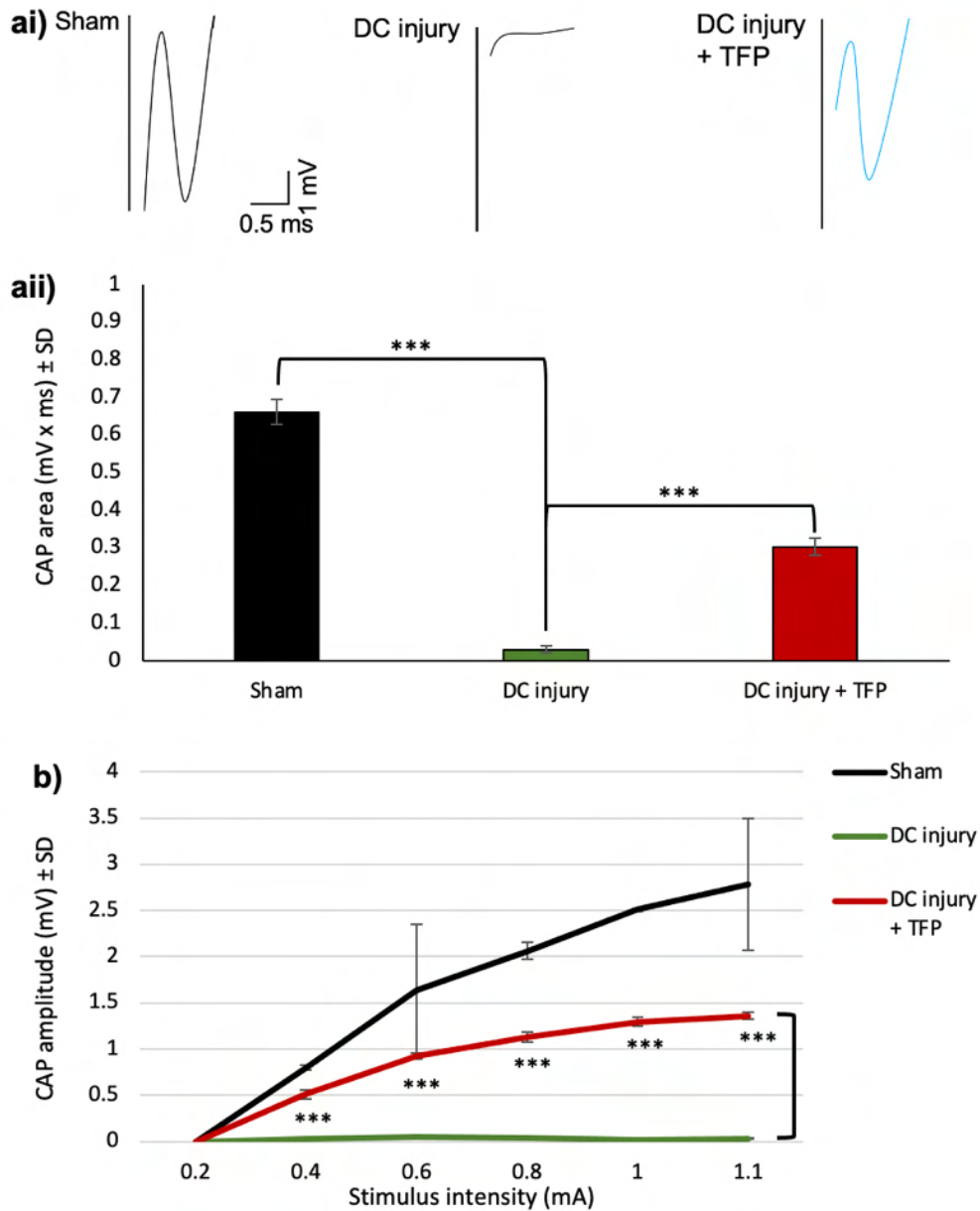


Figure 4-7 Compound action potential (CAP) areas (mV x ms) recorded at spinal cord level C4/5 after stimulation at level L1/2.

A) Representations of the processed traces obtained from animals from each treatment group.

B) Quantification of the average area within the processed traces of all animals from each treatment group. DC+Vehicle = T8 DC crush + PBS; DC+ CaMi = DC crush + intra-lesion injection of trifluoperazine (TFP); DC+PKAi = DC crush + intra-lesion injection of H89 (n=12).

Statistical significance was calculated by ANOVA followed by t-test with Bonferroni correction,

* indicates $p < 0.05$, ** indicates $p < 0.01$, and *** indicates $p < 0.001$.

4.3.5 Effect of PKA or CaM inhibition on neurite outgrowth

4.3.5.1 *TFP inhibits neurite outgrowth at concentrations 10 μ M or above*

Data obtained in section 4.3.4 demonstrated that TFP significantly improves the neuronal conductivity of injured dorsal column fibres across the injury site 6 weeks post-injury. This therefore raised the question as to whether reducing the onset of edema, as observed in section 4.3.1, is itself sufficient to create this improvement in conductivity, or whether TFP also has an effect in enhancing neurite outgrowth of dorsal column fibres, such as those that emanate from the dorsal root ganglia (DRG). To investigate whether TFP has any effect on neurite outgrowth, DRG neurons were cultured in 8-well chamber slides pre-coated with laminin, a permissive growth substrate for DRG neurons, and treated with increasing concentrations of TFP (0 – 100 μ M) until 72hrs after plating. Neurites were visualized by immunocytochemistry staining for β III-tubulin and fluorescence microscopy. Multiple features of neurite outgrowth were quantified; average length, number of branch points, and longest neurite. When neurites are treated with 1 μ M TFP, there is no measurable difference in neurite number or length compared to untreated controls (Figure 4-9, $p > 0.05$). When treated with 10 μ M TFP, there was a significant decrease in both the number of neurites and the length of the longest and average neurite (Figure 4-9, $p < 0.0001$). There was an even further significant decrease in both neurite length and number when treated with 100 μ M TFP (Figure 4-9, $p < 0.0001$ between 10 μ M TFP and 100 μ M TFP).

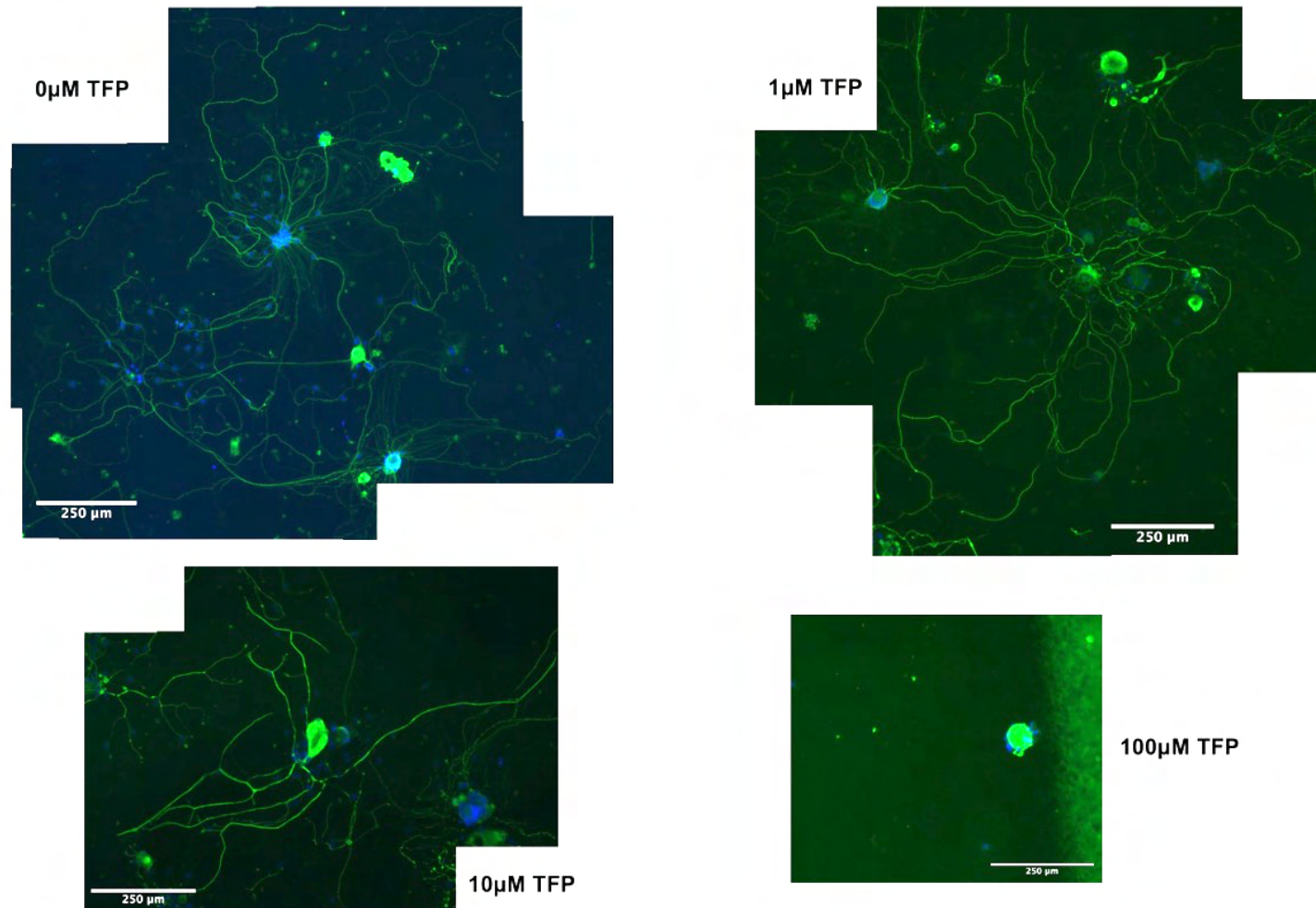


Figure 4-8 Representative images of DRGNs immunostained against β III-tubulin (green) and DAPI (blue) 72hrs after treatment with either 0µM, 1µM, 10µM, or 100µM TFP.

Images captured using an epifluorescence microscope at 10x magnification. All images are proportionate in size. Scale bar = 250µm.

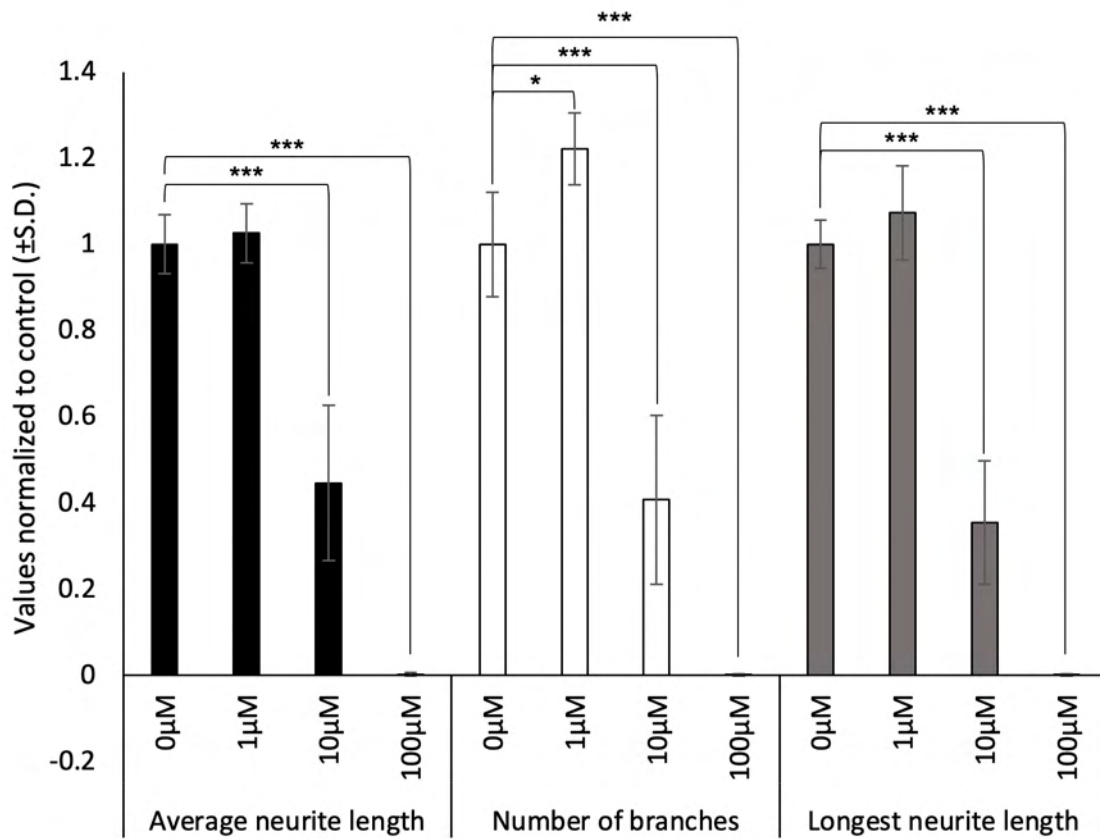


Figure 4-9 Quantification of various parameters of neurite outgrowth in cultured dorsal root ganglia neurons treated with increasing doses of trifluoperazine (TFP).

All values represent the means of each measurement normalized to respective controls in biological repeats (n = 3). * indicates $p < 0.05$, ** indicates $p < 0.01$, and *** indicates $p < 0.001$ by ANOVA followed by t-test with Bonferroni correction.

4.3.5.2 *TFP inhibition of neurite outgrowth is mediated through inhibition of Calmodulin*

Data in section 4.3.5.1, when DRGNs are treated with TFP at concentration of 10 µM or above, their ability to sprout neurons, both in length and in quantity, was significantly impaired. TFP as activity for a number of targets, the pharmacological targets were all investigated for their effect on neurite outgrowth

to determine which target is responsible for the TFP-mediated inhibition of neurite outgrowth observed. The off-target inhibitors selected were the same chosen to determine the pharmacology of the reduction in edema observed after spinal cord injury (see section 4.3.1.2). Of the inhibitory doses of TFP investigated for neurite outgrowth in DRG neurons, those treated with 100 μ M produce no neurite outgrowth, and appear to result in significant cell death, but those treated with 10 μ M TFP are still able to sprout neurites, 10 μ M TFP was selected as the proportionate drug concentration by which to calculate the doses of off-target inhibitors. To achieve this, the proportion of the relative half maximal inhibitory concentration of the receptor targets (IC_{50}) to which 10 μ M TFP occupies for each receptor was calculated, and the equivalent concentration of off-target inhibitor. Quantification of the all neurites across each treatment group demonstrated that, by comparison to non-treated control groups (Figure 4-11; average length: 1.00 ± 0.07 , length of longest neurite: 1 ± 0.07 , neurite number: 1 ± 0.10 , normalized arbitrary units), DRGNs treated with alternative calmodulin inhibitor, W-7 (Figure 4-11; DC + W-7), exhibited significant impairment for neurite outgrowth in both length and number (Figure 4-11; average length: 0.34 ± 0.09 , length of longest neurite: 0.27 ± 0.09 , neurite number: 0.23 ± 0.04). Treatment with either D2 receptor inhibitor L-741,626 (DC + D₂Ri), or α 1-receptor inhibitor terazosin (DC + A1Ri), had no significant effect on neurite outgrowth (Figure 4-11; D1Ri: average length: 0.89 ± 0.03 , length of longest neurite: 0.90 ± 0.06 , neurite number: 0.85 ± 0.10 ; A1Ri: average length: 0.97 ± 0.08 , length of longest neurite: 0.98 ± 0.07 , neurite number: 0.98 ± 0.11). These data suggest that the inhibition of neurite

outgrowth observed from treatment with 10 μ M TFP was due to the inhibitory activity of TFP for CaM in DRG neurons.

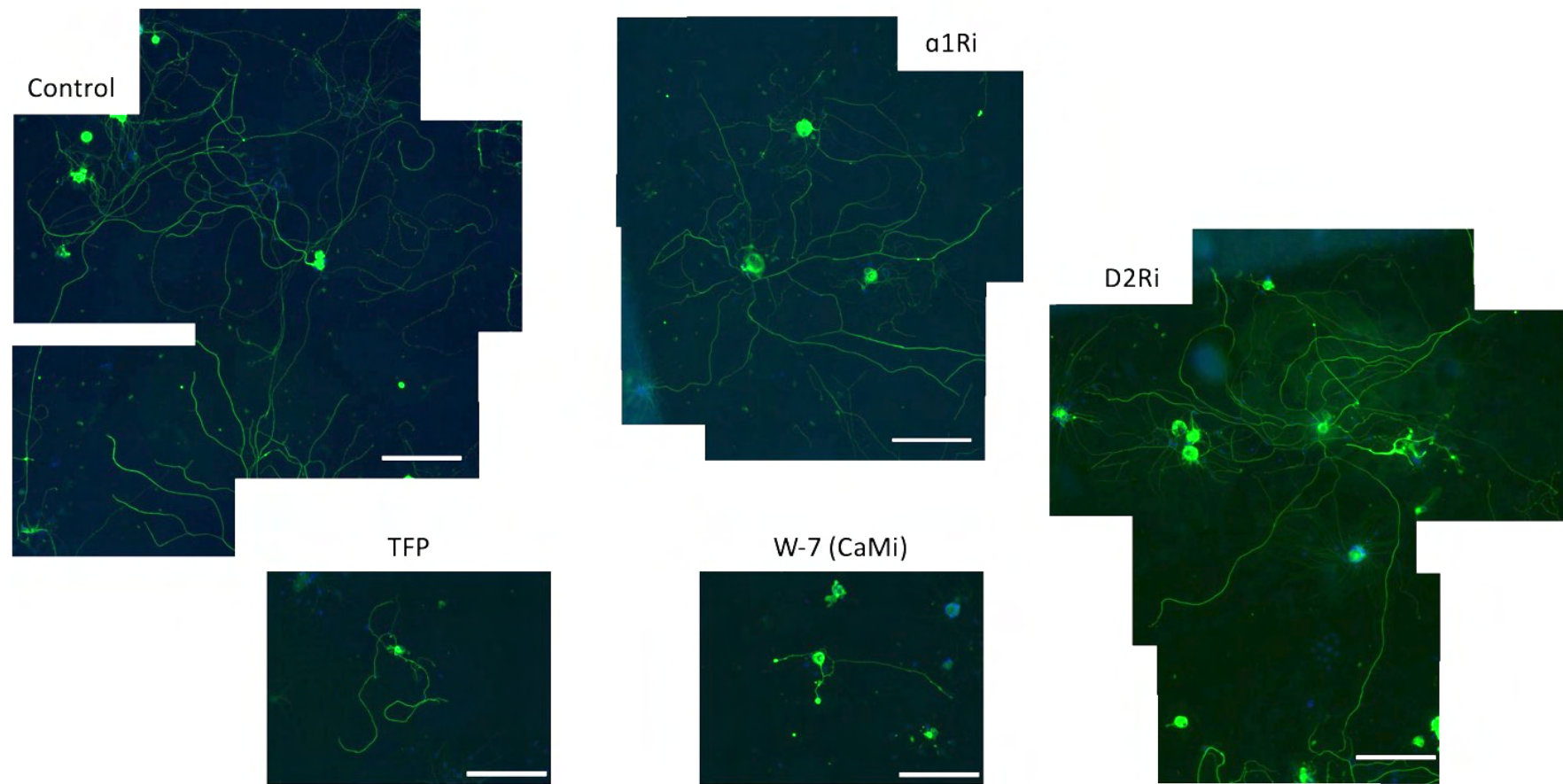


Figure 4-10 Representative images of DRGNs immunostained against β III-tubulin (green) and DAPI (blue) 72hrs after treatment with either 10 μ M TFP, 8.66 μ M W-7, 1.3 μ M L-741,626 (D2Ri), 0.724 μ M terazosin (A1Ri), or no treatment (control).

Images captured using an epifluorescence microscope at 10x magnification. All images are proportionate in size. Scale bar = 250 μ m.

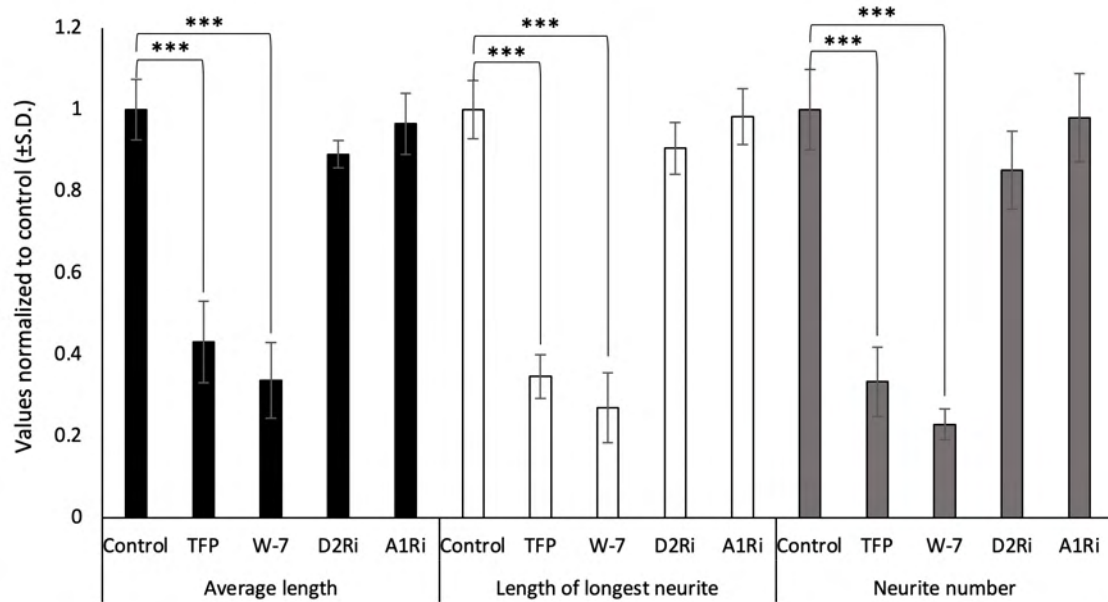


Figure 4-11 Quantification of various parameters of neurite outgrowth in cultured dorsal root ganglia neurons treated with 10 μ M TFP, 8.66 μ M W-7, 1.3 μ M L-741,626 (D2Ri), 0.724 μ M terazosin (A1Ri), or no treatment (control).

All values represent the means of each measurement normalized to respective controls in biological repeats (n = 3). * indicates p<0.05, ** indicates p<0.01, and *** indicates p<0.001 by ANOVA followed by t-test with Bonferroni correction.

4.4 Discussion

This study provides evidence that CaM and/or PKA inhibition could be utilized as a clinical therapeutic target for acute prevention of edema and salvaging neuronal functionality following traumatic spinal cord injury.

4.4.1 The effect of inhibiting CaM or PKA on CNS edema

In a rat DC crush injury model of SCI, the increase spinal cord water content, as a measure of edema, observed after injury appeared to be prevented when animals were treated with inhibitors of PKA or CaM. Spinal cord water content is frequently used as a measure of tissue edema (Manley et al., 2000; Saadoun et al., 2008; Kimura et al., 2010; Wu et al., 2014a). At 3 days post-injury, the most significant increase in percentage spinal cord water content was observed, in line with the literature (Saadoun et al., 2008). This increase appeared to persist by 7 days post-injury, but not by 28 days (Figure 4-2). Water content of spinal cords from injured rats treated with TFP (CaMi) or H-89 (PKAi) were significantly lower than those of injured, untreated cords at both 3dpi or 7dpi. These data suggest that treatment with inhibitors of PKA or CaM after a traumatic CNS injury, such as SCI, prevent the increase in spinal cord edema observed.

AQP4 has a biphasic contribution toward post-traumatic CNS tissue edema; facilitating the onset at acute timepoints after injury, and facilitating clearance at later stages. The former is thought to be as a response to cytotoxic cell swelling whereby cells, mostly astrocytes, increase water absorption, and the latter as a

response to blood-CNS barrier breakdown, causing serum to enter the tissue parenchyma (vasogenic edema). Given that in this model, the inhibitors were injected immediately following injury, and the results observed previously (see Chapter 3) demonstrate the ability of these inhibitors to prevent AQP4 redistribution to the perivascular endfeet, it is reasonable to infer that these inhibitors have an anti-oedemous effect after SCI by manipulating the response of astrocytes to relocate AQP4 to the blood-spinal cord barrier, therefore reducing the amount of edema formed. This is supported by data demonstrating that patients exhibiting extensive cytotoxic lesions after TBI appear to have worse clinical manifestation of injury than patients who exhibit vasogenic edema (Hudak et al., 2014).

In support of this, the albumin immunohistochemistry appears to match the time course for the water content. There is no evidence to demonstrate the clearance rate of extravasated albumin from neural tissue, particularly in sites of disrupted endothelial integrity and increased reactive gliosis, such as after SCI. Hence, the reduced albumin immunostaining observed in spinal cords from the PKAi and CaMi treatment groups is more indicative that there was less albumin extravasation as a result of CaMi or PKAi treatment, rather than the clearance of existing edema. Cytotoxic edema is thought to precede and worsen the onset of vasogenic edema. Endothelial cells contribute to the maintenance of ionic homeostasis in the interstitial fluid (ISF) of the brain parenchyma by altering ion movement into, and out of, the ISF (Mokgokong et al., 2014). As such, increased presence of water channels and water absorption into perivascular astrocyte

endfeet may cause disruption to the local ionic environment, causing water to move into the tissue from the blood, and causing breakdown of the tight barrier, leading to vasogenic edema. Interestingly, one previous study did report that inhibition of calcium/calmodulin-dependent kinase kinase (CaMKK), a downstream molecule of the CaM-signalling pathway, appears to be protective of endothelial cell viability, inhibition of which exacerbated BBB breakdown after ischemia (Sun et al., 2019). This might suggest that inhibition of CaM could to exacerbate BBB breakdown. However, albumin immunostaining at 28dpi demonstrated an insignificant difference between injured groups untreated or treated with TFP (Figure 4-5), suggesting that our CaM inhibitor TFP does not appear to exacerbate BSCB breakdown. AQP4 is also responsible for maintenance of the blood-brain barrier integrity, and therefore, the benefits of reducing excess water absorption and prevention ionic dysregulation may outweigh any potential damage to endothelial cells downstream of CaM.

One of the key considerations in this study is the evidence existence of syrinxes (fluid-filled cysts) within the spinal cord that develop by 7 days post-injury. These are identified as cell-free areas when imaged using immunohistochemistry, and indicate that a fluid-filled cavity has developed within the lesion area. Syringomyelia is a significant complication that can follow traumatic spinal cord injury, and manifests as syrinx's, which may result in enhanced sensory/motor disturbance, pain below the level of injury, and spasticity. Like edema, syringomyelia can currently only be treated by surgical decompression, which itself is both invasive and poses further risk to the spinal cord (Klekamp, 2012).

The mechanisms that result in formation of syringomyelia remain largely unknown, but are thought to include changes in dynamics of CSF flow within the spinal cord, and the acute onset of post-traumatic edema. Indeed, many patients have been described through MRI scans post-injury to exhibit a “pre-syrinx” enlargement of the spinal cord, which could be the onset of edema (Fischbein et al., 1999; Kleindienst et al., 2020). As such, data from this chapter suggests that reducing spinal cord edema may also reduce or prevent the onset of syrinx formation as early as 7 days post-injury in rat models, supporting the idea that post-traumatic edema may be part of the underlying pathophysiology leading to syrinx formation. It’s also interesting tied in with the data demonstrated in chapter 3 regarding the early increase in perivascular AQP4 following traumatic injury. A

TFP is an off-licensed drug used clinically in the treatment of schizophrenia due to its activity as a dopamine D2 receptor antagonist (Seeman, 2002; Koch et al., 2014; Li et al., 2016; Macdonald and Shields Watts, 1959). TFP is considered to be a very “dirty” drug due to its polypharmacology, which results in many unwanted side-effects, and is partly why the clinical use is now very infrequent. With this in mind, it is important to narrow down the pharmacology by which TFP prevents the increase in water content after spinal cord injury. The anti-psychotic effects of TFP have been attributed to its anti-dopaminergic and anti-adrenergic actions (Qin et al., 2009). Dopamine is known to decrease AQP4 expression in cultured astrocytes (Kuppers et al., 2008). As such, the anti-dopaminergic activity of TFP may result in increased AQP4 expression following TFP treatment and a concomitant worsening of the edema. This is exactly what we observed with the

selective D2 antagonist, L-741,626, which increased spinal cord water content above the DC + Vehicle control 3 dpi (Figure 4-3). The fact we observe the opposite with TFP, suggests that the CaM effects of TFP dominate the anti-dopaminergic effects in CNS edema. Anti-adrenergics are associated with delayed onset of edema after intracerebral haemorrhage in humans, but have no observable effect on patient outcome (Sansing et al., 2011). In our study we saw prevention of edema (rather than just delayed onset) and a strong effect on outcome with TFP, whereas the α 1R antagonist terazosin had no effect on spinal cord water content following DC crush injury. This suggests that the primary mediator of the effect of TFP in our model is via CaM inhibition, consistent with the well-established role of TFP as a CaM antagonist (Tanokura and Yamada, 1986). Previously published data using a mouse model of stroke demonstrated that treatment with TFP prevented the onset of brain edema, which was proposed to be via CaM inhibition stabilizing the integrity of the BBB. We suggest that the beneficial effects are due to a reduction in AQP4 peri-endothelial localization as seen in section 3.3.2.3, which was not measured in that study (Sato et al., 2003).

4.4.2 Neurite sparing and sprouting

Two of the main agendas of CNS trauma research are to a) reduce or inhibit the amount of damage done to neurons in the CNS in order to retain functionality, and b) enhance plasticity and regeneration of any damaged neurons to recover any potential lost functionality. Mammalian neurons are intrinsically unable to endogenously regenerate, meaning that tissue damage and neuronal death is critical to functionality. Data obtained from in vivo electrophysiology recordings of

CAPs in the spinal cord indicate that 6 weeks after DC injury, those treated with inhibitors of PKA or CaM demonstrated significantly improved neuronal conductivity across the spinal cord lesion site compared to those injured and untreated. This was demonstrated in both the CAP area (Figure 4-7a_{ii}) and CAP amplitudes in response to stimulation between 0.4 and 1 (Figure 4-7b). These data demonstrate that these inhibitors have the potential not only to reduce the edema seen after a SCI, but also to improve the functionality of the spinal cord at later timepoints after edema has resolved. This is also supported by behavioural data collected by my supervisor Zubair Ahmed prior to the start of my project. This data demonstrates that as soon as 1 week post-injury, and up to 6 weeks post-injury, there can be observed significant improvement in both tape sensation tests (Figure 4-12a) and ladder walking tests (Figure 4-12b) in rats treated with TFP or H-89 compared to injured rats without treatment. Some clinical data does demonstrate that there is a direct correlation between the severity of edema after injury and the long-term functional recovery of patients (Miyanji et al., 2007; Flanders et al., 1999). It is possible to suggest that the improvement in the CAPs recorded across the spinal cord lesion when treated with TFP are a consequence of the preservation of axons as a result of reduced edema. However, it's also possible that other factors, such as affecting neurite sprouting of spared axons, may also explain the significant improvement observed.

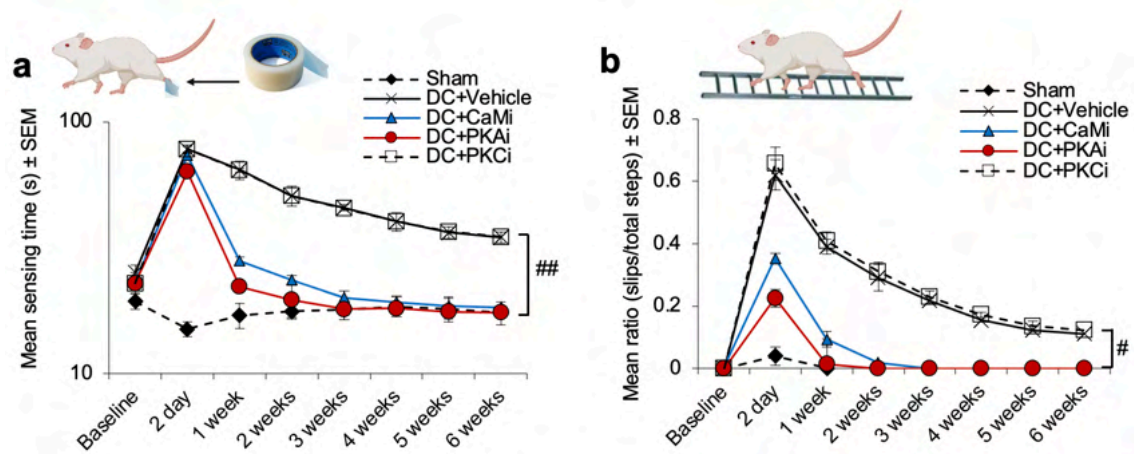


Figure 4-12 Treatment with inhibitors of AQP4 expression and subcellular relocation after cytotoxic edema in vivo improves sensory and locomotor functional recovery.

a) Both CaMi and PKAi treatment significantly improved the hind paw tape sensing and removal time and within 1 week, CaMi-treated and PKAi-treated rats recovered completely and were indistinguishable from Sham controls. b) The mean ratio of slips/total steps in a ladder-crossing test is significantly improved after CaMi and PKAi treatment, returning to Sham control levels by 1 week. For both tape sensing/removal and ladder crossing tests, significant deficits remained in both DC+Vehicle-treated and DC+PKCi treated rats, # = $p < 0.05$, linear mixed model and ## = $p < 0.05$.

The literature is divided on whether TFP is able to promote or inhibit neurite outgrowth. It was first reported that TFP promotes neurite outgrowth in primary hippocampal neurons up to a concentration of 2.5 μM (above which TFP produced inhibition) but only in the presence of inhibitory substrates, and has no effect at low doses on permissive substrates, such as laminin (Johnstone et al., 2012), although no dose-response was tested on permissive substrate. Subsequently, a high-throughput study in iPSC-derived neurons determined that TFP can promote neurite outgrowth on permissive laminin substrate with half-

maximal effective concentration (EC_{50}) of 21.3nM (Sherman and Bang, 2018). Whether this difference is due to the neuronal subtype tested is unknown, but it appears that on permissive substrates, TFP can enhance neurite outgrowth at nanomolar concentrations, but higher concentrations will result in neurite outgrowth inhibition. In the context of the electrophysiology data obtained in this study, it was prudent to determine whether TFP demonstrates any promotion of neurite outgrowth in spinal cord neurons, such as DRGNs, which project fibres through the dorsal column (i.e the area injured in the rat model), and so would be directly subject to intraspinal injection of TFP. In addition to reducing edema after spinal cord injury, which would decrease the intrathecal pressure of the cord and reduce the hypoxia and ischemia damaging the neurons, it is possible that TFP may also promote neurite outgrowth, which would aid the functional recovery observed here. As such, DRGN were cultured in increasing concentrations of TFP across the range determined from the aforementioned studies (0 – 100 μ M). It is important to note that the viability of DRGNs was poor when cultured on uncoated, or poly-D-lysine coated coverslips alone, and adherence could only be observed with pre-coating of laminin (data not shown). Interestingly, concentrations of 10 μ M or above appeared to significantly inhibit neurite outgrowth of DRGNs, and at 100 μ M, most DRGNs appeared completely unable to extend any neurite process at all. No cytotoxicity assay was performed, but many of the cell bodies observed when treated with 100 μ M TFP appeared apoptotic, and so this dose was considered toxic. It is possible that TFP causes inhibition of neurite outgrowth due to its effect on growth cone dynamics. CaM is known to affect neurite outgrowth by modulating growth cone motility (Polak et

al., 1991). Xi et al., 2019 demonstrate that inhibition of Ca^{2+} /Calmodulin-dependent protein kinase II (CaMKII), a downstream kinase activated by CaM, prevents actin extension within the growth cone.

4.4.3 Summary

The evidence presented in this chapter demonstrates that treatment with CaM inhibitor TFP or PKA inhibitor H-89 significantly reduce post-traumatic edema in a rat model of spinal cord injury, and that this reduction in edema facilitates better functionality across the spinal cord lesion site chronically. In the context of the discussed literature, it remains unknown whether the reduction in edema alone is enough to produce the significant improvement in neuronal function observed at 6 weeks post-injury. It appears as though TFP, at least when cultured on permissive substrate, inhibits the ability of neurites to sprout at concentrations of 10 μM and above. Given that the concentration injected directly into the spinal cord was significantly higher than the dose resulting in neurite outgrowth inhibition *in vitro*, it is unlikely that TFP promotion of neurite outgrowth is what produces the improved electrophysiology observed. Both TFP and H-89 were only injected once directly following injury, which suggests that the beneficial effect of the drugs on spinal cord electrophysiology may have been the result of preventing an acute pathology, rather than the facilitation axon regeneration, *per se*.

Chapter 5

Investigating the effect of AQP4 subcellular relocalization on astrocyte migration and its contribution to astrocytic scarring

5 Chapter 5

5.1 Rationale

Astrocytes are a type of glial cell with many functional responsibilities in the CNS, including neuroprotection. Astrocytes have a specialized morphology, including processes that ensheath the CNS vasculature and neuronal synapses. This allows them to facilitate clearance of excess neurotransmitters in order to reduce excitotoxicity, maintain ionic regulation to facilitate normal neuronal excitability, and maintain the integrity of the blood-CNS barriers (Verkhratsky and Nedergaard, 2018). However, in response to trauma, astrocytes take on a reactive phenotype, altering their protein expression, morphology, and function in a process known as reactive astrogliosis (Sofroniew, 2015). This reactivity occurs as a consequence of BBB damage and serum leakage, increased inflammation, and activation of astrocyte cell-surface receptors for various inflammatory stimuli, such as DAMPs and cytokine/chemokine receptors. Such signals influence changes in gene expression for proteins that contribute toward cell morphology, growth, and proliferation (Sofroniew, 2014; Hamby et al., 2012). The consequence of increased reactive gliosis following a traumatic injury to the spinal cord is proliferation of reactive astrocytes and migration of them to the lesion site to aid repair. Astrocytes, alongside other cell types such as microglia, macrophages, and NG2 cells, then facilitate the formation of a astrocytic scar; a dense multicellular formation containing a dense extracellular matrix composed mostly of laminin, fibronectin and collagen I, as an attempt to repair the wound. Proliferation and migration of astrocytes occurs within the acute stage of injury progression (around 1-3 days, Figure 5-1), followed by a period of clustering and overlapping of endfeet domains between 7 and 14 days post-injury, which forms the dense scar border (Wanner et al., 2013). This formation persists chronically, and in

most cases never fully heals, however the long-term size and severity of the scar depends on the severity of the primary injury. A recent multi-institute review recently addressed the nomenclature around astrocytes in their various states of reactivity, including in CNS scar formation, as a morphologically separate feature of the scar. They concluded that a reasonable term to describe astrocytes in this context would be as an “astrocytic scar” (Escartin et al., 2021). Therefore, will be referred to as such going forward.

Reactive astrogliosis increases the migratory capacity of astrocytes. The role of AQP4 in the onset of astrogliosis remains undetermined. AQP4, (as discussed in chapter 3), is mostly localized to perivascular and perisynaptic astrocyte endfeet. I showed that AQP4 localization around blood vessels increased after injury (see chapter 3), which we suggest contributes to the oedemous effect after spinal cord injury (see chapter 4). However, AQP4 also has other roles in astrocytes, including in migration, which is a key feature of reactive astrocytes that contributes towards the formation of the astrocytic scar. Many studies demonstrate that astrocytes within uninjured, extralesional tissue migrate into the lesion in response to local signalling, overlap in their special domains, and contribute to the development of the dense astroglial border of the scar (Wang et al., 2004; Saadoun, 2005; Rhodes et al., 2003; Homkajorn et al., 2010). Other studies suggest that long-distance migration does not occur, but newly proliferated astrocytes at the lesion border will reorganize in morphology along the lesion border at the extent of the damage, concurrent with reorganization of AQP4 along the lesion border (Wanner et al., 2013). Migration of astrocytes is in part dependent on the localization of AQP4 in the cell membrane. This is probably due to the requirement of compartmental water fluxes that create membrane protrusions for

cytoskeletal rearrangements that facilitate cell migration. Mechanistically, this is thought to be the result of local fluctuations in osmolarity, likely as a result of haemorrhage and ischemia, resulting in localized uptake of water within a region of a cell, causing membrane expansion (Jaeger et al., 1999) (Figure 5-2). The localized expansion is then stabilized by the extension of actin filaments into the newly formed space, creating the cell protrusion (Oster and Perelson, 1987; Loitto et al., 2009). Compartmentalized changes in osmolarity increase the rate of migration of the astrocytes, which is prevented when AQP4 is knocked out (Saadoun, 2005). Furthermore, astrocyte migration is significantly impaired in both transwell migration and scratch assays in the absence of AQP4 expression. AQP4 appears to be most densely expressed at the leading edge of the migrating astrocytes *in vitro* in the absence of any change in osmolarity, suggesting that local changes in osmolarity alone are not sufficient for the membrane protrusions, and perhaps the mechanism also involves localized increased water permeability by redistribution of AQP4 to the appropriate membrane compartments (Saadoun, 2005). Further to this, the border of the astrocytic scar is much farther from the lesion core in AQP4-null mice after brain stab injury than in wild-type mice (Saadoun, 2005).

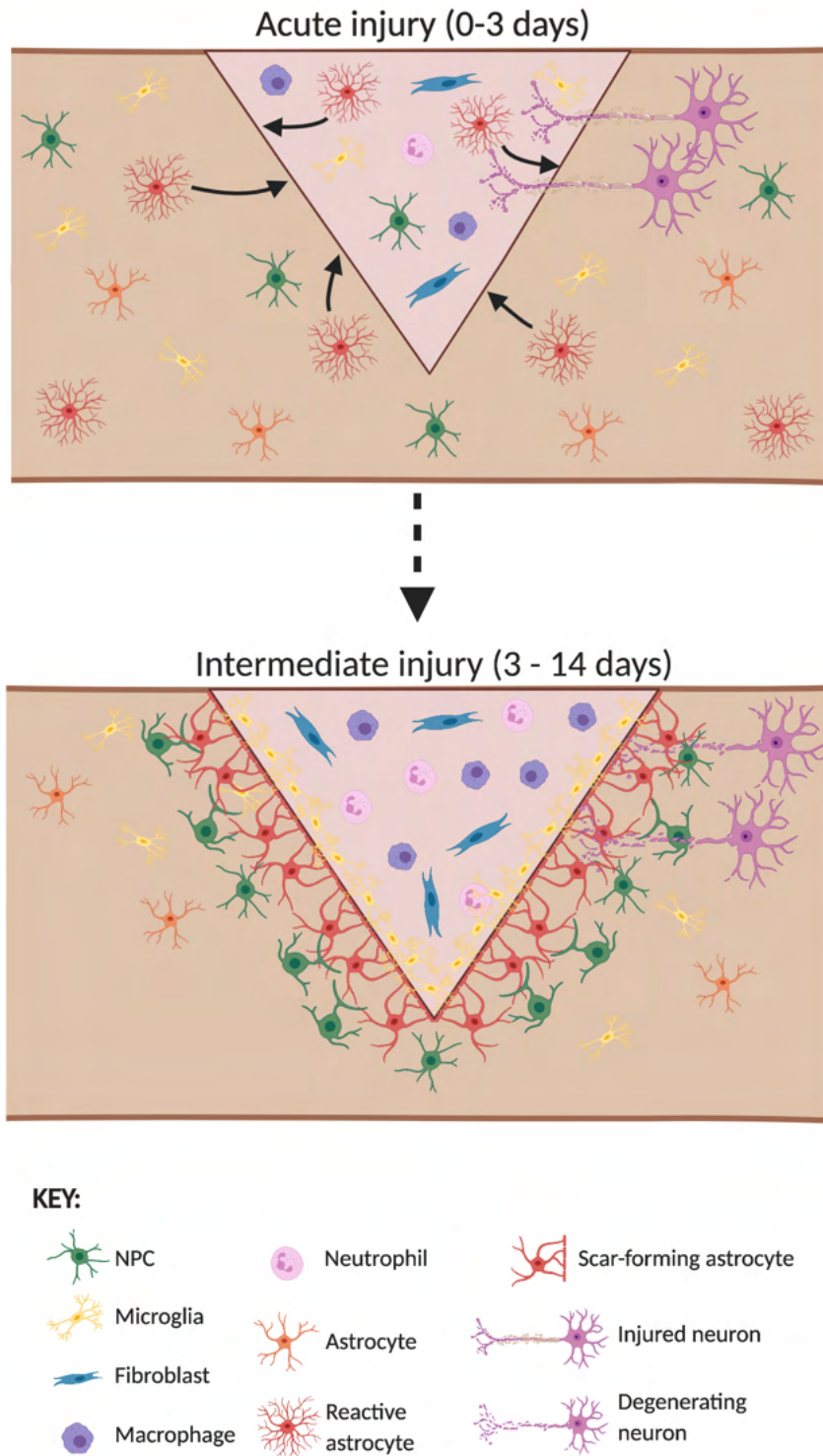


Figure 5-1 A schematic representing the distribution of cell types at various time periods after traumatic spinal cord injury.

The acute secondary injury phase (0 to ~3 days post-injury) involves early neuronal cell loss and demyelination in cells damaged by the primary injury, recruitment of blood-borne immune cells such as fibroblasts, macrophages and neutrophils to the site of injury, reactivity and

proliferation of microglia, and reactivity, proliferation, and migration of astrocytes to the site of injury. The subacute secondary injury phase (~3 to 14 days post-injury) involves more extensive neuronal loss and loss of myelination, deposition of extracellular matrix proteins from fibroblasts, and a border of lesion formation by the dense overlapping meshwork of astrocyte processes, termed the “astrocytic scar”, and the accumulation of reactive microglia between the astroglial border and the fibrotic scar.

Collectively, this evidence suggests that the dynamic subcellular localization of AQP4 may be important for the role of astrocytes in formation of the scar. Data from our group showed that AQP4 can be regulated in astrocytes by subcellular translocation in a manner dependent on protein kinase A (PKA) and calmodulin (CaM). Furthermore, this mechanism appears to be important for regulating the translocation of AQP4 *in vivo*; treatment immediately after traumatic spinal cord injury appears to prevent translocation of AQP4 to the perivascular endfeet acutely after injury, which is concurrent with a reduction in spinal cord edema. However, scarring is a more chronically persisting problem, and involves a slower progression. As such, this chapter aims to explore whether inhibiting the subcellular relocalization of AQP4 affects the migration of astrocytes, and to determine what effect, if any, this has on the overall size and morphology of the scar, and in particular, the astrocytic scar.

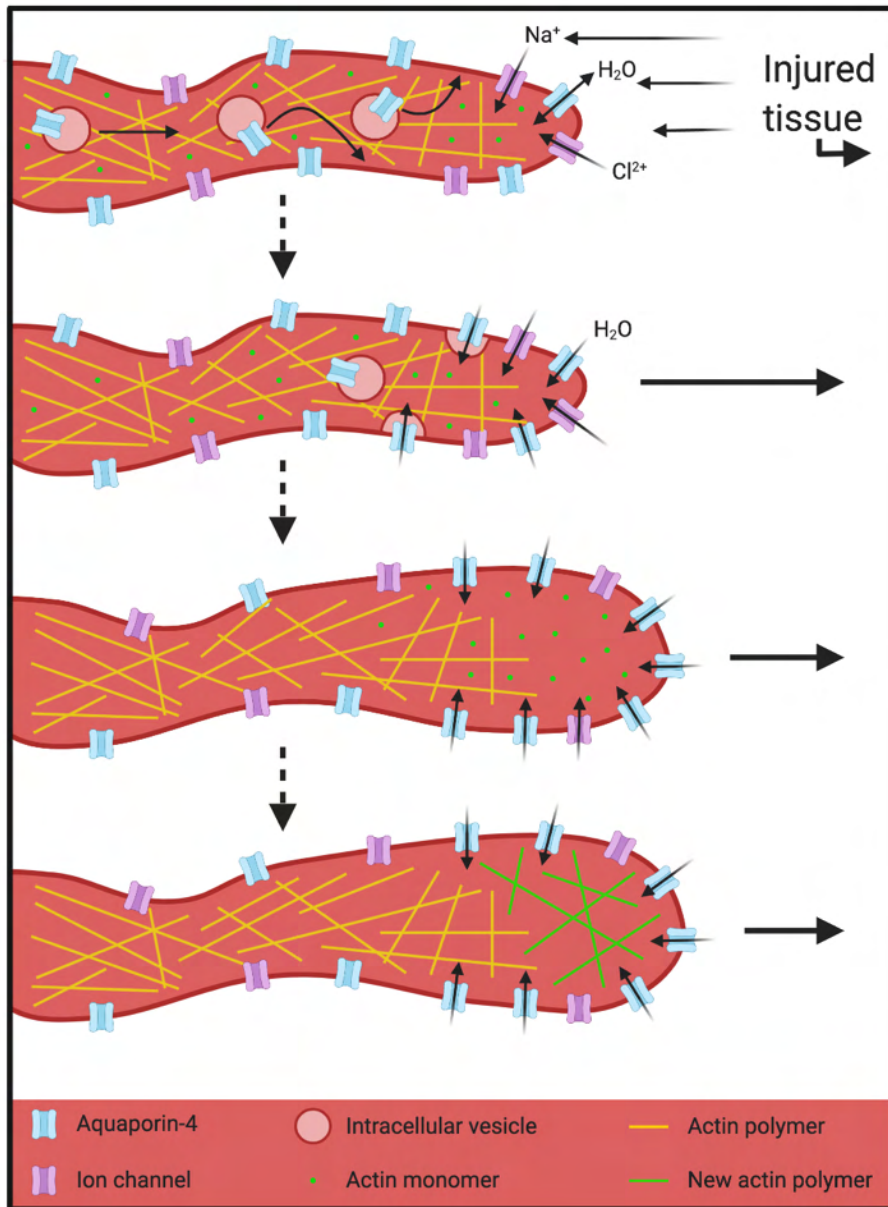


Figure 5-2 A schematic demonstrating the mechanisms of astrocyte membrane expansion and stabilization for the purpose of migration.

Briefly, in response to various traumatic stimuli and compartmentalized changes in tissue osmolarity, water permeability increases in a localized manner at the leading edge of the migrating astrocyte. Increased uptake of extracellular ions is followed by increase uptake of water to maintain the osmotic environment. Increase in water uptake results in membrane expansion, which is then stabilized by the polymerization of free-floating actin monomers.

5.2 Aims and hypothesis

I hypothesize that to facilitate the migration of astrocytes, AQP4 becomes relocalized to the leading edge of astrocytes, in a mechanism involving CaM and PKA. I further hypothesize that these inhibitor of CaM or PKA may be beneficial for limiting the progression of the dense astrocytic scar border formation *in vivo*.

Aims:

- To determine whether inhibition of PKA or CaM alters the morphology of the astrocytic scar in an *in vivo* spinal cord injury model
- To determine whether inhibition of PKA or CaM alters the rate of migration of primary astrocytes *in vitro*
- To establish a population of GFP-AQP4 expressing astrocytes from human induced pluripotent stem cells (hiPSCs)
- To determine whether AQP4 relocalization to the leading edge of migrating astrocytes is the mechanism facilitating astrocyte migration, which may be inhibited.

5.3 Results

5.3.1 Inhibition of CaM or PKA significantly decreased the overall size of the scar, as well as the GFAP immunoreactivity at the scar border

Tissue sections obtained from rats subject to dorsal column crush injury, as described in section 2.1.3.2. This was the same model used to determine AQP4 subcellular localization and edema in previous chapters. Sections were stained for GFAP to demarcate the scar border of the lesion site at 7 days post-injury, as in accordance with the literature (Figure 5-3). The area of the lesion, demarcated by the glial border of the scar, was significantly smaller in cords from rats treated with CaM inhibitor TFP or PKA inhibitor H-89 compared to that measured from injured, untreated cords (Figure 5-3A; $1.31 \pm 0.44\text{mm}^2$ or $1.35 \pm 0.33\text{mm}^2$, respectively, to $2.83 \pm 0.44\text{mm}^2$). In addition to lesion area, the density of astrocytes at the astrocytic scar border was measured by quantifying the intensity of GFAP immunostaining at the lesion border. These data demonstrated that the density of GFAP within the astrocytic scar was also significantly reduced in rats treated with either TFP or H-89 compared with that from injured, untreated rats at 7dpi (Figure 5-3B; 4.13 ± 2.02 or 5.73 ± 2.47 , respectively, to 12.08 ± 2.61 , arbitrary units of mean fluorescence minus background).

Sections of the same tissue were also immunostained for macrophages (CD68) to determine the overall size of the contained injury at 7dpi (Figure 5-4). Quantification of the area of positive immunofluorescence was significantly reduced in rats treated with either TFP or H-89 compared with injured, untreated rats (Figure 5-4; $54.7 \pm 24.4\%$ and $47.0 \pm 18.9\%$, respectively, to $100 \pm 40.8\%$)

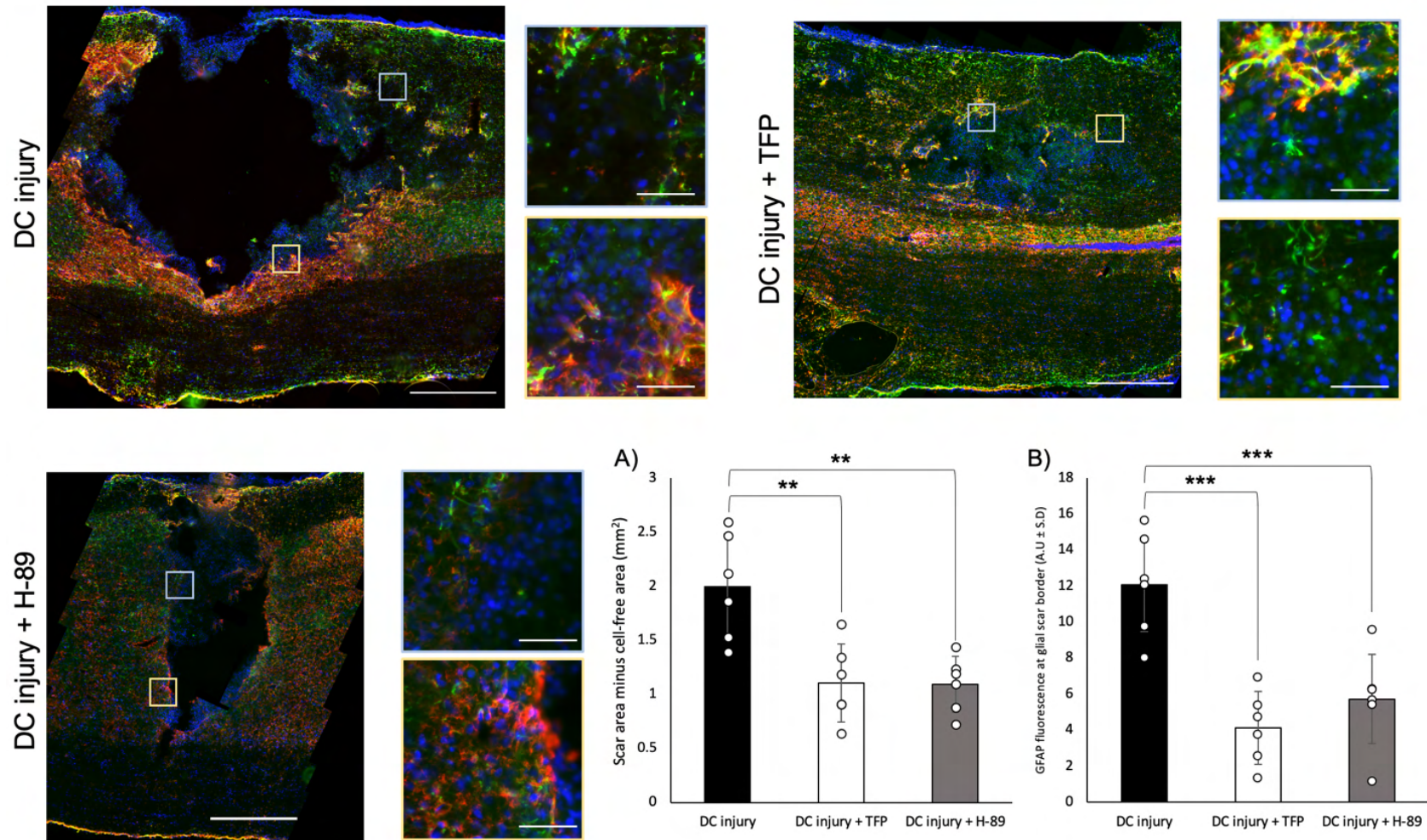


Figure 5-3 Immunohistochemistry of GFAP (green), AQP4 (red) and DAPI (blue) in rat spinal cord to demonstrate the morphology of the astrocytic scar barrier containing the entire lesion wound cavity at 7dpi.

Scale bar cords = 500 μ m, inserts = 150 μ m. (A) Quantification of the tissue-positive area within the astrocytic scar border, as determined by positive GFAP fluorescence. (B) Quantification of the fluorescence of GFAP at the astrocytic scar border, recorded as means of 8 randomized sections along the border per image (n=6 animals, n=3 sections/animal). For both methods of quantification, images were quantified using ImageJ, statistical significance was determined using a one-way ANOVA followed by Bonferroni post-hoc test; ** = $p < 0.01$, *** = $p < 0.001$.

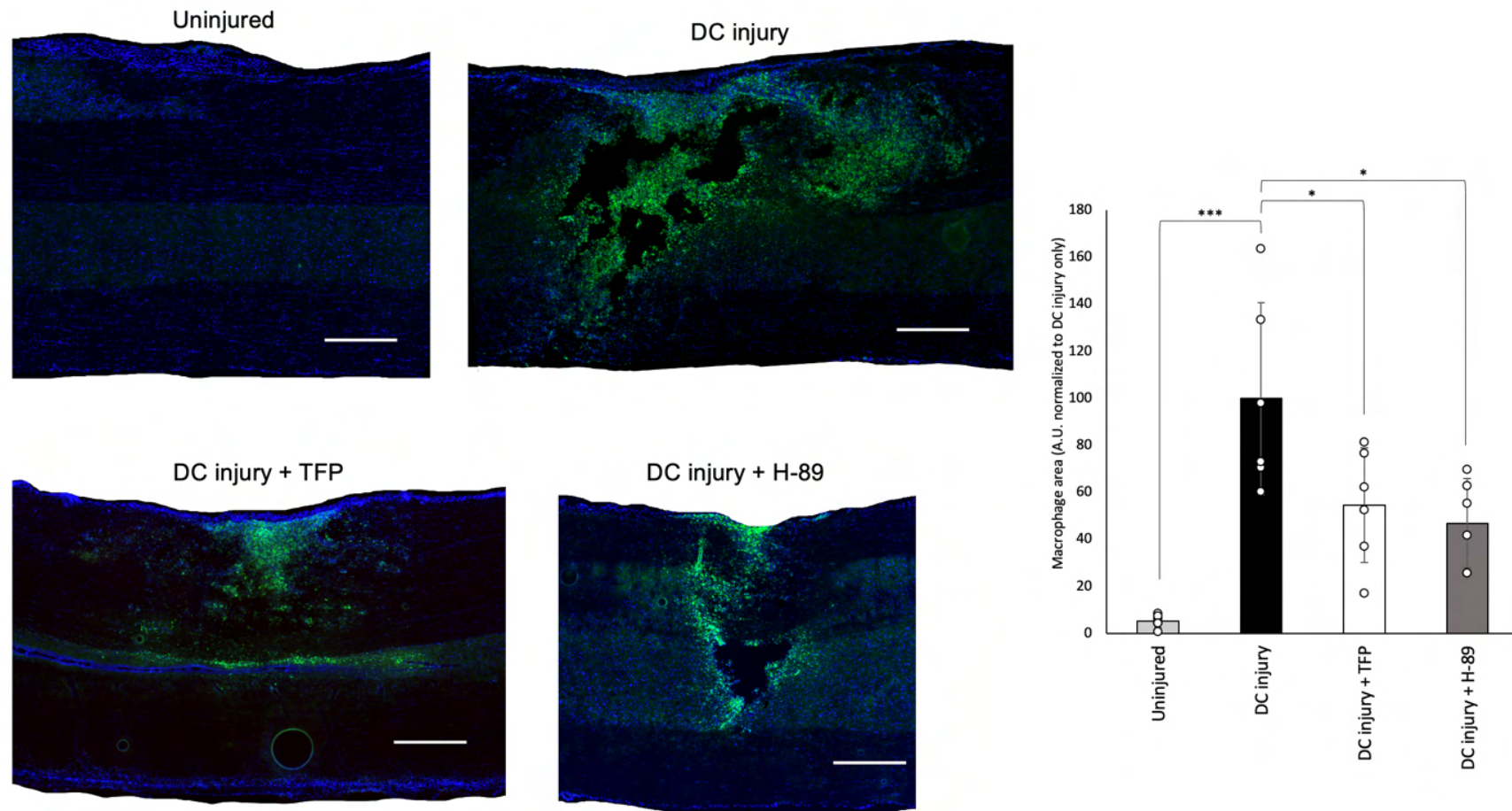


Figure 5-4 Immunohistochemistry of CD68 (green) and DAPI (blue) in rat spinal cord to demonstrate the extent of macrophage infiltration to the spinal cord lesion site at 7dpi.

Scale bar cords = 500 μ m, inserts = 150 μ m. Area contained within the astrocytic scar was measured using ImageJ and statistical significance determined using a one-way ANOVA followed by Bonferroni post-hoc test. *** = $p < 0.001$ (n=6 animals/treatment group, n=3 sections/animal).

5.3.2 Investigating the effect of calmodulin or PKA inhibition on the rate of astrocyte migration *in vitro*.

Given that inhibition of CaM or PKA both inhibits the subcellular relocalization of AQP4 *in vitro*, and appears to reduce the size of the scar formed after traumatic SCI, I next investigated whether these inhibitors also affected the rate of migration of astrocytes *in vitro* using two standard cell migration/invasion assays.

5.3.2.1 *Scratch wound closure assay*

Scratch wound closure assays are *in vitro* assays frequently used to investigate the effect of treatments or conditions on the rate of cell movement into a cell-free area when confluent adherent cells are removed by mechanical scratch (see methods section 2.2.4.2).

5.2.1.1.1 *Optimization of appropriate cell culture media to minimize proliferation*

Prior to conducting the scratch wound closure assays, appropriate culture/treatment conditions were established to ensure that extraneous factors do not confound the data. Firstly, to ensure that proliferation of the primary rat astrocytes was minimized as to prevent cell proliferation from clouding migration, a number of cell culture medias were trialled. Cells were treated for 72 h in either standard astrocyte culture media (DMEM with high glucose, pyruvate and glutamine) supplemented with either 20% or 1% serum, or AWESAM media (50% DMEM, 50% Neurobasal-A supplemented with B27, HB-EGF and Glutamax).

AWESAM media, developed by Wolfes and Dean (2018), is a culture media for the production of primary murine astrocytes in order to culture them *in vitro* in a stellate, *in vivo*-like morphology, behaviour and genetic expression profile (Figure 5-5D). In this media, primary astrocytes have been previously observed in our group to be highly limited in proliferation rate. Results demonstrate that cells cultured in standard primary rat astrocyte media (DMEM + 20% serum) had a significantly increased proliferation rate after 96 h of culture compared to baseline (Figure 5-5A: $261.11 \pm 65.46\%$ to 100 ± 8.51). By contrast, both DMEM + 1% serum and AWESAM media both prevent significant proliferation in astrocytes after 96hrs of treatment compared to baseline (Figure 5-5A: $133.33 \pm 10.88\%$ and $122.22 \pm 28.46\%$ to $100 \pm 8.51\%$). However, treatment with DMEM + 1% serum reduced the viability of the cells (Figure 5-5B: $83.33 \pm 2.69\%$), an effect not observed by treatment with AWESAM media (Figure 5-5B: $97.27 \pm 1.63\%$). Therefore, AWESAM media was used as the most appropriate media to culture astrocytes for scratch wound closure assays in this chapter.

5.2.1.1.2 *Optimizing drug treatment concentrations to avoid cytotoxicity*

To measure the concentrations of inhibitors of CaM or PKA that do not produce a significant cytotoxic effect on primary rat astrocytes that may impair the wound closure rate due to cell loss, cytotoxicity was measured in primary rat astrocytes after 96 h of treatment with varying doses of CaM inhibitors TFP and W-7, and PKA inhibitor H-89, using the MTT assay as a measure of cellular metabolic activity. In comparison to control, media-only treated cells (Figure 5-5C: 1.00 ± 0.24), astrocytes treated $12.7\mu\text{M}$ TFP, the reported IC_{50} of TFP for CaM

demonstrated no significant difference in metabolic rate (Figure 5-5C: 1.07 ± 0.13). However, treatment with 10x the IC_{50} of TFP for calmodulin ($127\mu\text{M}$) did produce a significantly impaired metabolic rate (Figure 5-5C: 0.58 ± 0.32). An alternative calmodulin inhibitor, W-7, was also tested for cytotoxicity at a concentration equal to its IC_{50} for calmodulin (MacNeil et al., 1988), as well as 10x higher than this dose. Treatment with $290\mu\text{M}$ W-7 significantly reduced the metabolic activity of the astrocytes (Figure 5-5C: 0.47 ± 0.25), but treatment with $29\mu\text{M}$ W-7 did significantly change the metabolic activity compared to control (Figure 5-5C: 0.93 ± 0.31). Finally, astrocytes were also treated with concentrations of either 500nM or $5\mu\text{M}$ H-89. The reported in vitro IC_{50} of H-89 for PKA is 50nM , and the reported inhibitory doses vary between $10\text{-}30\mu\text{M}$. However previous work by our group demonstrated that $5\mu\text{M}$ H-89 is effective at inhibiting AQP4 relocalization (Kitchen et al., 2015). Treatment with either 500nM or $5\mu\text{M}$ produced no significant changes to metabolic rate compared with control (Figure 5-5C: 1.06 ± 0.15 and 1.03 ± 0.15 , respectively).

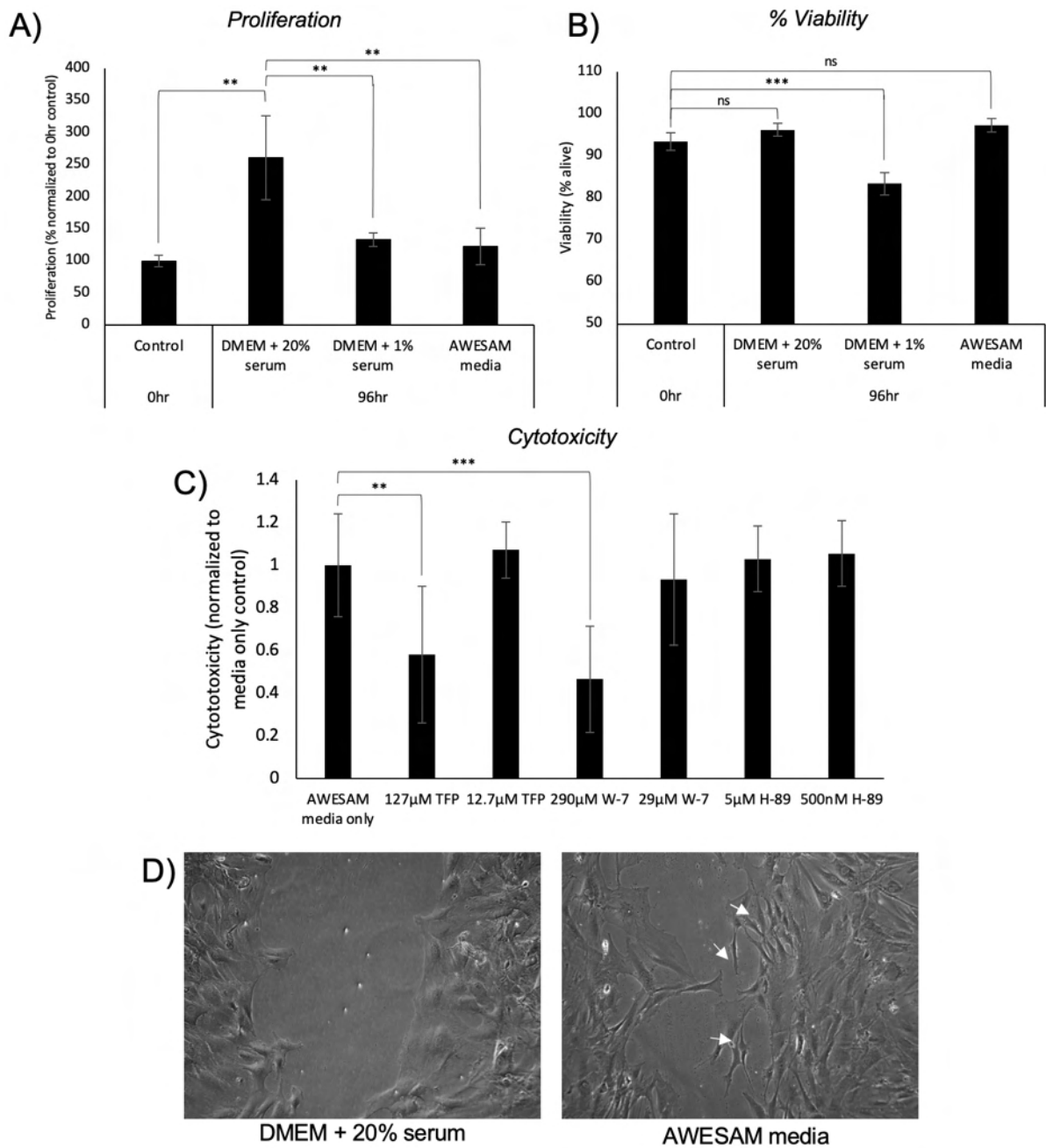


Figure 5-5 Optimization of cell culture conditions for an *in vitro* scratch wound closure assay using primary rat astrocytes.

The proliferation rate of cultured primary rat astrocytes was determined by manual cell counting from the day after plating (0hr) and again 96hrs later under various culture conditions. The viability of the cells was calculated by comparing the number of dead vs alive cells in the manual cell count. Cytotoxicity was measured using a standard MTT

assay to determine the dosage of inhibitors that may result in cytotoxicity after 96hrs of culture. For each drug, the lower concentration is equal to the reported IC50 for that drug against the intended drug target. For all graphs, * indicates $p < 0.05$, ** indicates $p < 0.01$, and *** indicates $p < 0.001$ by ANOVA followed by t-test with Bonferroni correction (n = 3).

5.2.1.1.3 *Inhibition of either CaM or PKA reduces rate of scratch wound closure in primary rat astrocytes*

Primary rat astrocytes were plated in 24-well plates, scratched along the centre of each well, and treated with either AWESAM media only, AWESAM media with 12.7 μ M TFP (CaM inhibitor) or AWESAM media with 500nM H-89 (PKA inhibitor). Astrocytes were then imaged by live-cell phase-contrast microscopy immediately following scratch and treatment, and every 12 hours until 96 hours. The area within the scratch was then measured in ImageJ at 0hr post-scratch and 96hrs post-scratch, and the difference was determined as the “area migrated”. Treatment with either TFP or H-89 significantly impaired the migration rate of astrocytes into the scratch wound area compared to untreated media-only controls (Figure 5-6: 0.43 ± 0.15 or 0.81 ± 0.08 , respectively, to 1.00 ± 0.15).

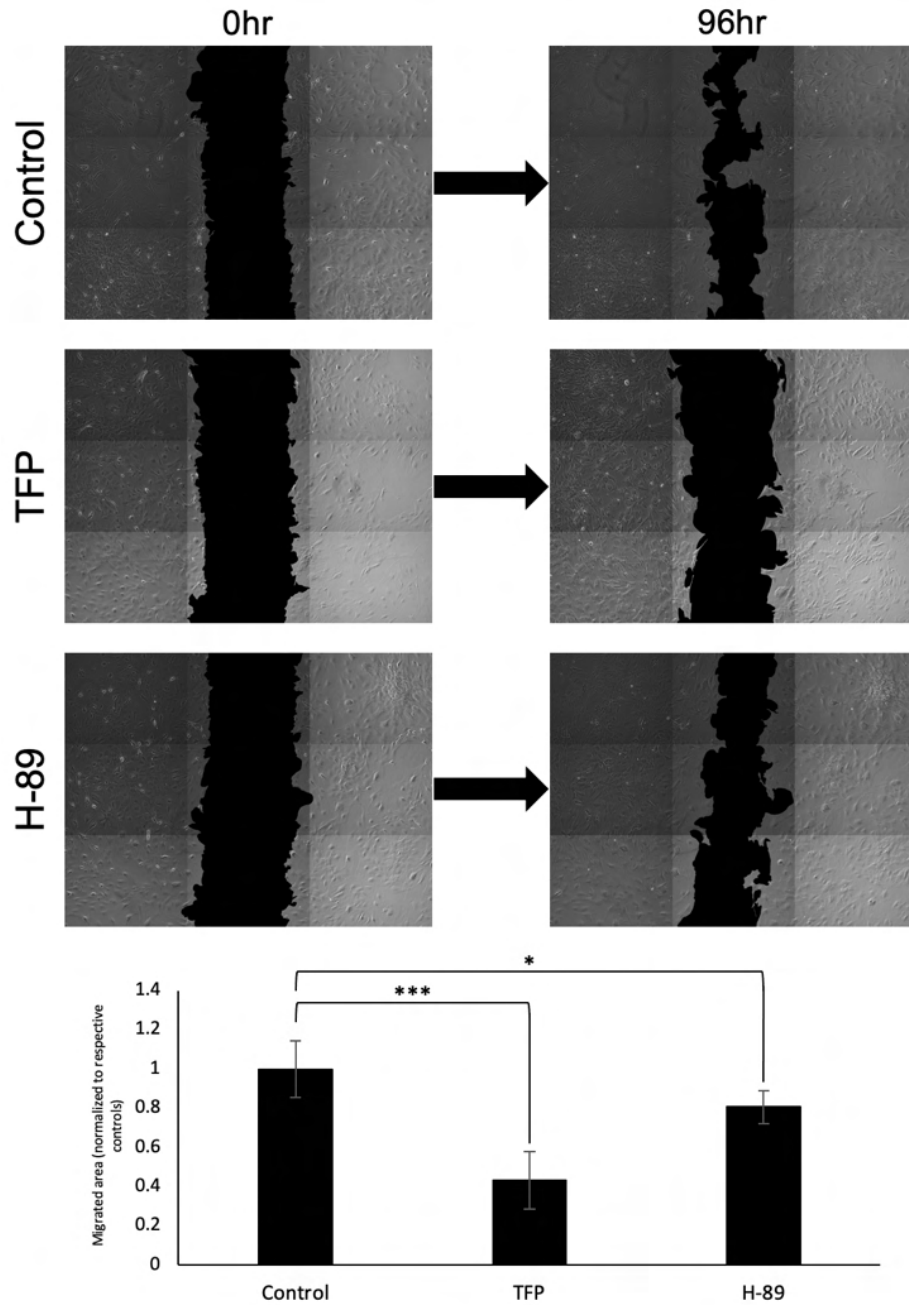


Figure 5-6 The effect of TFP or H-89 treatment on the rate of scratch wound closure in primary rat astrocytes.

A) Representative images of the scratch wound area at 0hr and 96hr post-scratch under each treatment condition. Representative images were selected as the closest calculated value to the overall mean across all biological repeats. B) Quantification of the migrated area into the scratch wound area of primary rat astrocytes after 96hrs of post-scratch incubation. Values are all normalized to the respective mean of each

biological repeat (n = 3). * indicates $p < 0.05$ and *** indicates $p < 0.001$ by ANOVA followed by t-test with Bonferroni correction.

5.3.2.2 *Transwell migration assay*

The second migration/invasion assay used to assess the effects of TFP/H-89 treatment on the migration rate of primary rat astrocytes involved a transwell setup (more details can be found in materials section 2.2.4.3).

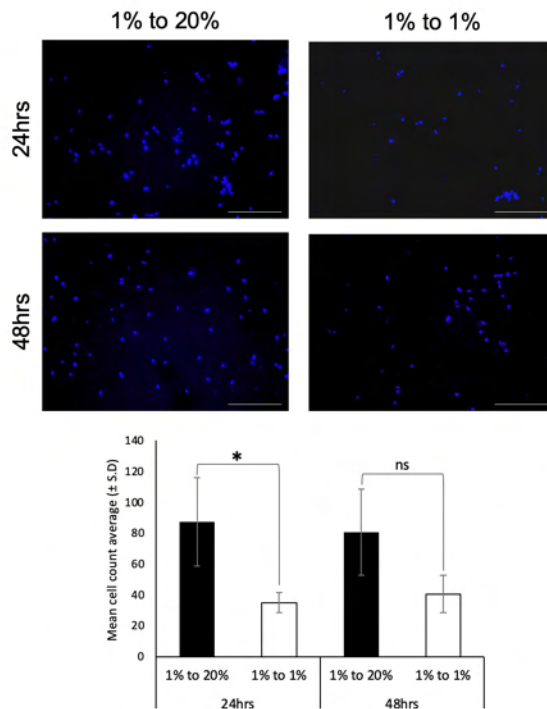
5.2.1.1.4 *Optimization of readout method for transwell migration assay*

To determine the effect of inhibitors on chemoattractant-mediated migration of primary rat astrocytes, the rate of migration across transwell membranes was calculated. The proportion of cells that migrated across the 8 μm diameter pores of the transwell membrane was compared using two methods. For each method, two conditions were compared to determine the effectiveness of migration; cells in the upper compartment were plated in media containing 1% serum, with the lower compartment containing either 20% serum as a chemoattractant to aid migration from the upper to the lower surface of the membrane, or 1% serum, which provides no chemoattractant to aid migration.

In the first method of quantification, cells on the upper surface of the transwell were removed by scraping, so that only those cells that migrated would remain on the membrane. The membrane was then removed, and mounted on a slide using mounting media containing DAPI. Cells were then counted across six randomized fields of view across the membrane at 10x magnification (Figure 5-7a).

The second method involved scraping the upper surface of the transwell membrane, and incubating those remaining in 8 μ m Calcein-AM, an acetomethoxy derivative of calcein, that is passively taken up into cells, and cleaved by esterases to release green fluorescence calcein in living cells only (Bratosin et al., 2005). These cells were then detached from the membrane using accutase, and the fluorescence read in triplicate per transwell (Figure 5-7b). Results from both methods of quantification indicate that the serum gradient generated using 20% serum in the lower compartment significantly increases the migration rate of primary rat astrocytes across the transwell membrane after 24hrs compared to wells with no serum gradient (Figure 5-7a: 87.28 ± 28.52 to 34.94 ± 6.48 ; Figure 5-7b: 296.41 ± 63.58 to 100.00 ± 8.12). After 48hrs, the migration rate as determined by the calcein fluorescence method also demonstrated a significant difference between the 20% to 1% and 1% to 1% groups (Figure 5-7b: 207.27 ± 55.55 to 100.00 ± 33.73), however no statistically significant difference was observed between these two groups using the cell counting method (Figure 5-7a: 80.71 ± 27.88 to 40.56). These results demonstrate that using 20% serum in the lower compartment is effective as a positive control for aiding migration of astrocytes across the transwell membrane going forward. Furthermore, it identifies that both methods of calculating migration rate produce the same interpretable result. From here, the calcein fluorescence method was used as the differences between the two groups are more significantly different, probably owing to the more consistent nature of the methodology.

A) Cell counting on transwell membrane



B) Calcein fluorescence

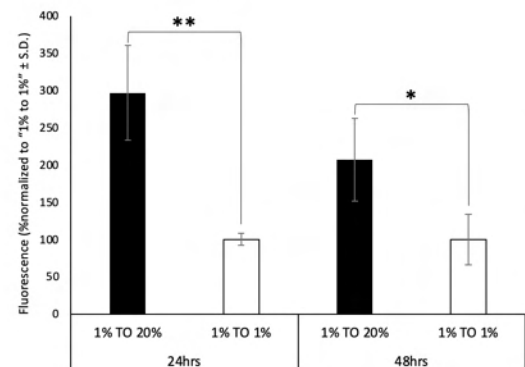


Figure 5-7 Initial optimization of two methods for calculating transwell migration.

Cells were cultured in media with 1% serum within the transwell insert atop the membrane. For positive control of migration, the lower chamber contained media containing 20% serum. Calcein fluorescence readout values were all normalized to the respective mean of each biological repeat. * indicates $p < 0.05$ and *** indicates $p < 0.001$ by ANOVA followed by t-test with Bonferroni correction. Error bars represent \pm S.E.M.

5.2.1.1.5 Inhibition of CaM by TFP reduces transwell migration rate of astrocytes

The proportion of cells that had migrated across the 8 μ m diameter transwell pores over 24 h was determined using the calcein fluorescence model optimized in section 5.2.1.1.4. Compared to the positive control (1% to 20%), the addition of TFP to both the top and bottom chamber significantly reduced migration (Figure 5-8; $100.00 \pm 5.04\%$ and $77.67 \pm 2.82\%$, respectively). Addition of H-89

to both chambers had no significant effect on migration compared to positive control (Figure 5-8; $100.00 \pm 5.04\%$ and $86.02 \pm 10.40\%$, respectively).

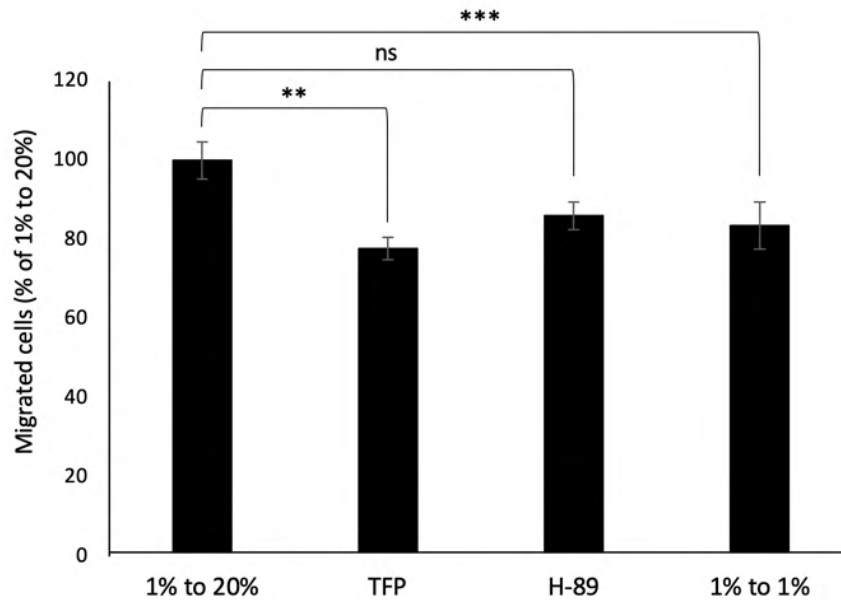


Figure 5-8 Percentage number of migrated cells 24hrs after plating, as determined using the Calcein fluorescence method.

Values are all normalized to the respective mean of the positive control group of each biological repeat. * indicates $p < 0.05$ and *** indicates $p < 0.001$ by ANOVA followed by Dunnett's post-hoc test comparing means of each group to positive control ($n = 3$). Error bars represent \pm S.E.M.

5.3.3 Investigating the effect of AQP4 membrane relocalization on astrocyte migration *in vitro*

Both TFP and H-89 appear to reduce the rate of migration in primary rat astrocytes in scratch wound closure assays, however the mechanism by which this occurs is unknown. Given the importance AQP4 in astrocyte migration

(Verkman et al., 2006; Auguste et al., 2007), and that both TFP and H-89 significantly inhibit subcellular membrane relocation of AQP4 under hypotonic, hypothermic, and hypoxic conditions (Kitchen et al., 2015; Salman et al., 2017; Kitchen et al., 2020), observing the subcellular localization in live-migrating astrocytes would be key for determining whether TFP/H-89 slow astrocyte migration by inhibiting the subcellular localization of AQP4.

5.3.3.1 *Transfection of eGFP-AQP4 into primary rat astrocytes*

In order to visualize AQP4 localization alongside migration in real time, an eGFP-AQP4 construct was transfected into primary rat astrocytes using polyethylenimine (PEI) according to a protocol previously used in our lab to transfect the same cDNA construct into HEK293 cells (Kitchen et al., 2015), and as detailed in section 2.2.3.1. After 2.5 h of incubation at 37°C with the DNA:PEI mixture, cells were imaged using phase-contrast microscopy on a Cell-IQ® live cell imaging system. The cells in all treatment groups that included PEI from 3mg (6:1 PEI:DNA ratio) to 0.5mg (1:1) per well had extensive cell shrinkage, cytoplasmic condensation, membrane blebbing, and detachment from cell-cell contact, suggesting they were highly stressed and beginning to die (Figure 5-9). None of these features were observed in the DNA-only treated well, even after 6hrs of incubation, suggesting that the toxic component in these conditions was the PEI.

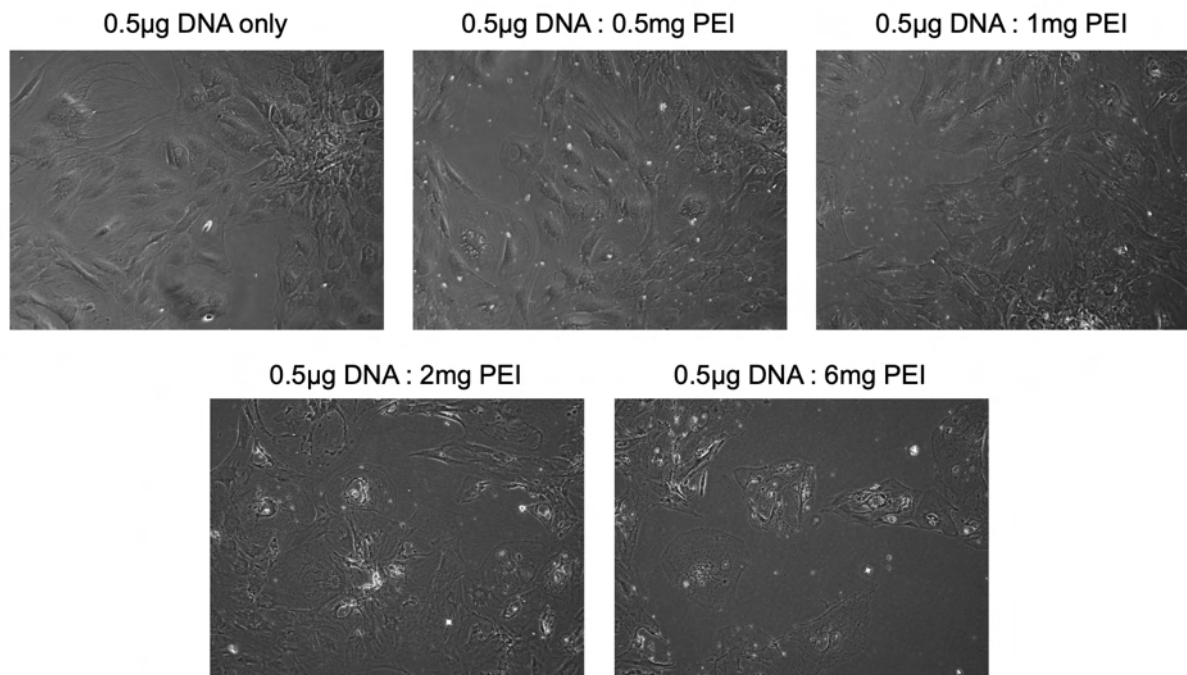


Figure 5-9 Representative phase-contrast images of primary rat astrocytes transfected with 0.5µg eGFP-AQP4 cDNA using various concentrations of polyethylenimine (PEI). Images obtained at 2.5 hours after transfection mix was added to cells.

To avoid PEI toxicity, the astrocytes were transfected with GFP-AQP4 was using lipofectamine, as described in section 2.2.3.2, optimized using the manufacturers recommended dilutions of cDNA:lipofectamine (500ng DNA combined with 3uL, 2uL, 1uL or 0.5uL LF2000 per well; dilutions 6:1, 4:1, 2:1, 1:1, respectively). Astrocytes were incubated for 48hrs post-transfection before being imaged using phase-contrast and fluorescence microscopy (Figure 5-10). The representative images shown demonstrate those with the highest amount of green fluorescence observed for each treatment group. Whilst the ratio of 2uL lipofectamine combined with 500ng cDNA yielded the best transfection efficiency overall, the

rates of transfection would still be insufficient to determine localization of AQP4 in a scratch wound closure model.

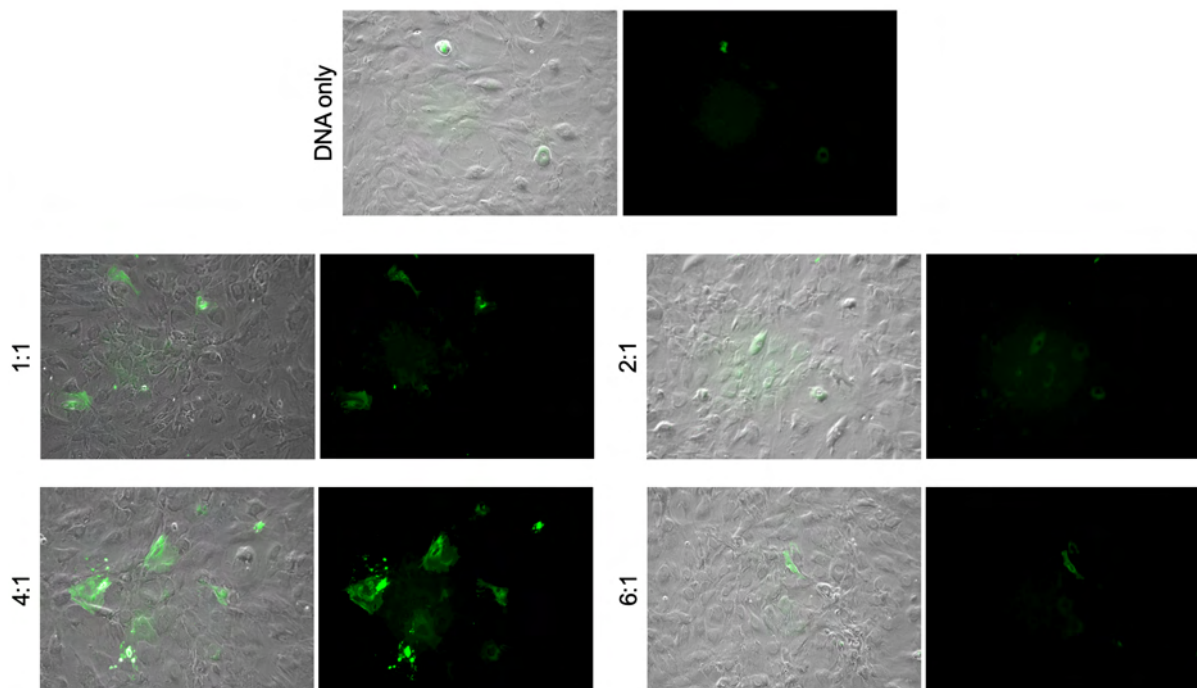


Figure 5-10 Optimization of Lipofectamine-2000-mediated transfection of eGFP-AQP4 cDNA construct into primary rat astrocytes.

Representative images were selected as those yielding the highest amount of GFP fluorescence across each treatment group after 48hrs. For each treatment group shown, images on the left depict a merge of both the phase-contrast and the GFP fluorescence of the primary rat astrocytes imaged in tandem. Images on the right represent the GFP fluorescence only.

5.3.3.2 *Differentiation of astrocytes from induced pluripotent stem (iPS) cell lines with EGFP-AQP4 knock-in*

In the absence of successful transfection of eGFP-AQP4 constructs into primary rat astrocytes, a hiPS cell line was generated with a eGFP reporter at the AQP4 locus with Applied StemCell, Inc. using CRISPR/Cas9 gene editing technology, details of which can be found in section 2.2.1.3. To differentiate naïve hiPSCs into astrocytes, they first needed to be differentiated into neural progenitor cells (NPCs).

5.2.1.1.6 hiPSC to NPC differentiation

As described in section 2.2.1.3.1, prior to differentiation, naïve hiPSCs need to be cultured into colonies. Once colonies form, the surrounding cells (potentially differentiated) are scraped off, and the remaining cells split into single cells and cultured in NPC differentiation medium. After 14 days of NPC differentiation, the cells formed rosette-like colonies within the culture, indicating according to manufacturer's instruction (Stemcell Technologies™) that they were ready for passage into NPC maintenance media (Figure 5-11, arrows) . To ensure that the cells had differentiated into NPCs, they were fixed with 2% formaldehyde, and immunolabelled on glass coverslips for markers of NPCs; Nestin, Pax6 and Sox1 (Figure 5-11). The cells positively expressed all markers, suggesting that they had successfully differentiated into NPCs, and could be cultured with NPC maintenance media until ready for astrocyte differentiation.

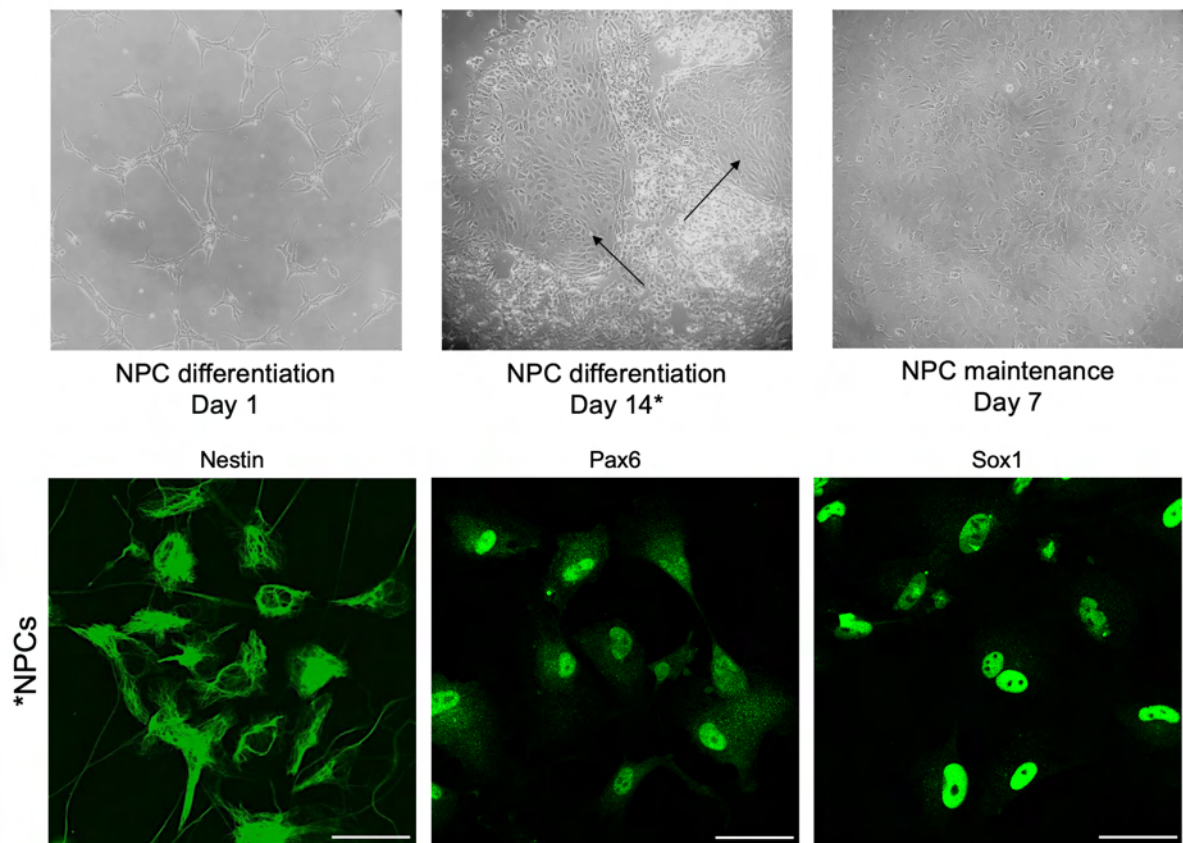


Figure 5-11 Characterization of hiPSC differentiation into hiNPCs.

A) Phase-contrast images of various stages of NPC differentiation and maintenance. Arrows indicate areas of colony formation to be isolated prior to NPC maintenance. B) Immunocytochemistry of NPCs after 7 days of maintenance using primary antibodies against NPC markers Nestin, Pax6 and Sox1. Images taken at 63x magnification using an upright confocal microscope. Scale bar = 25 μ m.

5.2.1.1.7 NPC to astrocyte differentiation

Characterized NPCs in NPC maintenance media were differentiated into astrocytes according to the protocol detailed by TCW et al., (2017). After 30 days of differentiation, as recommended, the morphology of the cells highly resembled that of astrocytes, with star-like processes extending and interacting with

neighbouring cells (Figure 5-12). At this time, cells were fixed and labelled using immunocytochemistry on glass coverslips for GFAP, a marker of astrocytes, and imaged using confocal microscopy. The cells stained positively for GFAP, suggesting that they had successfully differentiated into astrocytes. Furthermore, in primary antibody-omitted samples, GFP fluorescence was also detected in the cells, suggesting that the eGFP-AQP4 gene that was genetically inserted into the naïve hiPSCs had been expressed. AQP4 is a marker for astrocyte expression within the NPC lineage, providing further evidence the cells had successfully differentiated into astrocytes. However, the fluorescence pattern of the GFP expressed did not reflect the membranous localization of AQP4 expected (Figure 5-12, zoomed in).

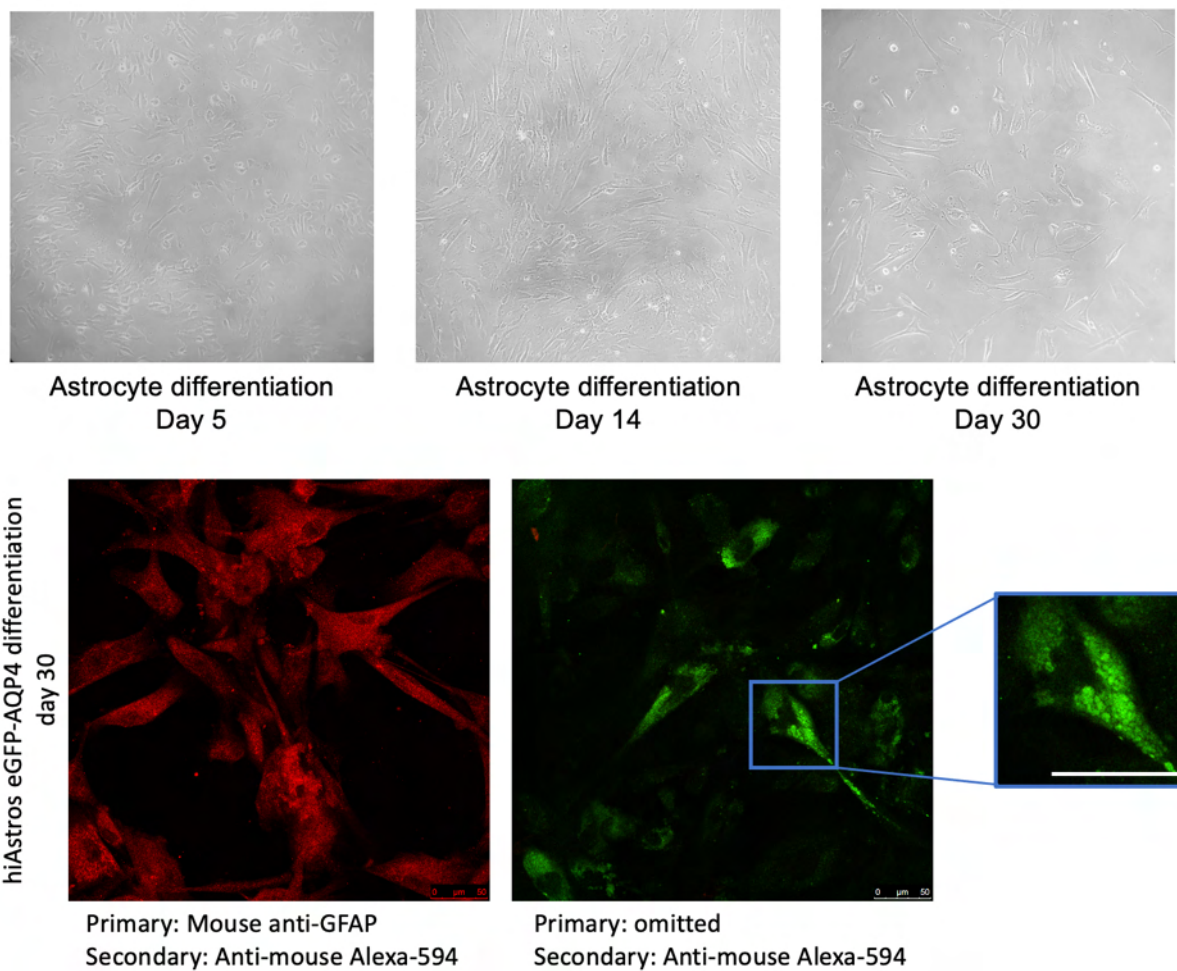


Figure 5-12 Characterization of hiNPC differentiation into hiPSC-derived astrocytes.

A) Morphology of astrocytes using phase-contrast microscope at various stages into astrocyte differentiation from hiNPCs. B) Immunocytochemistry of hiPSC-derived astrocytes at day 30 of astrocyte differentiation. Astrocytes were stained using (or omitted) mouse anti-GFAP primary antibody and goat anti-mouse Alexafluor-633 antibody (red). Green fluorescence represents endogenous AQP4-GFP expression genetically encoded into cells as hiPSCs. Zoom-in of primary-omitted demonstrates the typical fluorescence pattern observed. Imaged at 40x using an upright confocal microscope. Scale bar = 50 μ m.

5.2.1.1.8 *Live-cell imaging of eGFP-AQP4-expressing hiPSC-derived astrocytes in scratch wound closure assay*

HiPSC-derived astrocytes were plated in 24-well plates and scratched down the centre of each well and imaged using phase-contrast and fluorescence microscopy on a Cell-IQ® live cell imaging system (CM technologies) at 10x magnification at 15000ms exposure on the GFP channel. Fluorescence could be observed in some cells, particularly those in closer proximity to the scratch, however the distribution of the GFP fluorescence within the cells appeared to be mostly intracellular, and was difficult to differentiate across the cell. There also appeared to be areas of uneven illumination in the field of view in the imaging system used, which could not be fixed (asterisks, Figure 5-13).

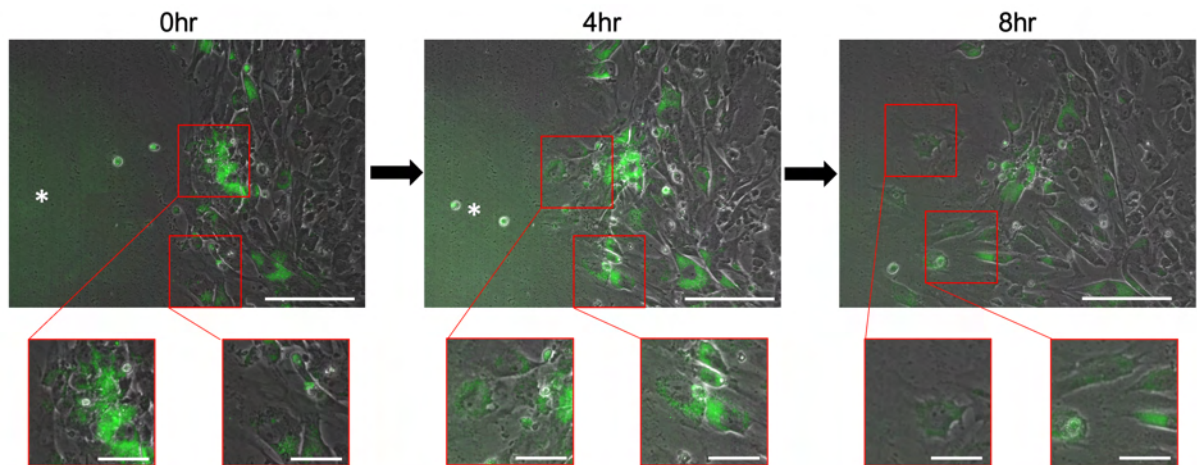


Figure 5-13 hiPSC derived astrocytes imaged at 0, 4, and 8hrs post-scratch using a CellIQ automated live-cell imaging machine.

Images represent the overlay of phase-contrast and fluorescence images taken simultaneously. Insert panels are zooms of the area-matched regions of interest outlined in red. Scale bar in top images = 200µm, scale bar in inserts = 50µm. Asterisk indicates area of uneven illumination.

5.4 Discussion

The data from this chapter demonstrates that inhibitors of CaM or PKA, which have been demonstrated to be involved in the mechanism resulting in AQP4 membrane relocalization in astrocytes, significantly slows the migration of astrocytes. Furthermore, when administered with these inhibitors, rats subject to dorsal column crush spinal cord injury developed a significantly smaller overall lesion and a sparser scar. This might provide an additional mechanism for the substantial recovery in functionality observed in rats treated with these inhibitors (see section 4.3.4). There is an absence of evidence to suggest that inhibiting onset of edema after a traumatic spinal cord injury is enough itself to fully recover or retain functionality after SCI, and therefore it is highly likely that these inhibitors may also offering additional benefits to recovery.

The total contribution of reactive astrocyte migration to the formation and/or stabilization of the scar following traumatic CNS injury remains unclear. Some studies suggest that reactive astrocytes do not migrate, but only proliferate within the lesion site (Wanner et al., 2013). However, other studies have demonstrated a correlation between the role of certain proteins in *in vitro* migration of astrocytes and changes to astrogliosis in tissue. For example, AQP4 knockout appeared to limit both astrocyte migration *in vitro* and size of the infarct area after stroke and spinal cord injury (Saadoun, 2005). Connexin-43 (Cx43) is a membrane channel protein that is a primary component of astrocyte gap junctions, which facilitate intracellular communication between adjacent cells (Giaume et al., 1991; Kotini et al., 2018). Previous studies have demonstrated that the absence of Cx43

significantly increased the area containing reactive astrocytes after focal brain ischemia in mice (Nakase et al., 2004), as well as the speed of wound closure in astrocyte scratch assays (Homkajorn et al., 2010). N-cadherin knockouts also affect astrocyte migration both *in vitro*, and the size of the GFAP+ area and immunoreactivity after brain stab injury (Kanemaru et al., 2013). Collectively, it appears that many of the targets investigated for their ability to alter astrocyte migration *in vitro* also appear to have an effect on the overall size of the lesion *in vivo*, and therefore there is a strong argument that migration does have a significant role to play in astrocytic scar formation after CNS injury. The exact role of AQP4 in particular, however, remains unclear.

5.4.1 AQP4 and astrocyte migration

Both CaM and PKA are involved in the mechanism resulting in subcellular relocalization of AQP4 to the cell membrane in response to changes in extracellular tonicity. However, no evidence yet exists to determine whether domain-specific subcellular localization occurs to facilitate directional migration, or indeed if inhibitors of AQP4 subcellular localization also inhibit this. The data in this chapter demonstrates that astrocyte migration can be inhibited by treatment with either CaM inhibitor TFP or PKA inhibitor H-89. When cultured primary rat astrocytes were subject to a central scratch, the rate of wound closure measured across treatment groups revealed that after 96hrs, treatment with TFP or H-89 significantly reduces the migration rate of astrocytes. Similar results were also shown using a transwell migration assay, where the migration rate of astrocytes toward a chemoattractant signal was slowed by TFP treatment. There

was no significant difference between the H-89 and control, however more experiments needed due to the high variance and error bars. Potentially this was due to the size of the error bars reporting, which may be overcome by increasing the number of biological repeats for this particular assay.

To further understand the role of AQP4 subcellular relocalization in astrocyte migration, the next step was to attempt to observe the movement of AQP4 within live, migrating astrocytes. To achieve this, the first attempt was to transfect an eGFP-AQP4 construct into the astrocytes to allow them to transiently express a green fluorescent AQP4 protein that can be observed in live-cell imaging. However, none of the transfection methods appeared to be appropriate or successful enough to produce enough GFP-positive astrocytes to quantify for their subcellular localization of AQP4 (Figure 5-9 and Figure 5-10). As an alternative method, commercially available hiPSCs CRISPR-edited to express eGFP-AQP4 were then differentiated into astrocytes. As such, any derivative cells of the hiPSCs that express AQP4, such as astrocytes, should express at least some eGFP-AQP4. Astrocytes were successfully derived from hiPSCs using NPCs as an intermediate cell type (Figure 5-11 and Figure 5-12). However, whilst the morphology of the cells appeared to be consistent with that of astrocytes, particularly in the way of extensive process morphology (Figure 5-12), and some positive GFP fluorescence could be observed, the GFP fluorescence that was observed was difficult to detect by either live-cell imaging using the Cell-IQ system, or using confocal microscopy in fixed, mounted hiPSC-derived astrocytes. The issues with detection were particularly problematic for live-cell

imaging because GFP fluorescence was only detected within the cytoplasm of the cell, and none at the membrane (Figure 5-12 and Figure 5-13). Time-permitting, it would be ideal to re-image these cells in a live-cell imaging system, or using an upright confocal microscope with a dipping lens, to observe any changes to localization of the green fluorescence in response to a hypotonic environment, an environment that has previously been demonstrated to result in AQP4 relocalization in astrocytes (Kitchen et al., 2015). Explaining the contribution of the AQP4 relocalization mechanism in migrating astrocytes will be a critical step in describing the mechanism by which TFP or H-89 limit astrocyte migration and understanding the cause of the reduced sized scar observed in rats treated with these inhibitors.

5.4.2 *In vivo* immunohistochemistry of the astrocytic scar

Data from this chapter demonstrates that the TFP and H-89 inhibitors of subcellular AQP4 relocalization, TFP and H-89, which limit the formation of edema post-injury, also appear to decrease the overall size and of the scar border as well as the density of GFAP present at the astrocytic scar in a dorsal column crush model of spinal cord injury. This suggests that, whilst astrocytes are not solely responsible for the formation of the scar, their post-injury response, particularly by way of migration or spatial rearrangement as facilitated by AQP4, contributes to the overall morphology of the scar. These data are contrasting to that obtained by Saadoun, et al. (2005), which claims that in AQP4 knockout mice, the overall size of the lesion contained within the astrocytic scar border was larger in the absence of AQP4. They suggest this was a consequence of reduced

migration of the astrocytes towards the site of the injury, resulting in ineffective scar formation. However, the authors make no attempt to quantify anything other than the overall size of the lesion at acute stages of injury, and therefore the measurement more accurately represents the overall size of the injury, rather than the scar itself. In this study, in addition to quantifying the overall size of injury contained by the astrocytic scar, only the area of cellular tissue (avoiding the cell-free cavities) within the scar as well as the intensity of reactive astrocytes at the astrocytic scar border were also quantified. Data from both of these quantification methods also demonstrated that in addition to a reduced size of injury, there was less overall injured tissue, and the overall density of the astrocytic scar border formed by reactive astrocytes was also reduced. This creates a clearer picture that the inhibitors of AQP4 relocalization are reducing the overall formation and/or morphology of the astrocytic scar. The precise contributions (i.e toward formation or maturation) remain to be determined.

It is important to address that the model used in this study, a rat dorsal column crush injury model, may not be the most suitable given that we've previously demonstrated that the model produced edema, which may confound any histological analysis. As a consequence, a stab injury model may have been a more ideal model to have used as it supposedly eliminates the potential contribution of cavitation and the development of syringomyelia, which can impact the overall measurement, and as we have previously demonstrated in chapter 4, these inhibitors to contribute to the reduction in tissue edema and syringomyelia-type cavity formation. Removing the area of the cell-free cavity

from the calculation of the scar size, the difference in scar area of spinal cords still remains significant between tissue from injured, untreated rats and injured rats treated with either TFP or H-89 (Figure 5-3). Saadoun et al (2005) attempted to reveal the role of AQP4 in astrocyte migration to the rate of astrocytic scar formation in mice raised completely null for AQP4, but did not attempt to factor in and secondary consequences of astrocytes being unable to express any AQP4, or compensatory mechanisms that may have occurred that impact the rate of SCI wound formation. In this study, I have explored the role of astrocyte migration after traumatic spinal cord injury in AQP4-expressing rats by altering the subcellular localization of AQP4. Here, endogenous AQP4 is still expressed, but instead the injury-induced upregulation and subcellular relocalization of AQP4 is impaired. Therefore, instead of completely blocking the functionality of the protein entirely, we prevent the pathology-induced changes that contribute to AQP4s role in astrocytes after traumatic injury.

I also demonstrate that the overall inflammatory area, as measured by area of positive macrophage (CD68/ED1+) immunofluorescence, was also significantly reduced in the injured area at 7 days post-injury (Figure 5-4). It was expected that if a reduction in astrocyte migration slowed or inhibited the formation of a scar border at this same timepoint, then the spread of the infiltrating inflammatory components recruited to the injury site may be more wide-spread, as there is a reduced barrier of separation. These data demonstrate that the overall amount of infiltrated macrophages was reduced by treatment with both TFP or H-89, however this could be attributed to the reduction in acute edema that results from

treatment with these same inhibitors (see Chapter 4), and therefore doesn't necessarily represent that the inhibitors also reduced the spread of inflammation. It would be ideal to find or develop an analysis method that can calculate the "spread" of positive cells, in order to determine whether despite a reduction in the overall inflammatory response, the spread of the injured area is also altered.

5.4.3 The "glial scar" debate

By comparison to scarring in many other tissues, which occurs acutely and resolves, the scar is chronic, and may be a pathology in itself due to the highly complex microenvironment of the CNS. The glial scar is an extremely inhibitory structure for axonal regeneration, and may enhance degeneration of spared fibres. One of the major debates around the glial scar is the definition itself; whilst many studies refer to the "glial scar" as the entire lesioned area encapsulated by the dense astrocytic border, others refer to the border itself as the "glial scar", whilst referring to the core of the scar as the "mesenchymal" or "fibrotic" scar. For the purpose of this study, we have considered the glial scar to incorporate the entire area contained by the astrocyte border, but that the astrocyte border itself is a separate feature, referred to as the astrocytic scar. The other major debate in the field of SCI is the beneficial or detrimental contribution that the scar has on the cord. Most of the data addressing the nature of the scar concur that scar formation is necessary to protect spared tissue and that the glial scar inhibits repair. However, it was demonstrated that the formation of a glial scar may facilitate axon regeneration. One study showed that the total targeted ablation of a scar failed to produce any axonal sprouting from transected fibres in the spinal

cord. Moreover, ablation of the scar significantly impaired the enhanced neurite outgrowth that can be obtained by treatment with growth-promoting factors, suggesting that even in an environment permissive for axonal sprouting, the is still required (Anderson et al., 2016). The data presented in this chapter demonstrates that treatment with either TFP or H-89 did not completely ablate the formation of a scar entirely, but reduced the overall size of the scar formed within the intermediate phase of secondary injury progression. In a previous chapter, I showed that these inhibitors significantly improved neuronal functionality at six weeks post-injury (section 4.3.4). It is feasible that reduction, but not ablation of the scar that occurred from treatment with these drugs created the most permissive environment for any growth repair or reduction in further damage; the scar remains to a degree that facilitates any attempts for neuronal sprouting, but not to a degree that may cause significant inhibition or damage to surviving neurons.

5.4.4 Summary

Astrocytes are important for the formation and maturation of a after traumatic spinal cord injury. The dynamics and morphology of scar formation play fundamental roles in the function of the cord in the long term. Many attempts at limiting scar formation have been attempted in order to reduce the inhibition of axon sprouting and regeneration. Data in this chapter suggests that the migration rate of astrocytes can be slowed by treatment with inhibitors of CaM or PKA, which have also been demonstrated to prevent subcellular relocalization of AQP4

in astrocytes. Treatment with these inhibitors also appears to limit the area and density of the astrocytic scar border formed at 7 days post-injury.

Chapter 6

Discussion

6 General discussion

6.1 General conclusions

CNS edema is a devastating secondary consequence of a number of CNS pathologies, including traumatic injury to the brain and/or spinal cord, stroke, brain tumours, and infections (Jha et al., 2019; Liang et al., 2007). Despite extensive efforts from industry to develop anti-edema drugs for traumatic CNS injuries, all have failed by phase III clinical trials. All current therapies for CNS edema do not focus on the underlying pathophysiology responsible. Only very few drugs currently in clinical trials are based on the primary underlying mechanisms causing edema, such as the dysregulation of water flow (Stokum et al., 2020). AQP4 represents an established drug target in the prevention of CNS edema owing to the extensive data demonstrating its role in the promoting CNS edema formation (Verkman et al., 2017; Manley et al., 2000; Sun et al., 2017; Saadoun et al., 2008). Most of the attempts at targeting AQP4 to reduce cerebral edema have come from identifying drugs that can block the pore of the channel. For example, AER-270 is a small molecule proposed to reduce CNS edema by inhibiting the AQP4 water channel pore, the pro-drug of which, AER-271, is currently in phase I clinical trials (NCT03804476). However, the mechanism by which AER-270 produces inhibition of CNS edema remains unclear.

This project investigated the role of subcellular localization of AQP4 within astrocytes in traumatic spinal cord injury. Previous work by our group established the intracellular molecular mechanism that facilitates the movement of intracellular stores of AQP4 to the plasma membrane, which results in cell swelling. This mechanism involves both CaM and PKA; inhibition of either inhibits AQP4 membrane trafficking.

The first aim of this study was to measure any observable differences in the subcellular localization of AQP4 *in vivo* following traumatic injury in astrocytes. Astrocytes are known to “swell” and facilitate the onset of edema after injury. Data from immunohistochemistry showed a measurably higher amount of AQP4 surrounding blood vessels (perivascular AQP4) within damaged rat spinal cord tissue after injury compared to uninjured tissue (Figure 3-8). This was despite no measurable differences in the subcellular localization of AQP4 across the cell bodies of astrocytes between injured and uninjured spinal cord tissue at acute stages after injury. These results were also seen when comparing the injured tissue with both uninjured tissue from the same cord, as well as from healthy tissue from uninjured animals. Furthermore, when treated with inhibitors of PKA or CaM after injury, I did not observe the same increased perivascular fluorescence as identified in uninjured, untreated tissue (Figure 3-8). These data suggest that within the injured area, local damage, most likely a combination of ischemia, hypoxia, and the release of extracellular glutamate from damaged neurons, triggers the polarized relocalization of AQP4 from intracellular pools or surrounding membrane regions to the endfeet surrounding blood vessels. It also suggests that the mechanism leading to the increased perivascular relocalization of AQP4 also involves PKA and CaM, as it does *in vitro*.

The second major aim of this study was to determine whether this polarized translocation of AQP4 has implications for the onset of edema after spinal cord injury, and to determine whether the molecules used to inhibit AQP4 relocalization have potential as preventative treatments clinically. The measurements of spinal cord water

content in this study showed that the dorsal column crush model generates edema at 3 and 7 days post-injury, and that CaM and PKA inhibitors significantly inhibited the onset of edema in this model (Figure 4-2). The CaM inhibitor used in this study is TFP, a molecule still in use in clinic for treatment of Schizophrenia due to its inhibitor activity at the dopamine D2 receptor. When considering the clinical use of a drug, it's important to determine the molecular targets by which it is having its desired effect. Pharmacological interrogation of this effect suggest that the prevention of edema observed was as a result of inhibition of CaM, and not the other main molecular targets of TFP. In the same injury model, inhibition of CaM or PKA improved the neuronal functionality of spinal cord fibres in the dorsal column at 6 weeks post-injury Figure 4-7. It is not clear whether this effect was directly due to the prevention of edema onset alone, and so it was then investigated whether TFP was able to alter neurite outgrowth *in vitro*. Interestingly, TFP inhibited neurite outgrowth on permissive substrates at concentrations much smaller than the injected dose *in vivo*. Furthermore, this inhibition appeared to be due to the inhibition of CaM. Due to these two effects, the precise molecular explanation for how TFP on improved the longer-term function of dorsal column fibres remains unknown.

The third aim of this study was to determine whether inhibiting AQP4 relocalization affected astrocyte migration both *in vitro* and *in vivo*. Astrocyte migration is an important contributor to the formation and maturation of the glial scar, a secondary reactive feature of traumatic injury that occurs in attempt to contain injury for healing, but can also be inhibitory for neurons. Chapter 5 demonstrates that both CaM and PKA inhibition significantly reduced the rate of astrocyte migration *in vitro*, and that treatment with these inhibitors also resulted in a significantly smaller scar area and

astrocyte border density at seven days post-injury (Figure 5-3). These data suggest that the improvement in neuronal function observed in Chapter 4 (Figure 4-7) may also be in part due to the reduction in the size of the scar formed and/or the density of the astrocytic scar border as a result of reduced astrocyte migration and/or spatial rearrangement during its formation.

Collectively, the data presented in this project indicate a mechanistic relationship between inhibition of AQP4 subcellular relocalization and the reduction in CNS edema, scarring, and improvement of neuronal function in traumatic SCI. In summary, this study suggests that inhibition of AQP4 subcellular relocalization is a viable therapeutic strategy for SCI.

6.2 Limitations of study

6.2.1 Investigating AQP4 subcellular distribution in spinal cord tissue

In this study, the subcellular localization of AQP4 using immunohistochemistry of spinal cord tissue and confocal microscopy was investigated. Using these methods facilitated the visualization of AQP4 down to a magnification and resolution that could confidently show both intracellular and membranous AQP4, as well as the localization of AQP4 between cell bodies, processes and endfeet. However, I was not able to determine whether AQP4 was definitively membranous, or whether it existed in pools of vesicles sitting just below the plasma membrane. However, imaging fluorescence in tissue using confocal microscopy can be limited by noise interference from lipids, calcium phosphates, and pigments, which increases the rejection of high-frequency signal, and limits the resolution. As such, the quantification methods used were

approximate, and it would be ideal to resolve the membrane vs sub-membrane localization. Superresolution microscopy is a good option for obtaining images with a higher diffraction limit. However, it still cannot interpret exact membrane interaction in the absence of cell-type specific membrane marker, and still does not overcome the magnification limitation as conventional superresolution microscopes, including those used for single-molecule imaging such as Stochastic Optical Reconstruction Microscopy (STORM), can't offer any higher objectives than that of a confocal microscope. For better resolution of AQP4 subcellular distribution in rat tissue, a method such as transmission electron microscopy (TEM) with the addition of immunogold labelling would be much superior. This method has previously been used to observe high resolution, high-magnification images of astrocyte-endothelial cell interactions, as well as to determine the localization of AQP4 at the astrocyte endfeet membranes using immunogold labelling. This method is similar to fluorescence immunohistochemistry, but utilizes the high electron density of colloidal gold particles, which are the conjugates of the secondary antibody. This method would allow us to determine the amount of AQP4 surrounding blood vessels with the confidence that each labelled protein is found within the membrane for more confident quantification. TEM experiments had been planned through collaboration with the University of Bristol, but were not possible due to the COVID-19 restrictions.

An alternative to electron microscopy would be the use of tissue clearing and expansion microscopy (Zhao et al., 2017; Chen et al., 2015). By using this method, we could increase the magnification of the tissue by physically expanding it up to tenfold; achieved by embedding pre-fluorescently labelled tissue in a hydrogel and cross-linking before expanding in water. We could also achieve increased resolution

of the fluorescently labelled antigens by clearing the extracellular debris causing refractive interference. It would be ideal to utilize the method of expansion microscopy to observe at a higher magnification the subcellular protein localization in tissue samples for labs without access to a transmission electron microscope, but the optimization of expansion microscopy in tissue samples would have required more time than this project had.

6.2.2 Measurement of spinal cord edema

The methodology for detecting and comparing levels of edema in the brain and spinal cord is very limited, owing to the virtually “invisible” nature of the pathology. Measuring water content using the wet weight/dry weight method, as utilized in this study, is a common technique used for animal edema measurement, as it requires equipment found in almost every lab, is simple to carry out, and multiple tissues can be handled consistently and at the same time. However, it does not delineate the contribution of the different types of edema involved. In this study, we attempted to quantify differences between uninjured, injured, and injured/treated groups in terms of the vasogenic edema formed. To quantify the level of vasogenic edema that occurred, sections from spinal cord tissue were immunostained for albumin, a mostly blood-borne protein, which is nearly absent from spinal cord tissue in uninjured controls (Figure 4-4 and Figure 4-5). Whilst this method allowed us to observe the spread of the vasogenic edema within the injured tissue area by visualizing the extravasated albumin, it limited the quantification of a select number of slices throughout the cord. An alternative method of calculating differences in vasogenic edema across the treatment groups would have been to perform Evans blue dye extravasation assays (Evans and Schulemann, 1914; Wang and Lai, 2014). This method involves the injection of Evans

blue dye into the blood stream of rats shortly before culling. The dye will appear within any tissue that has blood barrier breakdown, such as during the formation of vasogenic edema in the CNS, giving an indication of the integrity of the barrier. The cords from injected animals can be dissected, homogenized, and the dye extracted. Density of the dye present in the tissue is measured using absorbance on a plate reader and compared relatively across treatment groups.

Another alternative would be to use diffusion-weighted image (DWI) MRI (Hudak et al., 2014). This method is arguably an improvement on the use of tracer dyes such as Evans blue to measure BBB integrity, as it allows the imaging of edema in the same animal at multiple timepoints, giving a clearer picture of the dynamics of onset vs clearance, and can be used in both animal models and human patients. DWI MRI is also beneficial for reducing the number of animals required for experimentation as timepoints can all be obtained from the same animal (Ebisu et al., 1993). Furthermore, studies have shown that a combination of DWI and Fluid-Attenuated Inversion Recovery (FLAIR) imaging can delineate the contribution of cytotoxic versus vasogenic edema. FLAIR is a type of T2-weighted MRI scan in which high signal emerging from physiologically fluid-filled spaces (i.e ventricles or central canal), is suppressed, allowing for visualization of only pathological water (Hudak et al., 2014). This combined imaging methodology would allow an enhancement of our understanding of the temporal changes and/or contributions of different types of edema at different stages after injury in the same animal, which would be extremely useful for understanding the mechanisms involved more clearly. This method was not attempted in this study due to lack of access to MRI facilities for live animals.

6.2.3 SCI model

No rodent SCI model perfectly mimics human SCI, and therefore clinical translation using rodent models will always be limited. However, different models can simulate many of the features observed in human SCI, by modifying both the type of injury as well as the injury severity and level. This study utilized a dorsal column crush injury model at the level T8, which produces a moderate injury by using a compression force within the dorsal column tracts alone. This model does not produce a severe functional deficit, which would have been deemed unnecessary for the required experimental output, but does allow us to assess tissue for immunohistochemistry, protein expression, edema, and electrophysiology. However, there still are a number of factors associated with the model that may alter the physiological response to injury, and are not representative of human SCI. For example, the use of laminectomy, which is the removal of the spinal laminae adjacent to the injury site in order to access the tissue, is not something that occurs after human SCI, and therefore may affect the post-injury edema, as the removal of the laminae adjacent to the injured cord provides space for tissue to swell into, almost as a pre-decompression. As such, a model that doesn't involve laminectomy may have been more appropriate, for example a balloon compression model, which unfortunately was not available to us (Vanický et al., 2001).

6.2.4 Route of administration of drugs

For all animal injury treatment groups in this study, treatment was administered via injection directly into the spinal cord immediately following injury. Whilst this represents the most ideal drug delivery method for the purposes of investigating injury

mechanism, it isn't directly clinically translatable, as intrathecal/intraspinal injection of a substance would not be achievable for patients subject to first response or even acute medical care. There are a number of ways that we could repeat the study to more closely address whether the drugs investigated could be clinically relevant. TFP, our primary molecule of interest in this study due to its existing clinical use, is primarily administered orally, but can also be delivered more rarely via intramuscular injection (Brauzer and Goldstein, 1968). In SCI, most of the therapies evaluated through human clinical trials have administered drugs via IV bolus, intramuscular injection, or subcutaneous injection. Currently, TFP is only formulated to be administered either orally in tablet or liquid form, or via intramuscular injection. As such, a more clinically relevant model would have included these routes of administration to assess whether the beneficial outcomes through direct intraspinal injection are also exhibited via a clinical route. The use of intravenous or intramuscular injection was limited by our animal project licence.

6.2.5 Timepoints of drug administration

In this study, we administered the single dose of TFP immediately following the injury. Again, this doesn't represent a clinically plausible timepoint for treatment, and for the purposes of inhibiting edema, the study should be repeated with a later timepoint of administration no later than 24hrs after the primary injury, as patients who do not receive care within this timeframe have exhibited worse secondary complications (Middleton et al., 2012). However, no clinical data exists to demonstrate the average time of onset of edema after spinal cord injury in patients, probably due to the variance as a result of injury type, severity, and level. Clinical data demonstrates that at 24hrs after injury, edema can already be detected in most patients, which correlates with

functionally worse outcome (Miyanji et al., 2007), and as such, it would be ideal to test if TFP has a beneficial effect of reducing edema by administering within this 24hr window. In rat models of SCI, edema has been shown to occur as soon as 1hr after contusion injury (Yan et al., 2018), however most report the onset to be around 12hrs. Most recent data from the Nuffield Trust indicate that 90% of category 1 (life-threatening) calls are responded to within 15 minutes of calling 999, and 90% of category 2 (emergency) calls are responded to within 40 minutes (NHS England, 2020). Therefore, it could be possible to administer a drug within the first 40 minutes of injury from paramedics. A time-course of drug administration in our rat model between 40 mins and 24 h would be ideal to determine whether delayed administration within this clinically viable window would still be affective at reducing edema. This option was limited by our animal project licence due to the need to re-open an existing wound that had been stitched in recovering animals that had recently undergone surgery and anaesthesia.

6.3 Future work

6.3.1 TBI translation

The relationship between astrocytes and the vasculature in the brain is largely identical to that in the spinal cord; astrocytes ensheath blood vessels with tight restriction to reduce the passage of molecules between the blood and tissue parenchyma. Brain and spinal cord astrocytes are equally specialized in their ability to regulate water flow at this location via AQP4 in the endfeet surrounding blood vessels (Abbott, 2005). Many studies identify cytotoxic swelling of astrocytes to be the premorbid process facilitating edema onset across both SCI and TBI, making it an analogous mechanism

and potential drug target for both pathologies (Liang et al., 2007; Rosenblum, 2007; Stokum et al., 2015; Saadoun et al., 2008; Huang et al., 2019; Leonard and Vink, 2015; Manley et al., 2004; Ren et al., 2013). Accordingly, there is also no clinically available pharmacological therapy used for preventing the onset of edema after TBI. As such, treatment with inhibitors of AQP4 relocalization should, in theory, also reduce or prevent the formation of edema after TBI via the same mechanism as in SCI. However, the brain has a more complex three-dimensional structure than the spinal cord, as well as increased variability in the presence of astrocyte sub-types and gene expression profiles across different regions of the brain, most notably between grey and white matter (Nyúl-Tóth et al., 2016; Batiuk et al., 2020). This would therefore require a study considering multiple regions of the brain subject to TBI for clarity.

6.3.2 Scarring

Whilst the 2D *in vitro* migration assays employed in this study are useful tools for elucidating bulk differences in cell migration under different treatment regimes, they are still limited by their lack of a third dimension to exhibit or explain the intricate and comprehensive processes involved in *in vivo* cell migration. The third dimension is essential for integrating the role of key extracellular matrix components in the migration process, as well as interactions with multiple cell types. The development and increasing accessibility of high-resolution imaging equipment now makes it possible to visualize cell migration in 3D models. Organotypic cultures of brain slices simulate *in vivo*-like microenvironments by preserving some of the original structures and cell-cell interactions. Organotypic cultures have been developed in adult rodent tissues for modelling the migration of glioblastoma multiforme (GBM) (Eisemann et al., 2018). Using this model, hiPSC-derived astrocytes expressing fluorescently labelled AQP4,

as developed in chapter 5 (section 5.3.3.2), can be injected into organotypic brain and/or spinal cord slice cultures and allowed to migrate under various conditions in 3D, hosting a number of important elements of the *in vivo* environment. Astrocyte migration, as well as the subcellular localization of AQP4 within astrocytes, can then be observed by fixing and clearing tissue at various timepoints and imaged using confocal microscopy. However, this methodology is still restricted by its lack of ability to image the same cells at different timepoints. Ideally, these measured parameters could be visualized in real time using time-lapse confocal microscopy. Only recently has automated longitudinal imaging been developed for use in organotypic slice cultures (Linsley et al., 2019). This involves an automated spinning disc microscope that is programmed by set marks on a 96-well plate, allowing the lens to return to the same location on the imaging plate, even when the plate has been removed. This then facilitates imaging of the same cells within the slice culture over multiple imaging periods.

6.3.3 Alternative applications of AQP4 relocalization mechanism

6.3.3.1 *AQP4 and the glymphatic system: roles in sleep and neurodegeneration*

The clearance of excess compounds and solutes within any tissue is crucial for maintaining a functional homeostatic environment. The lymphatic system is a network of tissues throughout the human body contiguous with the cardiovascular system, which extends through many tissues, as well as the lymph nodes, and aids the movement of solutes, proteins, and fluid back to the circulatory system (Liao and Padera, 2013). The CNS, however, despite being a system with a relatively high

metabolic rate, does not contain any traditional form of lymphatic system. As such, an alternative mechanism must exist to facilitate waste and fluid clearance. As the CNS is excluded from the body's immune system, including immune cells and many pathogens, it was initially believed that the CNS had its own form of lymphatic system through CSF pathways (Ransohoff and Engelhardt, 2012). An early study by Rennels et al., (1985) demonstrated the first evidence of "paravascular CSF flow" in the brain and spinal cord. In this study, it was demonstrated that when horseradish peroxidase was injected into the CSF via the brain ventricles, it could be detected in brain slices using tetramethylbenzidine (TMB) surrounding blood vessels and within the tissue parenchyma itself. This generated the theory that CSF flow also occurs through tissue in a specific and contained location parallel to CNS vasculature. The glymphatic (glial-lymphatic) system, as it is now known, is a unique CNS system that permits the exchange of CSF and interstitial fluid (ISF) using a specialised paravascular route, with the function of distributing and clearing waste solutes from the brain and spinal cord, including glucose, proteins, amino acids, lipids, and ions. There are three main features required for the glymphatic system; periarterial space limited by glial endfeet facilitating flow of CSF from the subarachnoid space, through the Virchow-Robin spaces; perivenous space limited by glial endfeet facilitating flow of ISF back to larger CSF-producing structures and the lymphatic system; and parenchymal interstitium facilitating flow of fluid between the two (Figure 6-1) (Iliff et al., 2012, 2013). The pulsatility of blood vessels is thought to facilitate the flow of fluid in the same direction as the flow of blood (Mestre et al., 2018). Evidence for this system comes primarily from either MRI images following intrathecal or intravenous injection of contrast agents or stable isotopes, or two-photon microscopy following the injection of a radio-labelled

tracer into the *cisterna magna* (Iliff et al., 2012; Gaberel et al., 2014; Ringstad et al., 2017; Taoka et al., 2018; Sweeney et al., 2019).

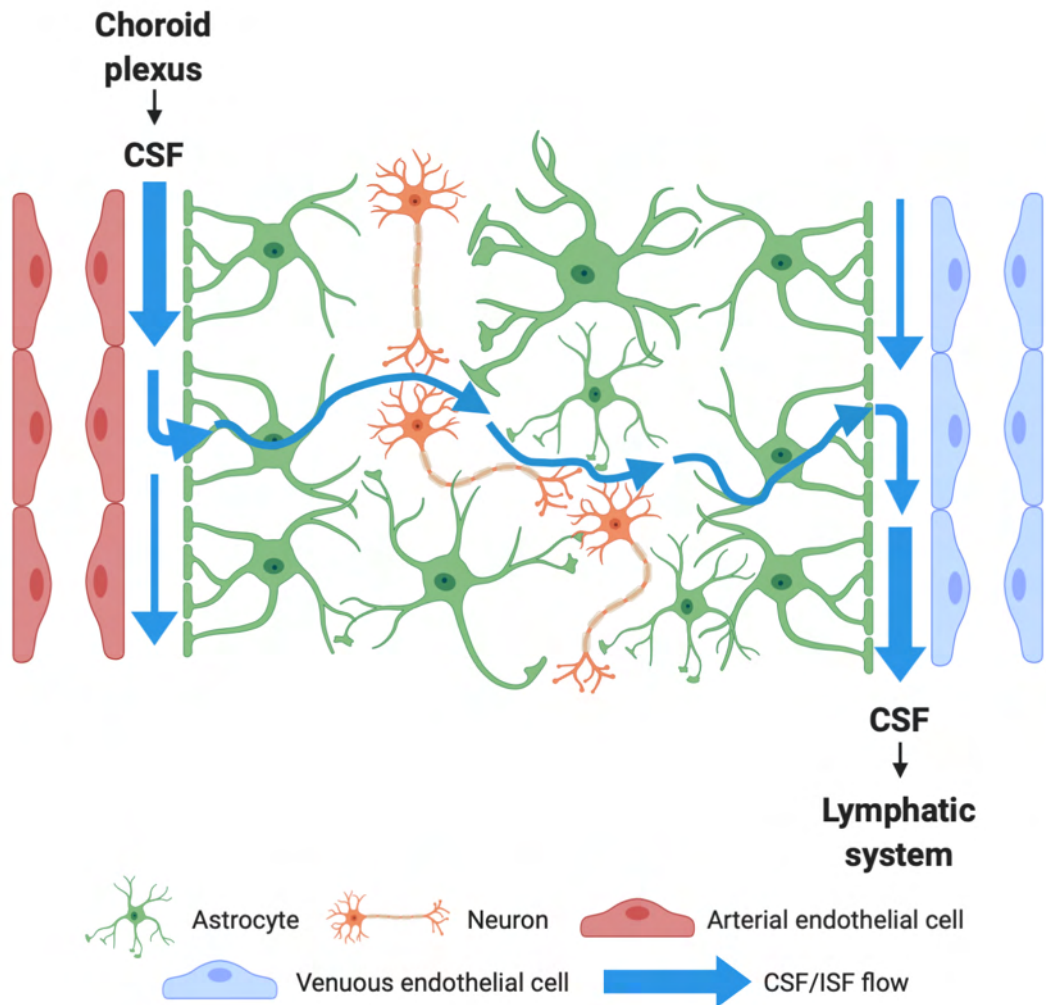


Figure 6-1 A schematic of the glymphatic system. CSF flows in paravascular spaces lined with astrocyte endfeet.

Water flow occurs through AQP4 in astrocyte endfeet surrounding the glymphatic structure at arterial blood vessels to enter the brain parenchyma. It then exits the parenchyma via AQP4 in astrocyte endfeet surrounding the glymphatic structure at venous blood vessels. Made using biorender.com.

AQP4 within the astrocytic endfeet that ensheath blood vessels in the brain facilitates CSF transport into the brain parenchyma. AQP4 knockout mice exhibit a much slower influx of CSF tracer into the brain parenchyma compared to wild-type controls (Iliff et al., 2012). It is well known that sleep, which is a conserved experience among many living species, is important for brain function. A lack of sleep can reduce cognition, impair learning, and in extreme cases of sleep deprivation, can be fatal (Twooroger et al., 2006). One study reported that the volume of the interstitial space in the brain parenchyma is smaller during wakefulness, which authors suggest resists flow of interstitial fluid across the tissue, and would ultimately restrict the movement of built-up solutes. However, it is unclear whether the reduced volume of interstitial space is a consequence or cause of lack of ISF flow. Furthermore, clearance of waste solutes and metabolites, namely β -amyloid, is significantly higher during sleep (Xie et al., 2013).

AQP4 perivascular localization appears to be significantly reduced in brains of patients with Alzheimer's Disease (AD) compared to young, pathology-free brains, and a loss of perivascular AQP4 is associated with increased GFAP-correlated AQP4 localization surrounding amyloid-beta plaques as well as worsened cognition (Zeppenfeld et al., 2017). This reduction in perivascular AQP4 can also be seen in aging mice, alongside an impairment in glymphatic function (Kress et al., 2014). AQP4 is essential for facilitating glymphatic flow for clearance of excess brain solutes (Iliff et al., 2012). AQP4 knockout mice exhibit reduced clearance of radio-labelled β -amyloid, a protein involved in the neurodegenerative mechanism causing AD, and enhanced aggregate formation (Xu et al., 2015). Increased perivascular AQP4 was also observed concurrently with increased glymphatic flow during sleep (Hablitz et al., 2020).

Collectively, this suggests that sleep deprivation, or sleep-related issues may facilitate the onset of neurodegenerative disorders due to inefficient solute clearance through the AQP4-mediated glymphatic clearance pathway. In this project, we demonstrated a pathological change in AQP4 subcellular localization in response to injury (see Chapter 3), however the physiological role of AQP4 turnover remains unknown. The distinct role of AQP4 in facilitating glymphatic clearance suggests that sleep-associated clearance can be attributed to the mechanism of AQP4-mediated CSF-ISF flow. Furthering an understanding of the dynamic regulation of AQP4 between sleep and wakefulness will be useful to elucidate potential molecular targets in the development and progression of neurodegenerative diseases. Understanding the role of AQP4 sub-cellular relocalization provides a novel perspective to understand physiological waste clearance, and opens up new treatment avenues to slow the progression of neurodegenerative conditions.

6.3.4 Glioblastoma multiforme (GBM)

The AQP family of water channel proteins have been linked to GBM recurrence. AQP1 and AQP4 are both expressed in the brain and under normal conditions they facilitate brain water homeostasis and the maintenance of cell volume (Nagelhus and Ottersen, 2013; Rash et al., 1998). Both AQP1 and AQP4 are also highly-expressed in GBM tumours (Oshio et al., 2005; Warth et al., 2007), where they have been suggested to have a role in GBM cell migration and invasion (Papadopoulos and Saadoun, 2015; Lan et al., 2017; Tome-Garcia et al., 2018). However, the underlying mechanisms by which they exert this effect are unclear and the importance of each AQP is unknown. In astrocytes, knockdown of AQP4 reduced migration in scratch and transwell migration assays and also limited scarring after injury, a response that involves AQP4

redistributing to the leading edge of the migrating cell (Saadoun, 2005). Silencing of AQP1 in GBM cells results in reduced migration *in vitro*, the formation of smaller tumours in a xenograft model, and reductions in invasion-facilitating proteins such as integrins and matrix metalloproteinases (Yang et al., 2018). AQP1 can also be observed at the leading edge of migrating GBM cells (McCoy and Sontheimer, 2007). The conceptually-novel approach of limiting cell migration by preventing AQP4 subcellular relocalization proposed in the context of SCI in this study may also translate to GBM. By controlling the subcellular translocation of AQPs, it may be possible to slow down GBM recurrence by halting GBM migration.

6.4 Summary

This thesis demonstrates that targeting subcellular relocalization of AQP4 is a viable therapeutic target for SCI. The CaM inhibitor used in this study, TFP, a drug licenced for human use (NICE, 2019), was administered to rats at a dose approximately equivalent to its licenced dose in humans. Treatment with TFP prevented the increase in perivascular AQP4 within the injury, inhibited the onset of post-injury edema as soon as 3 days post-injury, improved spinal cord function at 6 weeks post-injury, and markedly reduced the size and density of the scar formed at 7 days post-injury. There is still no pharmacological intervention to prevent the onset of edema after traumatic spinal cord injury. This study demonstrates a novel approach to applying molecular mechanistic understanding of water channel regulation to a new therapeutic framework for SCI sufferers globally.

References

- Abbott, N.J. (2005) Dynamics of CNS barriers: Evolution, differentiation, and modulation. *Cellular and Molecular Neurobiology*. doi:10.1007/s10571-004-1374-y.
- Abe, Y., Yamamoto, T., Sugiyama, Y., et al. (1999) Apoptotic cells associated with wallerian degeneration after experimental spinal cord injury: A possible mechanism of oligodendroglial death. *Journal of Neurotrauma*. doi:10.1089/neu.1999.16.945.
- Agre, P., King, L.S., Yasui, M., et al. (2002) Aquaporin water channels--from atomic structure to clinical medicine. *The Journal of physiology*, 542 (Pt 1): 3–16. doi:10.1113/jphysiol.2002.020818.
- Agre, P., Preston, G.M., Smith, B.L., et al. (1993) Aquaporin CHIP: the archetypal molecular water channel. *The American journal of physiology*, 265: F463–F476. doi:10.1085/jgp.79.5.791.
- Ahmed, Z., Read, M.L., Berry, M., et al. (2010) Satellite glia not DRG neurons constitutively activate EGFR but EGFR inactivation is not correlated with axon regeneration. *Neurobiology of Disease*, 39 (3): 292–300. doi:10.1016/j.nbd.2010.04.013.
- Ahuja, C.S., Wilson, J.R., Nori, S., et al. (2017) Traumatic spinal cord injury. *Nature Reviews Disease Primers*, 3: 17018. doi:10.1038/nrdp.2017.18.
- Alilain, W.J., Horn, K.P., Hu, H., et al. (2011) Functional regeneration of respiratory pathways after spinal cord injury. *Nature*. doi:10.1038/nature10199.
- Allen, A.R. (1911) Surgery of experimental lesion of spinal cord equivalent to crush injury of fracture dislocation of spinal column: A preliminary report. *Journal of the American Medical Association*. doi:10.1001/jama.1911.04260090100008.
- Amiry-Moghaddam, M., Williamson, A., Palomba, M., et al. (2003) Delayed K⁺ clearance associated with aquaporin-4 mislocalization: Phenotypic defects in brains of α -syn trophin-null

mice. *Proceedings of the National Academy of Sciences of the United States of America*. doi:10.1073/pnas.2336064100.

Anderson, D.K. and Means, E.D. (1985) Iron-induced lipid peroxidation in spinal cord: Protection with mannitol and methylprednisolone. *Journal of Free Radicals in Biology and Medicine*. doi:10.1016/0748-5514(85)90030-3.

Anderson, M.A., Ao, Y. and Sofroniew, M. V. (2014) Heterogeneity of reactive astrocytes. *Neuroscience Letters*. doi:10.1016/j.neulet.2013.12.030.

Anderson, M.A., Burda, J.E., Ren, Y., et al. (2016) Astrocyte scar formation AIDS central nervous system axon regeneration. *Nature*. doi:10.1038/nature17623.

Andrews, R.J., Bringas, J.R. and Muto, R.P. (1993) Effects of mannitol on cerebral blood flow, blood pressure, blood viscosity, hematocrit, sodium, and potassium. *Surgical Neurology*. doi:10.1016/0090-3019(93)90186-5.

Anwar, M.A., Al Shehabi, T.S. and Eid, A.H. (2016) Inflammogenesis of Secondary Spinal Cord Injury. *Frontiers in Cellular Neuroscience*, 10. doi:10.3389/fncel.2016.00098.

Arvanian, V.L., Schnell, L., Lou, L., et al. (2009) Chronic spinal hemisection in rats induces a progressive decline in transmission in uninjured fibers to motoneurons. *Experimental Neurology*. doi:10.1016/j.expneurol.2009.01.004.

Auguste, K.I., Jin, S., Uchida, K., et al. (2007) Greatly impaired migration of implanted aquaporin-4-deficient astroglial cells in mouse brain toward a site of injury. *The FASEB Journal*. doi:10.1096/fj.06-6848com.

Badaut, J., Brunet, J.F., Grollmund, L., et al. (2003) Aquaporin 1 and aquaporin 4 expression in human brain after subarachnoid hemorrhage and in peritumoral tissue. *Acta neurochirurgica. Supplement*, 86: 495–8. Available at: <http://www.ncbi.nlm.nih.gov/pubmed/14753493>.

Bai, C., Fukuda, N., Song, Y., et al. (1999) Lung fluid transport in aquaporin-1 and aquaporin-

4 knockout mice. *Journal of Clinical Investigation*. doi:10.1172/JCI4138.

Barbeau, H., McCrea, D.A., O'Donovan, M.J., et al. (1999) Tapping into spinal circuits to restore motor function. *Brain Research Reviews*. doi:10.1016/S0165-0173(99)00008-9.

Barnes, P.J. (1998) Anti-inflammatory actions of glucocorticoids: Molecular mechanisms. *Clinical Science*. doi:10.1042/cs0940557.

Barrett, C.P., Guth, L., Donati, E.J., et al. (1981) Astroglial reaction in the gray matter of lumbar segments after midthoracic transection of the adult rat spinal cord. *Experimental Neurology*. doi:10.1016/0014-4886(81)90272-7.

Batiuk, M.Y., Martirosyan, A., Wahis, J., et al. (2020) Identification of region-specific astrocyte subtypes at single cell resolution. *Nature Communications*. doi:10.1038/s41467-019-14198-8.

Becerra, J.L., Puckett, W.R., Hiester, E.D., et al. (1995) MR-pathologic comparisons of wallerian degeneration in spinal cord injury. *American Journal of Neuroradiology*.

Beggs, J.L. and Waggner, J.D. (1975) Vasogenic edema in the injured spinal cord: A method of evaluating the extent of blood-brain barrier alteration to horseradish peroxidase. *Experimental Neurology*, 49 (1): 86–96. doi:10.1016/0014-4886(75)90196-X.

Beitz, E., Wu, B., Holm, L.M., et al. (2006) Point mutations in the aromatic/arginine region in aquaporin 1 allow passage of urea, glycerol, ammonia, and protons. *Proceedings of the National Academy of Sciences*, 103 (2): 269–274. doi:10.1073/pnas.0507225103.

Benfenati, V., Caprini, M., Dovizio, M., et al. (2011) An aquaporin-4/transient receptor potential vanilloid 4 (AQP4/TRPV4) complex is essential for cell-volume control in astrocytes. *Proceedings of the National Academy of Sciences*, 108 (6): 2563–2568. doi:10.1073/pnas.1012867108.

Benfenati, V. and Ferroni, S. (2010) Water transport between CNS compartments: Functional and molecular interactions between aquaporins and ion channels. *Neuroscience*. 168 (4) pp.

926–940. doi:10.1016/j.neuroscience.2009.12.017.

Bering, E.A. (1955) Choroid plexus and arterial pulsation of cerebrospinal fluid: Demonstration of the choroid plexuses as a cerebrospinal fluid pump. *Archives of Neurology And Psychiatry*, 73 (2): 165–172. doi:10.1001/archneurpsyc.1955.02330080043012.

Binder, D.K., Yao, X., Zador, Z., et al. (2006) Increased seizure duration and slowed potassium kinetics in mice lacking aquaporin-4 water channels. *GLIA*. doi:10.1002/glia.20318.

Blight, A.R. (1991) Morphometric analysis of a model of spinal cord injury in guinea pigs, with behavioral evidence of delayed secondary pathology. *Journal of the Neurological Sciences*. doi:10.1016/0022-510X(91)90159-5.

Bose, B., Osterholm, J.L. and Kalia, M. (1986) Ganglioside-induced regeneration and reestablishment of axonal continuity in spinal cord-transected rats. *Neuroscience Letters*. doi:10.1016/0304-3940(86)90055-8.

Bozzo, A., Marcoux, J., Radhakrishna, M., et al. (2011) The Role of Magnetic Resonance Imaging in the Management of Acute Spinal Cord Injury. *Journal of Neurotrauma*, 28 (8): 1401–1411. doi:10.1089/neu.2009.1236.

Bracken, M.B. (2012) Steroids for acute spinal cord injury. *The Cochrane database of systematic reviews*, 1: CD001046. doi:10.1002/14651858.CD001046.pub2.

Bracken, M.B., Collins, W.F., Freeman, D.F., et al. (1984) Efficacy of Methylprednisolone in Acute Spinal Cord Injury. *JAMA: The Journal of the American Medical Association*. doi:10.1001/jama.1984.03340250025015.

Bracken, M.B., Shepard, M. jo, Collins, W.F., et al. (1990a) A randomized, controlled trial of methylprednisolone or naloxone in the treatment of acute spinal-cord injury: Results of the second national acute spinal cord injury study. *New England Journal of Medicine*. doi:10.1056/NEJM199005173222001.

Bracken, M.B., Shepard, M.J., Collins, W.F., et al. (1990b) A Randomized, Controlled Trial of

Methylprednisolone or Naloxone in the Treatment of Acute Spinal-Cord Injury. *New England Journal of Medicine*, 322 (20): 1405–1411. doi:10.1056/NEJM199005173222001.

Bracken, M.B., Shepard, M.J., Collins, W.F., et al. (1992) Methylprednisolone or naloxone treatment after acute spinal cord injury: 1-year follow-up data. Results of the second National Acute Spinal Cord Injury Study. *Journal of Neurosurgery*, 76: 23–31. doi:10.3171/jns.1992.76.1.0023.

Bracken, M.B., Shepard, M.J., Holford, T.R., et al. (1997) Administration of methylprednisolone for 24 or 48 hours or tirilazad mesylate for 48 hours in the treatment of acute spinal cord injury: Results of the Third National Acute Spinal Cord Injury randomized controlled trial. *Journal of the American Medical Association*. doi:10.1097/00132586-199808000-00011.

Bradbury, E.J. and Carter, L.M. (2011) Manipulating the glial scar: Chondroitinase ABC as a therapy for spinal cord injury. *Brain Research Bulletin*. doi:10.1016/j.brainresbull.2010.06.015.

Bradbury, E.J., Moon, L.D.F., Popat, R.J., et al. (2002) Chondroitinase ABC promotes functional recovery after spinal cord injury. *Nature*. doi:10.1038/416636a.

Bratosin, D., Mitrofan, L., Palii, C., et al. (2005) Novel fluorescence assay using calcein-AM for the determination of human erythrocyte viability and aging. *Cytometry Part A*. doi:10.1002/cyto.a.20152.

Braughler, J.M. and Hall, E.D. (1982) Correlation of methylprednisolone levels in cat spinal cord with its effects on (Na⁺ + K⁺)-ATPase, lipid peroxidation, and alpha motor neuron function. *Journal of neurosurgery*, 56 (6): 838–44. doi:10.3171/jns.1982.56.6.0838.

BRAUZER, B. and GOLDSTEIN, B.J. (1968) Comparative Effects of Intramuscular Thiothixene and Trifluoperazine in Psychotic Patients. *The Journal of Clinical Pharmacology and The Journal of New Drugs*. doi:10.1002/j.1552-4604.1968.tb00116.x.

Buss, A., Brook, G.A., Kakulas, B., et al. (2004) Gradual loss of myelin and formation of an

astrocytic scar during Wallerian degeneration in the human spinal cord. *Brain*. doi:10.1093/brain/awh001.

Byrnes, K.R., Fricke, S.T. and Faden, A.I. (2010) Neuropathological differences between rats and mice after spinal cord injury. *Journal of magnetic resonance imaging: JMRI*. doi:10.1002/jmri.22323.

Cabrera-Aldana, E.E., Ruelas, F., Aranda, C., et al. (2017a) Methylprednisolone Administration Following Spinal Cord Injury Reduces Aquaporin 4 Expression and Exacerbates Edema. *Mediators of Inflammation*, 2017: 1–7. doi:10.1155/2017/4792932.

Cabrera-Aldana, E.E., Ruelas, F., Aranda, C., et al. (2017b) Methylprednisolone Administration Following Spinal Cord Injury Reduces Aquaporin 4 Expression and Exacerbates Edema. *Mediators of Inflammation*, 2017. doi:10.1155/2017/4792932.

Cadotte, D.W. and Fehlings, M.G. (2012) "Spinal cord injury." *In Principles of Neurological Surgery*. doi:10.1016/B978-1-4377-0701-4.00027-0.

Casha, S., Zygun, D., McGowan, M.D., et al. (2012) Results of a phase II placebo-controlled randomized trial of minocycline in acute spinal cord injury. *Brain*. doi:10.1093/brain/aws072.

De Castro Ribeiro, M., Hirt, L., Bogousslavsky, J., et al. (2006) Time course of aquaporin expression after transient focal cerebral ischemia in mice. *Journal of Neuroscience Research*. doi:10.1002/jnr.20819.

Chang, V.T.W. and Chang, H.M. (2020) Review: Recent advances in the understanding of the pathophysiology of neuromyelitis optica spectrum disorder. *Neuropathology and Applied Neurobiology*. doi:10.1111/nan.12574.

Chen, F., Tillberg, P.W. and Boyden, E.S. (2015) Expansion microscopy. *Science*. doi:10.1126/science.1260088.

Chen, J.Q., Zhang, C.C., Jiang, S.N., et al. (2016) Effects of aquaporin 4 knockdown on brain edema of the uninjured side after traumatic brain injury in rats. *Medical Science Monitor*.

doi:10.12659/MSM.898190.

Chen, M.S., Huber, A.B., Van Der Haar, M.E.D., et al. (2000) Nogo-A is a myelin-associated neurite outgrowth inhibitor and an antigen for monoclonal antibody IN-1. *Nature*. doi:10.1038/35000219.

Cheriyian, T., Ryan, D.J., Weinreb, J.H., et al. (2014) Spinal cord injury models: A review. *Spinal Cord*. 52 (8) pp. 588–595. doi:10.1038/sc.2014.91.

Cho, K.J. and Kim, G.W. (2016) “RNAi Therapeutic Potentials and Prospects in CNS Disease.” *In RNA Interference*. doi:10.5772/62896.

Coleman, W. and Geisler, F. (2004) Injury severity as primary predictor of outcome in acute spinal cord injury: retrospective results from a large multicenter clinical trial. *Spine J*, 4 (4): 373–378. doi:10.1016/j.spinee.2003.12.006.

Conner, M.T., Conner, A.C., Bland, C.E., et al. (2012) Rapid aquaporin translocation regulates cellular water flow: Mechanism of hypotonicity-induced subcellular localization of aquaporin 1 water channel. *Journal of Biological Chemistry*. doi:10.1074/jbc.M111.329219.

Conner, M.T., Conner, A.C., Brown, J.E.P., et al. (2010) Membrane trafficking of aquaporin 1 is mediated by protein kinase C via microtubules and regulated by tonicity. *Biochemistry*. doi:10.1021/bi902068b.

Courtine, G., Song, B., Roy, R.R., et al. (2008) Recovery of supraspinal control of stepping via indirect propriospinal relay connections after spinal cord injury. *Nature Medicine*. doi:10.1038/nm1682.

Cui, Y. and Bastien, D.A. (2011) Water transport in human aquaporin-4: Molecular dynamics (MD) simulations. *Biochemical and Biophysical Research Communications*, 412 (4): 654–659. doi:10.1016/j.bbrc.2011.08.019.

Damoiseaux, J.G., Döpp, E.A., Calame, W., et al. (1994) Rat macrophage lysosomal membrane antigen recognized by monoclonal antibody ED1. *Immunology*.

- Day, R.E., Kitchen, P., Owen, D.S., et al. (2014) Human aquaporins: Regulators of transcellular water flow. *Biochimica et Biophysica Acta - General Subjects*. 1840 (5) pp. 1492–1506. doi:10.1016/j.bbagen.2013.09.033.
- Deen, P., Verdijk, M., Knoers, N., et al. (1994) Requirement of human renal water channel aquaporin-2 for vasopressin-dependent concentration of urine. *Science*, 264 (5155): 92–95. doi:10.1126/science.8140421.
- Derakhshanrad, N., Saberi, H., Yekaninejad, M.S., et al. (2018) Granulocyte-colony stimulating factor administration for neurological improvement in patients with postrehabilitation chronic incomplete traumatic spinal cord injuries: A double-blind randomized controlled clinical trial. *Journal of Neurosurgery: Spine*. doi:10.3171/2017.11.SPINE17769.
- Dergham, P., Ellezam, B., Essagian, C., et al. (2002) Rho signaling pathway targeted to promote spinal cord repair. *Journal of Neuroscience*. doi:20026637.
- Detmers, F.J.M., De Groot, B.L., Müller, E.M., et al. (2006) Quaternary ammonium compounds as water channel blockers: Specificity, potency, and site of action. *Journal of Biological Chemistry*. doi:10.1074/jbc.M513072200.
- Dietzel, I., Heinemann, U., Hofmeier, G., et al. (1980) Transient changes in the size of the extracellular space in the sensorimotor cortex of cats in relation to stimulus-induced changes in potassium concentration. *Experimental Brain Research*, 40 (4): 432–439. doi:10.1007/BF00236151.
- Duan, T., Tradtrantip, L., Phuan, P.W., et al. (2020) Affinity-matured ‘aquaporin-4 antibody’ anti-aquaporin-4 antibody for therapy of seropositive neuromyelitis optica spectrum disorders. *Neuropharmacology*. doi:10.1016/j.neuropharm.2019.107827.
- Dubreuil, C.I., Winton, M.J. and McKerracher, L. (2003) Rho activation patterns after spinal cord injury and the role of activated Rho in apoptosis in the central nervous system. *Journal of Cell Biology*. doi:10.1083/jcb.200301080.

Dumont, R.J., Okonkwo, D.O., Verma, S., et al. (2001) Acute spinal cord injury, part I: pathophysiologic mechanisms. *Clinical neuropharmacology*, 24 (5): 254–64. doi:10.1097/00002826-200109000-00002.

Ebert, E. (2012) Gastrointestinal involvement in spinal cord injury: a clinical perspective. *Journal of gastrointestinal and liver diseases: JGLD*, 21 (1): 75–82. Available at: <http://www.ncbi.nlm.nih.gov/pubmed/22457863>.

Ebisu, T., Naruse, S., Horikawa, Y., et al. (1993) Discrimination between different types of white matter edema with diffusion-weighted MR imaging. *Journal of Magnetic Resonance Imaging*. doi:10.1002/jmri.1880030612.

Edgerton, V.R., Tillakaratne, N.J.K., Bigbee, A.J., et al. (2004) PLASTICITY OF THE SPINAL NEURAL CIRCUITRY AFTER INJURY. *Annual Review of Neuroscience*. doi:10.1146/annurev.neuro.27.070203.144308.

Edgley, S.A. (2001) Organisation of inputs to spinal interneurone populations. *Journal of Physiology*. doi:10.1111/j.1469-7793.2001.0051b.x.

Eisemann, T., Costa, B., Strelau, J., et al. (2018) An advanced glioma cell invasion assay based on organotypic brain slice cultures. *BMC Cancer*. doi:10.1186/s12885-018-4007-4.

Eng, L.F. (1985) Glial fibrillary acidic protein (GFAP): the major protein of glial intermediate filaments in differentiated astrocytes. *Journal of Neuroimmunology*. doi:10.1016/S0165-5728(85)80063-1.

Eriksson, U.K., Fischer, G., Friemann, R., et al. (2013) Subangstrom resolution x-ray structure details aquaporin-water interactions. *Science*, 340 (6138): 1346–1349. doi:10.1126/science.1234306.

Escartin, C., Brouillet, E., Gubellini, P., et al. (2006) Ciliary neurotrophic factor activates astrocytes, redistributes their glutamate transporters GLAST and GLT-1 to raft microdomains, and improves glutamate handling in vivo. *Journal of Neuroscience*.

doi:10.1523/JNEUROSCI.0302-06.2006.

Escartin, C., Galea, E., Lakatos, A., et al. (2021) Reactive astrocyte nomenclature, definitions, and future directions. *Nature Neuroscience*. doi:10.1038/s41593-020-00783-4.

Evans, H.M. and Schulemann, W. (1914) The action of vital stains belonging to the benzidine group. *Science*. doi:10.1126/science.39.1004.443.

Evans, M.J. and Kaufman, M.H. (1981) Establishment in culture of pluripotential cells from mouse embryos. *Nature*. doi:10.1038/292154a0.

Faden, A.I., Chan, P.H. and Longar, S. (1987) Alterations in Lipid Metabolism, Na⁺, K⁺ - ATPase Activity, and Tissue Water Content of Spinal Cord Following Experimental Traumatic Injury. *Journal of Neurochemistry*, 48 (6): 1809–1816. doi:10.1111/j.1471-4159.1987.tb05740.x.

Faden, A.I., Jacobs, T.P. and Smith, M.T. (1984) Thyrotropin-releasing hormone in experimental spinal injury: Dose response and late treatment. *Neurology*. doi:10.1212/wnl.34.10.1280.

FADEN, A.I., VINK, R. and McINTOSH, T.K. (1989) Thyrotropin-Releasing Hormone and Central Nervous System Trauma. *Annals of the New York Academy of Sciences*. doi:10.1111/j.1749-6632.1989.tb54505.x.

Fan, Y., Kong, H., Shi, X., et al. (2008) Hypersensitivity of aquaporin 4-deficient mice to 1-methyl-4-phenyl-1,2,3,6-tetrahydropyridine and astrocytic modulation. *Neurobiology of Aging*. doi:10.1016/j.neurobiolaging.2007.02.015.

Farr, G.W., Hall, C.H., Farr, S.M., et al. (2019) Functionalized Phenylbenzamides Inhibit Aquaporin-4 Reducing Cerebral Edema and Improving Outcome in Two Models of CNS Injury. *Neuroscience*. doi:10.1016/j.neuroscience.2019.01.034.

Fawcett, J.W., Curt, A., Steeves, J.D., et al. (2007) Guidelines for the conduct of clinical trials for spinal cord injury as developed by the ICCP panel: Spontaneous recovery after spinal cord

injury and statistical power needed for therapeutic clinical trials. *Spinal Cord*. doi:10.1038/sj.sc.3102007.

Fehlings, M.G. and Hawryluk, G.W.J. (2010) Scarring after spinal cord injury. *Journal of Neurosurgery: Spine*. doi:10.3171/2009.11.SPINE09862.

Fehlings, M.G. and Nguyen, D.H. (2010) Immunoglobulin G: A potential treatment to attenuate neuroinflammation following spinal cord injury. *Journal of Clinical Immunology*. 30 (SUPPL. 1). doi:10.1007/s10875-010-9404-7.

Fehlings, M.G. and Perrin, R.G. (2006) The timing of surgical intervention in the treatment of spinal cord injury: A systematic review of recent clinical evidence. *Spine*. doi:10.1097/01.brs.0000217973.11402.7f.

Fehlings, M.G., Tator, C.H. and Linden, R.D. (1989) The effect of nimodipine and dextran on axonal function and blood flow following experimental spinal cord injury. *Journal of Neurosurgery*. doi:10.3171/jns.1989.71.3.0403.

Fehlings, M.G., Tetreault, L.A., Aarabi, B., et al. (2017) A Clinical Practice Guideline for the Management of Patients With Acute Spinal Cord Injury: Recommendations on the Type and Timing of Rehabilitation. *Global Spine Journal*. doi:10.1177/2192568217701910.

Fehlings, M.G., Theodore, N., Harrop, J., et al. (2011) A phase I/IIa clinical trial of a recombinant Rho protein antagonist in acute spinal cord injury. *Journal of Neurotrauma*. doi:10.1089/neu.2011.1765.

Fehlings, M.G., Vaccaro, A., Wilson, J.R., et al. (2012) Early versus delayed decompression for traumatic cervical spinal cord injury: Results of the surgical timing in acute spinal cord injury study (STASCIS). *PLoS ONE*. doi:10.1371/journal.pone.0032037.

Feigin, V.L., Nichols, E., Alam, T., et al. (2019) Global, regional, and national burden of neurological disorders, 1990–2016: a systematic analysis for the Global Burden of Disease Study 2016. *The Lancet Neurology*. doi:10.1016/S1474-4422(18)30499-X.

Feldblum, S., Arnaud, S., Simon, M., et al. (2000) Efficacy of a new neuroprotective agent, gacyclidine, in a model of rat spinal cord injury. *Journal of Neurotrauma*. doi:10.1089/neu.2000.17.1079.

Feng, X., Papadopoulos, M.C., Liu, J., et al. (2009) Sporadic obstructive hydrocephalus in Aqp4 null mice. *Journal of Neuroscience Research*, 87 (5): 1150–1155. doi:10.1002/jnr.21927.

Ferrari, G. and Greene, L.A. (1996) Prevention of neuronal apoptotic death by neurotrophic agents and ganglioside GM1: Insights and speculations regarding a common mechanism. *Perspectives on Developmental Neurobiology*.

Festoff, B.W., Ameenuddin, S., Arnold, P.M., et al. (2006) Minocycline neuroprotects, reduces microgliosis, and inhibits caspase protease expression early after spinal cord injury. *Journal of Neurochemistry*. doi:10.1111/j.1471-4159.2006.03799.x.

Feuerstein, G., Zukowska-Grojec, Z., Bayorh, M., et al. (1983) Leukotriene D4-induced hypotension is reversed by thyrotropin-releasing hormone. *Prostaglandins*. doi:10.1016/0090-6980(83)90056-4.

Fischbein, N.J., Dillon, W.P., Cobbs, C., et al. (1999) The “presyrinx” state: A reversible myelopathic condition that may precede syringomyelia. *American Journal of Neuroradiology*.

Flanders, A.E., Spettell, C.M., Friedman, D.P., et al. (1999) The relationship between the functional abilities of patients with cervical spinal cord injury and the severity of damage revealed by MR imaging. *AJNR. American journal of neuroradiology*, 20 (5): 926–34. Available at: <http://www.ncbi.nlm.nih.gov/pubmed/10369368> (Accessed: 18 May 2018).

Fleming, J.C., Bao, F., Chen, Y., et al. (2008) $\alpha 4\beta 1$ integrin blockade after spinal cord injury decreases damage and improves neurological function. *Experimental Neurology*, 214 (2): 147–159. doi:10.1016/j.expneurol.2008.04.024.

Fleming, J.C., Norenberg, M.D., Ramsay, D.A., et al. (2006) The cellular inflammatory response in human spinal cords after injury. *Brain*, 129 (12): 3249–3269.

doi:10.1093/brain/awl296.

Flynn, J.R., Graham, B.A., Galea, M.P., et al. (2011) The role of propriospinal interneurons in recovery from spinal cord injury. *Neuropharmacology*.

doi:10.1016/j.neuropharm.2011.01.016.

French, D.D., Campbell, R.R., Sabharwal, S., et al. (2007) Health care costs for patients with chronic spinal cord injury in the Veterans Health Administration. *The journal of spinal cord medicine*, 30 (5): 477–81. Available at: <http://www.ncbi.nlm.nih.gov/pubmed/18092564> (Accessed: 17 April 2018).

Frostell, A., Hakim, R., Thelin, E.P., et al. (2016) A review of the segmental diameter of the healthy human spinal cord. *Frontiers in Neurology*. doi:10.3389/fneur.2016.00238.

Fu, D., Libson, A., Miercke, L.J.W., et al. (2000) Structure of a glycerol-conducting channel and the basis for its selectivity. *Science*, 290 (5491): 481–486.

doi:10.1126/science.290.5491.481.

Fukuda, A.M., Adami, A., Pop, V., et al. (2013) Posttraumatic reduction of edema with aquaporin-4 RNA interference improves acute and chronic functional recovery. *Journal of Cerebral Blood Flow and Metabolism*, 33 (10): 1621–1632. doi:10.1038/jcbfm.2013.118.

Fukuda, A.M., Pop, V., Spagnoli, D., et al. (2012) Delayed increase of astrocytic aquaporin 4 after juvenile traumatic brain injury: Possible role in edema resolution? *Neuroscience*, 222: 366–378. doi:10.1016/j.neuroscience.2012.06.033.

Fukuda, S., Nakamura, T., Kishigami, Y., et al. (2005) New canine spinal cord injury model free from laminectomy. *Brain Research Protocols*. doi:10.1016/j.brainresprot.2005.01.001.

Furlan, J.C., Noonan, V., Cadotte, D.W., et al. (2011) Timing of decompressive surgery of spinal cord after traumatic spinal cord injury: An evidence-based examination of pre-clinical and clinical studies. *Journal of Neurotrauma*. doi:10.1089/neu.2009.1147.

Furman, C.S., Gorelick-Feldman, D.A., Davidson, K.G. V., et al. (2003) Aquaporin-4 square

array assembly: Opposing actions of M1 and M23 isoforms. *Proceedings of the National Academy of Sciences*, 100 (23): 13609–13614. doi:10.1073/pnas.2235843100.

Fushimi, K., Sasaki, S. and Marumo, F. (1997) Phosphorylation of serine 256 is required for cAMP-dependent regulatory exocytosis of the aquaporin-2 water channel. *Journal of Biological Chemistry*, 272 (23): 14800–14804. doi:10.1074/jbc.272.23.14800.

Gaberel, T., Gakuba, C., Goulay, R., et al. (2014) Impaired glymphatic perfusion after strokes revealed by contrast-enhanced MRI: A new target for fibrinolysis? *Stroke*. doi:10.1161/STROKEAHA.114.006617.

Gao, Y.J., Zhang, L., Samad, O.A., et al. (2009) JNK-induced MCP-1 production in spinal cord astrocytes contributes to central sensitization and neuropathic pain. *Journal of Neuroscience*. doi:10.1523/JNEUROSCI.3623-08.2009.

Gaviria, M., Privat, A., D'Arbigny, P., et al. (2000a) Neuroprotective effects of a novel NMDA antagonist, Gacyclidine, after experimental contusive spinal cord injury in adult rats. *Brain Research*. doi:10.1016/S0006-8993(00)02581-6.

Gaviria, M., Privat, A., D'Arbigny, P., et al. (2000b) Neuroprotective effects of gacyclidine after experimental photochemical spinal cord lesion in adult rats: Dose-window and time-window effects. *Journal of Neurotrauma*. doi:10.1089/neu.2000.17.19.

Geisler, F.H., Coleman, W.P., Dorsey, F.C., et al. (1991) Recovery of motor function after spinal-cord injury — A randomized, placebo-controlled trial with GM-1 ganglioside. *New England Journal of Medicine*. doi:10.1056/NEJM199106273242601.

Geisler, F.H., Coleman, W.P., Grieco, G., et al. (2001a) Recruitment and early treatment in a multicenter study of acute spinal cord injury. *Spine*. doi:10.1097/00007632-200112151-00013.

Geisler, F.H., Coleman, W.P., Grieco, G., et al. (2001b) The Sygen® multicenter acute spinal cord injury study. *Spine*. doi:10.1097/00007632-200112151-00015.

George, R. and Griffin, J.W. (1994) Delayed macrophage responses and myelin clearance

during Wallerian degeneration in the central nervous system: The dorsal radiculotomy model. *Experimental Neurology*. doi:10.1006/exnr.1994.1164.

Giaume, C., Fromaget, C., El Aoumari, A., et al. (1991) Gap junctions in cultured astrocytes: Single-channel currents and characterization of channel-forming protein. *Neuron*. doi:10.1016/0896-6273(91)90128-M.

Glober, N.K., Sprague, S., Ahmad, S., et al. (2019) Acetazolamide Treatment Prevents Redistribution of Astrocyte Aquaporin 4 after Murine Traumatic Brain Injury. *Neuroscience Journal*. doi:10.1155/2019/2831501.

Goldshmit, Y., Sztal, T.E., Jusuf, P.R., et al. (2012) Fgf-dependent glial cell bridges facilitate spinal cord regeneration in Zebrafish. *Journal of Neuroscience*. doi:10.1523/JNEUROSCI.0758-12.2012.

Goodman, J.H., Bingham, W.G. and Hunt, W.E. (1976a) Ultrastructural blood brain barrier alterations and edema formation in acute spinal cord trauma. *Journal of Neurosurgery*. doi:10.3171/jns.1976.44.4.0418.

Goodman, J.H., Bingham, W.G.J. and Hunt, W.E. (1976b) Ultrastructural blood-brain barrier alterations and edema formation in acute spinal cord trauma. *Journal of neurosurgery*, 44 (4): 418–424. doi:10.3171/jns.1976.44.4.0418.

GrandPré, T., Shuxin, L.I. and Strittmatter, S.M. (2002) Nogo-66 receptor antagonist peptide promotes axonal regeneration. *Nature*. doi:10.1038/417547a.

Green, B.A., Kahn, T. and Klose, K.J. (1980) A comparative study of steroid therapy in acute experimental spinal cord injury. *Surgical Neurology*.

De Groot, B.L., Hub, J.S. and Grubmüller, H. (2009) Dynamics and energetics of permeation through aquaporins. What Do we learn from molecular dynamics simulations? *Handbook of Experimental Pharmacology*. 190 pp. 57–76. doi:10.1007/978-3-540-79885-9_3.

Gruner, J.A. (1992) A Monitored Contusion Model of Spinal Cord Injury in the Rat. *Journal of*

Neurotrauma, 9 (2): 123–128. doi:10.1089/neu.1992.9.123.

Guerriero, R.M., Giza, C.C. and Rotenberg, A. (2015) Glutamate and GABA Imbalance Following Traumatic Brain Injury. *Current Neurology and Neuroscience Reports*. 15 (5). doi:10.1007/s11910-015-0545-1.

Guest, J.D., Hiester, E.D. and Bunge, R.P. (2005) Demyelination and Schwann cell responses adjacent to injury epicenter cavities following chronic human spinal cord injury. *Experimental Neurology*. doi:10.1016/j.expneurol.2004.11.033.

Guha, A., Tator, C.H., Endrenyi, L., et al. (1987a) Decompression of the spinal cord improves recovery after acute experimental spinal cord compression injury. *Spinal Cord*, 25 (4): 324–339. doi:10.1038/sc.1987.61.

Guha, A., Tator, C.H. and Piper, I. (1987b) Effect of a calcium channel blocker on posttraumatic spinal cord blood flow. *Journal of Neurosurgery*. doi:10.3171/jns.1987.66.3.0423.

Gunnarson, E., Zelenina, M., Axehult, G., et al. (2008) Identification of a molecular target for glutamate regulation of astrocyte water permeability. *GLIA*, 56 (6): 587–596. doi:10.1002/glia.20627.

Guo, X., Zahir, T., Mothe, A., et al. (2012) The Effect of Growth Factors and Soluble Nogo-66 Receptor Protein on Transplanted Neural Stem/Progenitor Survival and Axonal Regeneration After Complete Transection of Rat Spinal Cord. *Cell Transplantation*. doi:10.3727/096368911X612503.

Hablitz, L.M., Plá, V., Giannetto, M., et al. (2020) Circadian control of brain glymphatic and lymphatic fluid flow. *Nature Communications*. doi:10.1038/s41467-020-18115-2.

Hains, B.C., Saab, C.Y., Lo, A.C., et al. (2004) Sodium channel blockade with phenytoin protects spinal cord axons, enhances axonal conduction, and improves functional motor recovery after contusion SCI. *Experimental Neurology*. doi:10.1016/j.expneurol.2004.04.001.

Haj-Yasein, N.N., Jensen, V., Østby, I., et al. (2012) Aquaporin-4 regulates extracellular space volume dynamics during high-frequency synaptic stimulation: A gene deletion study in mouse hippocampus. *GLIA*, 60 (6): 867–874. doi:10.1002/glia.22319.

Haj-Yasein, N.N., Vindedal, G.F., Eilert-Olsen, M., et al. (2011) Glial-conditional deletion of aquaporin-4 (Aqp4) reduces blood-brain water uptake and confers barrier function on perivascular astrocyte endfeet. *Proceedings of the National Academy of Sciences*, 108 (43): 17815–17820. doi:10.1073/pnas.1110655108.

Hall, E.D. and Braughler, J.M. (1982) Glucocorticoid mechanisms in acute spinal cord injury: a review and therapeutic rationale. *Surgical neurology*, 18 (5): 320–7. Available at: <http://www.ncbi.nlm.nih.gov/pubmed/7179094>.

Halsey, A., Conner, A., Bill, R., et al. (2018) Aquaporins and Their Regulation after Spinal Cord Injury. *Cells*. doi:10.3390/cells7100174.

Hamby, M.E., Coppola, G., Ao, Y., et al. (2012) Inflammatory mediators alter the astrocyte transcriptome and calcium signaling elicited by multiple G-protein-coupled receptors. *Journal of Neuroscience*. doi:10.1523/JNEUROSCI.1256-12.2012.

Han, Z., Wax, M.B. and Patil, R. V. (1998) Regulation of aquaporin-4 water channels by phorbol ester-dependent protein phosphorylation. *Journal of Biological Chemistry*, 273 (11): 6001–6004. doi:10.1074/jbc.273.11.6001.

Harries, W.E.C., Akhavan, D., Miercke, L.J.W., et al. (2004) The channel architecture of aquaporin 0 at a 2.2-Å resolution. *Proceedings of the National Academy of Sciences*, 101 (39): 14045–14050. doi:10.1073/pnas.0405274101.

Hassannejad, Z., Youseffard, M., Azizi, Y., et al. (2019) Axonal degeneration and demyelination following traumatic spinal cord injury: A systematic review and meta-analysis. *Journal of Chemical Neuroanatomy*. doi:10.1016/j.jchemneu.2019.01.009.

Heimburger, R.F. (2005) Return of function after spinal cord transection. *Spinal Cord*.

doi:10.1038/sj.sc.3101748.

Hermelinda, S.C., Guizar-Sahagun, G., Feria-Velasco, A., et al. (1998) Spontaneous long-term remyelination after traumatic spinal cord injury in rats. *Brain Research*. doi:10.1016/S0006-8993(97)01252-3.

Hertz, L., Peng, L. and Dienel, G.A. (2007) Energy metabolism in astrocytes: High rate of oxidative metabolism and spatiotemporal dependence on glycolysis/glycogenolysis. *Journal of Cerebral Blood Flow and Metabolism*. doi:10.1038/sj.jcbfm.9600343.

Hesp, Z.C., Goldstein, E.A., Miranda, C.J., et al. (2015) Chronic oligodendrogenesis and remyelination after spinal cord injury in mice and rats. *Journal of Neuroscience*. doi:10.1523/JNEUROSCI.2568-14.2015.

Hirbec, H., Gaviria, M. and Vignon, J. (2001) Gacyclidine: A new neuroprotective agent acting at the N-methyl-D-aspartate receptor. *CNS Drug Reviews*. doi:10.1111/j.1527-3458.2001.tb00194.x.

Hoffmann, E.K., Lambert, I.H. and Pedersen, S.F. (2009) Physiology of Cell Volume Regulation in Vertebrates. *Physiological Reviews*, 89 (1): 193–277. doi:10.1152/physrev.00037.2007.

Holmseth, S., Scott, H.A., Real, K., et al. (2009) The concentrations and distributions of three C-terminal variants of the GLT1 (EAAT2; slc1a2) glutamate transporter protein in rat brain tissue suggest differential regulation. *Neuroscience*. doi:10.1016/j.neuroscience.2009.03.048.

Homkajorn, B., Sims, N.R. and Muyderman, H. (2010) Connexin 43 regulates astrocytic migration and proliferation in response to injury. *Neuroscience Letters*. doi:10.1016/j.neulet.2010.09.051.

Horsefield, R., Nordén, K., Fellert, M., et al. (2008) High-resolution x-ray structure of human aquaporin 5. *Proceedings of the National Academy of Sciences of the United States of America*, 105 (36): 13327–32. doi:10.1073/pnas.0801466105.

- Hu, A.M., Li, J.J., Sun, W., et al. (2015) Myelotomy reduces spinal cord edema and inhibits aquaporin-4 and aquaporin-9 expression in rats with spinal cord injury. *Spinal Cord*, 53 (2): 98–102. doi:10.1038/sc.2014.209.
- Hua, Y., Ying, X., Qian, Y., et al. (2019) Physiological and pathological impact of AQP1 knockout in mice. *Bioscience Reports*. doi:10.1042/BSR20182303.
- Huang, Y., Li, S.N., Zhou, X.Y., et al. (2019) The dual role of aqp4 in cytotoxic and vasogenic edema following spinal cord contusion and its possible association with energy metabolism via cox5a. *Frontiers in Neuroscience*. doi:10.3389/fnins.2019.00584.
- Hubbard, J.A., Hsu, M.S., Seldin, M.M., et al. (2015) Expression of the astrocyte water channel aquaporin-4 in the mouse brain. *ASN Neuro*, 7 (5). doi:10.1177/1759091415605486.
- Huber, V.J., Tsujita, M., Kwee, I.L., et al. (2009) Inhibition of Aquaporin 4 by antiepileptic drugs. *Bioorganic and Medicinal Chemistry*. doi:10.1016/j.bmc.2007.12.038.
- Hudak, A.M., Peng, L., De La Plata, C.M., et al. (2014) Cytotoxic and vasogenic cerebral oedema in traumatic brain injury: Assessment with FLAIR and DWI imaging. *Brain Injury*. doi:10.3109/02699052.2014.936039.
- Huerta Bahena, J., Villalobos Molina, R. and Garcia Sainz, J.A. (1983) Trifluoperazine and chlorpromazine antagonize alpha1- but not alpha2-adrenergic effects. *Molecular Pharmacology*.
- Igarashi, H., Huber, V.J., Tsujita, M., et al. (2011) Pretreatment with a novel aquaporin 4 inhibitor, TGN-020, significantly reduces ischemic cerebral edema. *Neurological Sciences*. doi:10.1007/s10072-010-0431-1.
- Iliff, J.J., Lee, H., Yu, M., et al. (2013) Brain-wide pathway for waste clearance captured by contrast-enhanced MRI. *Journal of Clinical Investigation*. doi:10.1172/JCI67677.
- Iliff, J.J., Wang, M., Liao, Y., et al. (2012) A paravascular pathway facilitates CSF flow through the brain parenchyma and the clearance of interstitial solutes, including amyloid β . *Science*

Translational Medicine. doi:10.1126/scitranslmed.3003748.

Inada, T., Takahashi, H., Yamazaki, M., et al. (2014) Multicenter prospective nonrandomized controlled clinical trial to prove neurotherapeutic effects of granulocyte colony-stimulating factor for acute spinal cord injury: Analyses of follow-up cases after at least 1 Year. *Spine*. doi:10.1097/BRS.0000000000000121.

Ishibashi, K., Kuwahara, M., Gu, Y., et al. (1998) Cloning and functional expression of a new aquaporin (AQP9) abundantly expressed in the peripheral leukocytes permeable to water and urea, but not to glycerol. *Biochemical and Biophysical Research Communications*, 244 (1): 268–274. doi:10.1006/bbrc.1998.8252.

Jaeger, M., Carin, M., Medale, M., et al. (1999) The osmotic migration of cells in a solute gradient. *Biophysical Journal*. doi:10.1016/S0006-3495(99)76977-8.

James, N.D., Shea, J., Muir, E.M., et al. (2015) Chondroitinase gene therapy improves upper limb function following cervical contusion injury. *Experimental Neurology*. doi:10.1016/j.expneurol.2015.05.022.

Jha, R.M., Kochanek, P.M. and Simard, J.M. (2019) Pathophysiology and treatment of cerebral edema in traumatic brain injury. *Neuropharmacology*. doi:10.1016/j.neuropharm.2018.08.004.

Johnstone, A.L., Reiersen, G.W., Smith, R.P., et al. (2012) A chemical genetic approach identifies piperazine antipsychotics as promoters of CNS neurite growth on inhibitory substrates. *Molecular and Cellular Neuroscience*. doi:10.1016/j.mcn.2012.04.008.

Kanemaru, K., Kubota, J., Sekiya, H., et al. (2013) Calcium-dependent N-cadherin up-regulation mediates reactive astrogliosis and neuroprotection after brain injury. *Proceedings of the National Academy of Sciences of the United States of America*. doi:10.1073/pnas.1300378110.

Kapoor, S., Kim, S.-M., Farook, J.M., et al. (2013) Foxo3a Transcriptionally Upregulates AQP4

and Induces Cerebral Edema Following Traumatic Brain Injury. *Journal of Neuroscience*. doi:10.1523/jneurosci.2756-13.2013.

Kaptanoglu, E., Beskonakli, E., Okutan, O., et al. (2003) Effect of magnesium sulphate in experimental spinal cord injury: Evaluation with ultrastructural findings and early clinical results. *Journal of Clinical Neuroscience*. doi:10.1016/S0967-5868(03)00031-6.

Katsura, T., Gustafson, C.E., Ausiello, D.A., et al. (1997) Protein kinase A phosphorylation is involved in regulated exocytosis of aquaporin-2 in transfected LLC-PK1 cells. *The American journal of physiology*, 272 (6 Pt 2): F817–F822.

Khakh, B.S. and Sofroniew, M. V. (2015) Diversity of astrocyte functions and phenotypes in neural circuits. *Nature Neuroscience*. doi:10.1038/nn.4043.

Kimelberg, H.K. (2004) Water homeostasis in the brain: Basic concepts. *Neuroscience*. 129 (4) pp. 851–860. doi:10.1016/j.neuroscience.2004.07.033.

Kimelberg, H.K. (2010) Functions of mature mammalian astrocytes: A current view. *Neuroscientist*. doi:10.1177/1073858409342593.

Kimura, A., Hsu, M., Seldin, M., et al. (2010) Protective role of aquaporin-4 water channels after contusion spinal cord injury. *Annals of Neurology*, 67 (6): 794–801. doi:10.1002/ana.22023.

Kirshblum, S.C., Burns, S.P., Biering-Sorensen, F., et al. (2011) International standards for neurological classification of spinal cord injury (Revised 2011). *Journal of Spinal Cord Medicine*. doi:10.1179/204577211X13207446293695.

Kitamura, K., Fujiyoshi, K., Yamane, J. ichi, et al. (2011) Human hepatocyte growth factor promotes functional recovery in primates after spinal cord injury. *PLoS ONE*. doi:10.1371/journal.pone.0027706.

Kitamura, K., Iwanami, A., Nakamura, M., et al. (2007) Hepatocyte growth factor promotes endogenous repair and functional recovery after spinal cord injury. *Journal of Neuroscience*

Research. doi:10.1002/jnr.21372.

Kitamura, K., Iwanami, A., Okano, H., et al. (2015) Intrathecal administration of recombinant human hepatocyte growth factor for acute spinal cord injury: the road from bench to clinical trial and future perspective. *Nihon rinsho. Japanese journal of clinical medicine*.

Kitchen, P., Day, R.E., Taylor, L.H.J., et al. (2015) Identification and molecular mechanisms of the rapid tonicity-induced relocalization of the aquaporin 4 channel. *Journal of Biological Chemistry*, 290 (27): 16873–16881. doi:10.1074/jbc.M115.646034.

Kitchen, P., Salman, M.M., Halsey, A.M., et al. (2020) Targeting aquaporin-4 subcellular localization as a novel approach to treat CNS edema. *Cell*, In Press. doi:CELL-D-19-01465_R2.

Kjell, J., Finn, A., Hao, J., et al. (2015) Delayed Imatinib Treatment for Acute Spinal Cord Injury: Functional Recovery and Serum Biomarkers. *Journal of Neurotrauma*. doi:10.1089/neu.2014.3863.

Kleindienst, A., Engelhorn, T., Roeckelein, V., et al. (2020) Development of pre-syrinx state and syringomyelia following a minor injury: a case report. *Journal of Medical Case Reports*. doi:10.1186/s13256-020-02568-6.

Klekamp, J. (2012) Treatment of posttraumatic syringomyelia: Clinical article. *Journal of Neurosurgery: Spine*. doi:10.3171/2012.5.SPINE11904.

Ko, H.Y., Ditunno, J.F., Graziani, V., et al. (1999) The pattern of reflex recovery during spinal shock. *Spinal Cord*. doi:10.1038/sj.sc.3100840.

Kotini, M., Barriga, E.H., Leslie, J., et al. (2018) Gap junction protein Connexin-43 is a direct transcriptional regulator of N-cadherin in vivo. *Nature Communications*. doi:10.1038/s41467-018-06368-x.

Kotter, M.R., Li, W.W., Zhao, C., et al. (2006) Myelin impairs CNS remyelination by inhibiting oligodendrocyte precursor cell differentiation. *Journal of Neuroscience*.

doi:10.1523/JNEUROSCI.2615-05.2006.

Krassioukov, A. and Claydon, V.E. (2006) "The clinical problems in cardiovascular control following spinal cord injury: an overview." In *AUTONOMIC DYSFUNCTION AFTER SPINAL CORD INJURY*. pp. 223–229. doi:10.1016/S0079-6123(05)52014-4.

Kress, B.T., Iliff, J.J., Xia, M., et al. (2014) Impairment of paravascular clearance pathways in the aging brain. *Annals of Neurology*. doi:10.1002/ana.24271.

Kucher, K., Johns, D., Maier, D., et al. (2018) First-in-man intrathecal application of neurite growth-promoting anti-nogo- a antibodies in acute spinal cord injury. *Neurorehabilitation and Neural Repair*. doi:10.1177/1545968318776371.

Kwon, B.K., Curt, A.N., Belanger, L.M., et al. (2009) Intrathecal pressure monitoring and cerebrospinal fluid drainage in acute spinal cord injury: A prospective randomized trial - Clinical article. *Journal of Neurosurgery: Spine*. doi:10.3171/2008.10.SPINE08217.

Lagord, C., Berry, M. and Logan, A. (2002) Expression of TGF β 2 but not TGF β 1 correlates with the deposition of scar tissue in the lesioned spinal cord. *Molecular and Cellular Neuroscience*, 20 (1): 69–92. doi:10.1006/mcne.2002.1121.

Laird, A.S., Carrive, P. and Waite, P.M. (2006) Cardiovascular and temperature changes in spinal cord injured rats at rest and during autonomic dysreflexia. *J Physiol*, 577 (Pt 2): 539–548. doi:10.1113/jphysiol.2006.116301.

Lan, Y.L., Wang, X., Lou, J.C., et al. (2017) The potential roles of aquaporin 4 in malignant gliomas. *Oncotarget*. doi:10.18632/oncotarget.16017.

Lasiene, J., Shupe, L., Perlmutter, S., et al. (2008) No evidence for chronic demyelination in spared axons after spinal cord injury in a mouse. *Journal of Neuroscience*. doi:10.1523/JNEUROSCI.4756-07.2008.

Laufs, U., Endres, M., Stagliano, N., et al. (2000) Neuroprotection mediated by changes in the endothelial actin cytoskeleton. *Journal of Clinical Investigation*. doi:10.1172/JCI9639.

- Lavrov, I., Gerasimenko, Y.P., Ichiyama, R.M., et al. (2006) Plasticity of spinal cord reflexes after a complete transection in adult rats: Relationship to stepping ability. *Journal of Neurophysiology*. doi:10.1152/jn.00325.2006.
- Lee, D.Y., Park, Y.J., Song, S.Y., et al. (2018) The importance of early surgical decompression for acute traumatic spinal cord injury. *CiOS Clinics in Orthopedic Surgery*. doi:10.4055/cios.2018.10.4.448.
- Lee, J.M., Yan, P., Xiao, Q., et al. (2008) Methylprednisolone protects oligodendrocytes but not neurons after spinal cord injury. *Journal of Neuroscience*. doi:10.1523/JNEUROSCI.5547-07.2008.
- Lee, S.M., Yune, T.Y., Kim, S.J., et al. (2003) Minocycline Reduces Cell Death and Improves Functional Recovery after Traumatic Spinal Cord Injury in the Rat. *Journal of Neurotrauma*. doi:10.1089/089771503770195867.
- Leonard, A. V., Thornton, E. and Vink, R. (2015) The relative contribution of edema and hemorrhage to raised intrathecal pressure after traumatic spinal cord injury. *Journal of Neurotrauma*. doi:10.1089/neu.2014.3543.
- Leonard, A. V. and Vink, R. (2015) Reducing intrathecal pressure after traumatic spinal cord injury: A potential clinical target to promote tissue survival. *Neural Regeneration Research*, 10 (3): 380–382. doi:10.4103/1673-5374.153683.
- Levinson, B. (2018) SUN13837 in Treatment of Acute Spinal Cord Injury, the ASCENT-ASCI Study. *Clinical Neurology and Neuroscience*. doi:10.11648/j.cnn.20180201.11.
- Leybold, B.G., Flanders, A.E. and Burns, A.S. (2008) The Early Evolution of Spinal Cord Lesions on MR Imaging following Traumatic Spinal Cord Injury. *American Journal of Neuroradiology*, 29 (5): 1012–1016. doi:10.3174/ajnr.A0962.
- Leybold, B.G., Flanders, A.E., Schwartz, E.D., et al. (2007) The impact of methylprednisolone on lesion severity following spinal cord injury. *Spine*.

doi:10.1097/01.brs.0000253964.10701.00.

Li, C., Chen, X., Qiao, S., et al. (2014) Melatonin lowers edema after spinal cord injury. *Neural Regeneration Research*, 9 (24): 2205–2210. doi:10.4103/1673-5374.147954.

Li, J., Jia, Z., Xu, W., et al. (2019) TGN-020 alleviates edema and inhibits astrocyte activation and glial scar formation after spinal cord compression injury in rats. *Life Sciences*. doi:10.1016/j.lfs.2019.03.007.

Li, J., Patil, R. V. and Verkman, A.S. (2002) Mildly abnormal retinal function in transgenic mice without Müller cell aquaporin-4 water channels. *Investigative Ophthalmology and Visual Science*, 43 (2): 573–579.

Li, J. and Verkman, A.S. (2001) Impaired Hearing in Mice Lacking Aquaporin-4 Water Channels. *Journal of Biological Chemistry*. doi:10.1074/jbc.M104368200.

Li, P., Tong, C., Mehrian-Shai, R., et al. (2008) Germline Competent Embryonic Stem Cells Derived from Rat Blastocysts. *Cell*. doi:10.1016/j.cell.2008.12.006.

Li, S. and Tator, C.H. (1999) Effects of MK801 on evoked potentials, spinal cord blood flow and cord edema in acute spinal cord injury in rats. *Spinal Cord*. doi:10.1038/sj.sc.3100941.

Li, W., Suwanwela, N.C. and Patumraj, S. (2016) Curcumin by down-regulating NF-kB and elevating Nrf2, reduces brain edema and neurological dysfunction after cerebral I/R. *Microvascular Research*. doi:10.1016/j.mvr.2015.12.008.

Liang, D., Bhatta, S., Volodymyr, G., et al. (2007) Cytotoxic edema: mechanisms of pathological cell swelling. *Neurosurg Focus*. doi:10.3171/foc.2007.22.5.3.

Liang, H., Paxinos, G. and Watson, C. (2011) Projections from the brain to the spinal cord in the mouse. *Brain Structure and Function*. doi:10.1007/s00429-010-0281-x.

Liao, S. and Padera, T.P. (2013) Lymphatic function and immune regulation in health and disease. *Lymphatic Research and Biology*. doi:10.1089/lrb.2013.0012.

- Linsley, J.W., Tripathi, A., Epstein, I., et al. (2019) Automated four-dimensional long term imaging enables single cell tracking within organotypic brain slices to study neurodevelopment and degeneration. *Communications Biology*. doi:10.1038/s42003-019-0411-9.
- Liu, L., Zhou, J., Wang, Y., et al. (2019a) Imatinib inhibits oxidative stress response in spinal cord injury rats by activating Nrf2/HO-1 signaling pathway. *Experimental and Therapeutic Medicine*. doi:10.3892/etm.2019.8270.
- Liu, N.-K. and Xu, X.-M. (2012) Neuroprotection and its molecular mechanism following spinal cord injury. *Neural regeneration research*, 7 (26): 2051–62. doi:10.3969/j.issn.1673-5374.2012.26.007.
- Liu, Z., Yang, Y., He, L., et al. (2019b) High-dose methylprednisolone for acute traumatic spinal cord injury: A meta-analysis. *Neurology*. doi:10.1212/WNL.0000000000007998.
- Lo, A.C., Saab, C.Y., Black, J.A., et al. (2003) Phenytoin Protects Spinal Cord Axons and Preserves Axonal Conduction and Neurological Function in a Model of Neuroinflammation In Vivo. *Journal of Neurophysiology*. doi:10.1152/jn.00434.2003.
- Lo, W.D., Betz, A.L., Schielke, G.P., et al. (1987) Transport of sodium from blood to brain in ischemic brain edema. *Stroke*, 18 (1): 150–7. Available at: <http://www.ncbi.nlm.nih.gov/pubmed/3810748> (Accessed: 11 May 2018).
- Logan, a, Berry, M., Gonzalez, a M., et al. (1994) Effects of transforming growth factor beta 1 on scar production in the injured central nervous system of the rat. *The European journal of neuroscience*, 6 (3): 355–63. Available at: <http://www.ncbi.nlm.nih.gov/pubmed/8019673>.
- Loitto, V.M., Karlsson, T. and Magnusson, K.E. (2009) Water flux in cell motility: Expanding the mechanisms of membrane protrusion. *Cell Motility and the Cytoskeleton*. doi:10.1002/cm.20357.
- Loo, D.D.F., Zeuthen, T., Chandy, G., et al. (1996) Cotransport of water by the Na⁺/glucose cotransporter. *Proceedings of the National Academy of Sciences*, 93 (23): 13367–13370.

doi:10.1073/pnas.93.23.13367.

Loy, D.N., Crawford, C.H., Darnall, J.B., et al. (2002) Temporal progression of angiogenesis and basal lamina deposition after contusive spinal cord injury in the adult rat. *Journal of Comparative Neurology*. doi:10.1002/cne.10168.

Lu, D.C., Zador, Z., Yao, J., et al. (2011) Aquaporin-4 Reduces Post-Traumatic Seizure Susceptibility by Promoting Astrocytic Glial Scar Formation in Mice. *Journal of Neurotrauma*. doi:10.1089/neu.2011.2114.

Lukovic, D., Moreno-Manzano, V., Lopez-Mocholi, E., et al. (2015) Complete rat spinal cord transection as a faithful model of spinal cord injury for translational cell transplantation. *Scientific Reports*. doi:10.1038/srep09640.

Luo, H., Xie, A., Hua, Y., et al. (2018) Aquaporin 1 gene deletion affects the amniotic fluid volume and composition as well as the expression of other aquaporin water channels in placenta and fetal membranes. *Clinica Chimica Acta*. doi:10.1016/j.cca.2018.04.001.

Ma, T., Yang, B., Gillespie, A., et al. (1997) Generation and phenotype of a transgenic knockout mouse lacking the mercurial-insensitive water channel aquaporin-4. *Journal of Clinical Investigation*. doi:10.1172/JCI231.

Ma, T., Yang, B., Gillespie, A., et al. (1998) Severely impaired urinary concentrating ability in transgenic mice lacking aquaporin-1 water channels. *Journal of Biological Chemistry*. doi:10.1074/jbc.273.8.4296.

MacNeil, S., Griffin, M., Cooke, A.M., et al. (1988) Calmodulin antagonists of improved potency and specificity for use in the study of calmodulin biochemistry. *Biochemical Pharmacology*. doi:10.1016/0006-2952(88)90434-0.

Magni, F., Sarto, C., Ticozzi, D., et al. (2006) Proteomic knowledge of human aquaporins. *Proteomics*. 6 (20) pp. 5637–5649. doi:10.1002/pmic.200600212.

Manley, G.T., Binder, D.K., Papadopoulos, M.C., et al. (2004) New insights into water

transport and edema in the central nervous system from phenotype analysis of aquaporin-4 null mice. *Neuroscience*. doi:10.1016/j.neuroscience.2004.06.088.

Manley, G.T., Fujimura, M., Ma, T., et al. (2000) Aquaporin-4 deletion in mice reduces brain edema after acute water intoxication and ischemic stroke. *Nature Medicine*, 6 (2): 159–163. doi:10.1038/72256.

Marcantoni, M., Fuchs, A., Löw, P., et al. (2020) Early delivery and prolonged treatment with nimodipine prevents the development of spasticity after spinal cord injury in mice. *Science Translational Medicine*. doi:10.1126/scitranslmed.aay0167.

Mathiisen, T.M., Lehre, K.P., Danbolt, N.C., et al. (2010) The perivascular astroglial sheath provides a complete covering of the brain microvessels: An electron microscopic 3D reconstruction. *GLIA*, 58 (9): 1094–1103. doi:10.1002/glia.20990.

McCoy, E. and Sontheimer, H. (2010) MAPK induces AQP1 expression in astrocytes following injury. *GLIA*, 58 (2): 209–217. doi:10.1002/glia.20916.

McCoy, E. and Sontheimer, H. (2007) Expression and function of water channels (aquaporins) in migrating malignant astrocytes. *GLIA*. doi:10.1002/glia.20524.

McDonough, A., Monterrubio, A., Ariza, J., et al. (2015) Calibrated Forceps Model of Spinal Cord Compression Injury. *Journal of Visualized Experiments*, (98). doi:10.3791/52318.

McIntosh, T.K., Fernyak, S., Hayes, R.L., et al. (1993) Beneficial Effect of the Nonselective Opiate Antagonist Naloxone Hydrochloride and the Thyrotropin-Releasing Hormone (TRH) Analog YM-14673 on Long-Term Neurobehavioral Outcome following Experimental Brain Injury in the Rat. *Journal of Neurotrauma*. doi:10.1089/neu.1993.10.373.

McKeon, R.J., Schreiber, R.C., Rudge, J.S., et al. (1991) Reduction of neurite outgrowth in a model of glial scarring following CNS injury is correlated with the expression of inhibitory molecules on reactive astrocytes. *Journal of Neuroscience*. doi:10.1523/jneurosci.11-11-03398.1991.

- McLaughlin, I., Dani, J.A. and De Biasi, M. (2017) The medial habenula and interpeduncular nucleus circuitry is critical in addiction, anxiety, and mood regulation. *Journal of Neurochemistry*. 142 pp. 130–143. doi:10.1111/jnc.14008.
- McTigue, D.M., Wei, P. and Stokes, B.T. (2001) Proliferation of NG2-positive cells and altered oligodendrocyte numbers in the contused rat spinal cord. *Journal of Neuroscience*. doi:10.1523/jneurosci.21-10-03392.2001.
- Mercadante, A.A. and Tadi, P. (2020) *Neuroanatomy, Gray Matter*.
- Mestre, H., Tithof, J., Du, T., et al. (2018) Flow of cerebrospinal fluid is driven by arterial pulsations and is reduced in hypertension. *Nature Communications*. doi:10.1038/s41467-018-07318-3.
- Metz, G., Curt, A., Van de meent, H., et al. (2000) Validation of the Weight-Drop Contusion Model in Rats: A Comparative Study of Human Spinal Cord Injury. *Journal of Neurotrauma*, 17 (1): 1–17. doi:10.1089/neu.2000.17.1.
- Michinaga, S. and Koyama, Y. (2015) Pathogenesis of brain edema and investigation into anti-edema drugs. *International Journal of Molecular Sciences*. doi:10.3390/ijms16059949.
- Middleton, P.M., Davies, S.R., Anand, S., et al. (2012) The pre-hospital epidemiology and management of spinal cord injuries in New South Wales: 2004-2008. *Injury*. doi:10.1016/j.injury.2011.12.010.
- Migliati, E., Meurice, N., DuBois, P., et al. (2009) Inhibition of aquaporin-1 and aquaporin-4 water permeability by a derivative of the loop diuretic bumetanide acting at an internal pore-occluding binding site. *Molecular Pharmacology*. doi:10.1124/mol.108.053744.
- Minnema, A.J., Mehta, A., Boling, W.W., et al. (2019) SCING - Spinal Cord Injury Neuroprotection with Glyburide: A pilot, open-label, multicentre, prospective evaluation of oral glyburide in patients with acute traumatic spinal cord injury in the USA. *BMJ Open*. doi:10.1136/bmjopen-2019-031329.

- Misawa, T., Arima, K., Mizusawa, H., et al. (2008) Close association of water channel AQP1 with amyloid-beta deposition in Alzheimer disease brains. *Acta neuropathologica*, 116 (3): 247–60. doi:10.1007/s00401-008-0387-x.
- Miyanji, F., Furlan, J.C., Aarabi, B., et al. (2007) Acute Cervical Traumatic Spinal Cord Injury: MR Imaging Findings Correlated with Neurologic Outcome—Prospective Study with 100 Consecutive Patients 1. *Radiology*, 243 (3): 820–827. doi:10.1148/radiol.2433060583.
- Moeller, H.B., Fenton, R.A., Zeuthen, T., et al. (2009) Vasopressin-dependent short-term regulation of aquaporin 4 expressed in *Xenopus* oocytes. *Neuroscience*, 164 (4): 1674–1684. doi:10.1016/j.neuroscience.2009.09.072.
- Mokgokong, R., Wang, S., Taylor, C.J., et al. (2014) Ion transporters in brain endothelial cells that contribute to formation of brain interstitial fluid. *Pflügers Archiv European Journal of Physiology*. doi:10.1007/s00424-013-1342-9.
- Mola, M.G., Sparaneo, A., Gargano, C.D., et al. (2016) The speed of swelling kinetics modulates cell volume regulation and calcium signaling in astrocytes: A different point of view on the role of aquaporins. *GLIA*, 64 (1): 139–154. doi:10.1002/glia.22921.
- Morest, D.K. and Silver, J. (2003) Precursors of neurons, neuroglia, and ependymal cells in the CNS: What are they? Where are they from? How do they get where they are going? *GLIA*, 43 (1): 6–18. doi:10.1002/glia.10238.
- Murata, K., Mitsuoka, K., Hirai, T., et al. (2000) Structural determinants of water permeation through aquaporin-1. *Nature*, 407 (6804): 599–605. doi:10.1038/35036519.
- Nagelhus, E.A. and Ottersen, O.P. (2013) Physiological roles of Aquaporin-4 in brain. *Physiological Reviews*. doi:10.1152/physrev.00011.2013.
- Nagoshi, N., Tsuji, O., Kitamura, K., et al. (2020) Phase I/II Study of Intrathecal Administration of Recombinant Human Hepatocyte Growth Factor in Patients with Acute Spinal Cord Injury: A Double-Blind, Randomized Clinical Trial of Safety and Efficacy. *Journal of Neurotrauma*.

doi:10.1089/neu.2019.6854.

Nakase, T., Söhl, G., Theis, M., et al. (2004) Increased apoptosis and inflammation after focal brain ischemia in mice lacking connexin43 in astrocytes. *American Journal of Pathology*. doi:10.1016/S0002-9440(10)63765-0.

Nave, K.A. and Werner, H.B. (2014) Myelination of the nervous system: mechanisms and functions. *Annual review of cell and developmental biology*. doi:10.1146/annurev-cellbio-100913-013101.

Neely, J.D., Amiry-Moghaddam, M., Ottersen, O.P., et al. (2001) Syntrophin-dependent expression and localization of Aquaporin-4 water channel protein. *Proceedings of the National Academy of Sciences*, 98 (24): 14108–14113. doi:10.1073/pnas.241508198.

Nejsum, L.N., Kwon, T.-H., Jensen, U.B., et al. (2002) Functional requirement of aquaporin-5 in plasma membranes of sweat glands. *Proceedings of the National Academy of Sciences of the United States of America*, 99 (1): 511–6. doi:10.1073/pnas.012588099.

Nesathurai, S., Graham, W.A., Mansfield, K., et al. (2006) Model of traumatic spinal cord injury in *Macaca fascicularis*: Similarity of experimental lesions created by epidural catheter to human spinal cord injury. *Journal of Medical Primatology*. doi:10.1111/j.1600-0684.2006.00162.x.

Nesic, O., Guest, J.D., Zivadinovic, D., et al. (2010) Aquaporins in spinal cord injury: the janus face of aquaporin 4. *Neuroscience*, 168 (4): 1019–1035. doi:10.1016/J.NEUROSCIENCE.2010.01.037.

Nesic, O., Lee, J., Ye, Z., et al. (2006) Acute and chronic changes in aquaporin 4 expression after spinal cord injury. *Neuroscience*, 143 (3): 779–792. doi:10.1016/j.neuroscience.2006.08.079.

NHS England (2020) *Statistical Note: Ambulance Quality Indicators (AQI)*.

Nicchia, G.P., Rossi, A., Mola, M.G., et al. (2008) Actin cytoskeleton remodeling governs

aquaporin-4 localization in astrocytes. *GLIA*. doi:10.1002/glia.20724.

Nielsen, S., DiGiovanni, S.R., Christensen, E.I., et al. (1993) Cellular and subcellular immunolocalization of vasopressin-regulated water channel in rat kidney. *Proceedings of the National Academy of Sciences of the United States of America*, 90 (24): 11663–11667. doi:8265605.

Nielsen, S., Nagelhus, E.A., Amiry-Moghaddam, M., et al. (1997) Specialized membrane domains for water transport in glial cells: high-resolution immunogold cytochemistry of aquaporin-4 in rat brain. *The Journal of Neuroscience*, 17 (1): 171–180. Available at: <http://www.ncbi.nlm.nih.gov/pubmed/8987746>.

Noble, L.J. and Wrathall, J.R. (1989) Distribution and time course of protein extravasation in the rat spinal cord after contusive injury. *Brain research*, 482 (1): 57–66. Available at: <http://www.ncbi.nlm.nih.gov/pubmed/2706482> (Accessed: 18 May 2018).

Nobuyuki, O. (1979) A Threshold Selection Method from Gray-Level Histograms. *IEEE Transactions on Systems, Man, and Cybernetics*. doi:10.1109/TSMC.1979.4310076.

Noda, Y. and Sasaki, S. (2005) Trafficking mechanism of water channel aquaporin-2. *Biology of the Cell*, 97 (12): 885–892. doi:10.1042/BC20040120.

Noell, S., Fallier-Becker, P., Beyer, C., et al. (2007) Effects of agrin on the expression and distribution of the water channel protein aquaporin-4 and volume regulation in cultured astrocytes. *European Journal of Neuroscience*, 26 (8): 2109–2118. doi:10.1111/j.1460-9568.2007.05850.x.

Noell, S., Fallier-Becker, P., Deutsch, U., et al. (2009) Agrin defines polarized distribution of orthogonal arrays of particles in astrocytes. *Cell and Tissue Research*. doi:10.1007/s00441-009-0812-z.

Nógrádi, A. and Vrbová, G. (2007) “Anatomy and Physiology of the Spinal Cord.” In *Transplantation of Neural Tissue into the Spinal Cord*. doi:10.1007/0-387-32633-2_1.

Novy, J. (2006) Spinal Cord Ischemia. *Arch Neurol*, 63.

Nyúl-Tóth, Á., Suciú, M., Molnár, J., et al. (2016) Differences in the molecular structure of the blood-brain barrier in the cerebral cortex and white matter: An in silico, in vitro, and ex vivo study. *American Journal of Physiology - Heart and Circulatory Physiology*. doi:10.1152/ajpheart.00774.2015.

Oklinski, M.K., Lim, J.S., Choi, H.J., et al. (2014) Immunolocalization of Water Channel Proteins AQP1 and AQP4 in Rat Spinal Cord. *Journal of Histochemistry and Cytochemistry*, 62 (8): 598–611. doi:10.1369/0022155414537495.

Oliet, S.H.R., Piet, R. and Poulain, D.A. (2001) Control of glutamate clearance and synaptic efficacy by glial coverage of neurons. *Science*. doi:10.1126/science.1059162.

Oliva, A.A., Kang, Y., Truettner, J.S., et al. (2011) Fluid-percussion brain injury induces changes in aquaporin channel expression. *Neuroscience*. doi:10.1016/j.neuroscience.2011.02.020.

Oshio, K. (2004) Reduced cerebrospinal fluid production and intracranial pressure in mice lacking choroid plexus water channel Aquaporin-1. *The FASEB Journal*. doi:10.1096/fj.04-1711fje.

Oshio, K., Binder, D.K., Liang, Y., et al. (2005) Expression of the aquaporin-1 water channel in human glial tumors. *Neurosurgery*. doi:10.1227/01.NEU.0000148904.57841.6B.

Oshio, K., Binder, D.K., Yang, B., et al. (2004) Expression of aquaporin water channels in mouse spinal cord. *Neuroscience*, 127 (3): 685–693. doi:10.1016/j.neuroscience.2004.03.016.

Oster, G.F. and Perelson, A.S. (1987) The physics of cell motility. *Journal of Cell Science*. doi:10.1242/jcs.1987.supplement_8.3.

Owens, G.P., Ritchie, A., Rossi, A., et al. (2015) Mutagenesis of the aquaporin 4 extracellular domains defines restricted binding patterns of pathogenic neuromyelitis optica IgG. *Journal of*

Biological Chemistry. doi:10.1074/jbc.M115.647149.

Pan, C.F., Zhu, S.M. and Zheng, Y.Y. (2010) Ammonia induces upregulation of aquaporin-4 in neocortical astrocytes of rats through the p38 mitogen-activated protein kinase pathway. *Chinese Medical Journal*. doi:10.3760/cma.j.issn.0366-6999.2010.14.011.

Papadopoulos, M.C. and Saadoun, S. (2015) Key roles of aquaporins in tumor biology. *Biochimica et Biophysica Acta - Biomembranes*. doi:10.1016/j.bbamem.2014.09.001.

Park, H.C., Shim, Y.S., Ha, Y., et al. (2005) Treatment of complete spinal cord injury patients by autologous bone marrow cell transplantation and administration of granulocyte-macrophage colony stimulating factor. *Tissue Engineering*. doi:10.1089/ten.2005.11.913.

Parker, A.J., Park, R.D. and Stowater, J.L. (1973) Reduction of trauma induced edema of spinal cord in dogs given mannitol. *American Journal of Veterinary Research*.

Pineau, I. and Lacroix, S. (2007) Proinflammatory cytokine synthesis in the injured mouse spinal cord: multiphasic expression pattern and identification of the cell types involved. *The Journal of comparative neurology*, 500 (2): 267–85. doi:10.1002/cne.21149.

Pirici, I., Balsanu, T.A., Bogdan, C., et al. (2018) Inhibition of aquaporin-4 improves the outcome of ischaemic stroke and modulates brain paravascular drainage pathways. *International Journal of Molecular Sciences*. doi:10.3390/ijms19010046.

Pitts, L.H., Ross, A., Chase, G.A., et al. (1995) Treatment with Thyrotropin-Releasing Hormone (TRH) in Patients with Traumatic Spinal Cord Injuries. *Journal of Neurotrauma*. doi:10.1089/neu.1995.12.235.

Plemel, J.R., Duncan, G., Chen, K.W.K., et al. (2008) A graded forceps crush spinal cord injury model in mice. *Journal of Neurotrauma*. doi:10.1089/neu.2007.0426.

Pointillart, V., Petitjean, M., Wiart, L., et al. (2000) Pharmacological therapy of spinal cord injury during the acute phase. *Spinal Cord*. doi:10.1038/sj.sc.3100962.

- Polak, K.A., Edelman, A.M., Wasley, J.W.F., et al. (1991) A novel calmodulin antagonist, CGS 9343B, modulates calcium-dependent changes in neurite outgrowth and growth cone movements. *Journal of Neuroscience*. doi:10.1523/jneurosci.11-02-00534.1991.
- Poon, P.C., Gupta, D., Shoichet, M.S., et al. (2007) Clip compression model is useful for thoracic spinal cord injuries: Histologic and functional correlates. *Spine*. doi:10.1097/BRS.0b013e31815b7e6b.
- Popovich, P.G., Lemeshow, S., Gensel, J.C., et al. (2012) Independent evaluation of the effects of glibenclamide on reducing progressive hemorrhagic necrosis after cervical spinal cord injury. *Experimental Neurology*. doi:10.1016/j.expneurol.2010.11.016.
- Post, M.W.M. and van Leeuwen, C.M.C. (2012) Psychosocial issues in spinal cord injury: a review. *Spinal Cord*, 50 (5): 382–389. doi:10.1038/sc.2011.182.
- Potokar, M., Stenovc, M., Jorgačevski, J., et al. (2013) Regulation of AQP4 surface expression via vesicle mobility in astrocytes. *GLIA*. doi:10.1002/glia.22485.
- Pottorf, W.J., Johanns, T.M., Derrington, S.M., et al. (2006) Glutamate-induced protease-mediated loss of plasma membrane Ca²⁺ pump activity in rat hippocampal neurons. *Journal of Neurochemistry*, 98 (5): 1646–1656. doi:10.1111/j.1471-4159.2006.04063.x.
- Praetorius, J. and Nielsen, S. (2006) Distribution of sodium transporters and aquaporin-1 in the human choroid plexus. *American journal of physiology. Cell physiology*, 291 (1): C59–C67. doi:10.1152/ajpcell.00433.2005.
- Preston, G.M., Carroll, T.P., Guggino, W.B., et al. (1992) Appearance of Water Channels in *Xenopus* Oocytes Expressing Red Cell CHIP28 Protein. *Science*, 256 (5055): 385–387. doi:10.1126/science.256.5055.385.
- Preston, G.M., Jung, J.S., Guggino, W.B., et al. (1993) The mercury-sensitive residue at cysteine 189 in the CHIP28 water channel. *Journal of Biological Chemistry*, 268 (1): 17–20.
- Qiu, G.P., Xu, J., Zhuo, F., et al. (2015) Loss of AQP4 polarized localization with loss of β -

dystroglycan immunoreactivity may induce brain edema following intracerebral hemorrhage. *Neuroscience Letters*. doi:10.1016/j.neulet.2014.12.053.

Rabchevsky, A.G., Fugaccia, I., Turner, A.F., et al. (2000) Basic fibroblast growth factor (bFGF) enhances functional recovery following severe spinal cord injury to the rat. *Experimental Neurology*. doi:10.1006/exnr.2000.7399.

Rabin, S.J., Bachis, A. and Mocchetti, I. (2002) Gangliosides activate Trk receptors by inducing the release of neurotrophins. *Journal of Biological Chemistry*. doi:10.1074/jbc.M203240200.

Raivich, G. (2005) Like cops on the beat: The active role of resting microglia. *Trends in Neurosciences*. doi:10.1016/j.tins.2005.09.001.

Ransohoff, R.M. and Engelhardt, B. (2012) The anatomical and cellular basis of immune surveillance in the central nervous system. *Nature Reviews Immunology*. doi:10.1038/nri3265.

Rash, J.E., Yasumura, T., Hudson, C.S., et al. (1998) Direct immunogold labeling of aquaporin-4 in square arrays of astrocyte and ependymocyte plasma membranes in rat brain and spinal cord. *Proceedings of the National Academy of Sciences of the United States of America*, 95 (20): 11981–11986. doi:10.1073/pnas.95.20.11981.

Ren, Z., Iliff, J.J., Yang, L., et al. (2013) “Hit & Run” model of closed-skull traumatic brain injury (TBI) reveals complex patterns of post-traumatic AQP4 dysregulation. *Journal of Cerebral Blood Flow and Metabolism*. doi:10.1038/jcbfm.2013.30.

Rennels, M.L., Gregory, T.F., Blaumanis, O.R., et al. (1985) Evidence for a “Paravascular” fluid circulation in the mammalian central nervous system, provided by the rapid distribution of tracer protein throughout the brain from the subarachnoid space. *Brain Research*. doi:10.1016/0006-8993(85)91383-6.

Rhodes, K.E., Moon, L.D.F. and Fawcett, J.W. (2003) Inhibiting cell proliferation during formation of the glial scar: Effects on axon regeneration in the CNS. *Neuroscience*.

doi:10.1016/S0306-4522(03)00285-9.

Ringstad, G., Vatnehol, S.A.S. and Eide, P.K. (2017) Glymphatic MRI in idiopathic normal pressure hydrocephalus. *Brain*. doi:10.1093/brain/awx191.

Rivlin, A.S. and Tator, C.H. (1978) Effect of duration of acute spinal cord compression in a new acute cord injury model in the rat. *Surgical neurology*, 10 (1): 38–43. Available at: <http://www.ncbi.nlm.nih.gov/pubmed/684604>.

Rong, H., Liu, Y., Zhao, Z., et al. (2018) Further standardization in the aneurysm clip: The effects of occlusal depth on the outcome of spinal cord injury in rats. *Spine*. doi:10.1097/BRS.0000000000002279.

Ropper, A.H. (2012) Hyperosmolar Therapy for Raised Intracranial Pressure. *New England Journal of Medicine*, 367 (8): 746–752. doi:10.1056/NEJMct1206321.

Rosenblum, W.I. (2007) Cytotoxic edema: Monitoring its magnitude and contribution to brain swelling. *Journal of Neuropathology and Experimental Neurology*. doi:10.1097/nen.0b013e3181461965.

Ross, I.B. and Tator, C.H. (1991) Further Studies of Nimodipine in Experimental Spinal Cord Injury in the Rat. *Journal of Neurotrauma*. doi:10.1089/neu.1991.8.229.

Rossi, A., Ratelade, J., Papadopoulos, M.C., et al. (2012) Neuromyelitis optica IgG does not alter aquaporin-4 water permeability, plasma membrane M1/M23 isoform content, or supramolecular assembly. *GLIA*. doi:10.1002/glia.22417.

Rungta, R.L., Choi, H.B., Tyson, J.R., et al. (2015) The cellular mechanisms of neuronal swelling underlying cytotoxic edema. *Cell*, 161 (3): 610–621. doi:10.1016/j.cell.2015.03.029.

Saadoun, S. (2005) Involvement of aquaporin-4 in astroglial cell migration and glial scar formation. *Journal of Cell Science*, 118 (24): 5691–5698. doi:10.1242/jcs.02680.

Saadoun, S., Bell, B.A., Verkman, A.S., et al. (2008) Greatly improved neurological outcome

after spinal cord compression injury in AQP4-deficient mice. *Brain*, 131 (4): 1087–1098. doi:10.1093/brain/awn014.

Saadoun, S., Papadopoulos, M.C., Davies, D.C., et al. (2002) Increased aquaporin 1 water channel expression in human brain tumours. *British Journal of Cancer*, 87 (6): 621–623. doi:10.1038/sj.bjc.6600512.

Saadoun, S., Papadopoulos, M.C., Hara-Chikuma, M., et al. (2005) Impairment of angiogenesis and cell migration by targeted aquaporin-1 gene disruption. *Nature*. doi:10.1038/nature03460.

Saberi, H., Derakhshanrad, N. and Yekaninejad, M.S. (2014) Comparison of Neurological and Functional outcomes after Administration of Granulocyte-Colony-Stimulating Factor in Motor-Complete versus Motor-Incomplete Postrehabilitated, Chronic Spinal Cord Injuries: A Phase I/II Study. *Cell Transplantation*. doi:10.3727/096368914x684943.

Sakuma, T., Yamazaki, M., Okawa, A., et al. (2012a) Neuroprotective therapy using granulocyte colony-stimulating factor for patients with worsening symptoms of compression myelopathy, part 1: A phase i and Ila clinical trial. *European Spine Journal*. doi:10.1007/s00586-011-2020-2.

Sakuma, T., Yamazaki, M., Okawa, A., et al. (2012b) Neuroprotective therapy using granulocyte colony-stimulating factor for patients with worsening symptoms of thoracic myelopathy: A multicenter prospective controlled trial. *Spine*. doi:10.1097/BRS.0b013e318260cc71.

Salman, M.M., Kitchen, P., Woodroffe, M.N., et al. (2017) Hypothermia increases aquaporin 4 (AQP4) plasma membrane abundance in human primary cortical astrocytes via a calcium/transient receptor potential vanilloid 4 (TRPV4)- and calmodulin-mediated mechanism. *European Journal of Neuroscience*, 46 (9): 2542–2547. doi:10.1111/ejn.13723.

Savage, D.F., Egea, P.F., Robles-Colmenares, Y., et al. (2003) Architecture and selectivity in

aquaporins: 2.5 Å X-ray structure of aquaporin Z. *PLoS Biology*, 1 (3). doi:10.1371/journal.pbio.0000072.

Schousboe, A., Bak, L.K. and Waagepetersen, H.S. (2013) Astrocytic control of biosynthesis and turnover of the neurotransmitters glutamate and GABA. *Frontiers in Endocrinology*. doi:10.3389/fendo.2013.00102.

Schwab, J.M., Zhang, Y., Kopp, M.A., et al. (2014) The paradox of chronic neuroinflammation, systemic immune suppression, autoimmunity after traumatic chronic spinal cord injury. *Experimental Neurology*. 258 pp. 121–129. doi:10.1016/j.expneurol.2014.04.023.

Seeman, P. (2002) Atypical antipsychotics: Mechanism of action. *Canadian Journal of Psychiatry*.

Sharif-Alhoseini, M., Khormali, M., Rezaei, M., et al. (2017) Animal models of spinal cord injury: A systematic review. *Spinal Cord*. doi:10.1038/sc.2016.187.

Sharma, H. (2005) Pathophysiology of Blood-Spinal Cord Barrier in Traumatic Injury and Repair. *Current Pharmaceutical Design*. doi:10.2174/1381612053507837.

Sherman, S.P. and Bang, A.G. (2018) High-throughput screen for compounds that modulate neurite growth of human induced pluripotent stem cell-derived neurons. *DMM Disease Models and Mechanisms*. doi:10.1242/dmm.031906.

Shields, D.C., Schaefer, K.E., Hogan, E.L., et al. (2000) Calpain activity and expression increased in activated glial and inflammatory cells in penumbra of spinal cord injury lesion. *Journal of Neuroscience Research*, 61 (2): 146–150. doi:10.1002/1097-4547(20000715)61:2<146::AID-JNR5>3.0.CO;2-C.

Simard, J.M., Tsybalyuk, O., Keledjian, K., et al. (2012) Comparative effects of glibenclamide and riluzole in a rat model of severe cervical spinal cord injury. *Experimental Neurology*. doi:10.1016/j.expneurol.2011.11.044.

Simard, M. and Nedergaard, M. (2004) The neurobiology of glia in the context of water and

ion homeostasis. *Neuroscience*. doi:10.1016/j.neuroscience.2004.09.053.

Skaper, S.D. and Leon, A. (1992) Monosialogangliosides, neuroprotection, and neuronal repair processes. *Journal of Neurotrauma*.

Smith, A.J., Jin, B.J., Ratelade, J., et al. (2014) Aggregation state determines the localization and function of M1- and M23-aquaporin-4 in astrocytes. *Journal of Cell Biology*, 204 (4): 559–573. doi:10.1083/jcb.201308118.

Smith, A.J. and Verkman, A.S. (2015) Superresolution Imaging of Aquaporin-4 Cluster Size in Antibody-Stained Paraffin Brain Sections. *Biophysical Journal*, 109 (12): 2511–2522. doi:10.1016/j.bpj.2015.10.047.

Soderblom, C., Luo, X., Blumenthal, E., et al. (2013) Perivascular fibroblasts form the fibrotic scar after contusive spinal cord injury. *Journal of Neuroscience*. doi:10.1523/JNEUROSCI.2524-13.2013.

Sofroniew, M. V. (2009) Molecular dissection of reactive astrogliosis and glial scar formation. *Trends in Neurosciences*. doi:10.1016/j.tins.2009.08.002.

Sofroniew, M. V. (2014) Multiple roles for astrocytes as effectors of cytokines and inflammatory mediators. *Neuroscientist*. doi:10.1177/1073858413504466.

Sofroniew, M. V. (2015) Astrogliosis. *Cold Spring Harbor Perspectives in Biology*. doi:10.1101/cshperspect.a020420.

Solenov, E. (2004) Sevenfold-reduced osmotic water permeability in primary astrocyte cultures from AQP-4-deficient mice, measured by a fluorescence quenching method. *AJP: Cell Physiology*, 286 (2): 426C – 432. doi:10.1152/ajpcell.00298.2003.

Song, Y. and Gunnarson, E. (2012) Potassium Dependent Regulation of Astrocyte Water Permeability Is Mediated by cAMP Signaling Barnes, S. (ed.). *PLoS ONE*, 7 (4): e34936. doi:10.1371/journal.pone.0034936.

Stirling, D.P., Khodarahmi, K., Liu, J., et al. (2004) Minocycline Treatment Reduces Delayed Oligodendrocyte Death, Attenuates Axonal Dieback, and Improves Functional Outcome after Spinal Cord Injury. *Journal of Neuroscience*. doi:10.1523/JNEUROSCI.5275-03.2004.

Stokum, J.A., Gerzanich, V., Sheth, K.N., et al. (2020) Emerging pharmacological treatments for cerebral edema: Evidence from clinical studies. *Annual Review of Pharmacology and Toxicology*. doi:10.1146/annurev-pharmtox-010919-023429.

Stokum, J.A., Mehta, R.I., Ivanova, S., et al. (2015) Heterogeneity of aquaporin-4 localization and expression after focal cerebral ischemia underlies differences in white versus grey matter swelling. *Acta neuropathologica communications*. doi:10.1186/s40478-015-0239-6.

Streijger, F., Lee, J.H.T., Manouchehri, N., et al. (2016) The Evaluation of Magnesium Chloride within a Polyethylene Glycol Formulation in a Porcine Model of Acute Spinal Cord Injury. *Journal of Neurotrauma*. doi:10.1089/neu.2016.4439.

Sturdivant, N.M., Smith, S.G., Ali, S.F., et al. (2016) Acetazolamide Mitigates Astrocyte Cellular Edema Following Mild Traumatic Brain Injury. *Scientific Reports*. doi:10.1038/srep33330.

Su, Y.F., Lin, C.L., Lee, K.S., et al. (2015) A modified compression model of spinal cord injury in rats: Functional assessment and the expression of nitric oxide synthases. *Spinal Cord*. doi:10.1038/sc.2014.245.

Sun, D. and Jakobs, T.C. (2012) Structural remodeling of astrocytes in the injured CNS. *Neuroscientist*. doi:10.1177/1073858411423441.

Sun, L., Li, M., Ma, X., et al. (2017) Inhibition of HMGB1 reduces rat spinal cord astrocytic swelling and AQP4 expression after oxygen-glucose deprivation and reoxygenation via TLR4 and NF-KB signaling in an IL-6-dependent manner. *Journal of Neuroinflammation*, 14 (1). doi:10.1186/s12974-017-1008-1.

Sun, P., Bu, F., Min, J.W., et al. (2019) Inhibition of calcium/calmodulin-dependent protein

kinase kinase (CaMKK) exacerbates impairment of endothelial cell and blood–brain barrier after stroke. *European Journal of Neuroscience*. doi:10.1111/ejn.14223.

Sung, J.K., Miao, L., Calvert, J.W., et al. (2003) A possible role of RhoA/Rho-kinase in experimental spinal cord injury in rat. *Brain Research*. doi:10.1016/S0006-8993(02)03717-4.

Surey, S., Berry, M., Logan, A., et al. (2014) Differential cavitation, angiogenesis and wound-healing responses in injured mouse and rat spinal cords. *Neuroscience*. doi:10.1016/j.neuroscience.2014.06.003.

Suzuki, H., Ahuja, C.S., Salewski, R.P., et al. (2017) Neural stem cell mediated recovery is enhanced by Chondroitinase ABC pretreatment in chronic cervical spinal cord injury. *PLoS ONE*. doi:10.1371/journal.pone.0182339.

Sweeney, A.M., Plá, V., Du, T., et al. (2019) In Vivo Imaging of Cerebrospinal Fluid Transport through the Intact Mouse Skull using Fluorescence Macroscopy. *Journal of visualized experiments: JoVE*. doi:10.3791/59774.

Taoka, T., Jost, G., Frenzel, T., et al. (2018) Impact of the Glymphatic System on the Kinetic and Distribution of Gadodiamide in the Rat Brain: Observations by Dynamic MRI and Effect of Circadian Rhythm on Tissue Gadolinium Concentrations. *Investigative Radiology*. doi:10.1097/RLI.0000000000000473.

Tator, C.H. and Fehlings, M.G. (1991) Review of the secondary injury theory of acute spinal cord trauma with emphasis on vascular mechanisms. *Journal of Neurosurgery*, 75 (1): 15–26. doi:10.3171/jns.1991.75.1.0015.

Tator, C.H. and Koyanagi, I. (1997) Vascular mechanisms in the pathophysiology of human spinal cord injury. *Journal of Neurosurgery*, 86 (3): 483–492. doi:10.3171/jns.1997.86.3.0483.

TCW, J., Wang, M., Pimenova, A.A., et al. (2017) An Efficient Platform for Astrocyte Differentiation from Human Induced Pluripotent Stem Cells. *Stem Cell Reports*. doi:10.1016/j.stemcr.2017.06.018.

Teeter, L., Gassaway, J., Taylor, S., et al. (2012) Relationship of physical therapy inpatient rehabilitation interventions and patient characteristics to outcomes following spinal cord injury: The SCIRehab project. *Journal of Spinal Cord Medicine*. doi:10.1179/2045772312Y.0000000058.

Teng, Y.D., Choi, H., Onario, R.C., et al. (2004) Minocycline inhibits contusion-triggered mitochondrial cytochrome c release and mitigates functional deficits after spinal cord injury. *Proceedings of the National Academy of Sciences of the United States of America*. doi:10.1073/pnas.0306239101.

Tham, D.K.L., Joshi, B. and Moukhles, H. (2016) Aquaporin-4 cell-surface expression and turnover are regulated by dystroglycan, dynamin, and the extracellular matrix in astrocytes. *PLoS ONE*. doi:10.1371/journal.pone.0165439.

Thomas, D., Bron, P., Ranchy, G., et al. (2002) Aquaglyceroporins, one channel for two molecules. *Biochimica et Biophysica Acta - Bioenergetics*, 1555 (1–3): 181–186. doi:10.1016/S0005-2728(02)00275-X.

Thrane, A.S., Rappold, P.M., Fujita, T., et al. (2011) Critical role of aquaporin-4 (AQP4) in astrocytic Ca²⁺ signaling events elicited by cerebral edema. *Proceedings of the National Academy of Sciences*, 108 (2): 846–851. doi:10.1073/pnas.1015217108.

Tome-Garcia, J., Erfani, P., Nudelman, G., et al. (2018) Analysis of chromatin accessibility uncovers TEAD1 as a regulator of migration in human glioblastoma. *Nature Communications*. doi:10.1038/s41467-018-06258-2.

Törnroth-Horsefield, S., Wang, Y., Hedfalk, K., et al. (2006) Structural mechanism of plant aquaporin gating. *Nature*, 439 (7077): 688–694. doi:10.1038/nature04316.

Totoiu, M.O. and Keirstead, H.S. (2005) Spinal cord injury is accompanied by chronic progressive demyelination. *Journal of Comparative Neurology*, 486 (4): 373–383. doi:10.1002/cne.20517.

- TwoRoger, S.S., Lee, S., Schernhammer, E.S., et al. (2006) The association of self-reported sleep duration, difficulty sleeping, and snoring with cognitive function in older women. *Alzheimer Disease and Associated Disorders*. doi:10.1097/01.wad.0000201850.52707.80.
- Uldall, M., Bhatt, D.K., Kruuse, C., et al. (2017) Choroid plexus aquaporin 1 and intracranial pressure are increased in obese rats: Towards an idiopathic intracranial hypertension model? *International Journal of Obesity*, 41 (7): 1141–1147. doi:10.1038/ijo.2017.83.
- Umenishi, F. and Schrier, R.W. (2002) Identification and characterization of a novel hypertonicity-responsive element in the human aquaporin-1 gene. *Biochemical and Biophysical Research Communications*, 292 (3): 771–775. doi:10.1006/bbrc.2002.6709.
- Underhill, S.M., Wheeler, D.S. and Amara, S.G. (2015) Differential regulation of two isoforms of the glial glutamate transporter EAAT2 by DLG1 and CaMKII. *Journal of Neuroscience*. doi:10.1523/JNEUROSCI.4365-14.2015.
- Vanický, I., Urdzík, L., Saganová, K., et al. (2001) A simple and reproducible model of spinal cord injury induced by epidural balloon inflation in the rat. *Journal of Neurotrauma*. doi:10.1089/08977150152725687.
- Verbavatz, J.M., Ma, T., Gobin, R., et al. (1997) Absence of orthogonal arrays in kidney, brain and muscle from transgenic knockout mice lacking water channel aquaporin-4. *Journal of cell science*, 110 (Pt 2: 2855–60. Available at: <http://www.ncbi.nlm.nih.gov/pubmed/9427293>.
- Verkhatsky, A. and Nedergaard, M. (2018) Physiology of astroglia. *Physiological Reviews*. doi:10.1152/physrev.00042.2016.
- Verkman, A.A.S. and Mitra, A.K.A.K. (2000) Structure and function of aquaporin water channels. *American Journal of Physiology- Renal Physiology*, 278 (1): 13. doi:10.2528/pier13111003.
- Verkman, A.S., Binder, D.K., Bloch, O., et al. (2006) Three distinct roles of aquaporin-4 in brain function revealed by knockout mice. *Biochimica et Biophysica Acta - Biomembranes*.

1758 (8) pp. 1085–1093. doi:10.1016/j.bbamem.2006.02.018.

Verkman, A.S., Smith, A.J., Phuan, P. wah, et al. (2017) The aquaporin-4 water channel as a potential drug target in neurological disorders. *Expert Opinion on Therapeutic Targets*. doi:10.1080/14728222.2017.1398236.

Vitellaro-Zuccarello, L., Mazzetti, S., Bosisio, P., et al. (2005) Distribution of aquaporin 4 in rodent spinal cord: Relationship with astrocyte markers and chondroitin sulfate proteoglycans. *GLIA*, 51 (2): 148–159. doi:10.1002/glia.20196.

Wagner, F.B., Mignardot, J.B., Le Goff-Mignardot, C.G., et al. (2018) Targeted neurotechnology restores walking in humans with spinal cord injury. *Nature*. doi:10.1038/s41586-018-0649-2.

Walz, T., Fujiyoshi, Y. and Engel, A. (2009) The AQP structure and functional implications. *Handbook of experimental pharmacology*, (190): 31–56. doi:10.1007/978-3-540-79885-9_2.

Wang, H.L. and Lai, T.W. (2014) Optimization of Evans blue quantitation in limited rat tissue samples. *Scientific Reports*. doi:10.1038/srep06588.

Wang, K., Bekar, L.K., Furber, K., et al. (2004) Vimentin-expressing proximal reactive astrocytes correlate with migration rather than proliferation following focal brain injury. *Brain Research*. doi:10.1016/j.brainres.2004.07.086.

Wang, X., Yigitkanli, K., Kim, C.Y., et al. (2014) Human NgR-Fc decoy protein via lumbar intrathecal bolus administration enhances recovery from rat spinal cord contusion. *Journal of Neurotrauma*. doi:10.1089/neu.2014.3355.

Wang, X., Zhou, T., Maynard, G.D., et al. (2020) Nogo receptor decoy promotes recovery and corticospinal growth in non-human primate spinal cord injury. *Brain*. doi:10.1093/brain/awaa116.

Wang, Y., Schulten, K. and Tajkhorshid, E. (2005) What makes an aquaporin a glycerol channel? A comparative study of AqpZ and GlpF. *Structure*, 13 (8): 1107–1118.

doi:10.1016/j.str.2005.05.005.

Wanner, I.B., Anderson, M.A., Song, B., et al. (2013) Glial scar borders are formed by newly proliferated, elongated astrocytes that interact to corral inflammatory and fibrotic cells via STAT3-dependent mechanisms after spinal cord injury. *Journal of Neuroscience*. doi:10.1523/JNEUROSCI.2121-13.2013.

Warms, C. a, Turner, J. a, Marshall, H.M., et al. (2002) Treatments for chronic pain associated with spinal cord injuries: many are tried, few are helpful. *The Clinical journal of pain*, 18 (3): 154–163. doi:10.1097/00002508-200205000-00004.

Warth, A., Simon, P., Capper, D., et al. (2007) Expression pattern of the water channel aquaporin-4 in human gliomas is associated with blood-brain barrier disturbance but not with patient survival. *Journal of Neuroscience Research*. doi:10.1002/jnr.21224.

Watson, C. and Harrison, M. (2012) The Location of the Major Ascending and Descending Spinal Cord Tracts in all Spinal Cord Segments in the Mouse: Actual and Extrapolated. *Anatomical Record*. doi:10.1002/ar.22549.

Watson, C. and Kayalioglu, G. (2009) "The Organization of the Spinal Cord." In *The Spinal Cord*. doi:10.1016/B978-0-12-374247-6.50005-5.

Weber, J.T. (2012) Altered calcium signaling following traumatic brain injury. *Frontiers in Pharmacology*, 3 APR. doi:10.3389/fphar.2012.00060.

Whiteneck, G., Gassaway, J., Dijkers, M.P., et al. (2012) Relationship of patient characteristics and rehabilitation services to outcomes following spinal cord injury: The SCIR rehab Project. *Journal of Spinal Cord Medicine*. doi:10.1179/2045772312Y.0000000057.

Wiedemann, C. (2010) Neuron-glia interactions: With a little help from glia. *Nature Reviews Neuroscience*, 11 (3): 152–153. doi:10.1038/nrn2818.

Wintmo, P., Johansen, S.H., Hansen, P.B.L., et al. (2017) The water channel AQP1 is expressed in human atherosclerotic vascular lesions and AQP1 deficiency augments

angiotensin II-induced atherosclerosis in mice. *Acta Physiologica*. doi:10.1111/apha.12853.

Wiseman, D.B., Dailey, A.T., Lundin, D.D., et al. (2009) Magnesium efficacy in a rat spinal cord injury model: Laboratory investigation. *Journal of Neurosurgery: Spine*. doi:10.3171/spi.2009.10.4.308.

Wolburg, H., Noell, S., Wolburg-Buchholz, K., et al. (2009) Agrin, aquaporin-4, and astrocyte polarity as an important feature of the blood-brain barrier. *Neuroscientist*, 15 (2): 180–193. doi:10.1177/1073858408329509.

Wolfes, A.C. and Dean, C. (2018) Culturing in vivo-like murine astrocytes using the fast, simple, and inexpensive awesam protocol. *Journal of Visualized Experiments*. doi:10.3791/56092.

World Health Organization (2013) Spinal Cord Injury. *Media Centre, Fact Sheets n°384*, 33 (December 1990): 798–807. doi:10.1016/B978-0-12-385942-6.00062-7.

Wu, J.C., Huang, W.C., Chen, Y.C., et al. (2011) Acidic fibroblast growth factor for repair of human spinal cord injury: A clinical trial - Clinical article. *Journal of Neurosurgery: Spine*. doi:10.3171/2011.4.SPINE10404.

Wu, J.C., Huang, W.C., Tsai, Y.A., et al. (2008) Nerve repair using acidic fibroblast growth factor in human cervical spinal cord injury: A preliminary Phase I clinical study. *Journal of Neurosurgery: Spine*. doi:10.3171/SPI/2008/8/3/208.

Wu, Q., Zhang, Y.-J., Gao, J.-Y., et al. (2014a) Aquaporin-4 Mitigates Retrograde Degeneration of Rubrospinal Neurons by Facilitating Edema Clearance and Glial Scar Formation After Spinal Cord Injury in Mice. *Molecular Neurobiology*, 49 (3): 1327–1337. doi:10.1007/s12035-013-8607-3.

Wu, Q., Zhang, Y.J., Gao, J.Y., et al. (2014b) Aquaporin-4 mitigates retrograde degeneration of rubrospinal neurons by facilitating edema clearance and glial scar formation after spinal cord injury in mice. *Molecular Neurobiology*, 49 (3): 1327–1337. doi:10.1007/s12035-013-

8607-3.

Xi, F., Xu, R.J., Xu, J.H., et al. (2019) Calcium/calmodulin-dependent protein kinase II regulates mammalian axon growth by affecting F-actin length in growth cone. *Journal of Cellular Physiology*. doi:10.1002/jcp.28867.

Xie, L., Kang, H., Xu, Q., et al. (2013) Sleep drives metabolite clearance from the adult brain. *Science*. doi:10.1126/science.1241224.

Xu, W., Wong, T.P., Chery, N., et al. (2007) Calpain-mediated mGluR1alpha truncation: a key step in excitotoxicity. *Neuron*, 53 (3): 399–412. doi:10.1016/j.neuron.2006.12.020.

Xu, Z., Xiao, N., Chen, Y., et al. (2015) Deletion of aquaporin-4 in APP/PS1 mice exacerbates brain A β accumulation and memory deficits. *Molecular Neurodegeneration*. doi:10.1186/s13024-015-0056-1.

Yan, X., Liu, J., Wang, X., et al. (2018) Pretreatment with AQP4 and NKCC1 Inhibitors Concurrently Attenuated Spinal Cord Edema and Tissue Damage after Spinal Cord Injury in Rats. *Frontiers in Physiology*, 9: 6. doi:10.3389/fphys.2018.00006.

Yang, B., Zador, Z. and Verkman, A.S. (2008a) Glial cell aquaporin-4 overexpression in transgenic mice accelerates cytotoxic brain swelling. *Journal of Biological Chemistry*, 283 (22): 15280–15286. doi:10.1074/jbc.M801425200.

Yang, B., Zhang, H. and Verkman, A.S. (2008b) Lack of aquaporin-4 water transport inhibition by antiepileptics and arylsulfonamides. *Bioorganic and Medicinal Chemistry*. doi:10.1016/j.bmc.2008.06.005.

Yang, W.Y., Tan, Z.F., Dong, D.W., et al. (2018) Association of aquaporin-1 with tumor migration, invasion and vasculogenic mimicry in glioblastoma multiforme. *Molecular Medicine Reports*. doi:10.3892/mmr.2017.8265.

Yeung, C.-H., Callies, C., Rojek, A., et al. (2009) Aquaporin Isoforms Involved in Physiological Volume Regulation of Murine Spermatozoa¹. *Biology of Reproduction*, 80 (2): 350–357.

doi:10.1095/biolreprod.108.071928.

Yoon, S.H., Shim, Y.S., Park, Y.H., et al. (2007) Complete Spinal Cord Injury Treatment Using Autologous Bone Marrow Cell Transplantation and Bone Marrow Stimulation with Granulocyte Macrophage-Colony Stimulating Factor: Phase I/II Clinical Trial. *Stem Cells*. doi:10.1634/stemcells.2006-0807.

Yu, X., Green, M., Gilden, D., et al. (2011) Identification of peptide targets in neuromyelitis optica. *Journal of Neuroimmunology*. doi:10.1016/j.jneuroim.2011.04.007.

Yune, T.Y., Lee, J.Y., Jung, G.Y., et al. (2007) Minocycline alleviates death of oligodendrocytes by inhibiting pro-nerve growth factor production in microglia after spinal cord injury. *Journal of Neuroscience*. doi:10.1523/JNEUROSCI.1661-07.2007.

Zeidel, M.L., Ambudkar, S. V., Smith, B.L., et al. (1992) Reconstitution of Functional Water Channels in Liposomes Containing Purified Red Cell CHIP28 Protein. *Biochemistry*, 31 (33): 7436–7440. doi:10.1021/bi00148a002.

Zeng, X.N., Xie, L.L., Liang, R., et al. (2012) AQP4 Knockout Aggravates Ischemia/Reperfusion Injury in Mice. *CNS Neuroscience and Therapeutics*, 18 (5): 388–394. doi:10.1111/j.1755-5949.2012.00308.x.

Zeppenfeld, D.M., Simon, M., Haswell, J.D., et al. (2017) Association of perivascular localization of aquaporin-4 with cognition and Alzheimer disease in aging brains. *JAMA Neurology*. doi:10.1001/jamaneurol.2016.4370.

Zeynalov, E., Chen, C.H., Froehner, S.C., et al. (2008) The perivascular pool of aquaporin-4 mediates the effect of osmotherapy in postischemic cerebral edema. *Critical Care Medicine*. doi:10.1097/CCM.0b013e3181847853.

Zhang, C., Hu, A., Jing, Y., et al. (2019) Mannitol reduces spinal cord edema in rats with acute traumatic spinal cord injury. *Letters in Drug Design & Discovery*. doi:10.2174/1570180816666190731112158.

Zhao, Y., Bucur, O., Irshad, H., et al. (2017) Nanoscale imaging of clinical specimens using pathology-optimized expansion microscopy. *Nature Biotechnology*. doi:10.1038/nbt.3892.

Zu, J., Wang, Y., Xu, G., et al. (2014) Curcumin improves the recovery of motor function and reduces spinal cord edema in a rat acute spinal cord injury model by inhibiting the JAK/STAT signaling pathway. *Acta Histochemica*. doi:10.1016/j.acthis.2014.08.004.